Microbial communities in submarine permafrost and their response to permafrost degradation and warming

Julia Mitzscherling
geb. Magritz

DISSERTATION

Zur Erlangung des akademischen Grades
„doctor rerum naturalium“
- Dr. rer. nat. -
in der Wissenschaftsdisziplin „Mikrobiologie“

eingereicht an der
Mathematisch-Naturwissenschaftlichen Fakultät
Institut für Biochemie und Biologie
der Universität Potsdam
und
GFZ Deutsches GeoForschungsZentrum, Helmholtz Zentrum Potsdam
Geomikrobiologie

Potsdam
Eingereicht am: 02.10.2019
Tag der Disputation: 27.05.2020

Prüfungskomission:

Hauptbetreuerin: Jun.-Prof. Dr. Susanne Liebner (Universtität Potsdam)
Betreuer: Prof. Dr. Dirk Wagner (Universtität Potsdam)
Gutachter: Prof. Dr. Tim Urich (Universität Greifswald)

Tag der Disputation: 27. Mai 2020

Published online in the
Institutional Repository of the University of Potsdam:
https://doi.org/10.25932/publishup-47124
https://nbn-resolving.org/urn:nbn:de:kobv:517-opus4-471240

„Je mehr ich weiß, umso mehr weiß ich, dass ich nicht(s) weiß.“

Albert Einstein

Statement of Original Authorship

I herewith assure that I have developed and written the enclosed PhD-thesis completely by myself and have not used sources or means without declaration in the text. Any thoughts from others or literal quotations are clearly marked. The PhD-thesis was not used in the same or in a similar version to achieve an academic grading or is being published elsewhere.

Julia Mitzscherling

Preface

This study was supported by the Helmholtz Association (HGF) in the framework of the Helmholtz Young Investigators Research Group "MicroCene – Microbial Communities of the terrestrial subsurface" by a grant to Susanne Liebner (VH-NG-919). It focused on the development of microbial abundance, bacterial communities, and the occurrence of anaerobic oxidation of methane (AOM) by anaerobic methane oxidizing archaea (ANME) in warming submarine permafrost of the East Siberian Arctic Shelf. Two study sites in the central and western Laptev Sea, sampled during the expedition COAST I in 2005 and the expedition Laptev Sea – Buor Khaya in 2012, were chosen for the analyses in this study. The laboratory work was mainly performed at GFZ German Research Centre for Geosciences, Helmholtz Centre Potsdam. Physicochemical analyses were performed at the Alfred Wegener Institute, Helmholtz Centre for Polar and Marine Research, Potsdam.

The thesis is written in English, organized as a publication-based cumulative dissertation and submitted to the Faculty of Science at the University of Potsdam. It consists of a general introduction comprising the motivation of the study, a scientific background about permafrost with a focus on submarine permafrost, the permafrost carbon feedback, and microbial life in permafrost. Following the introduction, aims and objectives of the study as well as a description of the study sites are described. The results of this work are presented in two manuscripts with first authorship and one manuscript with co-authorship, which are published in peer-reviewed scientific journals. The thesis finishes with a synthesis including conclusions, critical remarks and future prospects.

Acknowledgements

I wish to particularly thank *Jun.-Prof. Dr. Susanne Liebner* (GFZ) for giving me the chance to work in the great scientific and collegial atmosphere of her Junior Research group. I want to thank my "Doktormutti" for her optimism, for encouraging me, and standing behind me in all the periods of my PhD time. Thank you for making it possible to start a family during this intense time by enabling such family friendly working conditions. But most notably, I want to thank you for your enthusiasm that made me fall in love with my work on the fascinating (microbial) world of the Arctic permafrost.

I would like to acknowledge *Prof. Dr. Dirk Wagner* (GFZ) and *Prof. Dr. Tim Urich* (Universität Greifswald) for the evaluation of my dissertation. Special thanks also to *Dirk* and my mentor *Dr. Paul Overduin* (AWI Potsdam) for valuable discussions and critics during our advisory meetings. Furthermore, I want to thank *Paul* for the linguistic proofreading of all my manuscripts and for his scientific input from the permafrost-side of view.

I would like to thank …
… all my colleagues of the section Geomicrobiology at GFZ for good times in the lab and during our coffee breaks. I particularly would like to thank *Andrea Kiss, Anke Saborowski, Dr. Janine Heise, Nadja Torres Reyes, Stine Holm* and *Lisa Moskwa* for their moral support during our conversations and for just being the lovely persons they are. Many thanks also to *Dr. Matthias Winkel* and *Dr. Fabian Horn* for their scientific support and funny times on conferences.
… *Mirco Jarius (Wehle)* and *Linda Mahler* whose internship and master's thesis were of great additional value for my work.
… *Sybille Hahmann* for always being there with regard to organizational stuff and any other non-scientific question.

Zuguterletzt möchte ich meinem Mann und unseren Kindern danken, die mein Leben so lebenswert und liebenswert machen. Ich möchte mich auch bei meiner Familie und meiner besten Freundin bedanken. Obwohl ich euch nie wirklich erklären konnte, was ich eigentlich mache, habt ihr immer großes Interesse an meiner Arbeit gezeigt und mir das Gefühl gegeben etwas Großartiges zu leisten. Ihr habt dazu beigetragen, meine Arbeit als das zu sehen, was sie ist: etwas Einzigartiges und Faszinierendes.

List of publications

In the scope of this thesis the following articles and conference contributions were published:

Articles

Mitzscherling, J., Horn, F., Winterfeld, M., Mahler, L., Kallmeyer, J., Overduin, P. P., … Liebner, S. (2019) Microbial community composition and abundance after millennia of submarine permafrost warming. *Biogeosciences, 16*(19), 3941–3958. https://doi.org/10.5194/bg-16-3941-2019

Mitzscherling, J., Horn, F., Winterfeld, M., Mahler, L., Kallmeyer, J., Overduin, P. P., … Liebner, S. (2019) Microbial community composition and abundance after millennia of submarine permafrost warming. *Biogeosciences Discussions.* https://doi.org/10.5194/bg-2019-144

Winkel, M., **Mitzscherling, J**., Overduin, P. P., Horn, F., Winterfeld, M., Rijkers, R., … Liebner, S. (2018). Anaerobic methanotrophic communities thrive in deep submarine permafrost. *Scientific Reports, 8*(1), 1–13. http://doi.org/10.1038/s41598-018-19505-9

Mitzscherling, J., Winkel, M., Winterfeld, M., Horn, F., Yang, S., Grigoriev, M. N., … Liebner, S. (2017). The development of permafrost bacterial communities under submarine conditions. Journal of Geophysical Research: *Biogeosciences*, 122(7), 1689–1704. http://doi.org/10.1002/2017JG003859

Conference Contributions

Mitzscherling, J., Horn, F., Winterfeld, M., Mahler, L., Kallmeyer, J., Overduin, P.P., ... Liebner, S. (2020) Microbial community response to submarine permafrost warming and thaw. *Annual Meeting 2020 of the Association for General and Applied Microbiology (VAAM)*, Leipzig, Germany, 8-11 March 2020 (Abstract, Oral Presentation)

Mitzscherling, J., Winkel, M., Overduin, P. P., Winterfeld, M., Horn, F., Mahler, L., … Liebner, S. (2018) Sea water influence reduces bacterial abundance in submarine permafrost. *17th International Symposium on Microbial Ecology (ISME 17)*, Leipzig, Germany, 12-17 August 2018 (Abstract, Poster)

Mitzscherling, J., Winkel, M., Winterfeld, M., Horn, F., Yang, S., Grigoriev, M. N., … Liebner, S. (2017) The development of permafrost bacteria under submarine conditions. *14th Symposium on Bacterial Genetics and Ecology (BAGECO 14)*, Aberdeen, Scotland, 4-8 June 2017 (Abstract, Poster)

Magritz, J., Winkel, M., Mahler, L., Horn, F., Overduin, P., Thiele, M., … Liebner, S. (2016) Development of Cell Numbers and Microbial Community Composition along a Natural Temperature Gradient in Subsea Permafrost. *XI. International Conference on Permafrost (ICOP 6)*, Potsdam, Germany, 20-24 June 2016 (Abstract, Poster)

Winkel, M., **Magritz, J.**, Horn, F., Overduin, P., Knoblauch, C. and Wagner, D. (2016) Anaerobic oxidation of methane (AOM) at the thaw front of subsea permafrost, *Annual Meeting of the Association for General and Applied Microbiology (VAAM)*, Jena, Germany, 13-16 March 2016 (Abstract, Oral Presentation)

Magritz, J., Winkel, M., Overduin, P., Knoblauch, C., Wagner, D. & Liebner, S. (2015) Quantifying Microbial Communities of the Methane Cycle in two Subsea Permafrost Deposits of the Central Laptev Sea. *Annual Conference 2015 of the Association for General and Applied Microbiology (VAAM)*, 1-4 March 2015 (Abstract, Oral Presentation)

Magritz, J., Overduin, P. P., Knoblauch, C., Wagner, D., & Liebner, S. (2014) Quantifying Microbial Communities of the Methane Cycle in Subsea Permafrost Deposits of the Central Laptev Sea. *IV. European Conference on Permafrost (EUCOP 4)*, Évora, Spain, 18-21 June 2014 (Abstract, Poster)

Summary

The Arctic region is especially impacted by global warming as temperatures in high latitude regions have increased and are predicted to further rise at levels above the global average. This is crucial to Arctic soils and the shallow shelves of the Arctic Ocean as they are underlain by permafrost. Perennially frozen ground is a habitat for a large number and great diversity of viable microorganisms, which can remain active even under freezing conditions. Warming and thawing of permafrost makes trapped soil organic carbon more accessible to microorganisms. They can transform it to the greenhouse gases carbon dioxide, methane and nitrous oxide. On the other hand, it is assumed that thawing of the frozen ground stimulates microbial activity and carbon turnover. This can lead to a positive feedback loop of warming and greenhouse gas release.

Submarine permafrost covers most areas of the Siberian Arctic Shelf and contains a large though unquantified carbon pool. However, submarine permafrost is not only affected by changes in the thermal regime but by drastic changes in the geochemical composition as it formed under terrestrial conditions and was inundated by Holocene sea level rise and coastal erosion. Seawater infiltration into permafrost sediments resulted in an increase of the pore water salinity and, thus, in thawing of permafrost in the upper sediment layers even at subzero temperatures. The permafrost below, which was not affected by seawater, remained ice-bonded, but warmed through seawater heat fluxes.

The objective of this thesis was to study microbial communities in submarine permafrost with a focus on their response to seawater influence and long-term warming using a combined approach of molecular biological and physicochemical analyses. The microbial abundance, community composition and structure as well as the diversity were investigated in drill cores from two locations in the Laptev Sea, which were subjected to submarine conditions for centuries to millennia. The microbial abundance was measured through total cell counts and copy numbers of the 16S rRNA gene and of functional genes. The latter comprised genes which are indicative for methane production (*mcrA)* and sulfate reduction (*dsrB*). The microbial community was characterized by high-throughput-sequencing of the 16S rRNA gene. Physicochemical analyses included the determination of the pore water geochemical and stable isotopic composition, which were used to describe the degree of seawater influence. One major outcome of the thesis is that the submarine permafrost stratified into different so-called pore water units centuries as well as millennia after inundation: (i) sediments that were mixed with seafloor sediments, (ii) sediments that were infiltrated with seawater, and (iii) sediments that

were unaffected by seawater. This stratification was reflected in the submarine permafrost microbial community composition only millennia after inundation but not on time-scales of centuries.

Changes in the community composition as well as abundance were used as a measure for microbial activity and the microbial response to changing thermal and geochemical conditions. The results were discussed in the context of permafrost temperature, pore water composition, paleo-climatic proxies and sediment age. The combination of permafrost warming and increasing salinity as well as permafrost warming alone resulted in a disturbance of the microbial communities at least on time-scales of centuries. This was expressed by a loss of microbial abundance and bacterial diversity. At the same time, the bacterial community of seawater unaffected but warmed permafrost was mainly determined by environmental and climatic conditions at the time of sediment deposition. A stimulating effect of warming was observed only in seawater unaffected permafrost after millennia-scale inundation, visible through increased microbial abundance and reduced amounts of substrate.

Despite submarine exposure for centuries to millennia, the community of bacteria in submarine permafrost still generally resembled the community of terrestrial permafrost. It was dominated by phyla like *Actinobacteria*, *Chloroflexi*, *Firmicutes*, *Gemmatimonadetes* and *Proteobacteria*, which can be active under freezing conditions.

Moreover, the archaeal communities of both study sites were found to harbor high abundances of marine and terrestrial anaerobic methane oxidizing archaea (ANME). Results also suggested ANME populations to be active under *in situ* conditions at subzero temperatures. Modeling showed that potential anaerobic oxidation of methane (AOM) could mitigate the release of almost all stored or microbially produced methane from thawing submarine permafrost.

Based on the findings presented in this thesis, permafrost warming and thawing under submarine conditions as well as permafrost warming without thaw are supposed to have marginal effects on the microbial abundance and community composition, and therefore likely also on carbon mobilization and the formation of methane. Thawing under submarine conditions even stimulates AOM and thus mitigates the release of methane.

Zusammenfassung

Die globale Erwärmung beeinträchtigt die Arktische Region besonders stark. Im Vergleich zum globalen Mittel sind die Temperaturen in den hohen Breitengraden am stärksten gestiegen und werden voraussichtlich auch weiterhin am stärksten ansteigen. Das ist äußerst kritisch, da arktische Böden und die flachen Schelfgebiete des Arktischen Ozeans von Permafrost geprägt sind. Dieser mehrjährig gefrorene Boden ist ein Habitat für eine große Anzahl und Diversität von Mikroorganismen, die lebensfähig sind und auch unter gefrorenen Bedingungen aktiv sein können. Einerseits machen eine Erwärmung und das Tauen des Permafrosts gespeicherten organischen Kohlenstoff zugänglicher für die Mikroorganismen. Diese können den Kohlenstoff in die Treibhausgase Kohlenstoffdioxid, Methan und Distickstoffoxid umwandeln. Andererseits stimuliert das Tauen des gefrorenen Bodens die mikrobielle Aktivität und den Kohlenstoffumsatz. Das kann zu einem sich verstärkenden Rückkopplungsprozess aus Erwärmung und Freisetzung von Treibhausgasen führen.

Submariner Permafrost umfasst den größten Teil des Ostsibirischen Arktisschelfs und enthält ein großes, wenn auch nicht quantifiziertes Kohlenstoffreservoir. Der submarine Permafrost wird jedoch nicht nur durch Veränderungen des Wärmehaushalts beeinflusst, sondern auch durch drastische Veränderungen in der geochemischen Zusammensetzung. Durch den holozänen Meeresspiegelanstieg und durch Küstenerosion wurde der unter terrestrischen Bedingungen gebildete Permafrost überflutet. Ein Eindringen von Meerwasser führte in den Permafrostsedimenten zu einem Anstieg der Porenwasser-Salinität und dadurch zum Tauen des Permafrosts in den oberen Schichten, sogar bei Temperaturen unter 0 °C. Tiefer liegende Permafrostsedimente, die (noch) nicht vom Meerwasser beeinflusst wurden, blieben eis-gebunden, aber begannen sich durch den Wärmestrom des Meerwassers zu erwärmen.

Das Ziel dieser Dissertation war es, die mikrobiellen Gemeinschaften in submarinem Permafrost zu untersuchen. Der Fokus lag dabei auf der Reaktion der Gemeinschaften auf den Einfluss des Meerwassers und die Langzeiterwärmung. Die Arbeit nutzt dafür einen kombinierten Ansatz aus molekularbiologischen und physikochemischen Analysen. Die mikrobielle Abundanz, Gemeinschaftszusammensetzung und -struktur sowie die Diversität wurden in Sedimentbohrkernen zweier Standorte in der Laptew See untersucht, welche seit Jahrhunderten bis Jahrtausenden submarinen Bedingungen ausgesetzt waren. Die mikrobielle Abundanz wurde mit Hilfe von Zellzahlen und Kopienzahlen des 16S rRNA Gens sowie funktioneller Gene bestimmt, die kennzeichnend für die Methanproduktion (*mcrA*) und

Sulfatreduktion (*dsrB*) sind. Die mikrobielle Gemeinschaft wurde mit Hilfe der Hochdurchsatz-Sequenzierung des 16S rRNA Gens charakterisiert. Physikochemische Analysen beinhalteten die Untersuchung der geochemischen Zusammensetzung der Porenwassers und der stabilen Wasserisotopen. Beide Zusammensetzungen wurden genutzt, um den Grad des Meerwassereinflusses auf die Permafrostsedimente zu beschreiben. Ein Hauptergebnis der Arbeit ist, dass sich submariner Permafrost sowohl nach Jahrhunderten als auch nach Jahrtausenden der Überflutung in verschiedene Schichten, sogenannte Porenwassereinheiten, unterteilen lässt: (i) Sedimente, die sich mit dem Meeresboden vermischt haben, (ii) Sedimente, die vom Meerwasser infiltriert wurden und (iii) Sedimente, die vom Meerwasser unbeeinflusst sind. Diese Schichtenbildung spiegelt sich erst nach jahrtausendelanger Überflutung auch in der mikrobiellen Gemeinschaftszusammensetzung wider, nicht jedoch nach Jahrhunderten.

Änderungen sowohl in der Gemeinschaftszusammensetzung als auch in der Abundanz wurden als Maß für mikrobielle Aktivität und die mikrobielle Reaktion auf die sich ändernden thermischen und geochemischen Bedingungen genutzt. Die Ergebnisse wurden im Kontext von Permafrosttemperatur, Porenwasserzusammensetzung, paleoklimatischen Proxys und dem Sedimentalter diskutiert. Die Kombination aus Permafrosterwärmung und steigender Salinität, sowie die Permafrosterwärmung allein, resultierten auf Zeitskalen von Jahrhunderten in einer Störung der mikrobiellen Gemeinschaft. Dies drückte sich durch einen Verlust der mikrobiellen Abundanz und der bakteriellen Diversität aus. Gleichzeitig wurde die bakterielle Gemeinschaft im vom Meerwasser unbeeinflussten, aber erwärmten Permafrost hauptsächlich durch die Umweltbedingungen und das Klima zur Zeit der Sedimentablagerung geprägt. Ein stimulierender Einfluss der Erwärmung konnte im vom Meerwasser unbeeinflussten Permafrost erst nach jahrtausendelanger Überflutung beobachtet werden. Dies wurde durch einen Anstieg in der mikrobiellen Abundanz und einer Abnahme der organischen Substrate sichtbar.

Obwohl die bakteriellen Gemeinschaften des Permafrostes submarinen Bedingungen für Jahrhunderte bis Jahrtausende ausgesetzt waren, unterschieden sie sich kaum von den Gemeinschaften im terrestrischen Permafrost. Die Gemeinschaft des submarinen Permafrosts wurde von Phyla wie *Actinobacteria*, *Chloroflexi*, *Firmicutes*, *Gemmatimonadetes* und *Proteobacteria* dominiert, welche auch unter gefrorenen Bedingungen aktiv sein können. Darüber hinaus enthielten die archaellen Gemeinschaften an beiden Standorten eine hohe Anzahl von marinen und terrestrischen anaerob methan-oxidierenden Archaeen (ANME), bei denen eine Aktivität unter *in situ* Bedingungen bei Minusgraden angenommen wird. Eine Modellierung zeigte, dass die anaerobe Oxidation von Methan (AOM) potenziell fast die

gesamte Menge des gespeicherten und mikrobiell produzierten Methans in tauendem submarinem Permafrost reduzieren könnte.

Die Ergebnisse der Arbeit deuten darauf hin, dass das Tauen von Permafrost unter submarinen Bedingungen sowie eine Erwärmung ohne Tauen marginale Effekte auf die Abundanz und Zusammensetzung der mikrobiellen Gemeinschaften und somit wahrscheinlich auch auf die Mobilisierung von Kohlenstoff in Form von Methan hat. Das Tauen unter submarinen Bedingungen stimuliert sogar AOM und reduziert somit den Ausstoß von Methan.

Table of contents

Abbreviations

ACIA	Arctic Climate Impact Assessment
ANME	anaerobic methane oxidaizing archaea
ANOVA	analysis of variance
AOM	anaerobic oxidation of methane
BIT	branched and isoprenoid tetraether
BK2	submarine core drilled at Buor Khaya
BONCAT	bioorthogonal noncanonical amino acid tagging
BP	before present
C1	terrestrial core drilled at Mamontov Klyk
C2	submarine core drilled at Mamontov Klyk 11.5 km off the coast
C3	submarine core drilled at Mamontov Klyk 3 km off the coast
C4	submarine core drilled at Mamontov Klyk 1 km off the coast
CARD-FISH	catalyzed reporter deposition Fluorescence In Situ Hybridization
CCA	canonical correspondence analysis
CH_4	Methane
CO	carbon monoxide
CO_2	carbon dioxide
CTAB	cetyl trimethylammonium bromide
Cy3	cyanine dye
DDBJ	DNA Database of Japan
DHVEG 1	Deep Hydrothermal Vent Euryarchaeotal Group 1
DNA	deoxyribonucleic acid
dNTP	nucleoside triphosphate
DOC	dissolved organic carbon
DPANN	archaeal superphlyum
DSPEG	Deep Submarine Permafrost Euryarchaeotal Group
dsrB	dissimilatory sulfite reductase β-subunit
EDTA	ethylenediaminetetraacetic acid
EMBL	nucleotide sequence database of the European Molecular Biology Laboratory
EPS	extracellular polymeric substance
ESAS	East Siberian Arctic Shelf
FISH	fluorescence *in situ* hybridization
GDGT	glycerol dialkyl glycerol tetraether
GenBank	International Genetic Database
Gt	gigatons (=Pg)
H2	Hydrogen
HCl	hydrogen chloride
HGF	Helmholtz-Gemeinschaft Deutscher Forschungszentren
IBPT	ice-bonded permafrost table
ICP-OES	inductively coupled plasma - optical emission spectrometry
IPCC	International Panel on Climate Change
ka	thousand years
LPS	Lipopolysaccharide

m bs	meters below surface
m bsf	meters below seafloor
m bsl	meter below sea level
MAG	metagenome-assembled genome
MBG-x	Marine Benthic Group x
MCG	Miscellaneous Crenarchaeotal Group
mcrA	methyl-coenzyme M reductase α-subunit
MI	methane index
MID	multiple identifier
N_2O	nitrous oxide
NMDS	non-metric multi-dimensional scaling
OTU	operational taxonomic unit
PBS	paraformaldedhyde-phosphate-buffered saline
PC	principal component
PCA	principal component analysis
PCR	polymerase chain reaction
PerMANOVA	permutational multivariate analysis of variance
Pg	petagramm (=Gt)
PLFA	phospholipid fatty acid
PSU	pratical salinity unit
PW	pore water unit
PW II IL	pore water unit II interlayer
qPCR	quantitative (real time) PCR
RCP	representative concentration pathways
rRNA	ribosomal ribonucleic acid
SDS	sodium dodecyl sulfate
SIP	stable isotope probing
SMTZ	sulfate-methane transition zone
SOM	soil organic matter
SRB	sulfate reducing bacteria
TC	total carbon
TCC	total cell counts
TEA	terminal electron acceptors
Tg	Teragramm
TN	total nitrogen
TOC	total organic carbon
T-RFLP	terminal restriction fragment length polymorphism
Tris-	tris(hydroxymethyl)aminomethane
TS	total sulfur
V SMOV	a standard for water isotopes
VPDB	a standard for measuring $\delta^{13}C$
wt%	weight %
$\delta^{13}C$	isotopic signature, a measure of the ratio of stable isotopes ^{13}C : ^{12}C
$\delta^{18}O$	measure of the ratio of stable isotopes oxygen-18 (^{18}O) and oxygen-16 (^{16}O)
δD	measure of the ratio of stable isotopes hydrogen D/^{1}H

List of Figures

List of Tables

1 Introduction

1.1 Motivation

The Arctic plays an essential role in the earth's climate system. As the Arctic Ocean is intimately connected with the climate systems around it, the Arctic is more sensitive to changes in climate than Antarctica. Temperature in high-latitude regions have been rising twice as fast as the global average over the last 30 years [*IPCC in Climate Change 2013*, 2013] and are projected to experience the strongest increase across the world as a consequence of climate change in the future (Fig. 1-1) [*Kattsov et al.*, 2005; *IPCC in Climate Change 2013*, 2013].

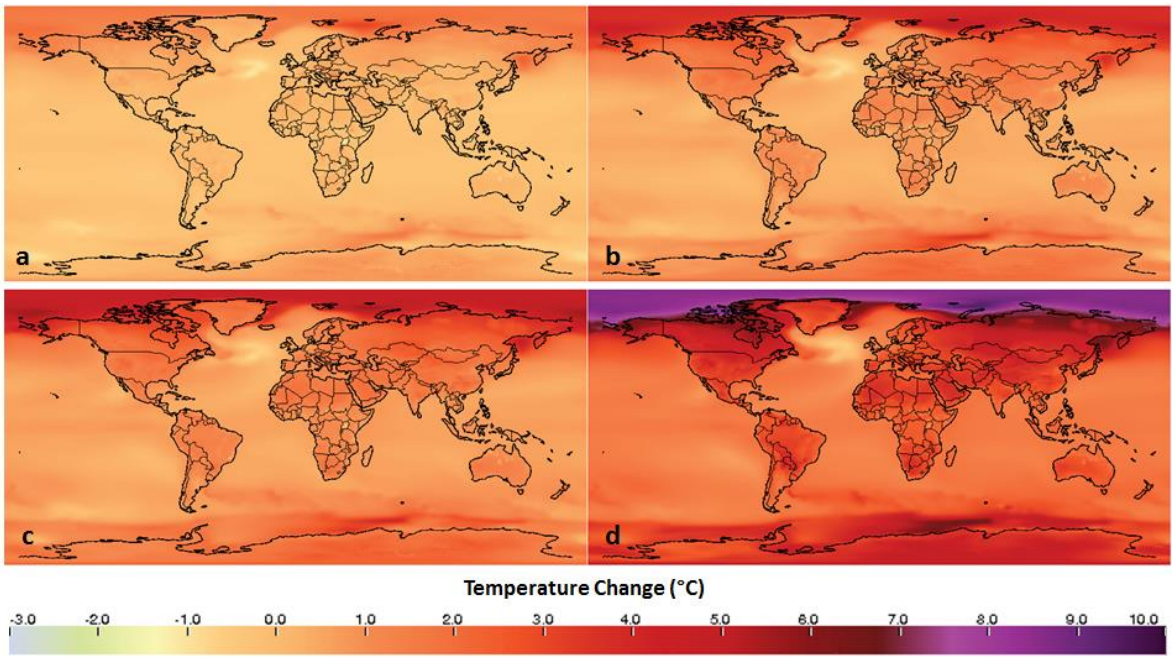

Figure 1-1: Mean annual temperature change between 2071-2090 and the reference period 1986-2005 based on different emission trajectories (i.e., Representative Concentration Pathways, RCPs). Representative Concentration Pathways provide concentrations of atmospheric greenhouse gas (GHG) and the trajectory that is taken over time to reach those concentrations. These RCPs are named according to the level of radiative forcing (enhanced greenhouse effect or warming) that they produce by the year 2100. The four RCPs include **a)** one low pathway in which radiative forcing peaks at 2.6 Watts per square meter (Wm^{-2}) before 2100 and is followed by a decline, two intermediate 'stabilization pathways' in which radiative forcing is stabilized at **b)** 4.5 Wm^{-2} and **c)** 6 Wm^{-2} after 2100, and **d)** one high pathway in which radiative forcing reaches 8.5 Wm^{-2} by 2100 (*Climate Inspector*. available from https://gisclimatechange.ucar.edu/ [accessed on 28-02-2019] [*Moss et al.*, 2011]).

Rising temperatures are causing changes in the physical condition of the otherwise permanently frozen ground (permafrost). On the regional scale this has socio-economic consequences including human settlement on uneven ground, destructive effects on the infrastructure and impacts on the regional economy [*Anisimov*, 2017]. However, besides regional effects, rising temperatures in the Arctic region have become a global problem. Permafrost soils, that are widespread in the Arctic region, have the potential to amplify the global climate change. Warming affects the soil/sediment stability and diffusivity and thereby unlocks large quantities of soil organic carbon. Several efforts have been made to model and predict the release of this carbon in the form of greenhouse gases into the atmosphere [*Shakhova et al.*, 2010b; *Schuur et al.*, 2015]. However, among those predictions, improvements are needed that include the physical and biological processes controlling the dynamics of permafrost carbon release. Biological processes include the microbial turnover of soil organic carbon. Therefore, it is necessary to understand the role and potential of microbial life in the cryosphere (i.e. sea, lake and river ice, snow cover, glaciers, ice caps and sheets, and frozen ground like permafrost) as these ecosystems are especially sensitive to climate changes. Although recently the interest in studying microorganisms in the cryosphere has grown, the current understanding of microbial diversity and activity in degrading frozen ground and of the role of micorobial populations in carbon turnover and release is limited.

Thus, the present thesis aims at reconstructing the response of microbial communities to permafrost degradation in the Arctic region by using a combination of geochemical and molecular biological analyses. Submarine permafrost, which started to warm hundreds to thousands of years ago because of seawater inundation, is used as a natural laboratory for studying the long-term response of microorganisms to permafrost warming. Furthermore, the thesis offers new insights into microbial life and its controls in permafrost thawing under submarine conditions.

1.2 Permafrost and the carbon feedback

Permafrost environments

In the Northern Hemisphere 24 % of the land surface (excluding glaciers and ice sheets) [*Zhang et al.*, 2003] and large areas of the Arctic shelves are underlain by perennially frozen ground (Fig. 1.2). This so called permafrost is defined as ground that remains at or below 0°C for at least two consecutive years [*van Everdingen*, 1998].

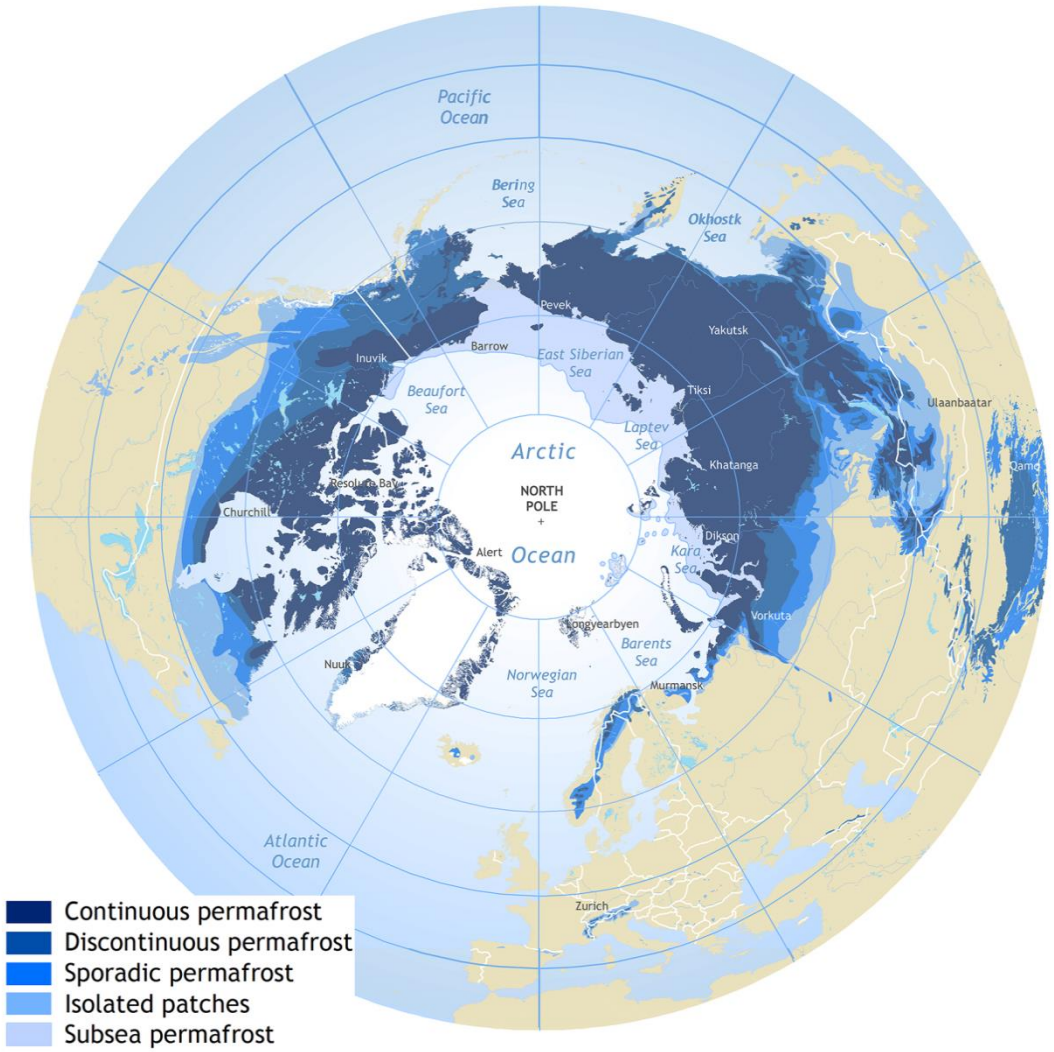

Figure 1-2: Circumpolar permafrost distribution of submarine and terrestrial permafrost. Terrestrial permafrost can be classified into continuous permafrost (underlying 90-100% of the landscape); discontinuous permafrost (50-90%); and sporadic permafrost (0-50%) (Source: [*Brown et al.*, 1997], International Permafrost Association).

In different geographical locations different types of permafrost exist with respect to permafrost structure, organic matter content and age. Traditionally, terrestrial permafrost is classified into continuous, discontinuous or sporadic permafrost by the amount of ice it contains (Fig. 1-2). It is overlain by the so-called "active layer", soil which is exposed to seasonal freeze-thaw cycles. A specific type of permafrost can be found in Northeast Siberia. The so called 'Yedoma' or 'Ice-complex' is characterized by high levels of organic matter (~2% carbon) and an ice content of 50-90%.

Recently, it was shown that owing to global warming the depth of the active layer has increased in many locations over the past few decades [*Walter et al.*, 2006; *Shur and Jorgenson*, 2007; *Romanovsky et al.*, 2010; *Vieira et al.*, 2010] and the permafrost temperature in the continuous and discontinuous permafrost zone as well as in mountain permafrost and Antarctica has risen. At a global scale permafrost has warmed by 0.3 °C within the last decade [*Biskaborn et al.*, 2019].

The permafrost carbon feedback

Research on permafrost has considerably advanced in recent years due to emerging concerns about the impacts of permafrost warming on the activation of indigenous microorganisms. Permafrost warming and thawing increases sediment permeability and can result in the release of stored methane into the atmosphere [*Shakhova et al.*, 2010a, 2014; *Portnov et al.*, 2013; *Thornton et al.*, 2016]. In addition, stored organic carbon released by permafrost thawing can become more accessible to microorganisms. The northern permafrost region is estimated to contain 1307–1580 Pg (=Gt) of organic [*Hugelius et al.*, 2014; *Schuur et al.*, 2015], twice as much as there is currently in the atmosphere [*Zimov et al.*, 2006; *Schuur et al.*, 2009]. Approximately 800 Pg of this organic carbon is stored in permafrost soils and deposits, while still unquantified amounts exist below the extensive shallow water areas of the Arctic continental shelf in submarine permafrost (Fig. 1-3). The organic carbon primarily originates from plant material and was buried by dust deposition, sedimentation in flood plains and peat development over decades to millennia [*Zimov et al.*, 2006; *Schuur et al.*, 2008].

Microorganisms are assumed to mineralize the organic carbon within the sediment in low-oxygen or anaerobic conditions promoting the formation of greenhouse gases, such as methane (CH_4), carbon dioxide (CO_2), and nitrous oxide (N_2O) [*Wagner et al.*, 2007; *Koch et al.*, 2009; *Mackelprang et al.*, 2011; *Graham et al.*, 2012].

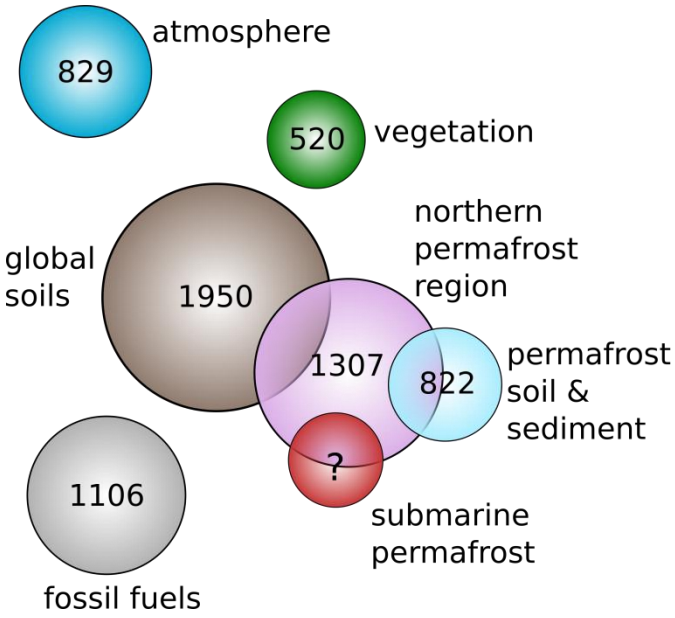

Figure 1-3: Terrestrial and atmospheric carbon stocks in relation to the carbon stored in the northern permafrost region and in perennially frozen ground. The surface area of the circles represents the size of the carbon stock. The stocks are given in Gt. For global soils, atmosphere, vegetation, and fossil fuels, means are taken of the minimum - maximum ranges given in [*Ciais et al.*, 2013]. The 1307 Gt of the northern circumpolar permafrost region and 822 Gt of permafrost soils and sediments were calculated in [*Hugelius et al.*, 2014]. Figure modified after [*Strauss*, 2014]**.**

Microbial conversion and release of just a fraction of the frozen carbon pool could alter the atmospheric greenhouse gas budgets significantly. This can generate positive feedbacks to the regional and global warming, even accelerating warming (Fig. 1-4) [*Shakhova et al.*, 2014]. However, the effect of rising permafrost temperature on microbial processes remains to be investigated.

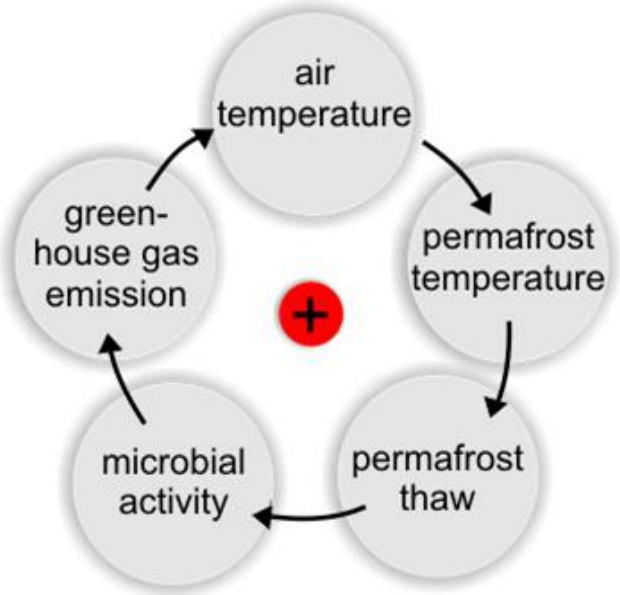

Figure 1-4: The permafrost carbon feedback loop generated by rising air temperatures in the Arctic.

1.3 Submarine permafrost

Dimension and formation

The shallow shelf areas of the Arctic Ocean are underlain by submarine permafrost (Fig. 1-2). The shelves reach from the coastline down to 100 m water depth [*Rachold et al.*, 2007]. They are found in the Barents Sea, Kara Sea, Laptev Sea, East Siberian Sea, Chukchi Sea, and the Beaufort Sea (Fig. 1-5). The shallowest and most spacious shelf of the World Ocean is the East Siberian Arctic shelf (ESAS) encompassed by the Laptev, East Siberian and the Russian part of the Chukchi Seas. It covers an area of 2 million km^2 or 14 % of the Arctic Ocean [*Berchet et al.*, 2016]. Thereby, it is almost three times larger as compared with the terrestrial Siberian wetlands and it comprises more than 80 % of the potential submarine permafrost in the Arctic (Fig 1-2) [*Overduin et al.*, 2015].

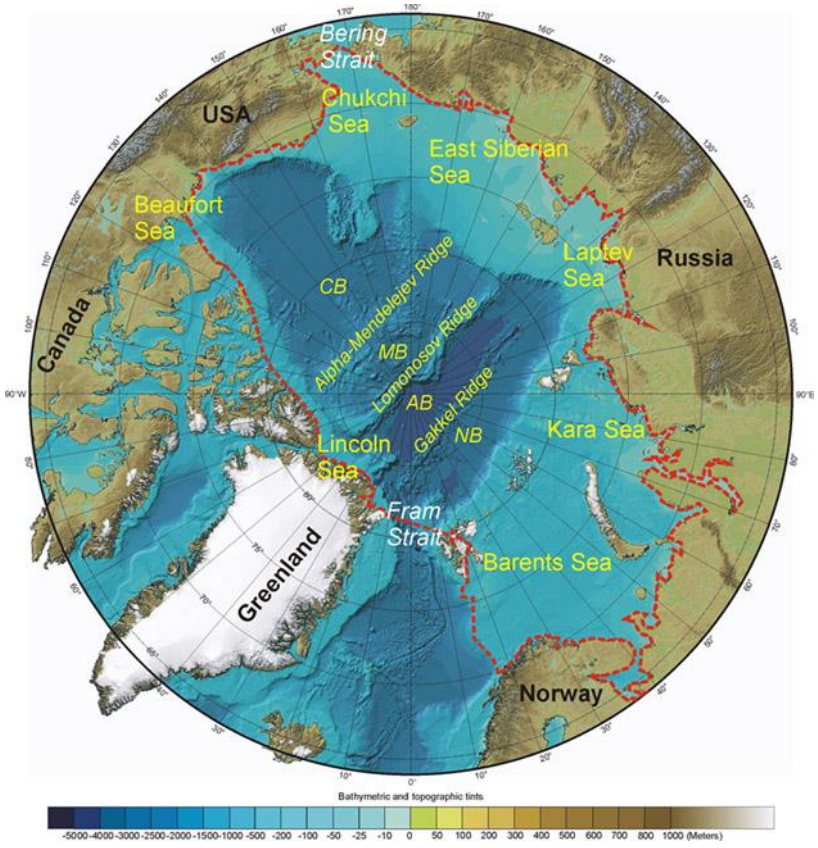

Figure 1-5: The Arctic Ocean and its constituent seas. The red dotted line indicates the limits of the Arctic Ocean. Main basins of the deep Arctic Ocean basin: NB – Nansen Basin, AB – Amundsen Basin, MB – Makarov Basin, CB – Canada Basin. (Włodarska-Kowalczuk, Maria (2013): *Arctic Ocean*. Available from http://www.coastalwiki.org/wiki/Arctic_Ocean [accessed on 16-01-2019])

Submarine permafrost on the Arctic sea shelves was formed as terrestrial permafrost when the non-glaciated shelves were exposed to subaerial conditions due to lower sea levels during the last glacial cycle. Subsequently, post-glacial sea level rise during the Holocene inundated the shelves [*Romanovskii and Hubberten*, 2001]. Since the stabilization of the sea level, 5 ka ago, coastal erosion is responsible for the formation of subsea permafrost. Degradation of permafrost coasts, which account for 34% of the coasts worldwide [*Lantuit et al.*, 2012], is thereby caused by a combined effect of declining sea ice cover, longer and warmer thawing seasons and sea level rise. Thus, waves can hit the coast higher and longer during the ice-free season [*Fritz et al.*, 2017]. Coastal erosion on the ESAS, with mean modern coastal erosion rates of 1 - 2 m yr^{-1} [*Lantuit et al.*, 2012] and a high local variability of up to 10 m yr^{-1} [*Lantuit et al.*, 2013], results in an annual formation of 10 km² of subsea permafrost [*Grigoriev*, 2008].

The average thickness of submarine permafrost within most of the shelf is 300 – 350 m, with a maximum thickness of 500 m and more [*Romanovskii et al.*, 2004]. Frozen sediments are thickest near the shore, where seawater submergence occurred more recently. Submarine permafrost depths in the nearshore zone of the Western Laptev Sea and along the coast of the East Siberian Sea range from 400 to 600 m and from 300 to 400 m, respectively [*Romanovskii et al.*, 2005]. With increasing distance to the shore, the depth of the ice-bonded permafrost table increases (Fig. 1-6) and consequently, the thickness of the cryotic (<0 °C), but ice-free sediment overlying the offshore permafrost, also increases. The increasing thickness of the unfrozen sediment layer above the permafrost table is an indicator for the increasing duration of seawater influence and progressive thawing of the ice-bonded sediment from above. Consequently, the outer shelf is now underlain by discontinuous, patchy permafrost [*Romanovskii et al.*, 2005; *Schuur et al.*, 2015].

Thermal regime of submarine permafrost

Upon sea transgression, the submerged permafrost on the shelf started to degrade as the relatively warm ocean water warmed the sediment. In the Laptev Sea, mean annual bottom water temperatures of -1.8 °C to -0.5 °C [*Osterkamp*, 2001] are 12 to 17 °C warmer than the annual average surface temperature of terrestrial permafrost [*Romanovskii et al.*, 2005]. Although thawing of frozen fresh-water sediments under the impact of low-temperature seawater proceeds very slowly, permafrost temperatures within the largest part of the shelf lie around -1.0 °C to -2.0 °C, within the range of freezing-thawing processes [*Romanovskii et al.*, 2004]. The remaining frozen sediments are therefore much more vulnerable to temperature increases than permafrost on land. Bottom-water warming due to decreasing sea-ice coverage

[*Stroeve et al.*, 2008], rising air temperatures in winter [*ACIA*, 2004] and water-mass inflow from the Atlantic and Pacific Oceans into the Arctic Ocean [*Walczowski and Piechura*, 2006; *Woodgate et al.*, 2006] thereby increase the degradation rates of submarine permafrost in the Laptev and East Siberian Seas. Besides top-down seawater heat and salt fluxes, bottom-up geothermal heat fluxes are also responsible for the degradation of submarine permafrost [*Osterkamp*, 2001; *Shakhova et al.*, 2010a].

Submarine permafrost degradation

Inundation and infiltration of seawater change the thermal regime and geochemical composition of submarine permafrost drastically [*Ulyantsev et al.*, 2016]. Thermal and chemical conditions of submarine permafrost are varying across the shelf and rely on many factors.

Permafrost degradation in the nearshore zone (<10 m water depth) is controlled by coastal erosion rates, wave dynamics, sediment supply and cross-shore transport, water column salinity and temperature as well as sea ice dynamics (especially the timing and duration of bottom-fast ice) and diffusive transport processes within the sediment column [*Overduin et al.*, 2012]. Close to the beach (**Zone 2**, Fig. 1-6) waves and high tides produce significant salt concentrations in the active layer. The active layer and temperature regime differ from that on land since coastal banks and bluffs often accumulate wind-blown snow. In shallow water regions (<1.5 - 2 m water depth, **Zone 3**), sea ice seasonally freezes to the seabed. The so-called bottom-fast ice couples the seabed conductively to the atmosphere. While the seabed is covered with relatively warm seawater in the summer, in the winter it becomes very cold and salt concentrations at the seabed are high. At greater water depths (**Zone 4**), where the ice does not or only sporadically freeze to the seabed, the under-ice circulation causes higher seawater salinities and lower temperatures above the seabed. In both settings there is an active layer at the seabed that thaws and freezes seasonally. Brine drainage from the growing sea ice increases water salinity and decreases temperatures of the bottom-water. This causes seasonal, partial freezing of the less saline pore waters in the sediments. Furthermore, due to their high salt concentrations brines are responsible for thawing the underlying submarine permafrost at negative sediment temperatures. This kind of circumstance is very important in the evolution of submarine permafrost as here the major proportion of salt infiltrates the sediment. Highly saline and dense brines infiltrate the seabed, even when it is partially frozen.

Regions further offshore (**Zone 5**), charachterized by water depths that guarantee normal seawater over the seabed throughout the year, have relatively constant chemical and thermal conditions since the ice-bonded permafrost no longer couples conductively to the atmosphere.

Thus, the permafrost thaws continuously throughout the year and depth to the ice-bonded permafrost increases rapidly with increasing distance from the shore [*Osterkamp*, 2001].

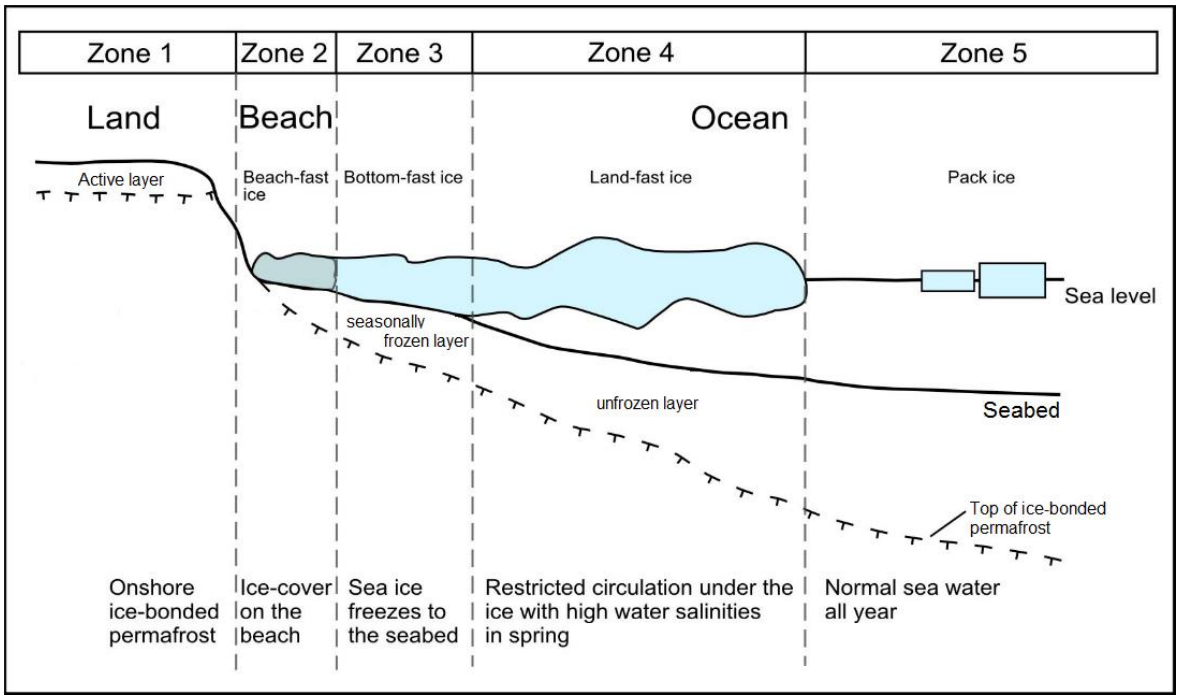

Figure 1-6: Model of the transition of terrestrial permafrost to submarine permafrost. Five zones with different thermal and chemical conditions can be distinguished (modified after [*Osterkamp*, 2001] and [*Eicken et al.*, 2005]).

1.4 Microbial life in permafrost

Limitations of microbial life in permafrost

Permafrost is a unique habitat for microorganisms and is colonized by Bacteria, Archaea and Fungi. There is a high variability in the composition and abundance of permafrost microorganisms. Organisms which are capable of growth and reproduction at low temperatures have been classified as psychrophiles, cryophiles, cold-tolerant or cold-adapted [*Feller and Gerday*, 2003; *Margesin and Collins*, 2019]. The temperature limit for cell reproduction and growth of bacteria, archaea, and unicellular eukaryotes lies at -20 °C [*Clarke*, 2014; *Bakermans*, 2017], while microbial activity in permafrost soils has been reported to be measurable down to -39 °C [*Panikov et al.*, 2006]. In the cryosphere, freezing temperature and water availability are the most important factors that limit microbial life and determine biomass, diversity and

community structure [*Pointing et al.*, 2009; *Yergeau et al.*, 2009; *Zeglin et al.*, 2009]. As freezing results in the removal of liquid water through the formation of ice, permafrost can be considered an environment of low water availability [*Franks*, 2003]. Thus, the true limiting factor for life in the cold is the lack of liquid water at low temperatures and not low temperature per se [*Clarke*, 2014; *Bakermans*, 2017]. Within permafrost, liquid water is only present as very thin films surrounding soil and ice particles. In Siberian permafrost, the thickness of water films was predicted to range between 15 nm at -1.5 °C to 5 nm at -10 °C (Fig. 1-7b) [*Rivkina et al.*, 2000]. Those water films, however, are too small to harbor microorganisms or to allow for the migration of microbial cells. Bacteria were found to be predominantly located in brine veins [*Junge et al.*, 2001, 2004] – that is liquid water in subzero environments, where increased solute and salt concentrations depress the freezing point [*Raymond-Bouchard et al.*, 2017] (Fig. 1-7a). Nevertheless, the thin water films are important for the survival and *in situ* activity of microorganisms, as they protect viable cells from destruction by ice crystals and serve as a nutrient medium for microbial growth [*Gilichinsky*, 2002].

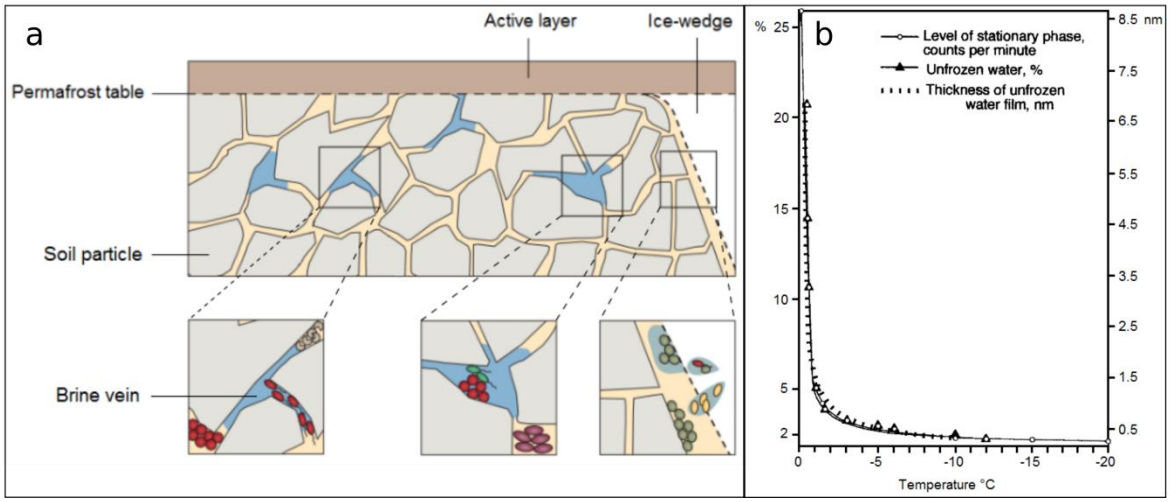

Figure 1-7: Permafrost features and water film thickness. a) The permafrost layer (grey) is overlain by a seasonally thawed active layer (brown). The bold dashed line indicates the surface of the permafrost table. Close-ups show individual soil microaggregates and microcolonies of bacterial or archaeal cells in the pores containing free water - called brine veins (modified after [*Jansson and Taş*, 2014]). **b)** Measured amounts of unfrozen water (filled triangle) and calculated thickness of unfrozen water films (dotted line) in permafrost as a function of temperature (modified after [*Rivkina et al.*, 2000]).

In addition to cryodessication, freezing causes physiological limitations for microbial cells. Proteins lose their flexibility or denature due to the cold. Cell membranes lose fluidity affecting

the nutrient transport [*Chattopadhyay*, 2006], and a higher stability of nucleic acids inhibits replication, transcription and translation [*D'Amico et al.*, 2006]. Furthermore, cells that have been preserved in permafrost for thousands to millions of years are also exposed to constant irradiation from native radio nuclides, which destroys the DNA of the ancient cells [*Gilichinsky et al.*, 2008].

Microbial survival strategies

In order to overcome the limitations and stresses charachteristic to the permafrost environment microbial cells have devloped several survival strategies (Fig. 1-8) [*Maayer et al.*, 2014; *Margesin and Collins*, 2019]. For example, Bacteria entrapped in frozen soil were found to be more resistant to irradiation than bacteria in thawed soil [*Gilichinsky et al.*, 2008] and to own DNA repair mechanisms [*Johnson et al.*, 2007].

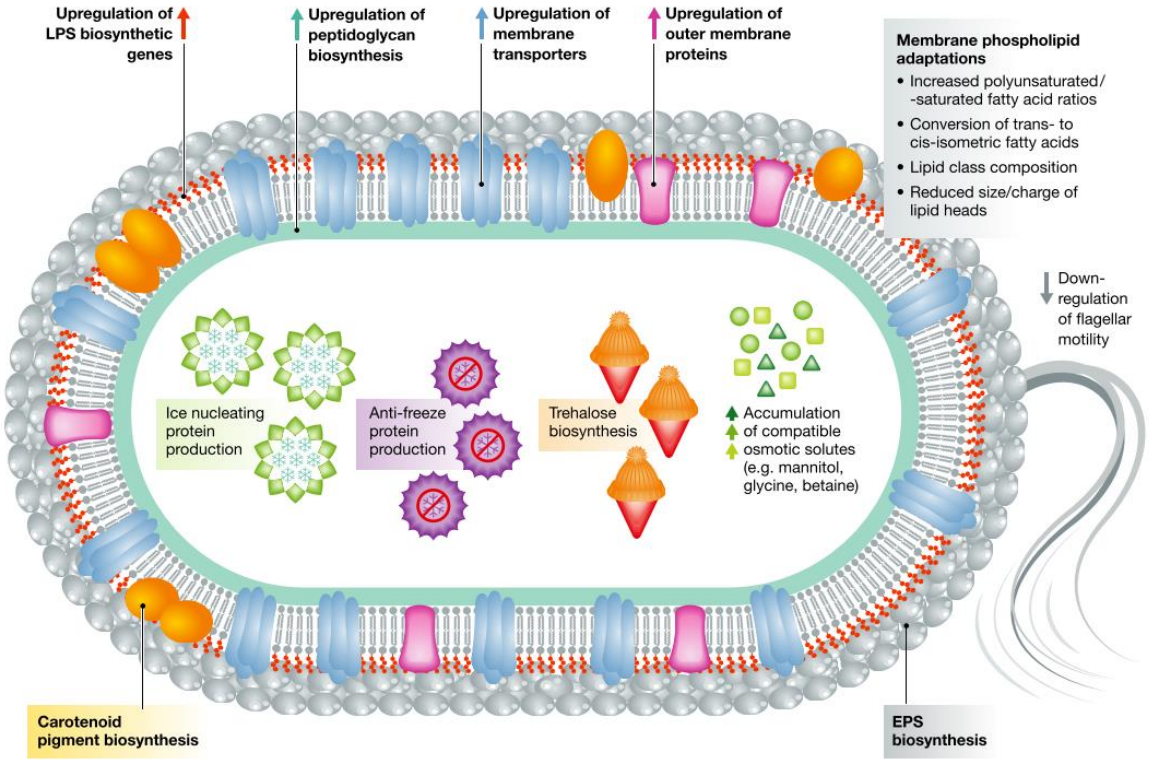

Figure 1-8: Physiological adaptations in a psychrophilic prokaryote [*Maayer et al.*, 2014]**.**

Strategies to survive subzero temperatures include entering a dormant state with low metabolic activity and production of cryoprotectants or similar molecules (ice nucleating molecules, anti-freeze proteins, compatible osmotic solutes) [*Bakermans et al.*, 2009; *Maayer et al.*, 2014]. Cold-adapted microorganisms shift their phospholipid metabolism to maintain membrane fluidity and functionality at subzero temperatures by regulating the branched-to-saturated fatty-acid production in the cell membranes [*Denich et al.*, 2003; *Unell et al.*, 2007; *Mykytczuk et al.*, 2013]. Further adaptation mechanisms include modifications to RNA transcription and protein folding [*Riley et al.*, 2008; *Ayala-del-Río et al.*, 2010], as well as the generation of carbon and energy reserves to overcome slow metabolism and rates of nutrient uptake [*Maayer et al.*, 2014].

Microbial Abundance and Viability

Abundance

Despite the existing limitations microorganisms are abundant in permafrost soils and sediments. Their abundance can vary by permafrost type and cell counts range from 10^3 to 10^8 cells g^{-1} sediment in Arctic permafrost, while seasonally frozen soils contain up to 10^9 cells g^{-1} sediment [*Steven et al.*, 2006; *Gilichinsky et al.*, 2008; *Jansson and Taş*, 2014]. In most cases, bacterial counts in permafrost environments are equal or even greater than those in other cryo-environments such as sea ice, glacier ice, marine sediments or lakes [*Steven et al.*, 2006]. Archaea are present in permafrost as well, though 200-1000 times lower in abundance [*Yergeau et al.*, 2010; *Altshuler et al.*, 2017]. In Siberian active layer soils Archaea were found to account for at least 1 to 12% of the total cell counts [*Kobabe et al.*, 2004; *Hoj et al.*, 2008].

Viability & Activity

Several studies using different isolation techniques and approaches have shown that viable bacteria can be abundant in Siberian permafrost (10^2-10^8 cells g^{-1}) [*Shi et al.*, 1997; *Vorobyova et al.*, 1997; *Vishnivetskaya et al.*, 2000]. Currenlty available data suggest that viability seems to be independent of temperature, but instead depends on the volume of ice and the age of permafrost. With increasing age and ice content, the number of viable cells decreases [*Gilichinsky et al.*, 1989, 1992; *Khlebnikova et al.*, 1990; *Steven et al.*, 2006]. In Arctic samples, the fraction of culturable cells is minor and represents only 0.1– 10% of the total cell counts [*Vishnivetskaya et al.*, 2000; *Steven et al.*, 2006]. An explanation for the low viable cell recovery might be the dominance of dwarfed cells in Siberian permafrost, which are viable but non-

culturable (Steven et al., 2009). However, at least up to 22% of cells were identified by staining to have intact cell membranes and were thus classified as live [*Mackelprang et al.*, 2017]. Since microorganisms can be viable they can also remain active at extremely low temperatures [*Rivkina et al.*, 2000; *Wagner et al.*, 2007]. *Buford Price and Sowers* [2004] proposed that microbial metabolic rates of cold-adapted communities can be classified into three groupings: (1) a rate sufficient for bacterial growth, (2) a rate for maintenance of metabolism but too low for growth, and (3) a rate for survival solely to repair macromolecular damage accumulated during prolonged storage over geological time scales in bacteria characterized as "largely dormant". Several studies reported of either activity or growth at temperatures substantially below the freezing point in frozen soils and permafrost [*Steven et al.*, 2006; *Nikrad et al.*, 2016]. For instance, early studies measured respiration and fluxes of CO_2 or N_2O (e.g. CO_2 respiration down to -18°C [*Elberling and Brandt*, 2003]), or evaluated the growth of isolates (acetate incorporation at -20°C [*Rivkina et al.*, 2000]). More recent studies focused on RNA-based methods like FISH [*Kobabe et al.*, 2004], microarray [*Yergeau et al.*, 2007] or T-RFLP analysis [*Männistö et al.*, 2013], as well as metatranscriptomics [*Coolen and Orsi*, 2015], and enzyme activity measurements [*Waldrop et al.*, 2010] in Arctic permafrost or tundra soils. Others determined the respiration and/or incorporation of labelled substrates such as ^{13}C-glucose (respiration down to -39°C [*Panikov et al.*, 2006]), ^{14}C-glucose (microbial uptake down to -15°C [*Gilichinsky et al.*, 2003]), ^{14}C-acetatic acid (^{14}C respiration at -15°C [*Steven et al.*, 2007b, 2008a]), or ^{13}C-acetate in combination with stable isotope probing (SIP) (bacterial genome replication down to -20°C [*Tuorto et al.*, 2014]). Two of the most recent studies performed either proteomic analysis of an permafrost isolate at -10°C [*Raymond-Bouchard et al.*, 2017]) or metaproteomics in permafrost soils [*Hultman et al.*, 2015]. All those studies underline that microbial life continues into the subzero temperature range. This activity contributes to carbon and nitrogen flux even under freezing conditions affecting global processes.

Microbial diversity and community composition

To study the diversity and community composition of (active) microorganisms in permafrost culture-independent methods like direct sequencing of environmental ribosomal RNA (rRNA) genes (clone libraries or high-throughput sequencing approaches) or various –omics approaches are used today [*Vishnivetskaya et al.*, 2006; *Steven et al.*, 2007a; *Liebner et al.*, 2008; *Yergeau et al.*, 2010; *Mackelprang et al.*, 2011; *Bakermans et al.*, 2014; *Frank-Fahle et al.*, 2014; *Ganzert et al.*, 2014; *Mitzscherling et al.*, 2017; *Winkel et al.*, 2018]. Culture-independent approaches revealed a higher and different bacterial diversity compared to culture-dependent

techniques [*Hultman et al.*, 2015]. In general, bacteria appear to be more diverse than archaea or fungi [*Jansson and Taş*, 2014; *Altshuler et al.*, 2017], and similar to abundance microbial diversity is lower in permafrost than in active-layer soils [*Taş et al.*, 2014].

Culture-independent approaches revealed that bacterial phyla such as Proteobacteria, Firmicutes, Chloroflexi, Acidobacteria Actinobacteria and Bacteroidetes commonly occur in Arctic permafrost [*Liebner et al.*, 2009; *Jansson and Taş*, 2014; *Mitzscherling et al.*, 2017; *Taş et al.*, 2018]. Isolated i.e. viable bacteria belonged to the phyla of Firmicutes, Actinobacteria, Bacteroidetes and Proteobacteria [*Jansson and Taş*, 2014 and references therein]. In addition, transcriptomic analysis and stable isotope probing demonstrated Chloroflexi and Gemmatimonadetes to be active under frozen conditions in permafrost [*Tuorto et al.*, 2014; *Coolen and Orsi*, 2015]. The most active members of the microbial communities are Proteobacteria, Acidobacteria, and Firmicutes [*Hultman et al.*, 2015].

The archaeal population is suggested to be diverse as well, as taxa that were detected in permafrost belong to the major archaeal domains Euryarchaeota, Crenarchaeota and Thaumarchaeota [*Rivkina et al.*, 2007; *Steven et al.*, 2007a, 2008b; *Yergeau et al.*, 2010; *Wilhelm et al.*, 2012; *Taş et al.*, 2014] Out of this pool Euryarchaeota were found to be one of the most transcriptionally active microbial groups under frozen conditions [*Coolen and Orsi*, 2015]. In Siberian and alpine permafrost, most of the archaeal community was composed of methanogenic species [*Steven et al.*, 2007a]. Also, the isolation of viable methane-producing strains suggests that permafrost is a favorable environment for methanogenesis [*Jansson and Taş*, 2014].

Methanogenesis and Methanotrophy

The existence of methanogens - methane producing archaea - is of concern as permafrost warming and thawing is expected to stimulate microbes and their contribution to carbon turnover [*Waldrop et al.*, 2010; *Mackelprang et al.*, 2011; *Graham et al.*, 2012; *Schuur et al.*, 2015] leading to the formation of the greenhouse gases CH_4 and CO_2. *Wei et al.* [2018] reported that permafrost thaw resulted in an increase of methane emissions accompanied with an increase in the abundance of methanogenic archaea and significant shifts in the archaeal community and their activities. Methanogens can be distinguished by their substrate. Hydrogenotrophic methanogens produce methane using H_2, CO_2 and sometimes formate as a carbon source, whereas acetoclastic methanogens use acetate as a carbon source. The latter group is responsible for approximately two-thirds of the biogenic methane that is produced annually on Earth [*Jansson and Taş*, 2014]. Besides methanogenic activity, metagenomic

analyses have identified functional pathways for methanotrophs in permafrost [*Mackelprang et al.*, 2011; *Taş et al.*, 2014]. Methanotrophic bacteria are able to aerobically metabolize methane as a source of carbon and energy. They can be divided into two distinct physiological groups. Type I methanotrophs assimilate formaldehyde produced from the oxidation of methane using the ribulose monophosphate pathway [*Anthony*, 1986]. Type II methanotrophs utilise the serine pathway for formaldehyde assimilation [*Hanson and Hanson*, 1996]. Functional pathways for both type I and type II methanotrophs have been detected in permafrost metagenomes. Due to the anoxic conditions in submarine permafrost systems another type of methanotrophy is more likely to occur: the anaerobic oxidation of methane (AOM). It is catalyzed by anaerobic methane oxidizing archaea (ANME). So far, AOM has mainly been studied in the so-called sulfate-methane transition zone (SMTZ) in the seabed [*Knittel and Boetius*, 2009]. In the ocean seabeds, >90% of the methane that is produced by methanogenesis is consumed by anaerobic oxidation of methane (AOM) [*Hinrichs and Boetius*, 2002; *Reeburgh*, 2007]. Hence, AOM efficiently controls the methane efflux from the ocean seafloor. AOM in marine sediments is coupled to sulfate reduction with penetrating sulfate from the seawater being utilized as the electron acceptor [*Iversen and Jør-gensen*, 1985]. ANME archaea of the marine clades ANME-1a/b, ANME-2a/b/c and ANME-3 [*Knittel and Boetius*, 2009] live in a syntrophic lifestyle with sulfate-reducing bacteria (SRB) [*Boetius et al.*, 2000; *Orphan et al.*, 2001; *Niemann et al.*, 2006] of the genera *Desulfosarcina*, *Desulfococcus*, *Desulfobulbus* and *Desulfofervidus* (Deltaproteobacteria) [*Knittel and Boetius*, 2009], and of the phylum *Thermodesulfobacteria* [*Krukenberg et al.*, 2016]. In addition to the marine ANME clades, there is evidence of terrestrial AOM in wetland and permafrost habitats [*Shcherbakova et al.*, 2016; *Narrowe et al.*, 2017] driven by ANME-2d [*Haroon et al.*, 2013; *Weber et al.*, 2017]. Furthermore, the coupling of AOM to alternative electron acceptors such as iron [*Beal et al.*, 2009; *Crowe et al.*, 2011], manganese [*Beal et al.*, 2009], nitrate [*Raghoebarsing et al.*, 2006; *Haroon et al.*, 2013] and humic substances [*Smemo and Yavitt*, 2011; *Scheller et al.*, 2016] has been suggested. So far, the microbial oxidation of methane in permafrost environments is only evident in aerobic soils and sediments [*Liebner et al.*, 2011; *Knoblauch et al.*, 2015], while communities that oxidize methane anaerobically in (thawing) deep subsurface permafrost remain to be detected and explored.

1.5 Aims and Objectives

Seawater inundation leads to permafrost warming and changes the pore water geochemical composition, as salt water infiltrates submarine permafrost sediments. This makes submarine permafrost more vulnerable to thawing and degradation than permafrost under subaerial conditions, and accordingly increases the potential for the release of methane and CO_2.
It is thus crucial to understand how microbial communities and abundance respond to warming, degradation and changing geochemical conditions with respect to carbon mobilization and greenhouse gas release. So far, our knowledge about the response of microbial communities in relict terrestrial permafrost to submarine conditions is limited to one study on the methanogenic communities [*Koch et al.*, 2009]. Thus, this thesis provides pioneer work in investigating the microbial ecology of submarine permafrost and the microbial response to permafrost warming and thawing under submarine conditions.
The work described in this thesis extends the current understanding on the structure and development of bacterial communities in dependence of pore water characteristics, stage of permafrost degradation, time of inundation and temperature in submarine permafrost. Furthermore, permafrost archaeal communities were analyzed with respect to potential anaerobic oxidation of methane under submarine conditions.

In this thesis, the following questions were addressed:

- **How does inundation of terrestrial permafrost change the pore water chemical conditions and physical state of permafrost?**
- **Is submarine permafrost a suitable natural laboratory to study the response of microbial communities to permafrost warming and thaw, and how do submarine permafrost communities differ from communities in onshore permafrost?**
- **What is the response of the indigenous microbial community to seawater infiltration and permafrost thaw?**
- **Do microbial communities already respond to permafrost warming without thaw on climate relevant time-scales and how does this occur?**
- **Is submarine permafrost a habitat for microbial assemblages involved in the anaerobic oxidation of methane and could they function as a filter for methane release?**

The methodologies applied to answer the questions are displayed in the flow chart on the following page. A combined approach of microbiological and physico- as well as geochemical analyses was used. Microbiological analyses of abundance and community composition were based on culture-independent techniques, while physico- and geochemical investigations were made on pore water and bulk material of the permafrost sediments.

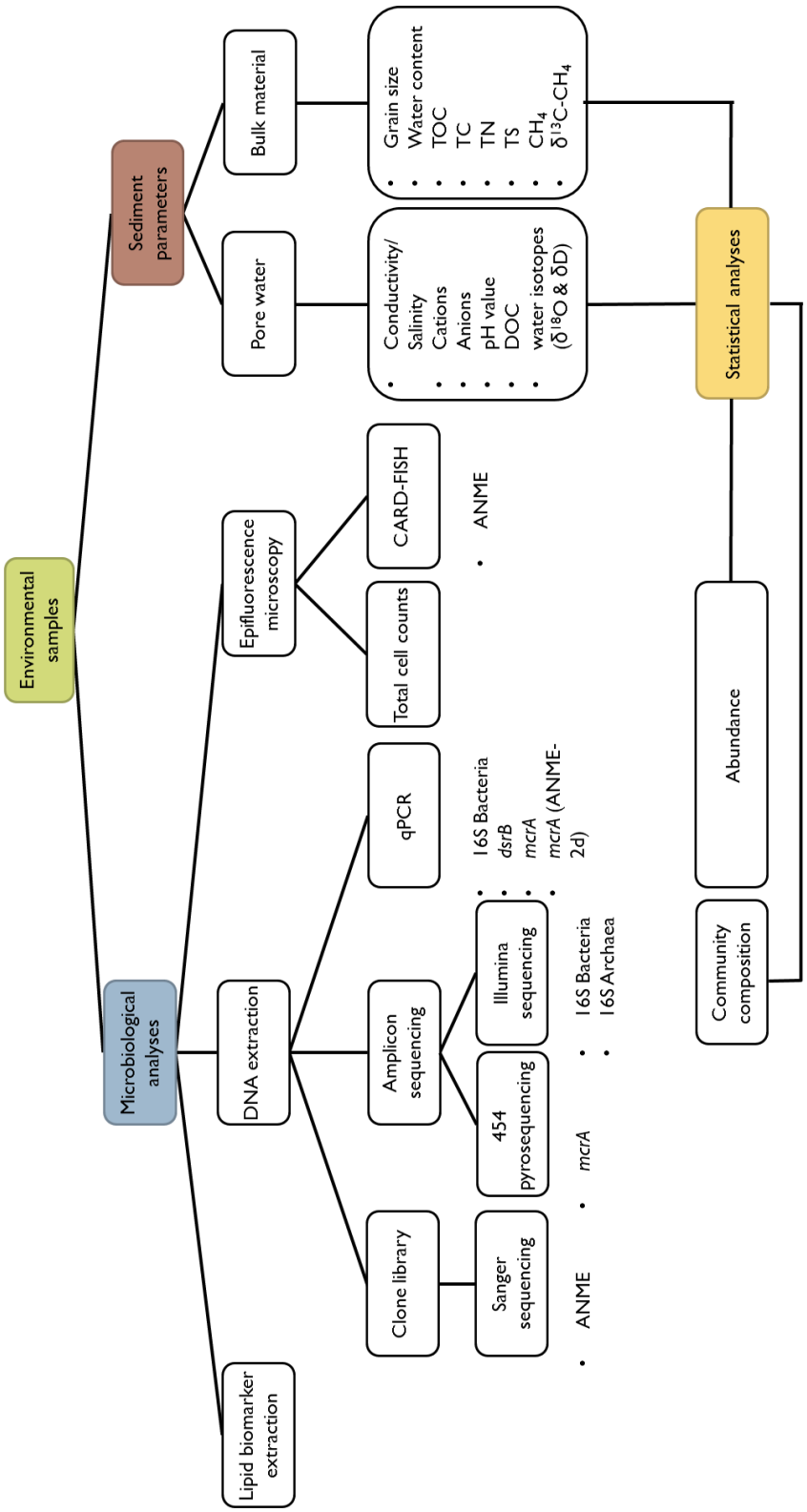

1.6 Overview of publications

Manuscript I (*Journal of Geophysical Research: Biogeosciences*, 2017, 122(7), 1689–1704, DOI: 10.1002/2017JG003859)

The article was highlighted as **Research Spotlight** (*Eos*, 2017, 98, DOI: 10.1029/2017EO080655)

The development of permafrost bacterial communities under submarine conditions

Authors: Julia Mitzscherling[1], Matthias Winkel[1], Maria Winterfeld[2], Fabian Horn[1], Sizhong Yang[1], Mikhail N. Grigoriev[3], Dirk Wagner[1,7], Pier P. Overduin[2] and Susanne Liebner[1,8]

Aims: The purpose of this study was to investigate the development of microbial abundance and bacterial community composition under submarine conditions with a focus on the combined effect of seawater intrusion and warming. Two sites in the Laptev Sea were studied, that were inundated for different time periods and thus represented different stages of permafrost degradation. They differed in depth and dimension of the phase boundary between unfrozen to frozen sediments, and in the pore water characteristics. The latter were analyzed to define the level of seawater infiltration and permafrost degradation. Bacterial communities and microbial abundance were related to physicochemical parameters in order to determine the effect of seawater inundation and to investigate the microbial response to warming.

Summary: Submarine permafrost is more vulnerable to thawing than permafrost on land. Besides increased heat transfer from the ocean water, the penetration of salt lowers the freezing temperature and accelerates permafrost degradation. Microbial communities in thawing permafrost are expected to be stimulated by warming but how they develop under submarine conditions is completely unknown. We used the unique records of two submarine permafrost cores from the Laptev Sea on the East Siberian Arctic Shelf, inundated about 540 and 2500 years ago, to trace how bacterial communities develop depending on duration of the marine influence and pore water chemistry. Combined with geochemical analysis, we quantified total cell numbers and bacterial gene copies, and determined the community structure of bacteria using deep sequencing of the bacterial 16S rRNA gene. We show that submarine permafrost is an extreme habitat for microbial life deep below the seafloor with changing thermal and chemical conditions. Pore water chemistry revealed different pore

water units reflecting the degree of marine influence and stages of permafrost thaw. Millennia after inundation by seawater, bacteria stratify into communities in permafrost, marine-affected permafrost, and seabed sediments. In contrast to pore water chemistry, the development of bacterial community structure, diversity and abundance in submarine permafrost appears site-specific, showing that both sedimentation and permafrost thaw histories strongly affect bacteria. Finally, highest microbial abundance was observed in the ice-bonded seawater unaffected but warmed permafrost of the longer inundated core, suggesting that permafrost bacterial communities exposed to submarine conditions start to proliferate millennia after warming.

Co-author's contribution: *P. P. Overduin* and *M. N. Grigoriev* conducted field work. *M. Winterfeld* and *P. P. Overduin* provided pore water and physicochemical data. *M. Winkel* and a masters student performed the cell counts. *F. Horn* preprocessed the sequence data and built OTU tables. *S. Yang* performed R applications. All authors contributed to the discussion and interpretation of the data and the writing of the paper.

Manuscript II (*Scientific Reports*, 2018, 8(1), 1–13, DOI: 10.1038/s41598-018-19505-9)

Anaerobic methanotrophic communities thrive in deep submarine permafrost

Authors: Matthias Winkel[1], Julia Mitzscherling[1], Pier P. Overduin[2], Fabian Horn[1], Maria Winterfeld[2], Ruud Rijkers[1], Mikhail N. Grigoriev[3], Christian Knoblauch[4], Kai Mangelsdorf[5], Dirk Wagner[1,7], and Susanne Liebner[1,8]

Aims: The submarine permafrost at both sites in the Laptev Sea was found to have deep sulfate-methane transition zones (SMTZ). As this is a potential habitat for anaerobic methane oxidizing archaea (ANME) this study aimed at identifying and quantifying microorganisms that are potentially involved in the anaerobic oxidation of methane (AOM) in thawing permafrost deep below the seafloor, and at evaluating their potential activity.

Summary: Thawing submarine permafrost is a source of methane to the subsurface biosphere. Methane oxidation in submarine permafrost sediments has been proposed, but the responsible microorganisms remain uncharacterized. We analyzed archaeal communities and identified distinct anaerobic methanotrophic assemblages of marine and terrestrial origin (ANME-2a/b, ANME-2d) both in frozen and completely thawed submarine permafrost

sediments. Besides archaea potentially involved in anaerobic oxidation of methane (AOM) we found a large diversity of archaea mainly belonging to Bathyarchaeota, Thaumarchaeota, and Euryarchaeota. Methane concentrations and δ^{13}C-methane signatures distinguish horizons of potential AOM coupled either to sulfate reduction in a sulfate methane transition zone (SMTZ) or to the reduction of other electron acceptors, such as iron, manganese or nitrate. Analysis of functional marker genes (*mcrA*) and fluorescence *in situ* hybridization (FISH) corroborate potential activity of AOM communities in submarine permafrost sediments at low temperatures. Modeled potential AOM consumes 72–100% of submarine permafrost methane and up to 1.2 Tg of carbon per year for the total expected area of submarine permafrost. This is comparable with AOM habitats such as cold seeps. We thus propose that AOM is active where submarine permafrost thaws, which should be included in global methane budgets.

Personal contribution: I carried out the molecular work including DNA extraction, quantification of the *mcrA* and *dsrB* genes via quantitative PCR and preparations of the Illumina sequencing of the archaeal 16S rRNA and of the pyrosequencing of *mcrA*. Furthermore, I contributed to the data interpretation and writing.

Manuscript III (*Biogeosciences*, 2019, *16*(19), 3941–3958. https://doi.org/10.5194/bg-16-3941-2019)

The article was **Highlight Article** in *Biogeosciences* (October)

Microbial community composition and abundance after millennia of submarine permafrost warming

Authors: Julia Mitzscherling[1], Fabian Horn[1], Maria Winterfeld[2], Linda Mahler[1], Jens Kallmeyer[1], Pier P. Overduin[2], Matthias Winkel[6], Mikhail N. Grigoriev[3], Dirk Wagner[1,7] and Susanne Liebner[1,8]

Aims: With this study, the response of microbial communities to submarine permafrost warming without thaw was investigated on the basis of changes in the microbial abundance and bacterial community composition. Along an onshore-offshore transect in the western Laptev Sea the sediment cores that were analyzed shared one lithostratigraphical unit. This unit was deposited at a similar time, in a similar environment and showed a high level of similarity with regard to pore water characteristics. The unit was so far unaffected of

penetrating seawater but warmed by > 10 °C due to centuries to millennia of inundation. The aim of this study was to investigate whether permafrost warming alone could already stimulate microbial activity and change the community composition.

Summary: Warming of the Arctic led to an increase of permafrost temperatures by about 0.3°C during the last decade. Permafrost warming is associated with increasing sediment water content, permeability and diffusivity and could on the long-term alter microbial community composition and abundance even before permafrost thaws. We studied the long-term effect (up to 2500 years) of submarine permafrost warming on microbial communities along an onshore-offshore transect on the Siberian Arctic Shelf displaying a natural temperature gradient of more than 10 °C. We analysed the in-situ development of bacterial abundance and community composition through total cell counts (TCC), quantitative PCR of bacterial gene abundance and amplicon sequencing, and correlated the microbial community data with temperature, pore water chemistry and sediment physicochemical parameters. On time-scales of centuries, permafrost warming coincided with an overall decreasing microbial abundance whereas millennia after warming the microbial abundance was similar to cold onshore permafrost. In addition, the dissolved organic carbon content of all cores was lowest in submarine permafrost after millennia-scale warming. Based on correlation analysis TCC unlike bacterial gene abundance showed a significant rank-based negative correlation with increasing temperature while bacterial gene copy numbers showed a strong negative correlation with salinity. Bacterial community composition correlated only weakly with temperature but strongly with the porewater stable isotopes $\delta^{18}O$ and δD, and with depth. The bacterial community showed substantial spatial variation and an overall dominance of Actinobacteria, Chloroflexi, Firmicutes, Gemmatimonadetes and Proteobacteria which are amongst the microbial taxa that were also found to be active in other frozen permafrost environments. We suggest that, millennia after permafrost warming by over 10°C, microbial community composition and abundance show some indications for proliferation but mainly reflect the sedimentation history and paleo-environment and not a direct effect through warming.

Co-author's contribution: *P. P. Overduin* and *M. N. Grigoriev* conducted field work. *M. Winterfeld* and *P. P. Overduin* provided pore water and physicochemical data. *F. Horn* conducted the bioinformatics analysis. *L. Mahler* performed and *J. Kallmeyer* advised the cell counting. All authors contributed to the discussion and interpretation of the data and the writing of the paper with particular contribution by *S. Liebner*.

Authors affiliation

[1]GFZ German Research Centre for Geosciences, Helmholtz Centre Potsdam, Section Geomicrobiology, 14473 Potsdam, Germany

[2]Alfred Wegener Institute, Helmholtz Centre for Polar and Marine Research, Periglacial Research, 14473 Potsdam, Germany

[3]Russian Academy of Sciences, Mel'nikov Permafrost Institute, Siberian Branch, Yakutsk, Russia

[4] University of Hamburg, Institute of Soil Science, 20146 Hamburg, Germany

[5]GFZ German Research Centre for Geosciences, Helmholtz Centre Potsdam, Section Organic Geochemistry, 14473 Potsdam, Germany

[6]GFZ German Research Centre for Geosciences, Helmholtz Centre Potsdam, Section Interface Geochemistry, 14473 Potsdam, Germany

[7]University of Potsdam, Institute of Geosciences, 14476 Potsdam, Germany

[8]University of Potsdam, Institute of Biochemistry and Biology, 14476 Potsdam, Germany

2 Study Area

2.1 Regional setting

The Laptev Sea is bordered by the Taymyr Peninsula to the west and the New Siberian Islands to the east. It is characterized by average water depths of less than 60 m. During the Weichselian glaciation (late Pleistocene, 18 ka BP) large areas of the non-glaciated arctic continental shelf [*Svendsen et al.*, 2004] was exposed to climatic conditions which led to the formation of cold, thick and continuous permafrost. Consequently, permafrost with high ice contents (ice-complex, ice contents of 80-98% [*Romanovskii et al.*, 2004]) formed on the Siberian coastal lowland and small islands close to the shore [*Romanovskii et al.*, 2000].

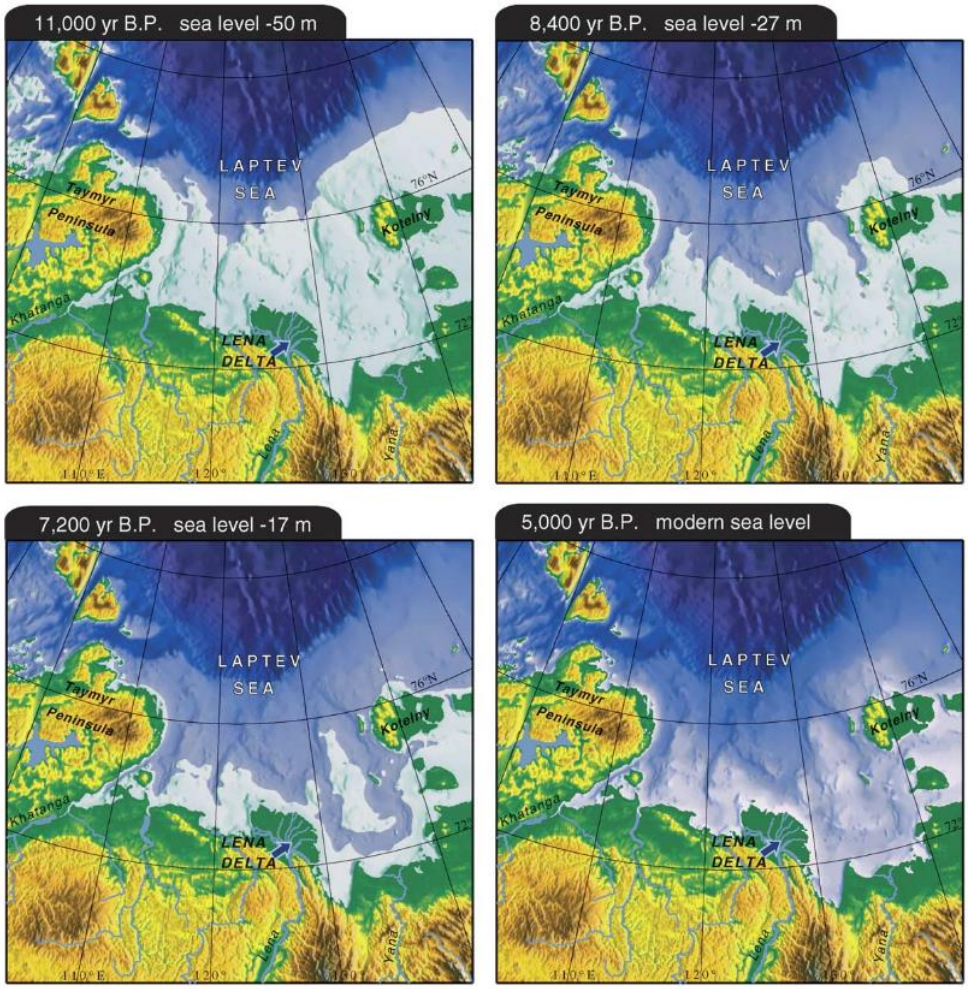

Figure 2-1: Time-slice reconstruction of the Holocene transgression for the Laptev Sea Shelf showing the retreat of the coastline [*Bauch and Kassens*, 2005]**.**

With the beginning of the climatic warming during the Holocene the sea level started to rise continually. A combination of coastal erosion, abrasion and warming led to the rapid degradation of the ice-rich terrestrial permafrost. As a consequence, the coastline shifted further south (Fig. 2-1). According to *Bauch et al.* [2001] the rates of sea level rise in the Laptev Sea region varied considerably. Between 11 and 10 ka BP the sea level rose at 5.4 mm yr^{-1}, for the period between 10 to 9 ka BP it was 13.3 mm yr^{-1} and in the final stage between 9 and 5 ka BP the sea level rose at 7.9 mm yr^{-1}. Due to the low topographic inclination angle, the final stage of sea level rise affected the largest area of the shelf. At the end of the transgression (~5 ka BP) the sea level showed signs of stabilization.

Mean modern annual ground temperatures of the terrestrial permafrost lie at -11 °C to -12 °C [*Romanovskii et al.*, 2005], while the mean annual bottom water temperatures in the Laptev Sea range between -1.8 °C to -0.5 °C [*Osterkamp*, 2001] leading to sediment temperatures of -1.0 °C and -2.0 °C within the largest part of the shelf [*Romanovskii et al.*, 2004]. Bottom-water salinity varies between 24 ‰ in the shallow coastal areas and 34 ‰ in the central shelf areas [*Zhigarev*, 1997].

The study sites within the Laptev Sea that were investigated in the present work are located at Cape Mamontov Klyk, in the western part, and in the Buor Khaya Bay, in the central Laptev Sea (Fig. 2-2). The site at Mamontov Klyk is located approximately 250 km westward and 550 km northward of the Buor Khaya site.

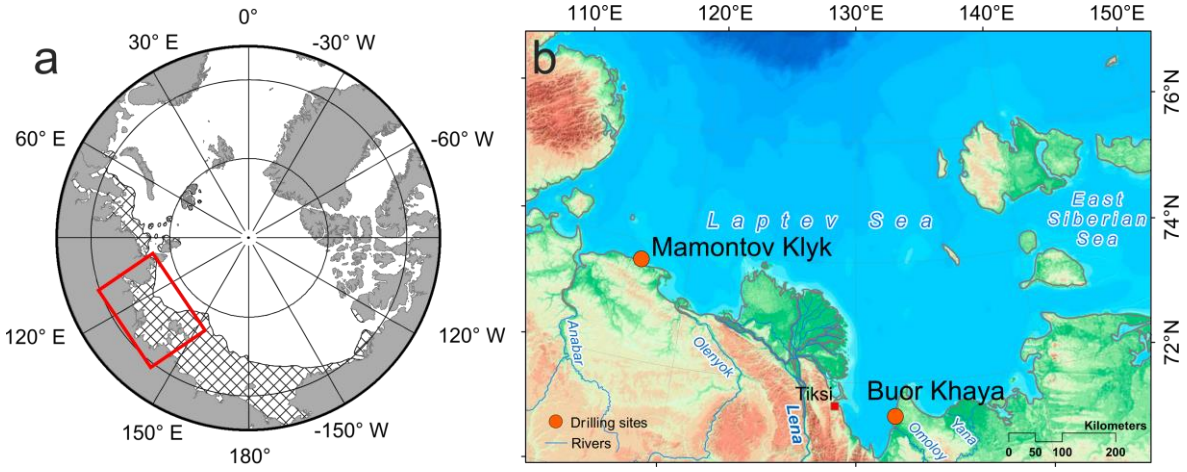

Figure 2-2: Geographical location of the study sites. (a) Location of the Laptev Sea on a circumpolar perspective map and the potential extent of submarine permafrost (striped area, based on *Brown et al.* [2002]) (b) Geographical location of the drilling sites at Cape Mamontov Klyk (C2) and in the Buor Khaya Bay (BK2), western and central Laptev Sea. (modified from *Overduin et al.* [2015])

2.2 Buor Khaya Study Site

The Buor Khaya peninsula is located in the central Laptev Sea, southeast of the Lena Delta and is part of the Yana-Indigirka lowland. The region is underlain by continuous permafrost which extends down to 450-650 m [*Romanovskii et al.*, 2004]. The climate of the study area is continental with mean annual air temperatures of -12.8°C and a precipitation of up to 321.5 mm. The mean temperature of the warmest month July is 8.7 °C, whereas the mean temperature of the coldest month January is -32.5°C [*Schirrmeister et al.*, 2016].

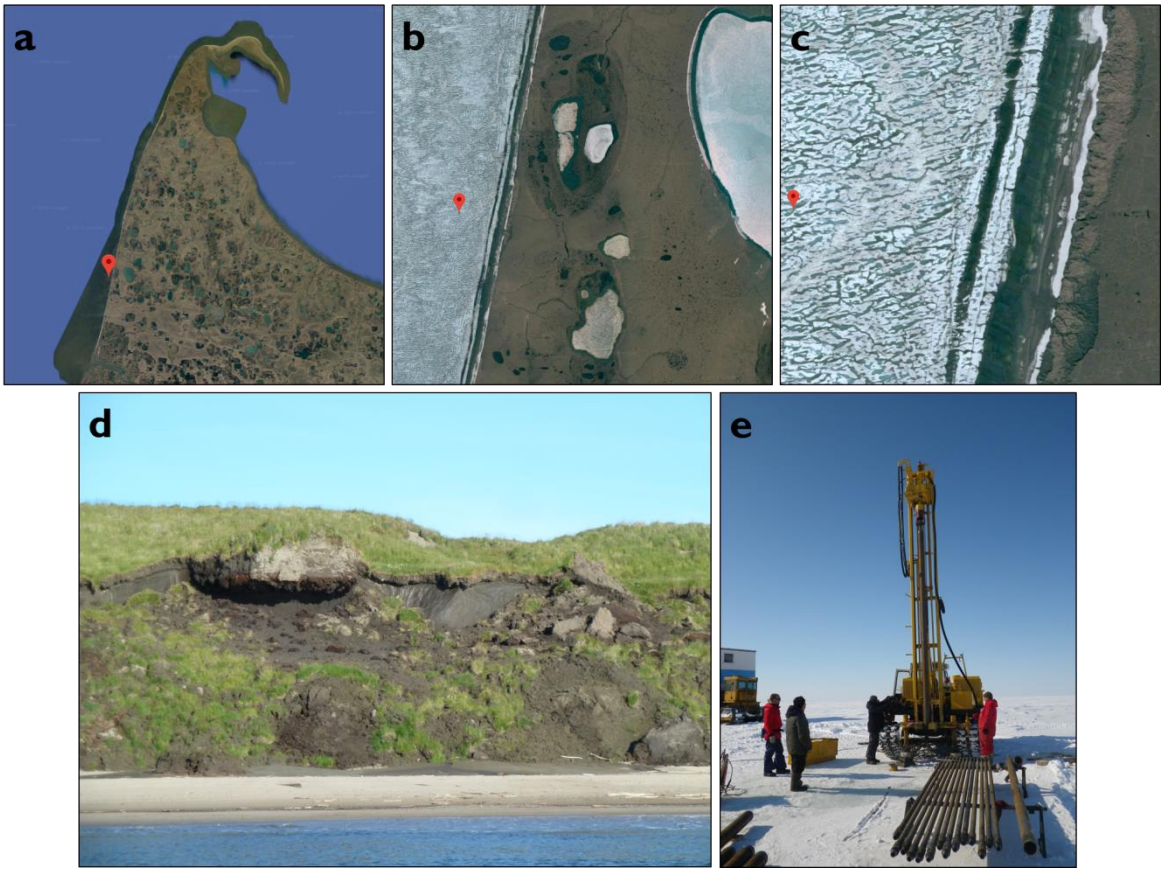

Figure 2-3: Study site at Buor Khaya. a-c) Buor Khaya Peninsula, the permafrost landscape and coast. The red mark indicates the drilling position of core BK2. **b)** Close-up of the permafrost landscape with thermokarst lakes. **c)** Close-up of the permafrost coast and sea ice near the drill site. (source of a,b and c: https://www.google.com/maps/, [accessed on 09-05-2019]) **d)** Permafrost coast near the drill site and signs of coastal erosion (Photo: P. P. Overduin, 2010) **e)** Portable drill rig (URB-4T) for submarine sediment sampling on the sea ice during the Expedition Laptev Sea – Buor Khaya in spring 2012 (Photo: L. Schirrmeister, 2012).

Along the western coastline of the Buor Khaya Peninsula, the mean annual coastal erosion rates range between 0.5 m yr^{-1} and 1.4 m yr^{-1} [*Günther et al.*, 2012]. Since the late glacial (late

Pleistocene) and Holocene warming the creation of submarine permafrost was primarily caused by the thermal erosion of the coast, which is mainly composed of high cliffs made up of ice-complex deposits and thermokarst features [*Schirrmeister et al.*, 2016]. The coastal retreat thereby eroded the Late Pleistocene Ice Complex and Holocene thermokarst deposits transporting this organic-rich sediment material into the ocean and exposing underlying Pleistocene alluvial sands to submarine conditions. The organic carbon content of the sandy sediment generally does not exceed 1–2 wt%. Values of the overlying deposits composed of Ice Complex and Holocene thermokarst deposits are substantially higher with mean total organic carbon (TOC) values of 3.2 wt% and 6.2 wt%, respectively [*Strauss et al.*, 2013].

Drilling at the study site 800 m off the Buor Khaya peninsula (71°25′20.3″N, 132°05′05.3″E) in 2013 revealed that ice-bonded permafrost can be found at a depth of 24.75 m below seafloor (m bsf). Ground temperatures in the unfrozen sediments ranged between -0.5 and 0.5 °C, and between -1.0 and -0.8 °C in the ice-bonded sediments. Modeled geothermal heat flux and modern seabed temperatures show the development of an area free of ice-bonded permafrost (talik) [*Nicolsky et al.*, 2012] in the central Buor Khaya Bay, indicating that this region is underlain by "warm" submarine permafrost which is sensitive to environmental changes. Based on the mean modern coastal erosion rate the borehole site was flooded approximately 540 years ago, meaning that the ice-bonded permafrost degraded at a mean rate of 5.3 cm yr^{-1} [*Overduin et al.*, 2015].

2.3 Cape Mamontov Klyk Study Site

Cape Mamontov Klyk (~73°60'N, 117°18'E) is situated about 150 km west of the Lena Delta (Fig. 2-4). The study area belongs to the Lena-Anabar lowland and is part of the continuous permafrost zone with thicknesses of 400 to 600 m. The climate on the coastal low-land is characterized by polar tundra climate. Mean temperatures of the warmest month range between 0 and 10 °C and the mean annual precipitation is low with 230 to 270 mm, 75% of it falling during summer. The mean annual air temperature is about -14°C. Mean winter air temperatures reach -22°C [*Dereviagin and Kunitsky*, 2004].

Since the end of the final stage of transgression, the ice-rich terrestrial permafrost eroded at average rates of 3 - 4.5 m yr^{-1} [*Grigoriev*, 2008] for the coastal section of Cape Mamontov Klyk. This caused a southward retreat of the shoreline of approximately 10-40 km [*Bauch et al.*, 2001; *Overduin et al.*, 2007]. Erosion and submergence of the permafrost landscape resulted in a submarine topography comprised of the remains of former thermokarst features (lakes and

lagoons), river valleys, and remnants of ice-bearing as well as ice-bonded permafrost, in particular of the ice-complex [*Overduin et al.*, 2007]. The organic carbon content of the sandy Pleistocene (early to middle Weichselian) sediment deposits is low with <0.1 to 1.9 wt%, whereas the late Pleistocene and Holocene deposits have higher organic carbon contents ranging from 1.0 to 3.9 wt% [*Winterfeld*, 2009].

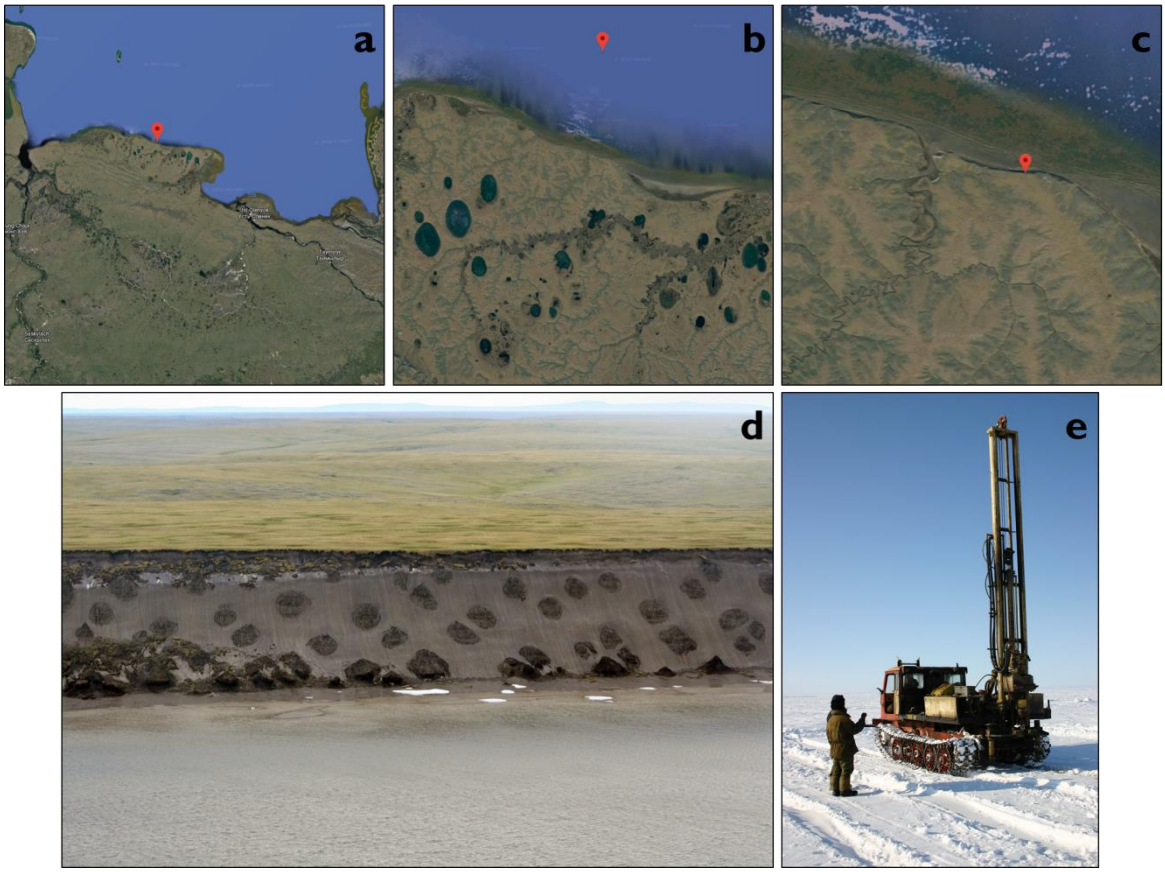

Figure 2-4: Study Site at Mamontov Klyk. a-c) Cape Mamontov Klyk, the permafrost landscape and coast. **b)** Close-up of the permafrost landscape with thermokarst lakes and river valleys. The red mark indicates the drilling position of the core furthest offshore (C2). **c)** Close-up of the permafrost coast at the drill site and position of the onshore core C1. (source of a, b and c: https://www.google.com/maps/, [accessed on 09-05-2019]) **d)** Coastal cliff at Cape Mamontov Klyk with an outcrop of the 'Yedoma' ice-complex. The dark spots represent fossil polygon centre and thermokarst mounds. (Photo: H.-W. Hubberten, 2008). **e)** Portable drill rig (URB-2A-2) for submarine sediment sampling on the sea ice during the Expedition COAST I in April 2005 (Photo: V. Rachold, 2005).

Drilling of 5 boreholes from the mainland to about 11.5 km offshore in a north-south transect (117°10'E) in 2005 revealed an increase in the depth to the ice-bonded permafrost table and in ground temperature with increasing distance to the shore [*Overduin*, 2007a; *Rachold et al.*,

2007]. The terrestrial core was completely frozen and exhibited the lowest average ground temperature of -14 °C. Going further offshore sediment temperatures increased from average -4.6 °C 1 km off the coast to -1.4 °C 3 km off the coast and -1.3 °C 11.5 km off the coast. Also, the thickness of the non-frozen sediment layer overlying the ice-bonded permafrost increased from 1.7 m 1 km off the coast, over 7.6 m 3 km off the coast to 29.0 m in 11.5 km distance from the coast.

Assuming a constant mean annual coastal erosion rate of 4.5 m yr^{-1} [*Grigoriev*, 2008] the drill site located furthest offshore (11.5 km) was inundated approximately 2500 years ago [*Rachold et al.*, 2007]. Accordingly, the drill sites located 3 km and 1 km off the coast, were inundated around 660 and 220 years ago, respectively. More recent analysis based on remote sensing shows that 40-year coastal erosion rates for the same stretch of coastline between 1965 and 2007 were slower (about 2.9 m yr^{-1} [*Günther et al.*, 2013b], which would translate into even longer inundation periods.

3 Manuscript I - The development of permafrost bacterial communities under submarine conditions

Abstract

Submarine permafrost is more vulnerable to thawing than permafrost on land. Besides increased heat transfer from the ocean water, the penetration of salt lowers the freezing temperature and accelerates permafrost degradation. Microbial communities in thawing permafrost are expected to be stimulated by warming but how they develop under submarine conditions is completely unknown. We used the unique records of two submarine permafrost cores from the Laptev Sea on the East Siberian Arctic Shelf, inundated about 540 and 2500 years ago, to trace how bacterial communities develop depending on duration of the marine influence and pore water chemistry. Combined with geochemical analysis, we quantified total cell numbers and bacterial gene copies, and determined the community structure of bacteria using deep sequencing of the bacterial 16S rRNA gene. We show that submarine permafrost is an extreme habitat for microbial life deep below the seafloor with changing thermal and chemical conditions. Pore water chemistry revealed different pore water units reflecting the degree of marine influence and stages of permafrost thaw. Millennia after inundation by seawater, bacteria stratify into communities in permafrost, marine-affected permafrost, and seabed sediments. In contrast to pore water chemistry, the development of bacterial community structure, diversity and abundance in submarine permafrost appears site-specific, showing that both sedimentation and permafrost thaw histories strongly affect bacteria. Finally, highest microbial abundance was observed in the ice-bonded seawater unaffected but warmed permafrost of the longer inundated core, suggesting that permafrost bacterial communities exposed to submarine conditions start to proliferate millennia after warming.

Introduction

Extensive shallow water areas of the Artic continental shelf are underlain by submarine permafrost [*Zhang et al.,* 1999*; Rachold et al.,* 2007]. The shallowest and most spacious shelf of the World‘s Ocean is the East Siberian Arctic Shelf (ESAS) encompassed by the Laptev,

East Siberian and the Russian part of the Chukchi Seas. It comprises more than 80% of the potential submarine permafrost in the Arctic [*Overduin et al.,* 2015].

Submarine permafrost is relict terrestrial permafrost that developed on land and was subsequently inundated by post-glacial sea level rise during the Holocene, 7 to 15 ka ago [*Romanovskii & Hubberten,* 2001]. Even today, especially Arctic permafrost coasts, that account for 34% of the coasts worldwide [*Lantuit*, 2012], are vulnerable to sea level rise, declining sea ice cover, and longer and warmer thawing seasons [*Fritz et al.*, 2017]. Resulting coastline collapses, with mean modern erosion rates of 1 to 2 m yr^{-1} [*Lantuit*, 2012] and local erosion rates of up to 25 m yr^{-1} [*Jones et al.*, 2009], lead to an annual formation of about 10 km^2 of submarine permafrost on the ESAS alone [*Grigoriev*, 2008]. This erosion of permafrost coasts is an abrupt form of permafrost degradation and results in yet unquantified fluxes of carbon and nutrients from thawing permafrost with presumably large consequences for the biogeochemical cycling of the shelf area [*Fritz et al.*, 2017].

The seawater inundation and infiltration causes drastic changes in the thermal regime and geochemical composition of submarine permafrost (Ulyantsev et al., 2016). With annual average bottom water temperatures of -1.8 °C to 1 °C [*Wegner et al.*, 2005], it is 12 to 17 °C warmer than the annual average surface temperature over on-land permafrost [*Romanovskii et al.*, 2005]. As temperatures in high latitudes have been rising faster than the global average over the past decades [*IPCC in Climate Change*, 2013], bottom-water warming further increases the degradation rates of submarine permafrost in the Laptev and East Siberian Seas. Besides top-down seawater heat and salt fluxes, bottom-up geothermal heat fluxes are responsible for the degradation of submarine permafrost [*Osterkamp*, 2001; *Shakhova et al.*, 2010]. The seabed temperature of much of the Artic shelf seas is cryotic (<0 °C). In coastal waters, submarine permafrost temperature is around -1 °C [*Overduin et al.*, 2015], the limit to maintain ice-bonded permafrost under submarine conditions [*Grigoriev*, 2008]. Warming and destabilization of submarine permafrost increases sediment permeability. On the one hand, this can result in the release of long preserved methane (CH_4) into the water column and atmosphere [*Shakhova et al.*, 2010; *Portnov et al.*, 2013; *Shakhova et al.*, 2014, *Thornton et al.*, 2016]. On the other hand, trapped organic material becomes more accessible to microorganisms after thawing, potentially inducing the decomposition of soil organic matter (SOM) and transforming complex organic compounds to soluble metabolites and gases, such as CH_4, CO_2, and N_2O [*Graham.*, 2012; *Mackelprang et al.*, 2011]. Its release is potentially relevant to global climate, since terrestrial and submarine permafrost store twice as much carbon as is currently in the atmosphere [*Schuur et al.*, 2009].

Microbial life in thawing permafrost is expected to be stimulated before permafrost thaws completely [*Schuur et al.*, 2015], i.e. activity and abundance should increase [*Waldrop et al.*, 2010; *Mackelprang et al.*, 2011; *Graham et al.*, 2012]. Submarine permafrost is thereby affected not only by rising temperatures but also by elevated salt concentrations [*Harrison and Osterkamp*, 1982]. In particular during the first decades of inundation, there may be an active layer at the seabed that thaws and freezes seasonally [*Osterkamp*, 2001]. Brine drainage from the growing sea ice increases water salinity and decreases temperatures of the bottom-water in fall and winter. Brines can infiltrate the seabed, even when it is frozen. They are responsible for thawing the underlying submarine permafrost at negative sediment temperatures. In contrast to rising temperatures and the release of substrate, the evolution of submarine permafrost with salt infiltration as the main process has been disregarded in assumptions how microbial life responds to submarine permafrost thaw. Osmotic stress is known to limit microbial growth and activity [*Galinski.*, 1995]. Although microbes have a number of features (fast growth rates, physiological flexibility and a rapid evolution i.e. mutation or horizontal gene transfer) to acclimate, adapt and recover, several studies showed that microbial community composition is sensitive to disturbances [reviewed by *Allison & Martiny*, 2008]. These studies observed shifts and no resilience in the microbial community composition within a few years. Therefore, we hypothesize that increasing salinity in terrestrial permafrost deposits might impair the indigenous microbial community before it is stimulated through rising temperatures. We expect the terrestrial community to change its composition in response to seawater infiltration. Assuming limited microbial growth and activity due to osmotic stress, as mentioned above, the community is initially expected to decrease in population size. To test this, we studied the pore water chemistry, and bacterial community composition, diversity and abundance by means of the bacterial 16S rRNA gene copy numbers, total cell counts and deep sequencing of the bacterial 16S rRNA gene of two submarine permafrost cores from the Western and Central Laptev Sea Shelf inundated for different time periods.

Materials and Methods

Regional setting and study areas

The Laptev Sea, bordered by the Taymyr Peninsula to the west and the New Siberian Island to the east, has an average water depth of less than 60 m. During the Weichselian glaciation (late Pleistocene) large areas of the non-glaciated arctic continental shelf were exposed to climatic conditions which led to the formation of cold, thick and continuous permafrost [*Svendsen et al.*,

2004]. Subsequently, a large portion of the ice-rich terrestrial permafrost that developed was inundated by a combination of the Holocene marine transgression and coastal thermoerosion [*Winterfeld et al.*, 2011].

The first study area at Cape Mamontov Klyk (Supplement Fig. A-1) was described by *Winterfeld et al.* [2011]. Cape Mamontov Klyk (~73°60'N, 117°18'E) is situated in the Western Laptev Sea. During a campaign in 2005 [*Rachold et al*. 2007; *Schirrmeister*, 2007], a submarine core (C2) was drilled about 11.5 km offshore. Assuming a mean annual coastal erosion rate of 4.5 m yr^{-1} [*Grigoriev*, 2008] the drill site was inundated 2500 years ago [*Rachold et al.*, 2007]. The core was retrieved in approximately 6 m water depth with a sea ice thickness of 1.35 m and bottom-water salinity of 29.2 PSU. Core material was retrieved between 6 and 77 m bsl (meters below sea level). Temperature measurements at the site of C2 were performed 1 to 11 days after drilling and are described and published elsewhere [*Junker et al.*, 2008; *Overduin et al.*, 2008]. Temperatures of the C2 borehole ranged between -1.5 and -0.8 °C.

The second study area is located in the Buor Khaya Bay (Supplement Fig. A-1). Within the framework of the Drilling Expedition Buor Khaya in 2012 [*Günther et al.*, 2013], the submarine sediment core BK2 was retrieved about 750 m off the coast west of the Buor Khaya Peninsula, in the Central Laptev Sea. Drilling was performed in 4.3 m deep water with a sea ice cover of 2.09 m and a bottom-water salinity of 5.9 PSU [*Günther et al.*, 2013]. Core material was retrieved between 6 and 51 m bsl. Borehole temperature of BK2 was recorded for 4 days after drilling. Measurement and temperature data of BK2 were published by *Overduin et al.* [2015]. Borehole temperatures ranged between 0.4 and -0.9 °C. Based on the distance of the borehole from the modern coastline and on the mean annual erosion rate of 1.4 ± 0.8m yr^{-1} [*Günther et al.*, 2012], the location of BK2 was flooded around 540 years ago [*Overduin et al.*, 2015]. Since the Buor Khaya Peninsula is covered by thermokarst depressions and characterized by an eroding Ice Complex coastal bluff, it is likely that the drill site was affected by Holocene thermokarst or thermokarst lake development prior to erosion and that it was frozen at the time of inundation.

Geochemical analyses

Pore water was extracted from thawed subsamples of the sediment cores using Rhizons™ (0.2 µm pore diameter). Electrical conductivity, salinity, cation (Ba^{2+}, Ca^{2+}, K^{+}, Mg^{2+}, Na^{+}, Si_{aq}) and anion (Cl^{-}, SO_4^{2-}, Br^{-}, NO_3^{-}) concentrations, stable isotope concentrations ($\delta^{18}O$, δD), and pH were measured for 94 samples of C2 (Cape Mamontov Klyk) and for 80 samples of BK2 (Buor Khaya Bay) (Supplement Tables A-1 and A-2). Electrical conductivity and salinity were

measured with a *WTW MultiLab 540* by using a standard conductivity cell (*TetraConR 325*) with four graphite electrodes. Total dissolved element concentration was determined via the analytical technique of ICP-OES (Inductively Coupled Plasma Optical Emission Spectrometry) using a *Perkin-Elmer ICP-OES Optima 3000XL*. In order to measure the concentration (mg/l) of dissolved anions, an ion chromatograph (*Dionex DX-320*), a latex-particle separation column and KOH as eluent were used. Values below detection limit were assigned values of half the detection limit for inclusion in PCA analyses. The determination of deuterium (δD) and oxygen isotope ($\delta^{18}O$) ratios was performed using a *Finnigan MAT Delta-S* mass spectrometer in combination with two equilibration units (MS Analysetechnik, Berlin).

Extraction of nucleic acids

Total nucleic acids were extracted as described by *Zhou et al.* [1996] in a slightly modified way. Sediment samples from 5 to 10 g were homogenized in liquid nitrogen and mixed with 13.5 ml of DNA extraction buffer (100 mM Tris-HCl [pH 8.0], 100 mM sodium EDTA [pH 8.0], 100 mM sodium phosphate [pH 8.0], 1.5 M NaCl, 1% CTAB) and 100 µl of proteinase K (10 mg/ml) in 50 ml centrifuge tubes. They were incubated with horizontal shaking for 1 h at 37 °C and 225 rpm. After the addition of 1.5 ml of 20% SDS, the samples were incubated in a water bath at 65 °C for 2 h with gentle inversions every 20 min. Supernatants were recovered by centrifugation at 6,000 *g* for 10 min at room temperature and collected in fresh 50 ml centrifuge tubes. The sediment pellets were extracted two more times as follows: addition of 4.5 ml of extraction buffer and 0.5 ml of 20% SDS, vortexing the tubes for 10 s, incubation at 65 °C for 10 min and centrifugation as described before. Supernatants of the three extraction cycles were combined and mixed with an equal volume of chloroform-isoamyl alcohol (24:1 v/v) and the coprecipitant GlycoBlue™ (1:300). After recovery of the aqueous phase by centrifugation, the DNA was precipitated with 0.6 volumes of isopropanol at room temperature for 1 h and pelleted by centrifugation at 16,000 *g* for 20 min. Finally, the DNA pellet was washed three times with 1 ml of ice-cold 70% ethanol and re-suspended in a final volume of 500 µl of sterile deionized water.

Genomic DNA was quantified with the QBIT2 system (Invitrogen, HS-quant DNA) and calculated per gram sediment wet weight. The crude DNA was purified using the HiYield PCR Clean-Up & Gel-Extraction Kit (Südlabor, Gauting, Germany) to reduce PCR inhibitors and the necessity to dilute the DNA extracts prior to PCR applications.

Quantification of the bacterial 16S rRNA genes

Quantitative PCR was performed using the CFX Connect™ Real-Time PCR Detection System (Bio-Rad Laboratories, Inc., Hercules, USA) and the following primer set: Eub341F and Eub534R [*Muyzer et al.*, 1993]. Each reaction (25 µl) contained 2x concentrate of iTaq™ Universal SYBR® Green Supermix (Bio-Rad Laboratories, Inc., Hercules, USA), 0.4 µM of the forward and reverse primer, sterile water and 5 µl of DNA template. The environmental DNA samples were diluted 5- to 100-fold and run in three technical replicates. The PCR reactions comprised an initial denaturation (5 min at 95 °C), followed by 40 cycles of 0.5 s at 95 °C, 30 s at an annealing temperature of 55.7 °C, 10 s at 72 °C and a plate read step at 80 °C for 0.3 s. Melt curve analysis from 65 to 95 °C with 0.5 °C temperature increment per 0.5 s cycle and gel electrophoresis on the PCR products was conducted at the end of each run to identify non-specific amplification of DNA. The qPCR assay was calibrated using known amounts of PCR amplified and cloned gene fragments from a pure *Escherichia coli* culture. Genomic standards were included in each qPCR run to ensure linearity and expected slope values of the Ct/log curves. PCR efficiency**,** based on the standard curve, was calculated using the BioRad CFX Manager software and varied between 95 and 100%. All cycle data were collected using the single threshold Cq determination mode. Abundances of the bacterial 16S rRNA gene and of cells were calculated per gram sediment wet weight.

Amplification and Illumina MiSeq sequencing of the bacterial 16S rRNA gene

We sequenced 19 samples from the core C2 and 10 samples from BK2. From BK2, two samples right above and below the ice-bonded permafrost table were pooled. The sampling depths are illustrated in Fig 2. PCR and sequencing were performed in two technical replicates for each sample. Bacterial 16S rRNA genes were amplified using the sequencing primers S-D-Bact-0341-b-S-17 and S-D-Bact-0785-a-A-21 (Supplement Table A-3) comprising different combinations of barcodes (Supplement Table A-4). Preparation and sequencing was performed in two technical replicates.

PCR amplification was carried out with a T100™ Thermal Cycler (Bio-Rad Laboratories, CA, USA) and the PCR mixture of 25 µl contained 0.025 U μl^{-1} of HotStarTaq DNA Polymerase (Qiagen), 1x PCR buffer (Tris-Cl, KCl, $(NH_4)_2SO_4$, 15 mM $MgCl_2$; pH 8.7, Qiagen), 0.4 µM of forward and reverse primer (Supplement Table A-3), dNTP mix (0.2 mM each; Thermo Fisher Scientific, Darmstadt, Germany), 2 µM of $MgCl_2$ (Qiagen), RNase-free water (EURx) and 2.5 µl of DNA extract. PCR conditions were as follows: initial denaturation at 95 °C for 5

min, followed by 30 cycles of denaturation (95 °C for 30 s), annealing (55 °C for 30 s) and elongation (72 °C for 1 min), and a final extension step of 72 °C for 10 min.

PCR products were purified from agarose gel with the HiYieldPCR Clean-Up & Gel-Extraction Kit (Südlabor, Gauting, Germany). Amplicons were quantified with the QBIT2 system (Invitrogen, HS-quant DNA), mixed in equimolar amounts and sequenced from both directions (GATC Biotech, Konstanz) based on the Illumina MiSeq technology. The library was prepared with the MiSeq Reagent Kit V3 for 2x 300 bp paired-end reads according to the manufacturer's protocols. For better performance due to different sequencing length, 15% PhiX control v3 library was used.

Sequence analyses and bioinformatics

The acquired raw data of bacterial sequences were analyzed starting with the quality control of the sequencing library by the tool FastQC (Quality Control tool for High Throughput Sequence Data (http://www.bioinformatics.babraham.ac.uk/projects/fastqc/) by S. Andrews). Demultiplexing of the sequence reads according to their barcodes and subsequent removal of the barcodes was performed with the CutAdapt tool [*Martin*, 2011]. Using PEAR [*Zhang et al.*, 2014] forward and reverse sequenced fragments with overlapping sequence regions were merged and the nucleotide sequence orientation was standardized. Low quality sequences were filtered and trimmed by Trimmomatic [*Bolger et al.*, 2014] and chimeras were removed by Chimera.Slayer. Finally, the QIIME pipeline was used to cluster sequences into Operational Taxonomic Units (OTUs) and to taxonomically assign them employing the Greengenes database with a cutoff value of 97% [*Caporaso,* 2010]. Older taxonomic assignments for bacteria were corrected manually after *Rinke et al.,* [2013] and *Nobu et al.,* [2016]. OP9 and JS1 were renamed to *Atribacteria*, OD1 to *Parcubacteria* and CD12 to *Aerophobetes.*

Statistical analyses

$OTU_{0.03}$ with reads <0.1% of the total read counts per sample, $OTU_{0.03}$ not classified as bacteria or classified as chloroplasts, and absolute singletons were removed prior to statistical analysis. Absolute read counts were transformed to relative abundances in order to standardize the data and to account for different sequencing depths. Variation in pore water and $OTU_{0.03}$ composition between samples and among pore water units, as well as correlations of the $OTU_{0.03}$ composition structure with pore water parameters, and determination of diversity were assessed using the Past 3.12 software [*Hammer et al.,* 2001]. Diversity indices and richness were calculated based on the mean relative abundance of all $OTU_{0.03}$ of duplicates. To visualize

the grouping patterns of sediment samples based on pore water data, principal component analyses based on the Euclidean distance of standardized ((x-mean)/stdev) pore water variables were used. Grouping patterns based on the $OTU_{0.03}$ composition of samples were determined by non-metric multidimensional scaling (NMDS) based on the Bray-Curtis distance measure. To test whether pore water units and their communities, as well as the total communities of the two study sites were significantly different, a Non-Parametric MANOVA/PerMANOVA was conducted [*Anderson*, 2001]. Mantel tests were used to study the relationship between pore water units and community structuring effects [*Mantel*, 1967].

Determination of the core community of $OTU_{0.03}$ in two different pore water units was performed using a custom R script. We filtered specialist $OTU_{0.03}$, which were present in all samples of one unit but not in the other.

Total Cell Counts

Fixation, sonication and filtration of sediment were performed as previously described [*Llobet-Brossa et al.*, 1998]. In order to prevent lysis of the cells during the hybridization process, macromolecules and cytoskeletal structures were stabilized by the fixation with formaldehyde. At the same time, the fixation makes the cell walls permeable. An amount of 0.5 g of sediment was fixed with 1.5 ml 4% paraformaldedhyde-phosphate-buffered saline (PBS, composed of 137 mM NaCl, 2.7 mM KCl, 15 mM Na_2HPO_4, and 1.7 mM KH_2PO_4 [pH 7.6 in water]) for 1 h at room temperature or at 4 °C over-night. After incubation the sediment was pelleted by centrifugation at 9600 *g* for 5 min and the supernatant was discarded. The paraformaldehyde fixed samples were washed twice in freshly sterile filtered 1.5 ml PBS and stored in 1.5 ml of PBS/ethanol (1:1) at -20 °C until further processing. The following sonication, according to [*Kousuke et al.*, 2004], was performed to relieve cells attached to sediment particles. A volume of 200 µl of the fixed sample was diluted 6-fold in PBS/ethanol (1:1), placed on ice and treated by low intensity sonication with a Sonotrode MS73 probe (Sonopuls HD3100, Bandelin, Berlin, Germany) for 30 s at a setting of 1.5 s sonication pulses (on/off 0.5 s/1.0 s) and an amplitude of 20%. Sonication was repeated two times. After each sonication step, the sample was resuspended. 200 µl of the supernatant was transferred to a fresh tube and replaced by 200 µl of PBS/ethanol. The collected supernatant was chilled on ice for 2 min or stored at -20 °C until further processing. The sonicated supernatant was diluted in PBS and filtered through a polycarbonate membrane filter. The filtration was performed by applying a vacuum and a pressure of around -5 mbar. Finally the filters were air dried at room temperature and stored at -20 °C until further processing [*Kousuke et al.*, 2004].

Total cell counts were determined by SYBR Green I. Filters were placed on a glass slide, mounted with 3 µl of SBYR Green I staining solution (1 volume of 1:40 SYBR Green I, 1 volume of 0.1% p-phenylenediamine and 1 volume of 4:1 Citifluor/Vecta Shield) and covered with a cover slip [*Kallmeyer et al.*, 2008]. Fluorescence microscopy was performed with a Leica DM2000 fluorescence microscope using the filter cube FI/RH for SYBR Green I.

Results

Pore water chemistry

According to the PCA of C2 and BK2 (Fig. 3-1) variance between the samples on the horizontal axis (PC1) is explained by the seawater influence represented by salinity, conductivity and most of the ion concentrations (Br^-, Cl^-, Na^+, Mg^{2+}), with non-saline sediments to the left and saline sediments to the right side. In each plot different clusters contained samples of consecutive depth, thus defining pore water units in the sediment. Pore water unit I (PW I) represented samples in the upper meters of both cores and is characterized by elevated salinity, conductivity and ion concentrations. Pore water unit II (PW II) represented samples located below PW I. These sediments showed a rapid decline of cations, anions, salinity and conductivity. The parameters mentioned before were lower than in PW I but still elevated in comparison to the underlying samples, which represented the pore water unit III (PW III). These were not influenced by seawater: salinity was less than 1 PSU for most samples.

In C2, clusters of PW II and PW III are not very distinct from each other (Fig. 3-1a), as the influence of the saline water (concentration of ions, etc.) decreased gradually with depth, leading to a smooth transition from one unit to the other. Furthermore, an additional cluster formed (PW IV), representing samples in the unfrozen sediments below PW III, located deepest in the core. Although clustering apart from PW I on the vertical axis, parameters were comparable (high salinity and ion concentrations). Pore water stable isotope signatures in PW I & IV laid in the range of -9 to -20 ‰ ($\delta^{18}O$) and -75 to -150 ‰ (δD), where increasing marine influence was shown by a tendency toward heavier values. PW III had values consistent with a glacial origin of pore water, with values from -30 to -20 ‰ ($\delta^{18}O$) and -150 to -230 ‰ (δD). A one-way PerMANOVA still revealed that the variance between each of the clusters was significantly higher than within single clusters ($p = 0.0001$, Supplement Table A-5). One single sample was located between the clusters of PW I and PW IV (Fig. 3-1a), representing the uppermost centimeters of sediment, namely the seabed.

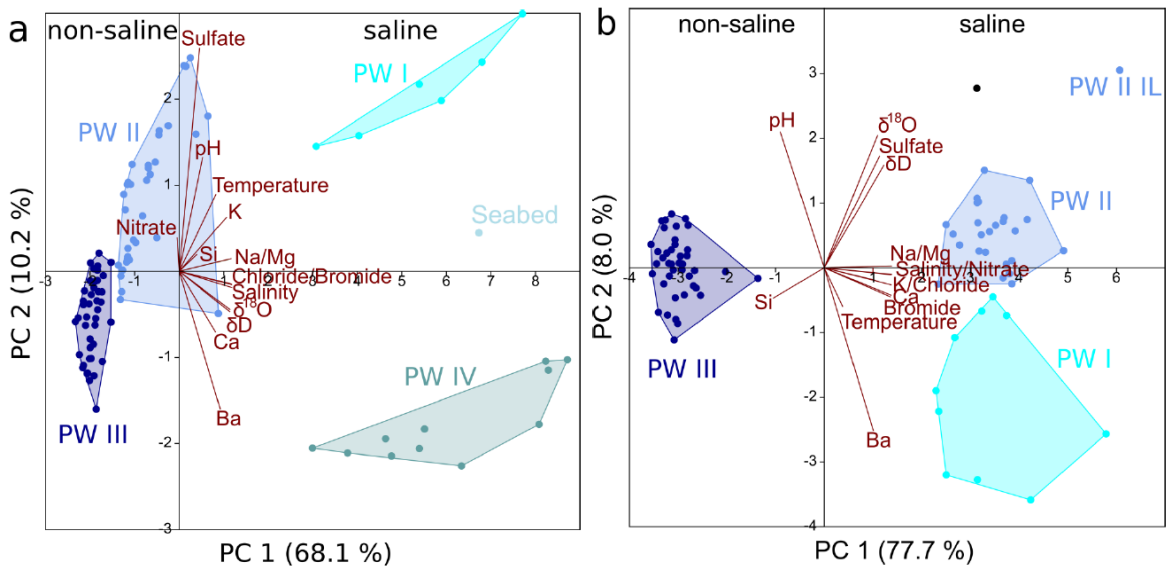

Figure 3-1: Principal component analyses (PCA) show the variation of sediment samples based on standardized pore water and temperature data (Euclidean distance). Pore water units (PW) were defined based on cluster analysis and are represented by different colors. The percentage of variation between samples described by principal components 1 and 2 (PC 1 and 2) is indicated on the axes. In total, PC1 and PC2 in **(a)** explained 78.3 % of the variance between samples of C2 (inundated ~2500 yrs ago). **(b)** PC1 and PC2 explained 85.7% of variance between samples of BK2 (inundated 540 yrs ago). Environmental variables are projected as dark red vectors.

In contrast to C2, the separation of PW II and PW III in BK2 was very clear (Fig. 3-1b). Salinity, conductivity and the concentrations of all ions showed a sudden drop at the depth of 28.75 m bsl, the same depth at which the ice-bonded permafrost table occurred. The seawater penetration abruptly stopped at this depth, leaving the underlying sediments (PW III) unaffected. In BK2, PW I and PW II clustered close together as both were comparably strongly influenced by seawater. Variations in pore water stable isotope signature for the Buor Khaya borehole were discussed in *Overduin et al.* [2015] and suggest a terrestrial cold climate origin not yet affected by the infiltration of seawater in PW III. Together with pH, barium and sulfate concentrations, isotopes were important in differentiating PW I from PW II sediments in BK2. However, the difference between all three clusters determined by one-way PerMANOVA was significant ($p = 0.0001$, Supplement Table A-6). Two samples were located apart from any cluster. One of them originated from the first few centimeters of sediment recovered (6 m bsl, black). However, the most deviant sample (PW II IL) originated from 12.35 m bsl depth, most closely located to PW II.

Analyses of samples from both cores in one principal component analysis (Supplement Fig. A-2) revealed that the PW III of both cores and PW II of C2 clustered together. Furthermore, the PW I of both cores, PW IV in C2 and PW II in BK2 clustered on the opposite site of the plot with increased influence of the salt water. PW II of C2 scattered between the PW I/PW II and PW III with most of the samples clustering close to PW III. In terms of pore water parameters, one-way PerMANOVA revealed no significant difference between both sediment cores ($p = 0.9999$; $F = -0.0005$).

Stratification of pore water units

Grouping the samples according to the previously shown clusters, resulted in a clear separation of the PW I and II in the PCA, which was reflected in the stratigraphy of C2 (Fig. 3-2a). PW I reached down to a depth of 29 m without interruption, whereas PW II and III showed some alternating layering effects in some depths. PW II reached down to a depth of 48.8 m bsl and was interrupted by PW III at between 44.7 and 45.2 m bsl. The largest zone of PW III extended to more than 10 meters from 48.8 to 62.3 m bsl with an interlayer of PW II at 60.5 m bsl. Below PW III again a layer of PW II occurred and reached down to a depth of 64.5 m bsl. This was followed by sediments which were similar to the PW I, namely pore water unit IV (PW IV).

PW I in BK2 reached down to a depth of 13.65 m bsl (Fig. 3-2b). An interlayer at the depth of 12.35 m bsl, resulting from the sample clustering far apart of any cluster (PW II IL in Fig. 3-1b), divided this unit into an upper and lower part. PW II reached down to a depth of 28.75 m bsl. Frozen sediment below the permafrost table, unaffected of marine waters, formed the PW III

Microbial abundance in submarine permafrost

DNA concentrations of C2 are illustrated in Fig. 3-2a and showed a high value of 265.2 ng g^{-1} in the upper centimeters right below the seafloor. A small DNA peak of of 84.3 ng g^{-1} was found in the PW II sediment at a depth of 40.4 m bsl. But the highest DNA concentrations with maxima between 89.9 and 341.5 ng g^{-1} were found at the depth interval of 54.6 to 56.1 m bsl in the frozen PW III. The depth profile of the microbial abundance showed the same trend. The uppermost sample just below the seafloor revealed high numbers of 9.2×10^6 cells and 3.5×10^8 gene copies, but total cell counts and bacterial 16S rRNA gene abundance peaked again between 54.6 to 56.1 m bsl, with ~5×10^7 cells g^{-1} and 2.7×10^8 gene copies.

In comparison, BK2 (Fig. 3-2b) exhibited three to four times lower DNA concentrations than C2 (Fig. 3-2a). Cell counts were 20 to 70 times lower and the abundance of the bacterial 16S

rRNA gene was even 50 to 250 times lower than in C2. In contrast to C2, the highest biomass here was found in the upper meters of the sediment core. In PW I and the thin interlayer of PW II DNA concentrations reached values of 68.3 to 87.9 ng g^{-1}. The lower part of PW II was characterized by very low values not exceeding 6 ng g^{-1}. Lowest DNA concentrations were obtained at the transition of frozen to unfrozen sediment with minimum values of 1.0 ng g^{-1} right above the ice-bonded permafrost table (IBPT). In the unaffected frozen unit (PW III) DNA concentrations peaked at a depth of 40.5 m bsl with 25.9 ng g^{-1}. Depth profiles of both bacterial gene copies and total cell counts were similar. Highest values in BK2 were obtained in the PW I and its interlayer with up to 2.4 x 10^6 cells and 6.2 x 10^6 gene copies. The second highest value of 1.1 x 10^6 gene copies was found in the ice-bonded part at a depth of around 40.5 m bsl, but generally cell counts in BK2 decreased with depth.

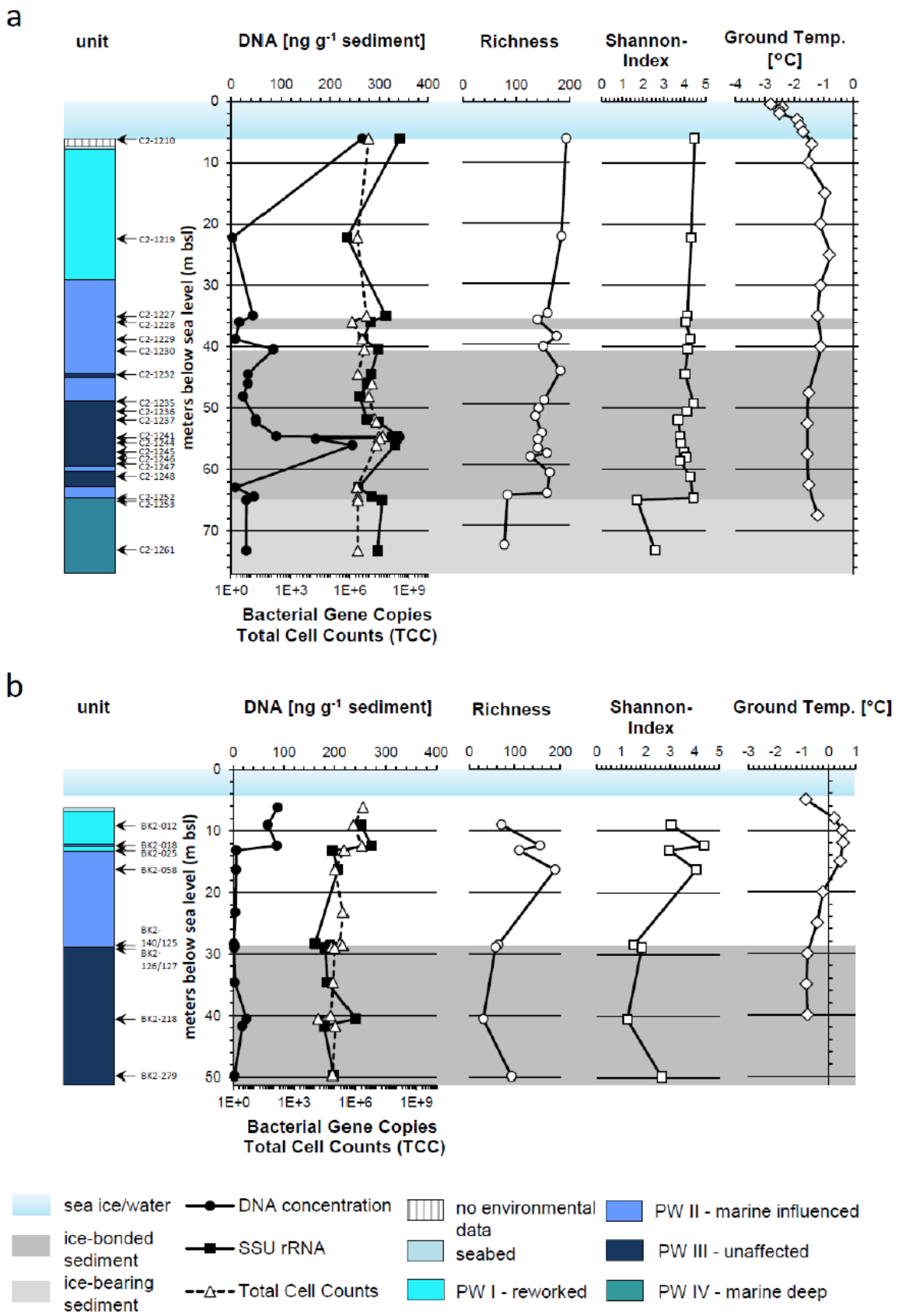

Figure 3-2: Sediment characteristics, from left to right: pore water units, depth of samples chosen for sequencing, DNA concentration (filled dots), bacterial 16S rRNA gene copy number (filled squares) and total cell counts (TCC, triangles) per gram sediment wet weight, Richness (no. of $OTU_{0.03}$, dots), Shannon-

Index (diversity, squares) and ground temperature (diamond) of **(a)** C2 (inundated ~2500 yrs ago) and **(b)** BK2 (inundated 540 yrs ago). Sea ice/water thickness is indicated at the top of the Figures; ice-bonded permafrost is shown in the graphs.

Diversity

The richness and diversity of C2 (Fig. 3-2a) were quite constant from the seabed to PW III, with the highest values in the marine sample and a slightly decreasing trend. Here, mean $OTU_{0.03}$ numbers of duplicates ranged between 127 and 194, in contrast to $OTU_{0.03}$ numbers of 78 to 84 in PW IV (Supplement Table A-7). Diversity indices behaved very similar (Shannon index 3.7 to 4.5; Simpson index > 0.9 in PW I-III, and Shannon index 1.7 to 2.6; Simpson index 0.5 to 0.8 in PW IV).

In BK2, values of the Shannon index and the richness of $OTU_{0.03}$ showed a similar trend (Fig. 3-2b). Both were highest in the unfrozen part (PW I and II) of BK2 and lowest in the permafrost unit PW III. Mean $OTU_{0.03}$ numbers of duplicates ranged between 31 and 189 per sample (Supplement Table A-7). A decrease could be observed right above the phase boundary and in the ice-bonded PW III. Those depths were highly dominated by few taxa.

Structure of the bacterial community

Using the relative abundances of $OTU_{0.03}$ and the Bray-Curtis distance measure, ordination plots were created (NMDS). The NMDS ordination of all samples from both cores showed some level of clustering of the bacterial communities in accordance with the separation by regional properties and environmental factors (Supplement Fig. A-3). Bacterial communities of both study sites formed two significant clusters (Supplement Table A-8).

Individually, C2 exhibited distinct microbial communities according to the pore water units (Fig. 3-3a). The NMDS plot showed an arrangement of the communities according to the depth location of pore water units. The community of the deep PW II was located between the PW II and PW III clusters showing the similarity to both of them. The microbial communities on the $OTU_{0.03}$ level differed significantly between the units (Supplement Table A-9). A Mantel test with the total community and pore water data, including temperature, revealed a significant correlation ($p = 0.001$, correlation $R = 0.46$). Mantel tests with the total community and single pore water parameters at the corresponding depths showed that there was no correlation with calcium, silicon and nitrate, and only a weak correlation with sulfate ($R < 0.25$) (Supplement Table A-10).

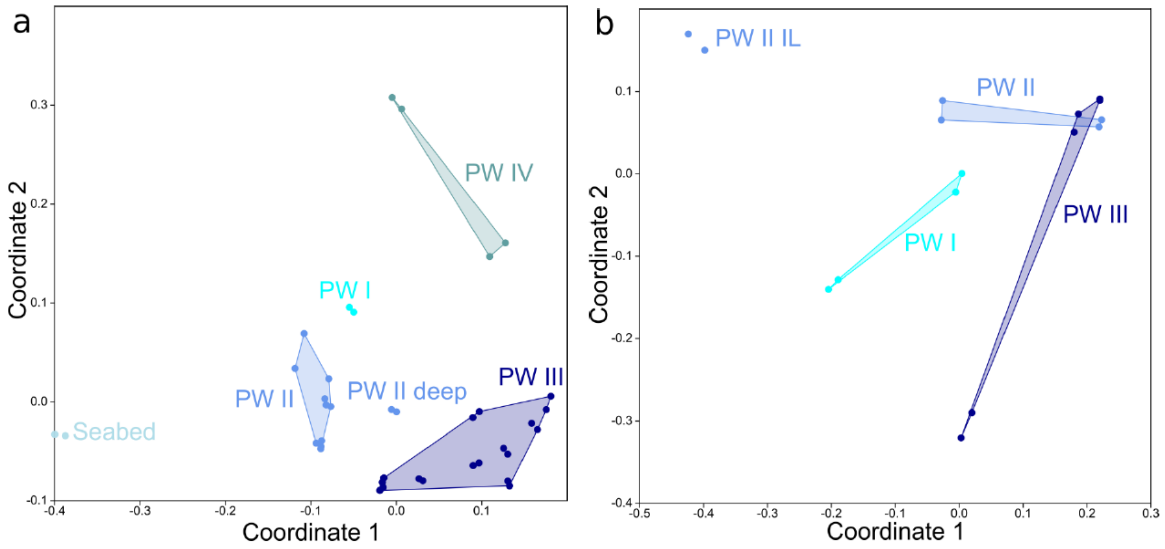

Figure 3-3: Non-metrical multidimensional scaling (NMDS) of the microbial community structure based on relative abundances of $OTU_{0.03}$ (Bray-Curtis dissimilarity). Colors represent the pore water units from which the $OTU_{0.03}$ originate. (a) NMDS of bacterial communities found in C2 (inundated ~2500 yrs ago). The seabed is not defined by pore water but by the shallow depth location of the sample. Stress: 0.12. (b) NMDS of bacterial communities found in BK2 (inundated 540 yrs ago). PW II IL means the interlayer of pore water unit II within PW I. Stress: 0.07.

In BK2, we did not observe bacterial community structures that were specific for any pore water unit (Fig. 3-3b). In addition to the corresponding pore water data, the bacterial community of the sample at 12.35 m depth (PW II IL) differed from the others. Grouping the samples according to the pore-water units showed an overall significant difference between those groups, but not when considered pairwise (Supplement Table A-11). Furthermore, there was no correlation of the overall community composition of BK2 to pore water parameters ($p = 0.357$, $R = 0.07$).

The most abundant phyla of C2 and BK2 on the order level are shown in Fig. 3-4a and b, and Supplement Tables A-12 and A-13. In BK2, 90 orders were identified (Supplement Table A-14), but only 17 had > 3% abundance. The bacterial community of C2 consisted of 138 identified orders with 34 exceeding a relative abundance of 3%, twice the number of BK2.

The composition and distribution of the most frequent orders (> 3%) of both sediment cores showed few similarities. Only *Clostridiales* were found to be abundant in several units of both cores. *Atribacteria* SB-45 was abundant in units with elevated salt concentrations (PW IV in C2 and PW I and II in BK2), *Burkholderiales* in units with low salinity and *Rhizobiales* throughout all PW units (Fig. 3-4).

In C2, no clear marine or terrestrial community was observed, except for the uppermost sample of C2 representing the seabed, because many of the observed taxonomic groups can be found in both, marine and terrestrial environments. The seabed was characterized by many marine related orders which were unique for that horizon, such as *Pirellulales* and orders of the *Deltaproteobacteria* (*Desulfobacterales*, MBNT15, *Myxococcales*) and *Gammaproteobacteria* (*Chromatiales, Thiotrichales, Marinicellales*). In regard of the dominant orders, PW I to PW III showed a quite similar community composition. Community characteristics of PW units and differences between them are described in the following. PW I mainly contained groups that could be found elsewhere in PW II or PW III sediments (*Acidimicrobiales*, *Actinomycetales*, *Gaiellales, Solirubrobacterales, Chloroflexi* Gitt-GS-136, *Gemmatimonadetes* Gemm-1, *Rhizobiales, Sphingomonadales*) and that were mostly absent from the shallowest and deepest layers (seabed and PW IV). Abundant groups, such as *Actinomycetales* and Gitt-GS-136, were found in all PW I to PW III. Both underwent a shift on family level from PW II to PW III. *Actinomycetales* in PW II were dominated by *Nocardioidiaceae*, whereas *Intrasporangiaceae* and *Actinotalea* dominated in PW III. Further, *Chloroflexi* Gitt-GS-136 was abundant in PW II, while in PW III *Chloroflexi* Ellin6529 was more abundant. Besides *Actinomycetales* and *Chloroflexi*, *Clostridiales* was among the most abundant orders in PW III. In addition, PW III contained numerous taxa that were unique for this pore water unit (for example *Acidobacteria* iii1-15, *Gaiellales, Bacteriodales* or *Gemmatimonadetes* N1423WL). The deepest unit PW IV was highly dominated by *Clostridiales* and SB-45 of the phylum *Atribacteria*. Due to the high dominance of *Clostridia*, there were only two other taxa (*Aerophobetes* and *Rhizobiales*) with a sequence abundance above 3%. In general, PW IV comprised less taxa, reflected in a lower diversity and richness compared to the other units (see Supplement Table A-7).

In BK2, a few taxa such as *Clostridiales* and *Rhizobiales* were highly abundant especially within PW III and right above the permafrost table. The bacterial community of the sample BK2-018 was very different from that of all other samples (Fig. 3-4b) coinciding with the pore water data (Fig. 3-1b, PW II IL) and the $OTU_{0.03}$ data (Fig. 3-3b, PW II IL). Except for *Clostridiales,* all other taxa (for example *Acidimicrobiales, Cytophagales, Ignavibacteriales, Chromatiales* and *Thiotrichales*) were only observed in BK2-018. Core groups of BK2 were *Clostridiales, Rhizobiales* and *Burkholderiales* and were found in all three pore water units of BK2.

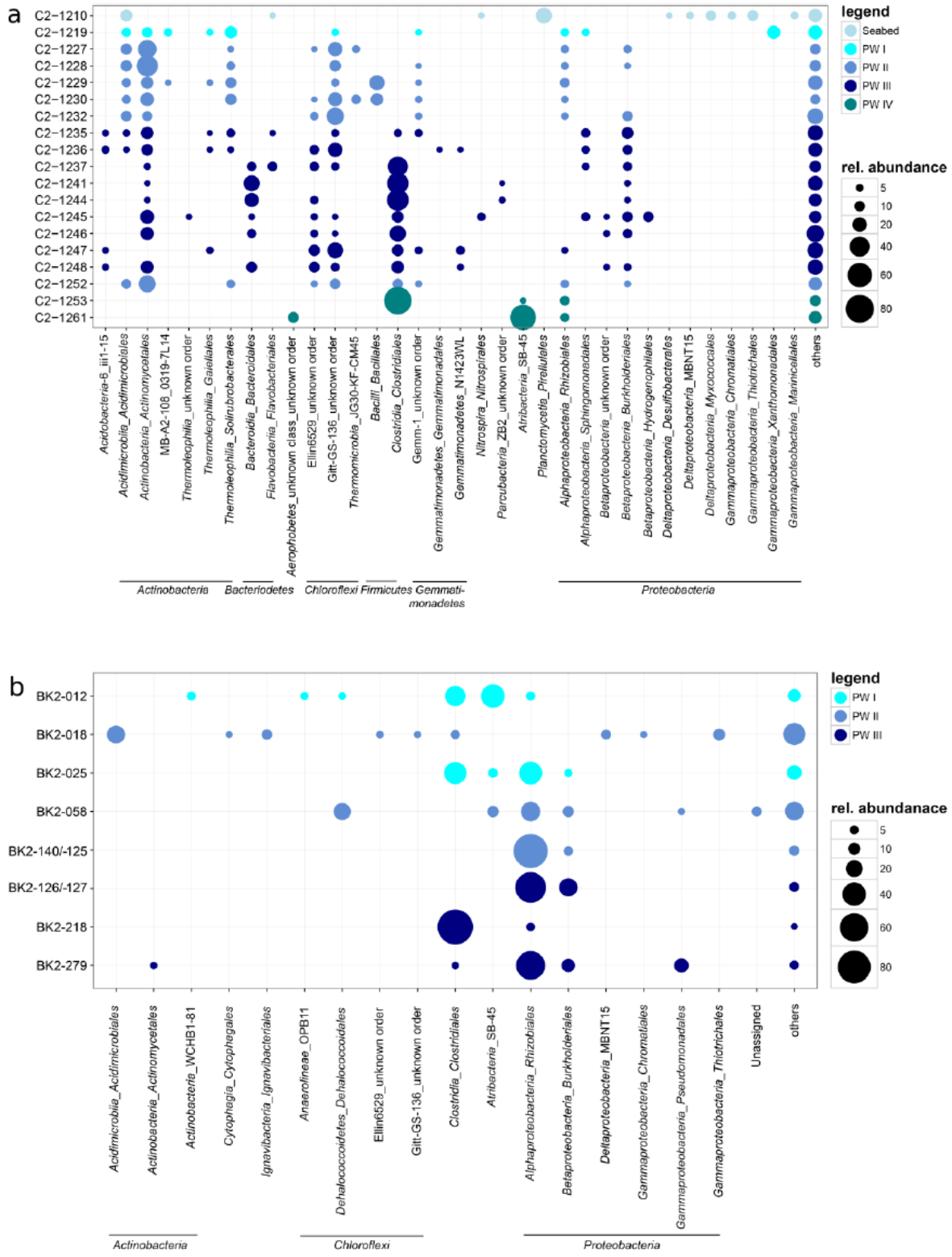

Figure 3-4: Relative abundance of bacterial orders of samples from **(a)** C2 (inundated ~2500 yrs ago) and **(b)** BK2 (inundated 540 yrs ago). Orders with an abundance of more than 3% are shown. The remaining orders are categorized as 'others'. Colors indicate the pore water unit.

In addition to the general community composition, we investigated the core communities of PW II and PW III in C2 (Supplement Table A-15). We excluded PW I due to the low sample number. Given the overall low sample number in BK2, a determination of the core communities was not reasonable. The core community of PW II in C2 was much more diverse than that of PWIII, counting 28 $OTU_{0.03}$. In contrast, the community of PW III in C2 contained only 8 shared $OTU_{0.03}$. Taxa such as *Acidimicrobia*, *Actinobacteria* and *Thermoleophilia* were represented by several $OTU_{0.03}$ in PW II, but completely absent in the core community of PW III. In contrast to the seabed, a clear marine origin of PWII taxa was not evident. Some taxa such as *Acidimicrobiales* (*Acidimicrobia*), *Nocardioidaceae* and *Geodermatophilaceae* (*Actinomycetales*), and *Hyphomicrobiaceae* (*Rhizobiales*) were, however, reported to be successful in marine environments [*Yi and Chun,* 2004; *Lee and Kim,* 2007; *Normand et al.*, 2014; *Oren and Xu,* 2014; *Zhang et al.,* 2014a; *Mizuno et al.,* 2015].

Discussion

Bacterial communities in two submarine permafrost settings from the East Siberian Arctic Shelf (BK2 and C2) were exposed to permafrost warming and thaw and the infiltration of seawater by inundation for about 540 and 2500 years, respectively. The inundation period was thereby based on recent rates of coastal retreat. Although the rate at which the sea transgresses over land is determined by many different factors, the degradation of permafrost in the nearshore zone is at least partially controlled by the coastal erosion rates [*Are*, 2003; *Overduin et al.*, 2016]. Due to a high mean annual coastal erosion rate of 4.5 m yr^{-1} over the past decades at the C2 site [*Grigoriev*, 2008], we assume an initially rapid submergence relative to BK2. The more rapid erosion at the C2 site leads to shorter times for seawater penetration for a particular distance from the coast, all other factors being equal. In contrast, the comparably low mean annual coastal erosion rate over the past decades of 1.4 m yr^{-1} means that inundation occurred more slowly at BK2. The proximity of BK2 to the coast and the shallower water suggests that seasonal changes in salinity and temperature are probably still large due to this proximity and that wave action will penetrate more deeply into the sediment [*Overduin et al.*, 2015]. The marine influence, characterized by a constant salinity in the unfrozen sediment of BK2, extended down to the ice-bonded permafrost table, suggesting convective downward transport of salt [*Overduin et al.*, 2015]. The coupling of heat with convective transport [*Osterkamp*, 2001], and higher terrestrial permafrost and geothermal heat fluxes in this region [*Nicolsky et al.*, 2012] likely also explain high sediment temperatures (-0.8 to 0.5 °C) of BK2.

Although both coring sites belong to the ice-rich syngenetic permafrost deposits called Yedoma or Ice Complex [*Schirrmeister et al.*, 2008, 2016; *Grosse et al.*, 2013], C2 is located 250 km westward and 550 northward of BK2. Despite their spatial separation and differing glacial sediment source regions, the sub-Yedoma terrestrial sandy sediment at both sites was deposited in similar local fluvial-alluvial environments with intermittent organic layers of woody and fibrous detritus [*Winterfeld et al.*, 2011; *Overduin et al.*, 2015]. The portions of the two cores undergoing submarine degradation have similar ages [*Winterfeld et al.*, 2011; *Schirrmeister et al.*, 2016]. Permafrost at the C2 site has a temperature close to -12 °C at the damping depth for annual temperature fluctuations; at BK2, the temperature is similar though closer to -10 °C, probably due to differences in regional climate. There were similarities between how pore water chemistry varied over depth in both cores, which reflected similar stages of permafrost degradation. PW III represents ice-bonded and warmed permafrost that was unaffected by the infiltration of seawater. PWI and II were found in permafrost of terrestrial origin that had been influenced by seawater. PW IV was only observed in one of the cores, where drilling penetrated through the frozen permafrost into a partially frozen marine layer. *Winterfeld et al.* [2011] suggested that the corresponding sediment layer was Eemian and marine in origin. The similarity of pore water units at the two sites suggests that they are characteristic of submarine permafrost. They can be partly explained by post-depositional and post-transgression processes: wave and ice turbation of the seabed (PWI), and infiltration of saline seawater into the sediment (PWII). In addition to warming of the sediment by the overlying seawater, these processes contribute to thawing of permafrost below the seabed after inundation. In C2, for example, PCA strongly suggests that seawater infiltrates into ice-bonded permafrost before thawing is complete. Higher solute concentrations decrease the temperature of freezing of the pore water and increase the liquid water content of the sediment [*Overduin et al.*, 2008]. Since freezing affects the volume of the habitable space in the sediment, and the concentration of solutes in that habitable space, depending on temperature and salinity, freezing is an important control on microbial activity. Determination of the *in situ* ice and liquid water content in the sediment at the time of sampling or during the period of warming following inundation is difficult for samples at or close to freezing temperature. Based on the measured pore water salinities, pore water solutions had freezing points of between -1.76 and -0.6 °C for PW I & IV and -0.9 and 0 °C for PW II & III. The almost isothermal temperature profile in Supplement Table A-1, for example, showed sediment at or near the freezing point, especially in PW IV. Permafrost dynamics and pore water composition in particular thus expand the bacterial habitat and have the potential to influence bacterial community composition.

The stratification of bacterial sub-communities at C2 (Fig. 3-3a) coincides with changes in the bacterial community composition (Fig. 3-4a). For example, the shallowest sample of C2, a few centimeters below the seafloor, harbored the highest number of unique phyla, and predominantly those typical for marine conditions such as *Pirellulales, Desulfobacterales, Thiotrichales, Marinicellales* [*Wang et al.*, 2012; *Campbell and Kirchman*, 2012]. The bacterial community composition of this layer thus shows a marine origin, so that we refer to it as the seabed. The underlying sub-communities of PWI and II lack an imprint of clearly marine taxa despite seawater infiltration and even though parameters such as salinity and pore water stable isotopes largely serve to explain their community patterns (Supplement Table A-10). At the same time they have evolved into sub-communities significantly different from those of the unaffected permafrost unit PWIII (Supplement Table A-9). The separation into individual sub-communities of PW II and III is further manifested through different core groups of both layers (Supplement Table A-15). So, although the bacterial community composition has changed in response to seawater infiltration, it reflects the bacterial assemblages of terrestrial permafrost even after centuries to millennia of exposure to submarine conditions. In C2, bacterial communities can consequently be classified as belonging to terrestrial permafrost, marine-affected permafrost, reworked permafrost sediments, or seabed. Continuing permafrost thaw will eventually lead to the complete loss of the original permafrost bacterial assemblages. They will probably shift to new assemblages like those of PWII but remain distinct in their composition from bacterial communities at the seabed. In contrast to C2, no significant correlation between community and environmental data along the BK2 core was observed, meaning that an assignment of bacterial communities consistent with pore water units was not possible. The statistical lack of significance may have been the result of low biomass in BK2. With total cell counts of 10^3 - 10^7 cells g^{-1} sediment the microbial abundances of both submarine permafrost cores were within the range of cell counts found in terrestrial long-term cryogenic formations such as frozen ground and buried soils [*Gilichinsky.*, 2008]. Cell numbers of C2 were comparable with microbial abundances from sub-seafloor sediments (10^6 – 10^7 cells ml^{-1} sediment) [*Parkes et al.*, 2014]. The depth profiles of total DNA concentration, bacterial gene copy numbers and total cell counts in both cores followed a similar trend. Still, in C2 the abundance of the bacterial 16S rRNA gene often exceeded that of the total cell counts by at least an order of magnitude (Supplement Tables A-16 and A-17). This cannot be solely due to multiple 16S rRNA gene copies per cell [*Schmidt,* 1998] but reflects the long-term preservation of extracellular DNA (up to 400 000 years) due to low temperature conditions in permafrost [*Stokstad,* 2003; *Willerslev et al.*, 2004]. A large proportion of external DNA has frequently

been observed in marine sediments as well [*Corinaldesi et al.*, 2005; *Alawi et al.*, 2014; *Kirkpatrick et al.*, 2016]. Future cell separation approaches will shed light on the extent and distribution of external DNA versus DNA of intact cells. In sub-seafloor sediments the microbial abundance usually shows an exponential decrease with depth [*Kallmeyer et al.*, 2012]. In C2, however, maximum microbial abundances, bacterial gene copy numbers and DNA concentrations occurred in the unaffected permafrost unit, which confirms that even in frozen sediments microbial cells can be conserved and survive within thin brine veins [*Steven et al.*, 2007a; *Wagner et al.*, 2007; *Bischoff et al.*, 2013]. C2 also exhibited a quite constant diversity and richness in all pore water units except for PW IV. The diversity of this submarine permafrost site is thereby comparable with the permafrost active layer and permafrost thaw ponds [*Liebner et al.*, 2008; *Crevecoeur et al.*, 2015], though lower than in marine and deep-sea hydrothermal sediments [*Wang et al.*, 2012; *Cerqueira et al.*, 2015]. Recalling the clear stratification of bacterial assemblages according to the degree of marine influence, C2 displays thus a very unusual sub-seafloor habitat where permafrost table depth, stage of permafrost degradation, and time of inundation are constraints for the abundance and structure of bacteria and where permafrost is a bottom-up source for sub-seafloor life. “Bottom-up” refers in this case to its vertical position and the fact that, due to permafrost thaw, it is being continuously released at the lower boundary of the thawed sediment layer. Since C2 can be considered representative for submarine permafrost after millennia of exposure to submarine conditions its unique features as a subsurface habitat are likely applicable to large areas of the Siberian Arctic Shelf.

The origin and development of bacterial community structure and diversity differ between the two submarine permafrost cores. β-diversity, the variation in community composition, increases with distance and when local environmental conditions differ [*Lindström and Langenheder*, 2012]. Given that the terrestrial sediment at both sites was deposited in similar local fluvial-alluvial environments, we assign the high β-diversity of the bacterial communities to the large spatial distance and different glacial sediment source regions. Not even the infiltration of seawater into the units PW I and II resulted in similar bacterial community structure of C2 and BK2 (Supplement Fig. A-3, Table A-8) even though dispersal, i.e. the movement of an individual taxon from one location to another by passive or active mechanisms [*Hanson et al.*, 2012] through seawater should be high [*Lindström and Langenheder*, 2012]. For example, abundant taxa of PW II in BK2 were *Rhizobiales* and *Burkholederiales*, whereas PW II in C2 harbored predominantly *Acidimicrobiales*, *Actinomycetales* and *Chloroflexi* Gitt-GS-136. The heterogeneity of bacterial communities in shelf sediments of the Laptev Sea is in line with a

substantial β-diversity of bacterial communities in deep marine subsurface sediments from different continental margin sites in the Pacific Ocean [*Fry et al.*, 2008]. A large β-diversity even in sediment layers influenced by seawater for decades and hundreds of years could reflect i) that marine bacterial taxa did not establish in the new location of formerly terrestrial sediment, ii) the movement of seawater through the sediment matrix is too slow or iii) the movement of seawater through the sediment matrix occurs at very different rates in C2 compared to BK2. Our results indeed show that sediments of terrestrial origin in C2 are less influenced by marine inundation than sediments in BK2. The more gradual transition between PW II and PW III (Fig. 3-1a) in C2, compared to BK2, indicates that the penetration of seawater into the sediment takes place more slowly in C2. This can be due to different seabed conditions caused by wave and sea ice action, which drive the diffusive penetration into the seabed, and/or distinct sediment column properties that affect the penetration rate [*Ulyantsev et al.*, 2016]. As a consequence of the relatively deep water column and the low sea ice thickness, seasonal changes in seabed temperature and salinity were likely lower in amplitude at the C2 site. Still, bottom water salinity in the western part of the Laptev Sea is higher than in the central Laptev Sea, which is influenced by fluvial discharge [*Schirrmeister*, 2007; *Charkin et al.*, 2011; *Günther et al.*, 2013]. The concentration profile in C2 [*Winterfeld et al.*, 2011] suggests a predominantly diffusive transport of dissolved constituents of the pore water through the sediment column, whereas the BK2 profile suggests either more rapid diffusion and/or advective transport [*Osterkamp*, 2001].

C2 furthermore appears to host bacterial communities that have been stimulated by warming and started to proliferate, an assumption that was made before in the context with submarine permafrost [*Koch et al.*, 2009] and that is generally associated with the development of microbes in thawing permafrost [*Graham et al.*, 2012; *Schuur et al.*, 2015]. Thereby, stimulation of the microbes may be facilitated by a rising water content in warming permafrost [*Overduin et al.*, 2008]. This is supported by highest total cell counts, DNA concentrations and bacterial gene copy numbers of all units in the ice-bonded unaffected permafrost unit of C2, when neglecting the seabed sample. We cannot, however, rule out that cell numbers were high before transgression. The drop in microbial abundance between the unaffected permafrost unit (PWIII) and the terrestrial units that are marine-influenced (PWI and II) further indicate that in C2 the microbial community was disturbed by seawater infiltration. This would be in line with observed decreases in soil microbial abundance after exposure to elevated salt concentrations [*Rietz & Haynes*, 2003]. In BK2, microbial cell numbers decrease with depth which is typical for sub-seafloor habitats. In addition, the microbial data along BK2, for example the lowest

microbial abundance in the seawater unaffected permafrost sediments, do not show any indication for proliferation due to warming. The ice-bonded permafrost is still characterized by sub-zero temperatures, an environment where water activity, rates of nutrient exchange and growth rates are low [*Rivkina et al.*, 2000]. Microorganisms must resist exposure to subzero temperatures for prolonged periods of time [*Wagner et al., 2007*]. This is highly selective for cells and may be the reason for the small bacterial diversity and population size (10^4 cells g^{-1} sediment) in BK2. In addition, a high mean acetate concentration of 132.6 µM in the unaffected sediments (Supplement Fig. A-4) indicate that despite the temperature increase bacterial activity and growth in the permafrost unit were not yet stimulated. In fact three orders of magnitude less microbial cells in PWIII of BK2 compared to C2 suggest that the reaction of the permafrost bacterial community in BK2 to inundation is more strongly determined by disturbance than by the beneficial increase in temperature. As a corollary, this would suggest that bacterial communities in C2 reflect a later stage in the reaction of permafrost bacterial communities to marine transgression of permafrost.

Conclusions

This study highlights that submarine permafrost is a suitable natural laboratory for studying the response of permafrost bacterial communities both to temperature and salinity increase on geological timescales. It shows that concentrations and stable isotopes of pore water solutes can be used to distinguish sediments affected by reworking in the marine environment from the terrestrial permafrost thawed *in situ* beneath the seabed. Further we show that seawater infiltrates into frozen ice-bonded permafrost before thawing is complete. The effect of these processes is also reflected in the bacterial communities found in thawed and frozen submarine permafrost. Submarine permafrost originates as terrestrial permafrost but is warmer and has more saline pore water as a result of inundation by seawater. These differences change bacterial community structure, abundance and diversity, but the communities themselves remain terrestrial. The exposure to warming and increasing pore water salinity is a disturbance that probably results in a decrease of the community size followed by increasing proliferation on a time scale of millennia. Further work is needed to clarify whether differences in the community size and structure are a result of different inundation processes or spatial differences, and whether microbes in unaffected sediments exposed to warming are actively proliferating.

Acknowledgments

Sequences of the submarine permafrost communities presented in this work were deposited at the NCBI Sequence Read Archive (SRA) with the Project number BioProject ID# PRJNA352907. Bacterial 16S rRNA gene sequences have the accession numbers SRR5184420-SRR5184446 and are available from Genbank, EMBL and DDBJ. Pore water data for the C2 and BK2 cores are available at https://doi.pangaea.de/10.1594/PANGAEA.873837. Coring was supported by the German Ministry for Education and Research, a Joint Russian German Research Group (HGF-JRG100) of the Helmholtz Association of German Research Centres and by the EU's INTAS program. Susanne Liebner is grateful for the funding of the Helmholtz Young Investigators Group (grant VH-NG-919). Our thanks go to Anke Saborowski, Monique Thiele, Linda Mahler, Antje Eulenburg, Ute Bastian and Katja Hockun for excellent laboratory support, André Friese for acetate and formate measurements, and Jens Kallmeyer for sharing his knowledge in the field of cell counts. We further thank Aleksandr Maslov (SB RAS, Mel'nikov Permafrost Institute, Yakutsk, Russia), who provided indispensable drilling expertise and we thank Tiksi Hydrobase staff members Viktor Bayderin, Viktor Dobrobaba, Sergey Kamarin, Valery Kulikov, Dmitry Mashkov, Dmitry Melnichenko, Aleksandr Safin, and Aleksandr Shiyan for their field support.

4 Manuscript II - Anaerobic methanotrophic communities thrive in deep submarine permafrost

Abstract

Thawing submarine permafrost is a source of methane to the subsurface biosphere. Methane oxidation in submarine permafrost sediments has been proposed, but the responsible microorganisms remain uncharacterized. We analyzed archaeal communities and identified distinct anaerobic methanotrophic assemblages of marine and terrestrial origin (ANME-2a/b, ANME-2d) both in frozen and completely thawed submarine permafrost sediments. Besides archaea potentially involved in anaerobic oxidation of methane (AOM) we found a large diversity of archaea mainly belonging to *Bathyarchaeota*, *Thaumarchaeota*, and *Euryarchaeota*. Methane concentrations and δ^{13}C-methane signatures distinguish horizons of potential AOM coupled either to sulfate reduction in a sulfate-methane transition zone (SMTZ) or to the reduction of other electron acceptors, such as iron, manganese or nitrate. Analysis of functional marker genes (*mcrA*) and fluorescence *in situ* hybridization (FISH) corroborate potential activity of AOM communities in submarine permafrost sediments at low temperatures. Modeled potential AOM consumes 72-100% of submarine permafrost methane and up to 1.2 Tg of carbon per year for the total expected area of submarine permafrost. This is comparable with AOM habitats such as cold seeps. We thus propose that AOM is active where submarine permafrost thaws, which should be included in global methane budgets.

Introduction

Terrestrial permafrost landscapes, which developed during glacial cold periods, are known to be a large reservoir of organic carbon (~1300 Pg) [*Hugelius et al.*, 2014]. Permafrost thaw and the following microbial production of carbon dioxide and methane from liberated organic matter may act as a positive feedback to climate warming [*Schuur et al.*, 2015]. Methane has 34 times higher global warming potential over a 100 year period [*IPCC in Climate Change 2013*, 2013] and is a more critical greenhouse gas than carbon dioxide. The amount and the

release rates of methane are not well constrained although they are critical for evaluating future climate change.

Several Arctic sources of methane have been identified, including methane bursts during soil freezing [*Mastepanov et al.*, 2008], thermokarst lakes [*Walter et al.*, 2006], lakes and ponds [*Wik et al.*, 2016], wetlands [*Petrescu et al.*, 2015], gas hydrates [*Ruppel and Kessler*, 2017] and submarine permafrost [*Shakhova et al.*, 2010a]. Submarine permafrost on continental shelves of the Arctic Ocean is a consequence of the inundation of terrestrial permafrost by seawater during the Holocene marine transgression [*Osterkamp*, 2001; *Rachold et al.*, 2007]. Coastal submarine permafrost froze under subaerial terrestrial conditions in alluvial/fluvial settings and has remained frozen since then [*Winterfeld et al.*, 2011; *Overduin et al.*, 2015]. Submarine permafrost is much more susceptible to thawing than permafrost on land, because of overlying warm marine water causing diffusion of salt water into the sediments from the top, and because of geothermal heat flux from below [*Shakhova et al.*, 2010a]. Based on thermal modeling of permafrost development over glacial/interglacial cycles, submarine permafrost is likely to have persisted in deep sediment layers for hundreds of millennia [*Romanovskii and Hubberten*, 2001]. Over those millennial timescales submarine permafrost reaches its freezing point, between -2 and -1 °C, after which it slowly starts degrading due to the influence of high salt concentration [*Osterkamp*, 2001; *Romanovskii et al.*, 2004]. Our knowledge of evolving carbon pools and carbon turnover in submarine permafrost is, however, scarce.

Arctic submarine permafrost regions have the potential to emit large amounts of methane to the atmosphere [*Shakhova et al.*, 2014], however flux measurements are controversial. First estimates suggest a release of 8.0 Tg of methane per year from the East Siberian Arctic Shelf (comprising Laptev Sea, East Siberian Sea and the Russian part of the Chukchi Sea), which would equal the release of methane from the entire world ocean [*Shakhova et al.*, 2010a]. In contrast, recent estimates for the Laptev and East Siberian Seas are almost three times lower (2.9 Tg y^{-1}) [*Thornton et al.*, 2016]. Methane is mainly released from the sediment but the source is unclear [*Shakhova and Semiletov*, 2007]. It is expected that permafrost degradation can create pathways for the release of gas captured within submarine permafrost sediment or within gas hydrates underneath [*Shakhova et al.*, 2014]. Low $\delta^{13}C\text{-}CH_4$ values indicate a biogenic or thermogenic origin of methane released from submarine permafrost [*Koch et al.*, 2009; *Overduin et al.*, 2015]. A previous study demonstrated a drop of methane concentrations at the permafrost thaw front deep inside the sediments, which coincided with increasing $\delta^{13}C\text{-}CH_4$ values from -70‰ to -35‰ that points to anaerobic oxidation of methane (AOM) [*Overduin et al.*, 2015]. Sulfate penetrating from the seabed into the sediment created a deep

sulfate-methane transition zone (SMTZ) similar to other geological formations in the subsurface [*D'Hondt et al.*, 2004], with sulfate being a potential electron acceptor for AOM [*Thornton and Crill*, 2015].

Most studies on AOM in the marine system have focused on ANME archaea that couple the oxidation of methane to the reduction of sulfate via a syntrophic lifestyle with sulfate-reducing bacteria (SRB) [*Boetius et al.*, 2000; *Orphan et al.*, 2001; *Niemann et al.*, 2006]. Three main marine clades, ANME-1a/b, ANME-2a/b/c, and ANME-3 have been identified so far [*Knittel and Boetius*, 2009]. These clades are associated with sulfate-reducing bacteria of the genera *Desulfosarcina*, *Desulfococcus*, *Desulfobulbus* and *Desulfofervidus*, which belong to the class *Deltaproteobacteria* [*Knittel and Boetius*, 2009] and of the phylum *Thermodesulfobacteria* [*Krukenberg et al.*, 2016]. Besides the marine ANMEs there is evidence of terrestrial AOM driven by the ANME-2d clade [*Haroon et al.*, 2013; *Weber et al.*, 2017]. ANME-2d sequences were detected in wetland and permafrost habitats [*Kao-Kniffin et al.*, 2015; *Shcherbakova et al.*, 2016; *Narrowe et al.*, 2017] so they might mitigate the release of methane in these environments. A recent study on wetlands showed that even low amounts of sulfate (µM) are sufficient to couple AOM with sulfate reduction in terrestrial environments [*Segarra et al.*, 2015]. In addition, alternative electron acceptors for AOM such as iron [*Beal et al.*, 2009; *Crowe et al.*, 2011], manganese [*Beal et al.*, 2009] as well as nitrate [*Raghoebarsing et al.*, 2006; *Haroon et al.*, 2013] and humic substances [*Smemo and Yavitt*, 2011; *Scheller et al.*, 2016] have been suggested. To date, the microbial mitigation of methane emissions from permafrost environments is only evident in aerobic soils and sediments [*Liebner et al.*, 2011; *Knoblauch et al.*, 2015], while communities that oxidize methane anaerobically in thawing permafrost in the deep subsurface remain unexplored [*Ruppel and Kessler*, 2017]. We hypothesize that active marine and terrestrial ANME clades exist in thawing submarine permafrost similar to microorganisms found in terrestrial enrichments [*Raghoebarsing et al.*, 2006; *Haroon et al.*, 2013] or marine SMTZ [*Oni et al.*, 2015; *Ruff et al.*, 2015], and that these clades could function as an efficient methane filter for a diffusive methane release.

We investigated AOM in two deep submarine permafrost cores (48 m and 71 m) from the Siberian Shelf with different stages of submarine permafrost thaw [*Mitzscherling et al.*, 2017] that were inundated for about 540 and 2,500 years, respectively [*Rachold et al.*, 2007; *Overduin et al.*, 2015]. To identify microbial assemblages involved in AOM, we performed high-throughput sequencing of archaeal and bacterial 16S rRNA genes and of the functional marker gene methyl co-enzyme reductase (*mcrA*) that is encoded by both methanogens and anaerobic methanotrophs. We quantified *mcrA* and dissimilatory sulfate reductase (*dsrB*) gene markers

by quantitative PCR (qPCR) and correlated their abundance with the 16S rRNA gene abundance of AOM-related microorganisms. We visualized AOM-related microorganisms by catalyzed reporter deposition fluorescence *in situ* hybridization (CARD-FISH) and constructed ANME-specific 16S rRNA gene clone libraries to resolve their diversity in submarine permafrost sediments. Pore water geochemistry i. e. concentrations of methane, nitrate, sulfate, iron, and manganese, was analyzed to verify potential horizons of methane consumption. Analysis of stable carbon isotope geochemistry of methane and microbial membrane lipid biomarker were performed to evaluate the activity of AOM communities *in situ*.

Results

Isotopic evidence of AOM and potential electron acceptors

Methane concentrations were low (average 48 µM) in the ice-bonded permafrost section of the Cape Mamontov Klyk core (hereafter C2) inundated for ~2,500 years [*Koch et al.*, 2009] and peaked at approximately 52 m below seafloor (bsf) with a concentration of 990 µM (Fig. 4-1A). In contrast, methane concentrations in the ice-bonded permafrost section of the Buor Khaya core (hereafter BK2) were on average 8 times higher than in C2 (Fig. 4-2A) [*Overduin et al.*, 2015]. $\delta^{13}C$ values of methane in the ice-bonded permafrost of BK2 showed values between -71 and -53‰ typical for a biological origin [*Avery et al.*, 1999] (Fig. 4-2A). Above the ice-bonded permafrost, $\delta^{13}C$ values of methane ranged from -37 to -30‰ within a few meters on top of the thaw front and stayed constant to a depth of about 12 mbsf [*Overduin et al.*, 2015]. Above 12 mbsf $\delta^{13}C$-values of methane showed high dynamics with values ranging between -67 to -32‰ (Fig. 4-2A). $\delta^{13}C$ values of methane in the C2 core were only measurable in parts of the ice-bonded permafrost and showed ^{13}C values between -72‰ to -37‰ (Fig. 4-1A). Independently of one another, both cores showed opposing dynamics of methane concentration and $\delta^{13}C$ values with a clear signal of AOM at the SMTZ of BK2. Estimated release rates of methane from the ice-bonded permafrost of BK2 together with the modeled fraction of methane that was oxidized yielded potential AOM rates of 1.7 - 2.1 nmol cm^{-3} d^{-1}± 0.9 - 1.2 nmol cm^{-3} d^{-1} [*Overduin et al.*, 2015] in the SMTZ.

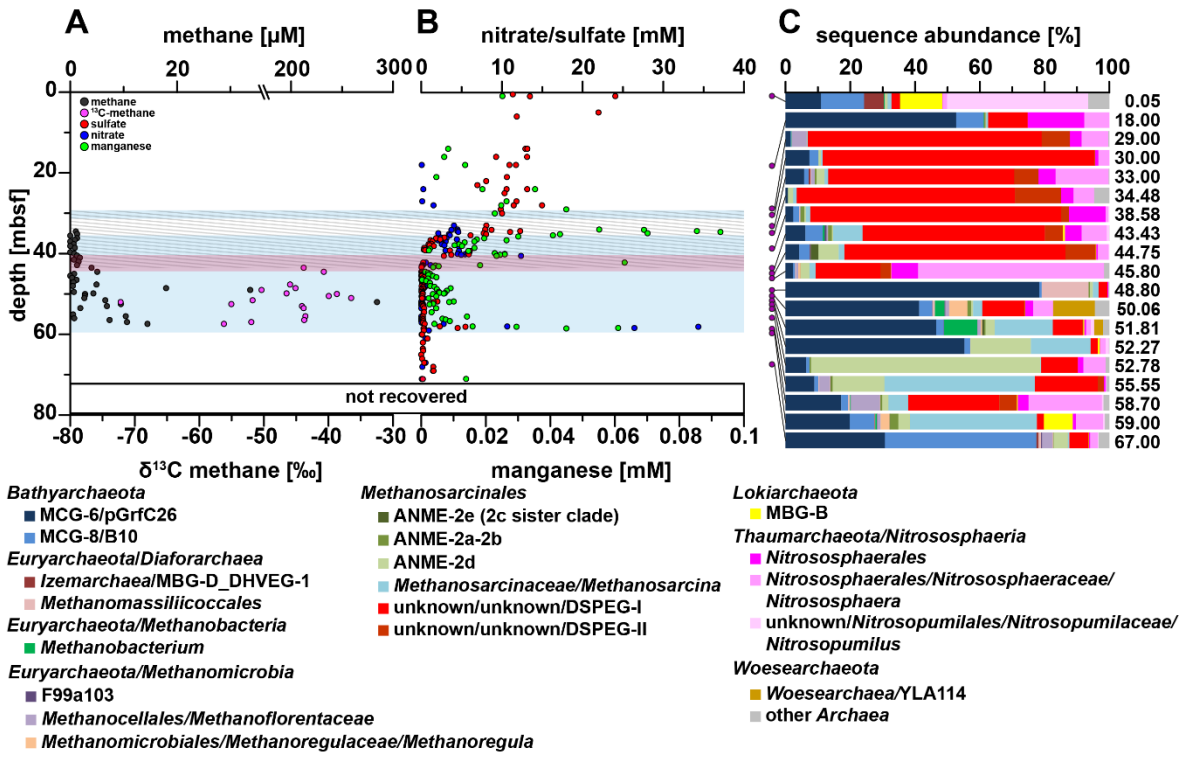

Figure 4-1: Pore water profiles of methane, nitrate, sulfate, manganese and relative archaeal abundance in the Mamontov Klyk core C2. **(A)** Methane concentrations are shown in black and corresponding δ^{13}C-values in magenta [*Koch et al.*, 2009]. **(B)** Nitrate concentrations are shown in blue, sulfate concentrations in red, manganese concentrations in green, and iron concentrations in light blue. **(C)** Purple dots on the left shows depth location in the core. Relative abundance of archaeal sequences are shown as bar plots. Colors of bars refer to the taxa in the legend below figure. Numbers on the right refer to the exact depth in the core. ANME= ANaerobic MEthanotrophic archaea, DHVEG-1= Deep Hydrothermal Vent Euryarchaeotal Group 1, DSPEG= Deep Submarine Permafrost Euryarchaeotal Group, MBG-B= Marine Benthic Group B, MBG-D= Marine Benthic Group D, MCG= Miscellaneous Crenarchaeotal Group. The shaded area represents the permafrost degradation zone, the red area a sulfate-methane transition zone, and the light blue areas ice-bonded permafrost. All uncolored areas of the plots correspond to unfrozen submarine permafrost and marine sediments.

Sulfate from seawater penetrated into the ice-bonded permafrost section of core C2 and into the thaw front of core BK2 indicating the presence of a SMTZ (Fig. 4-1B and 4-2B). Sulfate concentrations of 12 to 24 mM in the unfrozen part of the C2 core decreased with depth and penetrated almost 10 m into the ice-bonded permafrost. Here, sulfate concentrations were still high with up to 12.5 mM. Below 40 mbsf sulfate concentrations were low (< 0.4 mM) with the exception of ~52 mbsf (~1.5-2 mM) and the lower permafrost thaw front at ~58 mbsf (2.3 to 5.5 mM). Sulfate in the marine-affected layers of BK2 showed low concentrations (< 0.5 mM) in the first 5 mbsf and brackish concentration of 2 to 7 mM between 5 mbsf and the ice-bonded

permafrost. Inside the ice-bonded permafrost sulfate concentrations were low (average 0.08 mM) (Fig. 4-2B). In core C2, other potential terminal electron acceptors (TEA) such as nitrate, manganese, and iron were detected in the permafrost sediment layers (Fig. 4-1B). The latter two were only detected as total ions with no information on the oxidative state. Nitrate and manganese concentrations displayed high fluctuations in ice-bonded layers showing marine influence [*Mitzscherling et al.*, 2017] in the sediment i.e. between 29 and 43 mbsf. A high concentration of nitrate and manganese was also observed at the lower boundary of the ice-bonded permafrost (58.5 mbsf). In the ice-bonded permafrost part of BK2, manganese, iron and nitrate were close to or even below the detection limit. In the unfrozen part, manganese and iron concentrations were an order of magnitude higher and iron concentrations showed an increase towards the surface (Fig. 4-2B).

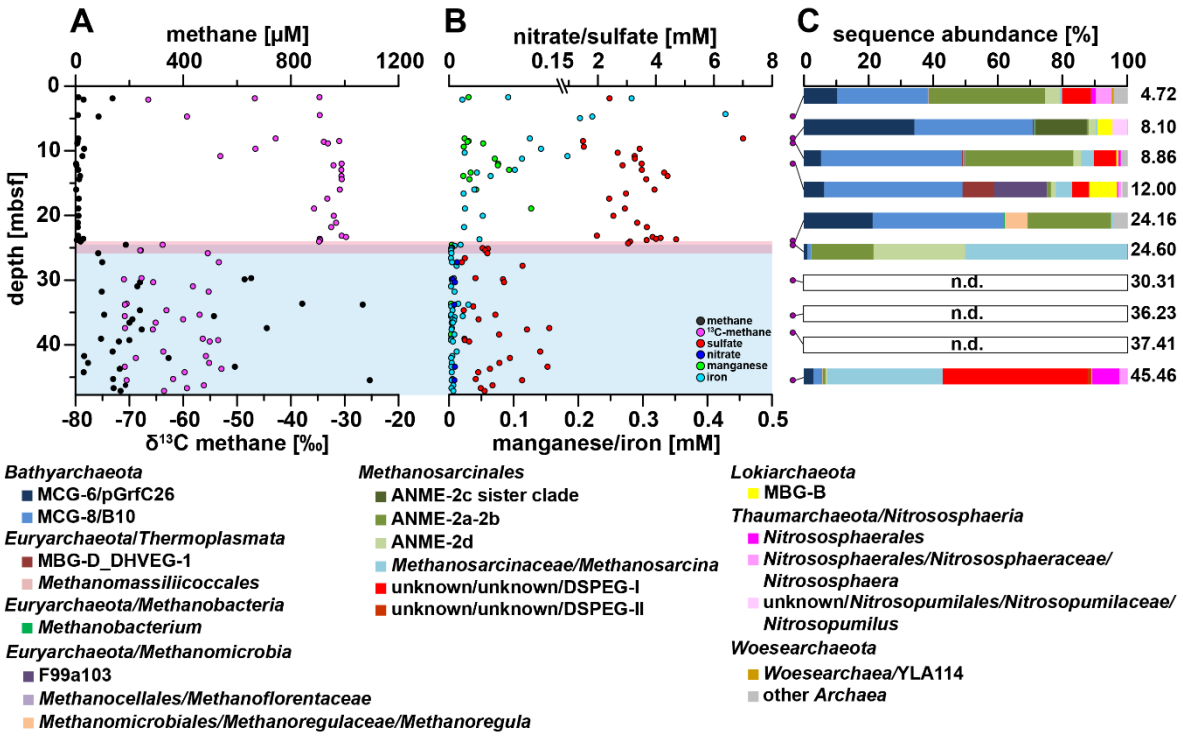

Figure 4-2: Pore water profiles of methane, nitrate, sulfate, iron, manganese and relative archaeal abundance in the Buor Khaya core BK2. (A) Methane concentrations are shown in black and corresponding δ13C-values in magenta [*Overduin et al.*, 2015]. **(B)** Nitrate concentrations are shown in blue, sulfate concentrations in red, manganese concentrations in green, and iron concentrations in light blue. **(C)** Purple dots on the left shows depth location in the core. Relative abundance of archaeal sequences are shown as bar plots. Colors of bars refer to the taxa in the legend below figure. Numbers on the right refer to the exact depth in the core. ANME= ANaerobic MEthanotrophic archaea, DHVEG-1= Deep Hydrothermal Vent Euryarchaeotal Group 1, DSPEG= Deep Submarine Permafrost Euryarchaeotal Group,

MBG-B= Marine Benthic Group B, MBG-D= Marine Benthic Group D, MCG= Miscellaneous Crenarchaeotal Group. The red area represents a sulfate-methane transition zone and the light blue area ice-bonded permafrost. All uncolored areas of the plots correspond to unfrozen submarine permafrost and marine sediments. n.d. – not detected.

Archaeal community structures of degrading permafrost

The upper layer of core C2, inundated for 2,500 years, was dominated by sequences of typical marine archaeal taxa. They were represented by aerobic ammonia-oxidizing *Thaumarchaeota* of the genus *Nitrosopumilus* (~44%), *Lokiarchaeota* found at hydrothermal vents (~15%), marine benthic group D (6%) and other marine taxa such as marine group II (~2%, Fig. 4-1C). At 18 mbsf *Bathyarchaeota* sequences of the MCG-6/pGrfC26 clade dominated (~53%) the archaeal community. This clade includes members able to degrade polymeric carbohydrates in the sulfate reduction zone [*Lazar et al.*, 2016]. In the same depth a shift towards taxa that are commonly found in terrestrial environments such as the ammonia-oxidizing *Nitrososphaerales* (~25%) was observed. Here we also detected a so far unknown clade, which we designated as Deep Submarine Permafrost Euryarchaeotal Group I (DSPEG I, ~12%). This new clade is closely related to *Methanomassiliicoccales* of the superclass *Diaforarchaea*. DSPEG I increased in relative sequence abundance with depth (Fig. 4-1C and 4-3). DSPEG I and a sister clade (designated DSPEG II) were most dominant in the sediment horizons between 29 and 44.8 mbsf, where they represented between 62 to 84% of all archaeal sequences (Fig. 4-1C). Both groups showed less than 82% sequence similarity values to the next cultured representative *Methanomassiliicoccus luminyensis* [*Dridi et al.*, 2012] placing them in a putative new order. Other abundant sequences belong to *Methanoflorentaceae* (~0.1-5%), ANME-2d (~0.2-6%), *Methanosarcina* (~0.2-9%), *Bathyarchaeota* MCG-6 and MCG-8 (~0.8-11%), as well as *Nitrososphaerales* (~3.7-22%). At 45 mbsf there was a pronounced shift towards *Nitrososphaerales* sequences (~65%). In the sediment layers between 49-52 mbsf, where most of the electron acceptors showed low concentrations, *Bathyarchaeota* of the MCG-6/pGrfC26 clade dominated (~41-78%). In these sediment horizons, many methanogen-related sequences appeared, such as *Methanoregula* (~0.1-6% between 50.06-52.3 mbsf), *Methanosarcina* (~2-18%), *Methanobacterium* (~3-10% 50.1-52.3 mbsf) and *Methanomassiliicoccaceae* (0.7-14% between 48.8-50.6 mbsf). Between 50.1 and 51.8 mbsf *Woesearchaeota* of the YLA114 clade were present (~3-13%). In core C2 ANME-2d sequences increased in relative abundance from less than 1% at 48.80 mbsf to 18% at 52.3 mbsf and up to 70% at 52.8 mbsf. The high abundance of anaerobic methane-oxidizers coincides around the

highest peak of the methane concentration profile in the ice-bonded permafrost (284 µM) at 52 mbsf (Fig. 4-1). In the same depth, about 1.1% of sequences are related to *Methanosarcinaceae*/ANME-3 as described by reference [*Niemann et al.*, 2006] (Table B-1). A second, much smaller peak of the methane concentration profile (10 µM) at 55.6 mbsf showed 16% ANME-2d sequences. At the same depth *Methanosarcina* represented the most abundant group (~47% of all archaeal sequences) and DSPEG I and II related sequences were the second most abundant (~21%, Fig. 4-1C). Towards the lower boundary of the ice-bonded permafrost at 58.7 mbsf, the DSPEG I and II increased again in sequence abundance (~33%). The sediment horizon directly underneath the permafrost contained some sequences related to marine environments, such as *Lokiarchaeota* (~9%), and ANME-2a/b (2.5%). The deepest sediment sample showed mostly *Bathyarchaeota* sequences of subgroups MCG-6 and MCG-8 (~77%) and DSPEG I and II, ANME-2d, *Methanoflorentaceae* and *Nitrososphaerales* (~6%, 4%, 3% and 2%, respectively) sequences.

The more recently inundated core BK2 contained a mixture of marine and terrestrial archaeal sequences in the depth between 4.7 and 12 mbsf. Marine clades were represented by ANME-2a/2b (~0.5-35%), *Methanomicrobia* of clade F99a103 (~0.1-16%) that were first discovered at a hydrothermal chimney, ANME-2c sister clade (~16%, 8.1 mbsf), Marine Benthic Group D (~0.1-10%), *Lokiarchaeota* (~0.7-9), and *Nitrosopumilales* (~0.3-4%). Terrestrial clades were represented by *Methanosarcinales*/*Methanosarcina* (~0.7-15%), DSPEG I and II (~0.1-9%), and *Nitrososphaerales* (~0.2-5%). The high numbers of ANME-2a/b sequences (Fig. 4-2C) at depths of ~5 and ~9 mbsf correlated with highest δ^{13}C-methane values in the uppermost 12 m that were characterized by highly variable methane δ^{13}C-values (-67 to -31‰, Fig. 4-2C). Still, *Bathyarchaeota*-related sequences of the clades MCG-6 and MCG-8 (~40-71%) dominated throughout the layers above the ice-bonded permafrost. In contrast, they drastically decreased (~2%) in the upper layer of the ice-bonded permafrost. The sediment horizon between 24.0 and 24.7 mbsf was characterized by opposing gradients of sulfate and methane. In the upper part of this layer that is strongly marine influenced ANME-2a/b made up about 26% of all archaeal sequences while in the lower and still partially ice-bonded part of the permafrost thaw front both ANME-2a/b and ANME-2d clades were detected in high abundances (about 19% and 28%, respectively, Fig. 4-2C). In the ice-bonded permafrost of core BK2, archaea were only detected in about 45.46 mbsf. Here, *Methanosarcina* (~37%) and DSPEG I and II (~46%) related sequences dominated. A detailed description of the bacterial community structure and diversity of both cores was described elsewhere [*Mitzscherling et al.*, 2017].

Figure 4-3: Phylogenetic affiliation of submarine Permafrost archaeal sequences based on 16S rRNA gene. Taxonomic cluster in red contain sequences of submarine permafrost. Numbers in brackets show the number of OTUs per cluster. The scale bar represents 10 percent sequence divergence. The tree was rooted with the DPANN superphlyum.

Diversity of ANME-related groups in degrading permafrost

Both cores displayed layers where ANME sequences dominated the archaeal community. The two major groups, ANME-2a/b and ANME-2d showed a remarkably high diversity with 23 and 17 operational taxonomic units (OTUs), respectively (Fig. 4-3 and 4-4A). ANME-2d separated into 4 different clusters (Fig. 4-4B), with the majority of all sequences falling into cluster 1. This cluster also contained *Candidatus* Methanoperedens nitroreducens BLZ1 [*Arshad et al.*, 2015], known to either use nitrate [*Haroon et al.*, 2013] or iron [*Ettwig et al.*, 2016] as electron acceptor for methane oxidation. Besides the two dominant ANME-groups, we also detected sequences in a sister clade of ANME-2c (designated ANME-2e) with 5 OTUs (Fig. 4-3 and 4-4 for details see also Fig. B-1 and B-2). Other sequences of this group were retrieved from cold seep sites and mud volcanoes. Moreover, we detected 1 OTU that fell into the ANME-3 cluster

(Fig. 4-3 and 4-4, for details see also Fig. B-2). Clone libraries of the SMTZ, using specific ANME-2a primers revealed mainly ANME-2a/b sequences but also ANME-2d as well as one sequence of the ANME-2e cluster (Fig. 4-4A, for details see also Fig. B-1). Corroborative CARD-FISH analysis of the SMTZ detected ANME-2a consortia with the specific ANME-2a-647 probe, while detection with a specific probe for *Desulfosarcina*/*Desulfococcus* showed no signal in any consortium (Fig. B-3).

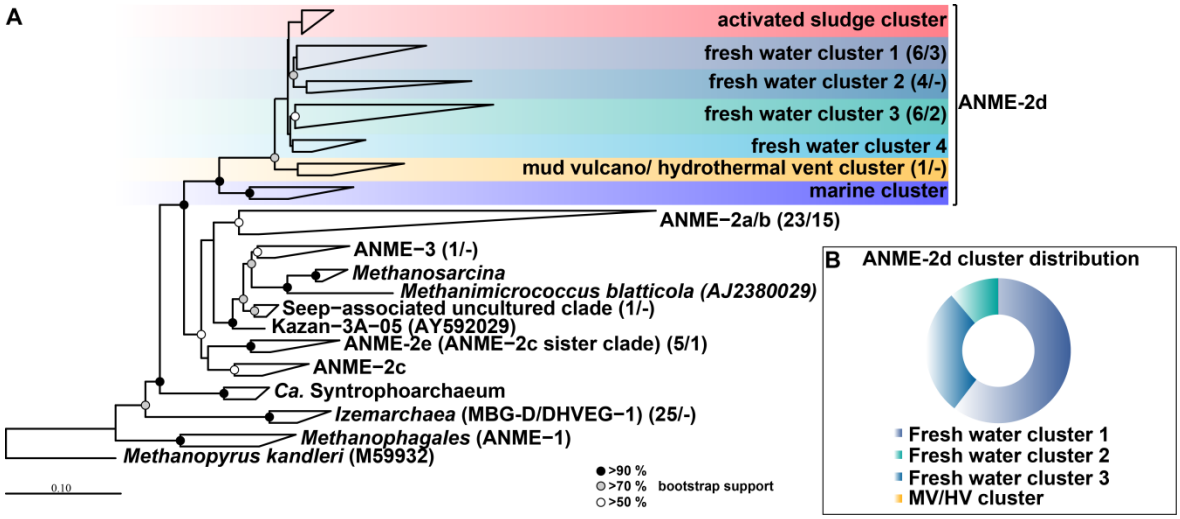

Figure 4-4: Phylogenetic affiliation of ANME sequences based on 16S rRNA gene. **(A)** The first number in the parenthesis represents the number of OTUs from the Illumina sequencing, while the second number represents the number of sequences of the clone library with ANME-specific primers. *Methanopyrus kandleri* was used as outgroup. The scale bar represents 10 percent sequence divergence. **(B)** The ring diagram represents the whole relative abundance of all ANME-2d sequences in both submarine permafrost cores.

Canonical correspondence analysis (CCA) illustrated that ANME-2a/b and ANME-2e clustered with other marine-related archaea and are mainly influenced by salinity, iron and sulfate (Fig. 4-5). Spearman rank correlations revealed that the abundance of ANME-2a/b significantly correlated with iron concentrations ($R=0.65$, $p< 0.03$). ANME-2d sequences clustered together with sequences of *Methanosarcina* and *Bathyarchaeota* of the MCG-6/pGrfC26 clade and fall in the terrestrial methane-influenced quadrant of the plot. However Spearman correlation revealed no significant correlation.

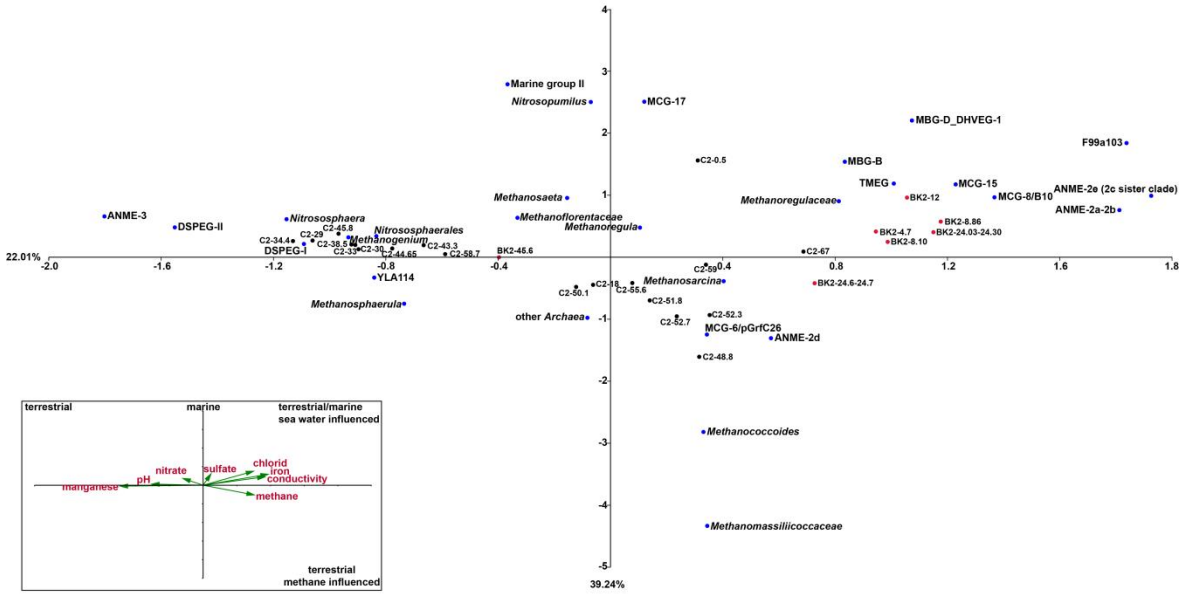

Figure 4-5: Canonical correspondence analysis (CCA) of environmental factors and archaeal taxa that contributed with more than 1% in any of the depth. Inlet: Environmental factors are plotted as triplot with scaling 3. Samples of core C2 are projected as black dots and samples of BK2 as red dots. The archaeal taxa are shown as blue dots. Percentages at axes represent the 'Eigenvalues' that explain the variability for the first two axes.

Functional groups responsible for methane cycling

Quantitative detection of the methyl co-enzyme reductase subunit A (*mcrA*) as functional marker for methane production (methanogens) and AOM (ANME) showed a decrease with depth in the unfrozen permafrost of both cores (0 to 29 mbsf for C2, and 0 to 24 mbsf for BK2, respectively, Fig. B-4A and B-4B). In the ice-bonded permafrost of core C2 we detected an increase in *mcrA* copy numbers with the highest copy numbers ($0.3 – 1.2 \times 10^5 \pm 0.4 - \times 10^3$ g^{-1} wet weight) between ~45 and 52 mbsf. At 53 mbsf total *mcrA* copy numbers decreased, while 16S rRNA gene sequences at the same depth were almost exclusively affiliated with ANME-2d (Fig. 4-1C and Fig. B-4A). 454 amplicon analyses of the *mcrA* sequences showed a relative increase of ANME-2d-related *mcrA* genes towards the layers with highest ANME-2d-related 16S rRNA gene sequences between 52.3 and 55.6 mbsf (Fig. 4-2C and Fig. B-5). Quantification of ANME-2d with recently designed *mcrA* primers in the ice-bonded permafrost [*Vaksmaa et al.*, 2017] showed up to $1.2 \pm 0.5 \times 10^5$ copy numbers g^{-1} wet weight at approximately 57 mbsf and an average copy number of $5.1 \pm 1.5 \times 10^4$ g^{-1} wet weight over the whole core (Fig. B-6).

Analysis of the dissimilatory sulfate reductase subunit B (*dsrB*) for SRB mainly followed the depth distribution of *Desulfosporosinus* 16S rRNA sequences in the C2 core, with a few exceptions (29.0, 30.0, 34.4 and 38.5 mbsf) where an increase in the *dsrB* could not be related to any known sulfate-reducers (Fig. B-7A).

McrA copy numbers in BK2 slightly increased at the SMTZ and may be underestimated due to a primer bias against ANME *mcrA* genes [*Vaksmaa et al.*, 2017], while 16S rRNA gene sequences showed 25-47% ANME-related sequences at the SMTZ (Fig. B-4B). The *dsrB* copy numbers slightly increased at the SMTZ, although SRB represented < 1% of the total bacterial 16S rRNA gene sequences (Fig. B-7B). Phylogenetic reconstruction of SRB at the SMTZ indicated that all sequences of the upper part belonged to typical marine clades SEEP-SRB1 and another seep-associated *Desulfobacterium anilini*-group (red OTUs, Fig. B-8). In the lower part of the SMTZ that is dominated by ANME-2d sequences, seep-associated SRB were below detection limit, while only *Desulfosporosinus*-related sequences (blue OTU, Fig. B-8) could be observed.

Lipid biomarker measurements revealed very low concentrations that prevented a precise isotopic analysis to conclude activity of AOM microbial communities. However, calculated branched and isoprenoid tetraether (BIT) indices showed values of terrestrial origin ranging from 0.99 to 1 [*Hopmans et al.*, 2004]. Moreover calculated methane indices (MI) for isoprenoid glycerol dialkyl glycerol tetraethers (GDGTs) showed values between 0.85 to 0.99 in the unfrozen sediment layer and 1 at the SMTZ [*Zhang et al.*, 2011]. The ratio of archaeal to bacterial ether lipids showed dominant archaeal values in the SMTZ (Fig. B-9). For further discussion on lipid biomarker see supplementary material.

Methane oxidation rates in submarine permafrost

The fraction of produced methane that, based on carbon isotopic signature change, was oxidized varied between 72-86% for the C2 core and 79-100% for the BK2 core, respectively. Methane release rates depend on the permafrost degradation rate and the methane concentration in the pore space of the core section. Assuming that our cores are representative for the whole submarine permafrost area with an estimated distribution of 3 million square kilometer (E. A. G. Schuur et al., 2015), modeling for the C2 core resulted in 0.0001 – 0.0984 Tg C y^{-1} (average 0.004-0.005 Tg C y^{-1}, highest and lowest oxidation, respectively) and 0.0242 – 1.1889 Tg C y^{-1} (average 0.1712 – 0.2167 Tg C y^{-1}, highest and lowest oxidation, respectively) for the BK2 core.

Discussion

Atmospheric methane concentration has been increasing again for the last decade, but the sources and mechanisms for this increase are not fully understood [*Saunois et al.*, 2016]. One potentially large but highly controversial source of methane is submarine permafrost, which faces drastic changes due to global temperature increase and associated Arctic sea ice reduction [*Richter-Menge et al.*, 2016]. Our study provides multiple lines of evidence that ANME communities are present in submarine permafrost layers where methane is being consumed. We thus propose the microbial mitigation of methane release from thawing deep submarine permafrost on the Siberian Arctic Shelf. We detected both marine and terrestrial ANME clades likely involved in the AOM process at various depths, not only at the permafrost thaw front, but also in still ice-bonded permafrost that undergoes degradation. Our study indicates that AOM could occur at temperatures below 0°C [*Mitzscherling et al.*, 2017] (Table B-2).

Pore water methane concentrations in the two cores were in the typical range of deep sediments and soils [*D'Hondt et al.*, 2004; *Wagner et al.*, 2007]. The permafrost thaw front at the BK2 site, inundated about 540 years ago reflects a deep SMTZ. We identified a steep decline of methane concentration above the SMTZ. This is in accordance with core (IID-13) [*Sapart et al.*, 2017] in close proximity that also showed a large decrease (10^6 to 10^3 nM) in methane concentrations at the thaw boundary while δ^{13}C-values of methane from unfrozen layers above (~15 to 4 m) of this core are not reported. Altogether the study of *Sapart et al.* [2017] finds no evidence for AOM, which might be due to regional influences such as river water, land surface run off and warming by river discharge. Our δ^{13}C-values of methane in the unfrozen part clearly show a large shift that can only be explained by microbial oxidation. The calculated potential rates based on methane release and the fraction of methane oxidized (1.7 - 2.1 nmol cm^{-3} d^{-1}± 0.9 - 1.2 nmol cm^{-3} d^{-1}) [*Overduin et al.*, 2015] are typical for margin SMTZ and exceed those of subsurface SMTZ [*Knittel and Boetius*, 2009].

At the permafrost thaw front of BK2, we detected marine and terrestrial ANME clades that potentially mitigate the methane release into overlying sediment layers. The upper unfrozen part of the SMTZ represents a typical marine sulfate-dependent AOM community of ANME-2a/b (Fig. 4-2C) affiliated with SEEP-SRB1/seep-associated *Desulfobacterium anilini*-group (Fig. B-7A). These sulfate-dependent AOM communities are of marine origin and are often found in mud vulcanoes, and in methane and hydrocarbon seeps [*Dekas et al.*, 2016]. Visualization of ANME-2a *in situ* using CARD-FISH further supports their occurrence at the permafrost thaw front of BK2. The molecular detection of associated SRB is, however, not conclusive. This might be due to SEEP-SRB partners that are not targeted by the DSS685 probe

[*Schreiber et al.*, 2010] or by yet unidentified bacterial partners [*Hatzenpichler et al.*, 2016]. The lower part of the SMTZ was characterized by a clear transition to a terrestrial AOM community closely related to *Candidatus* Methanoperedens nitroreducens (ANME-2d) that might be capable of using alternative TEA such as nitrate and iron [*Haroon et al.*, 2013; *Ettwig et al.*, 2016], although no information on the oxidative state of iron is available. A recent genomic study proposed that these organisms have the genetic repertoire for an independent AOM process without a bacterial partner [*Arshad et al.*, 2015]. Besides the analysis of AOM assemblages via a DNA approach we also found high ether lipid MI values in the SMTZ of BK2 that further supports a potential involvement of AOM communities [*Zhang et al.*, 2011]. The high abundances of marine-derived ANME-2a/b sequences in several depths above the SMTZ of BK2 with BIT indices towards an exclusively terrestrial origin show that terrestrial and marine sediments were mixed in the upper meters of BK2 (Fig. 4-2). The terrestrial sediments were thus influenced by seawater penetrating down to the permafrost table and thereby transport of marine organisms into deeper layers occurred (Fig. 4-2). This is consistent with profiles of other environmental parameters (pH, temperature, isotopes and ion concentrations) and the stratification and composition of the bacterial communities [*Mitzscherling et al.*, 2017].

In core C2 the layer between 29 and 43 mbsf is characterized by alternating frozen and partly thawed sediments (Fig. 4-1) and showed high fluctuations in the concentrations of nitrate and manganese. These fluctuations indicate degradation of thawing permafrost (shaded area, Fig. 4-1) and an increase in microbial activity resulting in the consumption of labile carbon pools [*Hodgkins et al.*, 2014]. Active processes in ice-bonded permafrost close to thawing (mean temperature: -1.2 ± 0.2 °C, Table B-2) can occur in liquid water films surrounding mineral particles, which form a network in which microbial activity is expected [*Jansson and Taş*, 2014]. Microbial activity may thereby be supported through sulfate as additional electron acceptor [*Hultman et al.*, 2015] penetrating into the ice-bonded sediment. Indeed, sulfate concentrations decreased and *dsrB* copy numbers increased with depth pointing towards active sulfate reduction and effective anaerobic organic matter decomposition [*Canfield et al.*, 1993]. In C2, the SMTZ occurred below the actual permafrost thaw front but inside the ice-bonded permafrost and was characterized by high manganese and nitrate concentration. Nitrate and manganese concentrations at the SMTZ and in the lower thaw boundary were in the higher µM to mM ranges that exceeded those typically reported for subsurface environments [*D'Hondt et al.*, 2004] by an order of magnitude (http://publications.iodp.org/). So far it is not clear why nitrate as favorable electron acceptor is not quickly consumed under anaerobic conditions.

Nevertheless, the high concentrations of nitrate and manganese could promote AOM with alternative TEA [*Raghoebarsing et al.*, 2006; *Beal et al.*, 2009] and shows ongoing degradation of ice-bonded permafrost. Also, the detection of ANME-2a/b in this layer shows their migration into permafrost by downward marine water intrusion [*Mitzscherling et al.*, 2017]. Unlike in core BK2, the ice-bonded layer of C2 was almost free of methane. At the same time ANME-2d occurred almost entirely throughout this layer. The relatively low copy numbers of ANME-2d detected with specific *mcrA* primers and compared with total cell counts [*Mitzscherling et al.*, 2017] are still in the range of North Sea and River sediment [*Vaksmaa et al.*, 2017]. The highest abundance of ANME-2d coincided with the highest methane concentration, which we consistently detected by several molecular approaches (16S rRNA, *mcrA* and ANME-2d-specific *mcrA*). Taken all this together we suggest that ANME-2d members are responsible for AOM in the ice-bonded permafrost before it completely thaws. An alternative explanation for the low methane concentrations and the low abundance of ANMEs in most of the ice-bonded layers are a relic of AOM communities that were active under different environmental conditions in the past. Whether methane was trapped in the permafrost during freezing or it was produced by microbial degradation of organic matter under recent *in situ* conditions cannot be resolved since radiocarbon analysis would give similar results in both cases.

Even though sulfate reduction might be relevant for organic matter mineralization61, links to sulfate-dependent AOM were not observed in the core C2. While C2 exhibited high copy numbers of *dsrB* and of SRB-related sequences, sulfate reducers were almost exclusively linked to *Desulfosporosinus* that have not been observed in AOM consortia so far. This genus belongs to the phylum *Firmicutes* and has been found in natural terrestrial environments such as peatlands, aquifer and permafrost [*Pester et al.*, 2010; *Mayeux et al.*, 2013]. Other TEA than sulfate, such as nitrate, iron and manganese, could also be related to AOM, and showed relatively low concentrations at the highest occurrence of ANME-2d sequences at 52 mbsf. This serves further as an indication of methane consumption during the process of AOM as known from physiological studies of ANME-2d enrichments [*Haroon et al.*, 2013; *Ettwig et al.*, 2016] but direct evidence is missing. Finally, besides the detected electron acceptors, other TEA such as humic acids could serve in the AOM process. Humic acids were shown to be involved in AOM [*Smemo and Yavitt*, 2011; *Scheller et al.*, 2016] in peatlands where they were detected in high concentrations. Humic acids are produced during organic matter degradation and soil formation [*Ghabbour and Davies*, 2007] and could thus play a role in thawing permafrost, too. Two clades, which we named DSPEG I and DSPEG II, mainly occurred in submarine permafrost layers that showed relatively high concentrations of iron and manganese in the pore

water (Fig. 4-1B, C). This could point towards an involvement in iron (III) and manganese (IV) reduction within the anaerobic oxidation of organic matter, in addition to sulfate reduction [*Pester et al.*, 2010]. Since the oxidative state of both metals has not been determined it is not clear whether these metals are used as TEA. Future analysis should focus on oxidative states of metals in these environments to further clarify a potential role in organic matter degradation and AOM. Nevertheless, Spearman rank analysis showed significant correlations between DSPEG I and DSPEG II and manganese concentration ($R= 0.58$, $p< 0.006$ and $R= 0.53$, $p< 0.02$, respectively) and negative correlations with methane ($R= -0.57$, $p< 0.02$ and $R= -0.64$, $p< 0.004$, respectively) as illustrated in the CCA (Fig. 4-5). We propose that these two groups reflect indicator taxa (Table B-3) for degrading permafrost. This is also supported by high occurrence of DSPEG I and DSPEG II (~19 to 28%, Fig. 4-1C) at the lower boundary of the ice-bonded permafrost, representing bottom-up permafrost thaw. Here, high concentrations of sulfate, nitrate, and manganese show an upwardly directed thaw process (Fig. 4-1B). Both groups were also dominant (47%) in the deepest sample of BK2, while degradation and an upward thaw cannot be concluded from our data. Environmental sequences affiliated with the DSPEG groups were mainly retrieved from cold environments [*Ayton et al.*, 2010; *Daae et al.*, 2013] and pristine aquifers [*Flynn et al.*, 2013], which further support an active role in low temperature habitats.

Taken together our molecular and biogeochemical data from two submarine permafrost cores indicate several microbial assemblages that have the potential to prevent the release of trapped or recently produced methane into the overlying unfrozen sediment following submarine permafrost thaw. Therefore, we challenge the assumption that high methane emissions reported for the Siberian Arctic Shelves originate from degrading submarine permafrost itself9 and suggest different mechanisms to be responsible, such as diffusion or ebullition through discontinuities in permafrost or the release from gas hydrates [*Kohnert et al.*, 2017; *Ruppel and Kessler*, 2017] at a limited spatial scale. Microbial assemblages in deep permafrost environments are usually associated with slow growth rates [*Rivkina et al.*, 2000] and low abundances [*Waldrop et al.*, 2010], and their activity is difficult to measure. New approaches such as BONCAT-FISH [*Hatzenpichler et al.*, 2016] have the potential for more direct detection of active microorganism and the analysis of their genomic potential.

The calculated fraction of methane that was oxidized in the SMTZ of BK2 showed high efficiencies, pointing towards an effective biological methane filter. While methane oxidation within the intact ice-bonded permafrost section of BK2 is unlikely, C2 showed several layers with heavier stable isotopes (≥-45‰) and high fractions (72 to 86%) of methane that were

oxidized. Actual methane oxidation rates may be even higher, since methane production of freshly available organic material is not taken into account. Still, on a global scale the estimated submarine permafrost area (~3 million km²) [*Schuur et al.*, 2015], could consume 0.0001 to 1.1889 Tg y^{-1} of methane from newly degraded permafrost assuming AOM activities similar to those in our cores. This only account for the methane released, since it is difficult to determine the total sediment volume in which AOM activity takes place. Submarine permafrost is thus comparable to AOM in other environments with high methane fluxes such as seep sites (< 10 Tg C y^{-1}) [*Boetius and Wenzhöfer*, 2013], while AOM in wetlands (200 Tg C y^{-1}) [*Segarra et al.*, 2015] and marine SMTZ (< 50 Tg C y^{-1}) [*Boetius and Wenzhöfer*, 2013] clearly show higher consumption rates. The latter two span areas that are 6 to 40 times larger than those of submarine permafrost.

Our study provides first molecular evidence of microbial communities in thawing submarine permafrost that are likely involved in AOM processes. In addition, many archaeal taxa such as the newly designated DSPEG groups, a large diversity of *Bathyarchaeota*, and *Thaumarchaeota* closely related to nitrogen cycling organisms are detected. Their function is unknown and need further investment to understand their contribution in organic matter degradation of permafrost thaw processes.

Materials and Methods

Site description and sampling

Sediment cores were drilled along two transects from terrestrial permafrost to offshore, submarine permafrost in the Siberian Laptev Sea: Mamontov Klyk (2005) and Buor Khaya (2012) (Table B-2). The outermost submarine permafrost cores influenced longest by inundation were chosen for chemical and microbial investigation. The Mamontov Klyk study site was located in the western Laptev Sea (Fig. B-10). The core drilled 11.5 km offshore is characterized by three different lithostratigraphical units and contains two ice-bonded permafrost layers between 29.5 - 30.4 mbsf and 34.3 – 58.7 mbsf, respectively [*Winterfeld et al.*, 2011]. The core had a total length of 71 m and contained sandy loam sediment with on average 0.38 % organic carbon and an average C/N ratio of 14.

The study site of Buor Khaya is located in the central Laptev Sea on the western part of the Buor Khaya peninsula (Fig. B-10). The submarine core contained again three lithological units with an ice-bonded permafrost layer between 24.7 – 47.6 mbsf [*Overduin et al.*, 2015]. The

core had a total length of 47.7 m. The retrieved sediment material consisted of fine sand and contained about 1% organic carbon with a C/N ratio of 14.

The drilling was performed with a mobile drilling rig (URB-2A-2/ URB-4T) and is described elsewhere [*Winterfeld et al.*, 2011; *Overduin et al.*, 2015]. Cores were kept frozen at -20°C and transported to the laboratories in Germany under frozen conditions. The frozen cores were split along the vertical axis under aseptic conditions. One half was used as an archive, whereas the other half was split into quarters for microbiological and for geochemical, sedimentological and micropalaeontological analyses.

Geochemical analysis

The cores were sectioned at different intervals. The core of the Mamontov Klyk site (C2) was separated into 118 horizons that were used for pore water analyses in 2007, 2 years after the drilling took place. The core was constantly stored at -20°C between drilling and subsampling. The Buor Khaya site (BK2) was divided into 80 horizons. After thawing of subsamples in 2013, one year after the drilling, pore water was collected using Rhizones© with an effective pore diameter of 0.1 µm. The concentration of sulfate and nitrate was determined via a KOH eluent and a latex particle separation column on a Dionex DX-320 ion chromatograph. Total manganese and iron ions were measured by a Perkin-Elmer 'Inductively Coupled Plasma Optical Emission Spectrometry' (ICP-OES) Optima 3000 XL.

For methane measurements, 3 g of frozen material were retrieved with ice screws and immediately immersed in 20 ml serum vials containing a saturated NaCl solution (315 g l^{-1}). Serum vials were sealed with butyl-rubber stopper and a crimp seal. Headspace gas was measured in triplicates with different setups. In brief, gas was analyzed with an Agilent 689019 or 7890A13 gas chromatograph equipped with a flame ionization detector and with a carbon plot capillary column or HP-Plot Q (Porapak-Q) column. The temperature of the oven, injector and detector were 40, 120, and 160°C, respectively. In both cases, helium was used as carrier gas. The amount of gas in the vials was calculated from headspace concentrations, gas pressure and solubility, and the volume of liquid in the bottles. Methane concentrations are reported relative to sediment pore water volume, regardless of whether present as ice or water, based on calculated total sediment water content. The $\delta^{13}C\text{-}CH_4$ was determined with an isotope ratio mass spectrometer (Finnigan Delta Plus) equipped with a PreCon and a GC/C III interface (Thermo, Bremen, Germany). The precision of replicated measurements was better than 0.5‰ VPDB. Methane $\delta^{13}C$-signatures were linked to the VPDB scale using internal (-43.8‰ VPDB) and external (RM8561; -73.27‰ VPDB) standards measured at least every 10 analyses.

DNA extraction, 16S rRNA Illumina sequencing and analysis

In 2014, genomic DNA of 4.7-13 g homogenized sediment from different depth (C2: 19 samples and BK2: 10 samples, Table B-2) was extracted after the protocol of *Zhou et al.* [1996]. DNA concentrations were quantified with Nanophotometer® P360 (Implen GmbH) and Qubit® 2.0 Flurometer (Thermo Fisher Scientific).

The 16S rRNA gene for bacteria was amplified with the primer combination S-D-Bact-0341-b-S-17 and S-D-Bact-0785-a-A-21. The 16S rRNA gene for archaea was amplified in a nested approach with the primer combination S-D-Arch-0020-a-S-19 and S-D-Arch-0958-a-A-19 in the first PCR for 40 cycles and S-D-Arch-0349-a-S-17 and S-D-Arch-0786-a-A-20 in the second PCR for 35 cycles, respectively. The primers were labelled with different combinations of barcodes that are listed together with primer sequences in Tables B-4 and B-5. The PCR mix contained 1x PCR buffer (Tris•Cl, KCl, $(NH_4)_2SO_4$, 15 mM MgCl2; pH 8.7) (QIAGEN), 0.5 µM of each primer (Biomers), 0.2 mM of each deoxynucleoside (Thermo Fisher Scientific), and 0.025 U μl^{-1} hot start polymerase (QIAGEN). The thermocycler conditions were 95°C for 5 min (denaturation), followed by 40 cycles of 95°C for 1 min (denaturation), 56°C for 45 sec (annealing) and 72°C for 1 minute and 30 sec (elongation), concluded with a final elongation step at 72°C for 10 min. PCR products were purified with a Hi Yield® Gel/PCR DNA fragment extraction kit (Süd-Laborbedarf). We performed technical duplicates of one DNA sample and PCR products of 3 individual runs per sample were combined. PCR products of different samples were pooled in equimolar concentrations and reduced to a final volume of 10 µl with a concentration of 200 ng μl^{-1} in a vacuum centrifuge Concentrator Plus (Eppendorf).

Illumina sequencing has been performed by GATC Biotech AG using 300 bp paired-end mode. For better performance due to different sequencing lengths, we used 15% PhiX control v3 library.

The quality and taxonomic classification of the Illumina sequences were analyzed with a customized QIIME pipeline [*Caporaso et al.*, 2010]. For details see Supplementary material and methods.

Construction of ANME-specific clone libraries

DNA of permafrost thaw horizons and methane peaks were investigated to amplify ANME communities with specific primers. Therefore we used an ANME-specific probe as reverse primer and a universal archaeal primer as forward primer (Table B-4). PCR mixes (25 µl) contained 1 x PCR buffer, 0.2 mM dNTP's, 2 mM $MgCl_2$, 0.08 mg ml^{-1} bovine serum albumin, and 0.02 units HotStart Taq Plus Polymerase (QIAGEN) and were performed under the

following conditions: initial denaturation 94 °C for 10 min, 30 cycles of denaturation 94 °C for 30 sec, annealing 59 °C for 1 min, extension 72 °C for 3 min, and a final elongation at 72 °C for 10 min. PCR amplicons were purified with the HiYield® Gel/PCR DNA Extraction Kit (Süd-Laborbedarf). Purified PCR products were cloned with the TOPO® TA Cloning® Kit (Invitrogen). Positive clones were directly sequenced by Sanger sequencing (GATC Biotech).

Phylogenetic reconstruction

For phylogenetic analyses of 16S rRNA gene of archaeal and bacterial sequences, the ARB software package was used [*Ludwig et al.*, 2004]. After manual refinement of representative sequences of OTUs achieved by the Illumina sequencing and partial sequences of clone libraries against the alignment of the SILVA 16S rRNA gene SSU reference database release 115 [*Quast et al.*, 2012], phylogenetic trees were calculated. Phylogenetic reconstructions were based on the maximum-likelihood algorithm (PHYLIP-ML, 100 bootstraps) implemented in ARB with reference sequences (> 1400 bp for bacteria and > 850 bp for archaea) and the implement archaeal or bacterial position variability filters. Our own partial sequences were added to the tree using the maximum parsimony algorithm without allowing changes in tree topology.

454 pyrosequencing of functional genes and analysis

The *mcrA* fragment was amplified using the primer set mlas and *mcrA*-rev (Table B-4). In a touchdown PCR denaturation, annealing and elongation time was set at 1 min. The PCR conditions were as follows: initial denaturation at 95°C for 3 min, 15 cycles with a stepwise temperature decrement from 65°C to 50°C, followed by 15 cycles with an annealing temperature of 55°C and a final elongation at 72°C for 10 min. Tagging of amplicons with unique multiple identifier (MID) tags (Table B-6) for 454 sequencing was conducted in a second PCR using amplicons from the touchdown PCR as template and 15 cycles with a constant annealing temperature of 55°C. PCR reactions were performed in several separate reactions and pooled until reaching at least 150 ng final product. We used the same chemicals as for 16S rRNA gene amplifications. PCR products were purified with a Hi Yield® Gel/PCR DNA fragment extraction kit (Süd-Laborbedarf). Amplicons were quantified with the Qubit 2.0 system using the ds DNA HS assay kit (Invitrogen), mixed in equimolar amounts and sequenced from both directions by Eurofins Genomics using Roche/454 GS FLX++ technology.

454 *mcrA* sequences were analyzed with the mothur software [*Schloss et al.*, 2009] by a customized standard operating procedure. For details see Supplementary material and methods.

Quantification of functional genes

Quantitative PCR was performed using the CFX Connect™ Real-Time PCR Detection System (Bio-Rad Laboratories). Each reaction contained iTaq™ Universal SYBR® Green Supermix (12.5 µl per reaction of 2x concentrate, Bio-Rad Laboratories), PCR primers (0.5 µl containing 20 µM each), sterile water (6.5 µl) and DNA template (5 µl) added to a final volume of 25 µl. Primers targeting the functional genes *mcrA* and *dsrB* were used (Table B-4). The PCR reactions comprised an initial denaturation (5 min at 95°C), followed by 40 cycles of 5 s at 95°C, 30 s at the specific annealing temperature (see Table B-4), 10s at 72°C and a plate read step at 80°C for 3 s. Melt curve analysis from 65 to 95°C with a 0.5°C temperature increment per cycle (5 sec) was conducted at the end of each run to check for non-specific amplification of DNA. The qPCR assays were calibrated using known amounts of PCR amplified and cloned gene fragments from corresponding taxa (standards of pure cultures) in the range of $10^6 – 10^1$ copies μl^{-1}. Prior to qPCR analysis, DNA templates were diluted 5- to 100-fold and triplicates were analyzed for each sample. The PCR efficiency based on the standard curve was calculated using the BioRad CFX Manager software and varied between 88 and 100%, depending on the standard. All cycle data were collected using the single threshold cq determination mode.

Quantification of ANME-2d

The DNA was diluted 1:100 to prevent inhibition of amplification by environmental compounds, e.g. humic acids, and to keep the cq value of the samples within detectable limits. The abundance of ANME-2d archaea was quantified by qPCR with specific *mcrA* primers (Table B-4). The PCR mix consisted of 10 µl KAPA HiFi SYBR green mix (KAPA Biosystems), primers (0.04 µl containing 100 mM each), $MgCl_2$ solution (0.5 µl of 50 mM), bovine serum albumin (BSA) (0.3 µl), sterile water (9.02 µl) and 1 µl DNA template. qPCR amplifications were performed by 10 min 98°C initialization; 40 cycles of 5 second denaturation at 95°C, 30 second of annealing at 60°C, 1 min of elongation at 72°C, 2 seconds at 82°C for fluorescence detection; and finally a melting curve from 55°C to 95°C with a 0.5°C increment every 5 seconds. For quantification, a tenfold dilution series of *mcrA*156F/*mcrA*345R product cloned into a pGEM-T easy plasmid of a known copy number was used as a standard [*Vaksmaa et al.*, 2017]. The PCR product specificity was checked by melt analysis and compared to the standard with a melting temperature of 82 °C.

Microbial lipid biomarker extraction

Different fractions of lipids were extracted from sediment of the SMTZ. For a detailed method description see supplementary material.

Catalyzed reporter deposition fluorescence in situ hybridization (CARD-FISH)

For CARD-FISH, sediments were fixed for 1 h at room temperature with 4 % formaldehyde (Fluka). For amplification, a fluorescine-labelled tyramide was used. The protocol for CARD-FISH followed the description published earlier [*Winkel et al.*, 2014]. For details see supplementary material and methods.

Statistical analysis of archaeal community

Statistical analysis was performed with the PAST 3.14 software [*Hammer et al.*, 2001]. Canonical correlation analysis (CCA) was performed with 7 environmental parameters (chloride, pH, conductivity, methane, sulfate, manganese, iron, and nitrate) as explanatory variables and relative abundance of archaeal genera to families. Explanatory variables were standardized by log10 transformation prior to computation, with the exception of pH and conductivity. Chloride, pH and conductivity were used to account for the marine influence of seawater penetration into the permafrost. The significance of canonical axes was tested via permutation computed for N = 999. Spearman correlation analysis was performed with the implemented tools in PAST 3.14.

Modeling of methane oxidation rates in submarine permafrost

For the modeling we used the highest change in stable isotope signature of dissolved methane in both cores to calculate the fraction of produce CH_4 that got oxidized ($f_{ox,i}$). For that we used the formula [*Liptay et al.*, 1998]:

$$f_{ox,i} = \frac{\delta_o - \delta_p}{1000 * (\propto_{ox} - \propto_{trans})}$$

δ_o and δ_p are the $\delta^{13}C$ values (in ‰) of CH_4 in the oxidized submarine permafrost layers (>-37‰) and of CH_4 produced or trapped in subjacent submarine permafrost layers (< -52‰), respectively. α_{ox} and α_{trans} are the fractionation factors for anaerobic oxidation of CH_4 and CH_4 transport, respectively.

We assumed that CH_4 is transported by diffusion and used a fractionation factor for soil of α_{trans} =1.001 [*Preuss et al.*, 2013]. Fractionation factors (α_{ox}) for sulfate-dependent (S-) AOM in

marine enrichments range between 1.009 -1.039 [*Holler et al.*, 2009]. Therefore, we used the highest and lowest value for calculations. Since the submarine permafrost is a former freshwater system we also used fractionation factors for S-AOM (α_{ox}= 1.030) [*Schubert et al.*, 2011], iron-dependent (Fe-) AOM (α_{ox}= 1.031) [*Nordi et al.*, 2013], nitrate-dependent (N-) AOM (α_{ox}= 1.032) [*Norði and Thamdrup*, 2014] and extracellular electron transfer (EEL-) AOM (α_{ox}= 1.0174) [*Gao et al.*, 2017], latter likely reflecting humic acids as potential electron acceptor. Calculated fractions of oxidized methane for the low marine S-AOM and the EEL-AOM revealed values over 1 and seems to not represent suitable AOM fractionation factors and were not considered further.

To compare the AOM activity of submarine permafrost to that of other habitats, we took the lowest, highest and average methane concentration of ice-bonded permafrost for both cores and calculated the methane release rate due to permafrost degradation rate for the cores. The permafrost degradation rate is calculated by the mean coastal erosion rate and the permafrost table depth [*Winterfeld et al.*, 2011; *Overduin et al.*, 2015] and gave values of 0.6 cm per year for C2, and 5.3 cm per year for BK2 [*Günther et al.*, 2013b], respectively. Assuming the AOM activity of our cores to be representative for submarine permafrost, we further extrapolated methane concentration to the whole area of submarine permafrost (3 million square kilometers) [*Schuur et al.*, 2015]. As last step we used the highest and lowest fraction of methane that got oxidized to calculate specific rates for both cores.

Acknowledgements

We thank Antje Eulenburg, Ute Bastian, Katja Hockun, Cornelia Karger, Maria Bade and Anke Saborowski for excellent laboratory support. We further thank Aleksandr Maslov (SB RAS, Mel'nikov Permafrost Institute, Yakutsk, Russia) who provided indispensable drilling expertise. We further thank Annika Vaksmaa of Radboud University, Nijmegen to kindly provide an ANME-2d *mcrA* standard. We thank Tiksi Hydrobase staff members Viktor Bayderin, Viktor Dobrobaba, Sergey Kamarin, Valery Kulikov, Dmitry Mashkov, Dmitry Melnichenko, Aleksandr Safin, and Aleksandr Shiyan for their field support and Birgit Schwinge (Universität Hamburg) for her help with the methane isotope measurements. We further thank Aurèle Vuillemin for helpful discussion on the manuscript and two anonymous reviewers for good comments and suggestions to improve the manuscript.

5 Manuscript III - Microbial community composition and abundance after millennia of submarine permafrost warming

Abstract

Warming of the Arctic led to an increase of permafrost temperatures by about 0.3°C during the last decade. Permafrost warming is associated with increasing sediment water content, permeability and diffusivity and could on the long-term alter microbial community composition and abundance even before permafrost thaws. We studied the long-term effect (up to 2500 years) of submarine permafrost warming on microbial communities along an onshore-offshore transect on the Siberian Arctic Shelf displaying a natural temperature gradient of more than 10 °C. We analysed the in-situ development of bacterial abundance and community composition through total cell counts (TCC), quantitative PCR of bacterial gene abundance and amplicon sequencing, and correlated the microbial community data with temperature, pore water chemistry and sediment physicochemical parameters. On time-scales of centuries, permafrost warming coincided with an overall decreasing microbial abundance whereas millennia after warming microbial abundance was similar to cold onshore permafrost. In addition, the dissolved organic carbon content of all cores was lowest in submarine permafrost after millennia-scale warming. Based on correlation analysis TCC unlike bacterial gene abundance showed a significant rank-based negative correlation with increasing temperature while bacterial gene copy numbers showed a strong negative correlation with salinity. Bacterial community composition correlated only weakly with temperature but strongly with the porewater stable isotopes δ18O and δD, and with depth. The bacterial community showed substantial spatial variation and an overall dominance of Actinobacteria, Chloroflexi, Firmicutes, Gemmatimonadetes and Proteobacteria which are amongst the microbial taxa that were also found to be active in other frozen permafrost environments. We suggest that, millennia after permafrost warming by over 10°C, microbial community composition and abundance show some indications for proliferation but mainly reflect the sedimentation history and paleo-environment and not a direct effect through warming.

Introduction

Temperatures in high-latitude regions have been rising twice as fast as the global average over the last 30 years [*IPCC in Climate Change 2013*, 2013] and are predicted to experience the globally strongest increase in the future [*Kattsov et al.*, 2005; *IPCC in Climate Change 2013*, 2013]. In the northern hemisphere, 24 % of the land surface [*Zhang et al.*, 2003] and large areas of the Arctic shelves are underlain by permafrost [*Brown et al.*, 1997]. With 1672 Pg carbon [*Schuur et al.*, 2008], the northern circumpolar permafrost zone stores about twice as much carbon as currently found in the atmosphere [*Zimov et al.*, 2006; *Schuur et al.*, 2009]. About 88% of this carbon occurs in permafrost soils and deposits [*Tarnocai et al.*, 2009]. Permafrost harbours numerous ancient but viable cells [*Wagner et al.*, 2007; *Gilichinsky et al.*, 2008; *Koch et al.*, 2009; *Mackelprang et al.*, 2011; *Graham et al.*, 2012; *Bischoff et al.*, 2013] that can remain active at extremely low temperatures [*Rivkina et al.*, 2000; *Hultman et al.*, 2015]. With increasing permafrost age, microbial communities show adaptations to the permafrost biophysical environment and specialize towards long-term survival strategies such as increased dormancy, DNA repair or stress response [*Johnson et al.*, 2007; *Mackelprang et al.*, 2017]. Following the trend of air temperature increase in the northern hemisphere, continuous permafrost warmed by about 0.3°C over the last decade at a global scale [*Biskaborn et al.*, 2019]. Warming of permafrost can substantially increase liquid water content, sediment diffusivity and permeability [*Rivkina et al.*, 2000; *Watanabe and Mizoguchi*, 2002; *Overduin et al.*, 2008] potentially mobilizing carbon in the form of trapped methane [*Shakhova et al.*, 2010a, 2010b, 2014; *Portnov et al.*, 2013; *Thornton et al.*, 2016]. Microbial community composition was reported to be responsive to temperature changes [*Zogg et al.*, 1997; *Zhang et al.*, 2005; *Weedon et al.*, 2012; *Luo et al.*, 2014; *Rui et al.*, 2015; *Xu et al.*, 2015]. However, results on the extent of these community changes and their dependence on exposure time are contradictory [*Allison et al.*, 2010; *Schindlbacher et al.*, 2011; *Xiong et al.*, 2014; *Zhang et al.*, 2016; *Weedon et al.*, 2017; *Walker et al.*, 2018]. In general, the microbial community response to warming appears to be delayed [*DeAngelis et al.*, 2015] and the effect of warming might take decades to affect the microbial community composition [*Rinnan et al.*, 2007; *Radujković et al.*, 2018]. Not only microbial community composition can be responsive to temperature but also microbial abundance especially in systems with weak energy constraints. Microbial abundance correlates with enzymatic activities and methane production [*Taylor et al.*, 2002; *Waldrop et al.*, 2010], which are sensitive to temperature. Microbial growth, respiration and carbon uptake can correlate with microbial biomass [*Walker et al.*, 2018]. Thus, substantial permafrost warming

on long time-scales could affect microbial community composition and abundance before permafrost thaws.

Submarine permafrost provides an analogue for rising permafrost temperatures over time-scales of centuries and millennia. Submarine permafrost of the Arctic Sea shelves originally formed under terrestrial (subaerial) conditions and was inundated by post-glacial sea level rise during the Holocene [*Romanovskii and Hubberten*, 2001]. Upon sea transgression, permafrost degraded over thousands of years as the relatively warm ocean water warmed the submerged seafloor. Mean annual bottom water temperatures in the Laptev Sea (East Siberian Arctic shelf) are 12 to 17 °C warmer than the annual average surface temperature of terrestrial permafrost [*Romanovskii et al.*, 2005]. Even today, new submarine permafrost is created by erosion of Arctic permafrost coasts [*Fritz et al.*, 2017], which account for 34% of the coasts worldwide [*Lantuit et al.*, 2012]. In a recent study, we compared submarine sediment cores from two locations on the Siberian Arctic Shelf and looked at the combined effect of permafrost inundation time and seawater intrusion on microbial communities. We showed that flooding by sea water reduced permafrost bacterial abundance and changed bacterial community composition due to the penetration of seawater into a former freshwater habitat [*Mitzscherling et al.*, 2017]. It was suggested that in addition to the effect of seawater infiltration, the sediment warming taking place over millennia could lead to proliferation. However, the specific effect of long-term permafrost warming independent of thawing has not been assessed so far. Here we hypothesize that millennial-scale permafrost warming directly increases microbial abundance and alters microbial community composition. We used submarine permafrost sediments of comparable age and physicochemical properties that differed in temperature by more than 10 °C due to different periods of inundation and sediment warming and assessed total microbial and bacterial abundances and community composition relative to temperature, pore-water chemistry and sedimentation history.

Materials and Methods

Study site and drilling

The study area (~73°60'N, 117°18'E) is situated in the western part of the Laptev Sea, on the East Siberian Arctic Shelf (Fig. 5-1). Mean annual bottom water temperatures in the Laptev Sea range between -1.8 °C to -1 °C [*Wegner et al.*, 2005] leading to sediment temperatures of -1.0 °C and -2.0 °C within the largest part of the shelf [*Romanovskii et al.*, 2004]. We investigated four cores (C1-C4, Fig. 5-2a) that were retrieved along an onshore-offshore transect in the

coastal region of Cape Mamontov Klyk in 2005 [*Overduin*, 2007a; *Rachold et al.*, 2007]. Cores were named after the order of drilling and we kept this order (C1, C4, C3, C2) for better comparability with previous studies [*Overduin et al.*, 2008; *Koch et al.*, 2009; *Mitzscherling et al.*, 2017; *Winkel et al.*, 2018].

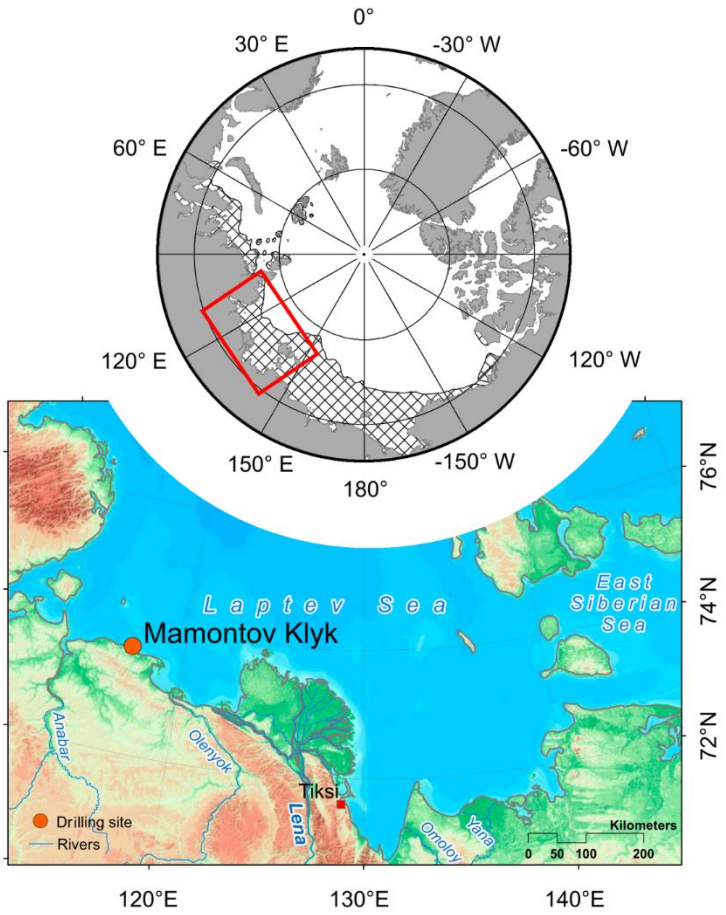

Figure 5-1: Geographical location of the study site. Location of the Laptev Sea on a circumpolar perspective map and the potential extent of submarine permafrost (striped area, based on [*Brown et al.*, 2002]), as well as the geographical location of the drilling site at Cape Mamontov Klyk in the western Laptev Sea. (modified from [*Overduin et al.*, 2015]).

From onshore to offshore all cores were characterized by an increase in water depth, in depth to the ice-bonded permafrost table (Fig. 5-2a, Table C-1) and in ground temperature (Table C-2) [*Overduin*, 2007a; *Rachold et al.*, 2007]. The transect was characterized by a temperature gradient that covered an increment of more than 10 °C compared to the onshore permafrost. Thereby, each core displayed its own unique temperature range (Fig. 5-2b).

Assuming a constant mean annual coastal erosion rate of 4.5 m yr^{-1} [*Grigoriev*, 2008] the drill site located furthest offshore (C2, 11.5 km off the coast) was inundated approximately 2500 years ago [*Rachold et al.*, 2007]. Accordingly, the drill sites C3 and C4, located 3 km and 1 km off the coast, were inundated around 660 and 220 years ago, respectively. More recent analysis based on remote sensing shows that 40-year coastal erosion rates for the same stretch of coastline between 1965 and 2007 were slower (about 2.9 m yr^{-1}) [*Günther et al.*, 2013b], which would translate into even longer inundation periods. However, in the present study we refer to *Grigoriev* [2008], which are based on direct observations of coastal erosion at the C1 coring site. Drilling was performed with a hydraulic rotary-pressure system (Drilling Technologies Factory, St. Petersburg, Russia, Model URB-2A-2) and without the use of any drilling fluid. All samples were frozen immediately after recovery and were kept at -22 °C until further processing. Temperature measurements at all sites were done using thermistors and infra-red sensors [*Junker et al.*, 2008].

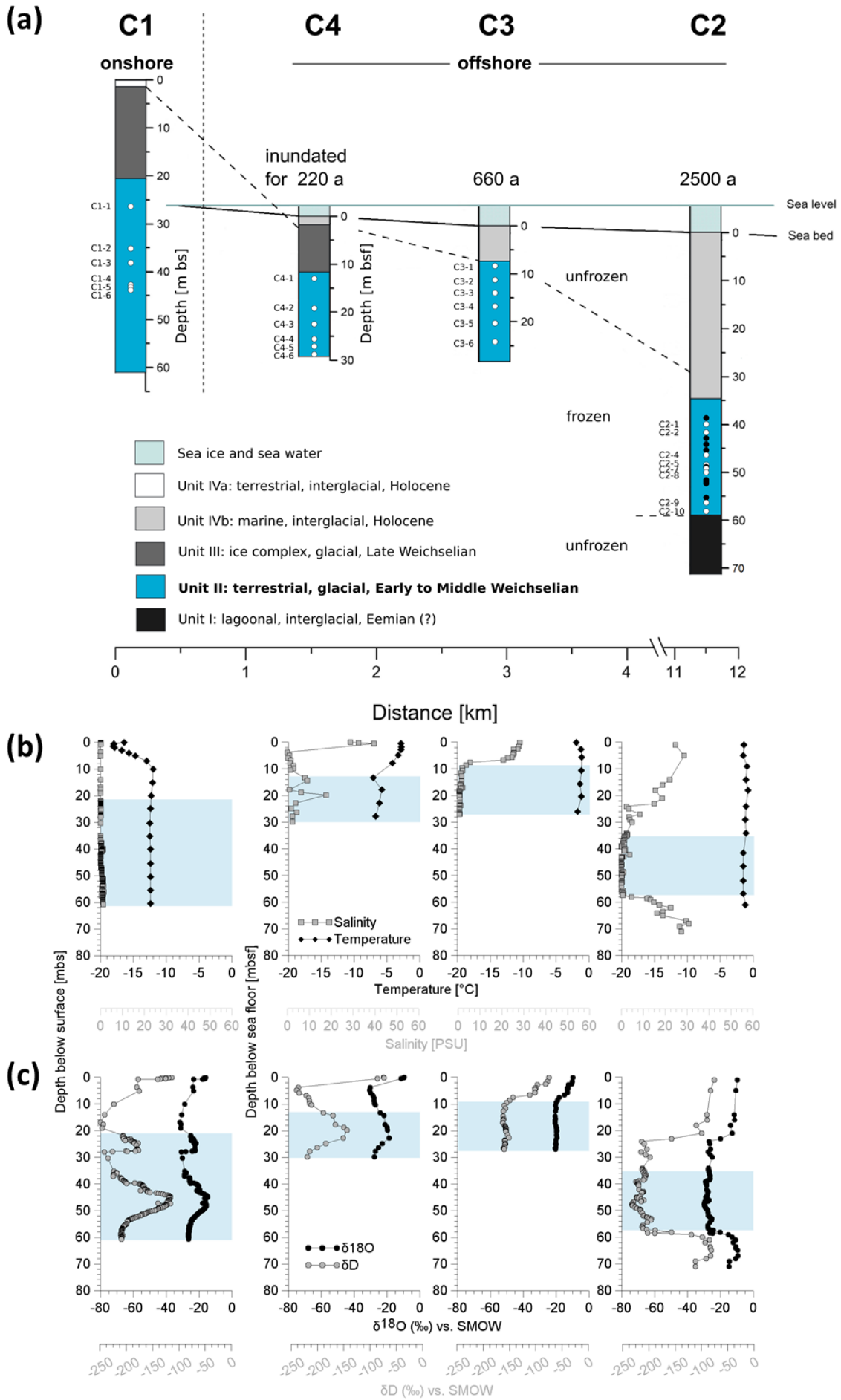
(a)
C1
C4
C3
C2
onshore
offshore
inundated for 220 a
660 a
2500 a
Sea level
Sea bed
Depth [m bs]
Depth [m bsf]
unfrozen
frozen
unfrozen
C1-1
C1-2
C1-3
C1-4
C1-5
C1-6
C4-1
C4-2
C4-3
C4-4
C4-5
C4-6
C3-1
C3-2
C3-3
C3-4
C3-5
C3-6
C2-1
C2-2
C2-4
C2-5
C2-7
C2-8
C2-9
C2-10
Sea ice and sea water
Unit IVa: terrestrial, interglacial, Holocene
Unit IVb: marine, interglacial, Holocene
Unit III: ice complex, glacial, Late Weichselian
Unit II: terrestrial, glacial, Early to Middle Weichselian
Unit I: lagoonal, interglacial, Eemian (?)
Distance [km]
(b)
Depth below surface [mbs]
Depth below sea floor [mbsf]
Salinity
Temperature
Temperature [°C]
Salinity [PSU]
(c)
δ18O
δD
δ18O (‰) vs. SMOW
δD (‰) vs. SMOW

Figure 5-2: Overview of the coring transect, position and characteristics of the terrestrial and the submarine sediment cores. a) Periods of inundation are indicated above each submarine core. Core depth of the terrestrial core is given in m below surface (m bs) and depth of the submarine cores in meters below seafloor (m bsf). The core depths are proportional to each other, whereas the distance scale is only schematic. Affiliation of sediment deposits to discrete sediment units (Unit I - IVb), accumulated under similar environmental conditions in the same glacial or interglacial period, are distinguished by colours. Dots show the depth of the molecular samples. White dots represent samples from this study. Their denomination is indicated to the left. Black dots represent samples from a previous study. **b)** Depth profiles of temperature (black diamonds) and salinity (grey squares) as well as of c) the pore water stable isotopes $\delta^{18}O$ (black circles) and δD (grey circles) from the cores C1, C4, C3 and C2. The blue shaded area represents Unit II.

Sample selection

Each of the four drill cores exhibited different sedimentological units. Lithostratigraphic Unit II was identified in all cores (Fig. 5-2a) and was entirely located within the ice-bonded permafrost. Irrespective of the permafrost temperature Unit II sediments of all cores were cemented mainly by pore ice but were also characterized by terrestrial permafrost features like ice lenses, ice veins and ice-wedges. Photographs of [*Winterfeld et al.*, 2011] show similar ice and sediment structures of the terrestrial core C1 and the outermost submarine core C2. Depth location of Unit II within each core can be found in Table C-1. This unit was deposited during the late Pleistocene, was warmed without thawing, and had so far remained unaffected of seawater infiltration. On the basis of a PCA analysis (see next chapter and Fig. 5-3) and previous lithostratigraphic descriptions [*Winterfeld et al.*, 2011] all further analysis was conducted on samples from Unit II. The ages of the sediment are published in *Winterfeld et al.* [2011]. The present study refers to sediment ages determined by optically stimulated luminescence (OSL) on quartz and infrared optically stimulated luminescence (IR-OSL) on feldspars. OSL ages of Unit II sediments from core C1 range from 30.5 ± 2.0 ka at 22 m below surface (m bs) to 114 ± 6 ka at 50 m bs. OSL ages range from 97 ± 6 to 112 ± 8 ka between 23 and 30 m below seafloor (m bsf) in core C3 and from 133 ± 8 to 148 ± 14 ka between 37 and 53 m bsf, and increase with depth. IR-OSL ages date back to 59 ± 5.8 ka at around 15 m bsf in C4 and 86 ± 5.9 ka at 44 m bsf and 111 ± 7.5 ka at 77 m bsf in C2. Consequently, sediments of Unit II were deposited during the early to middle Weichselian [*Winterfeld et al.*, 2011].

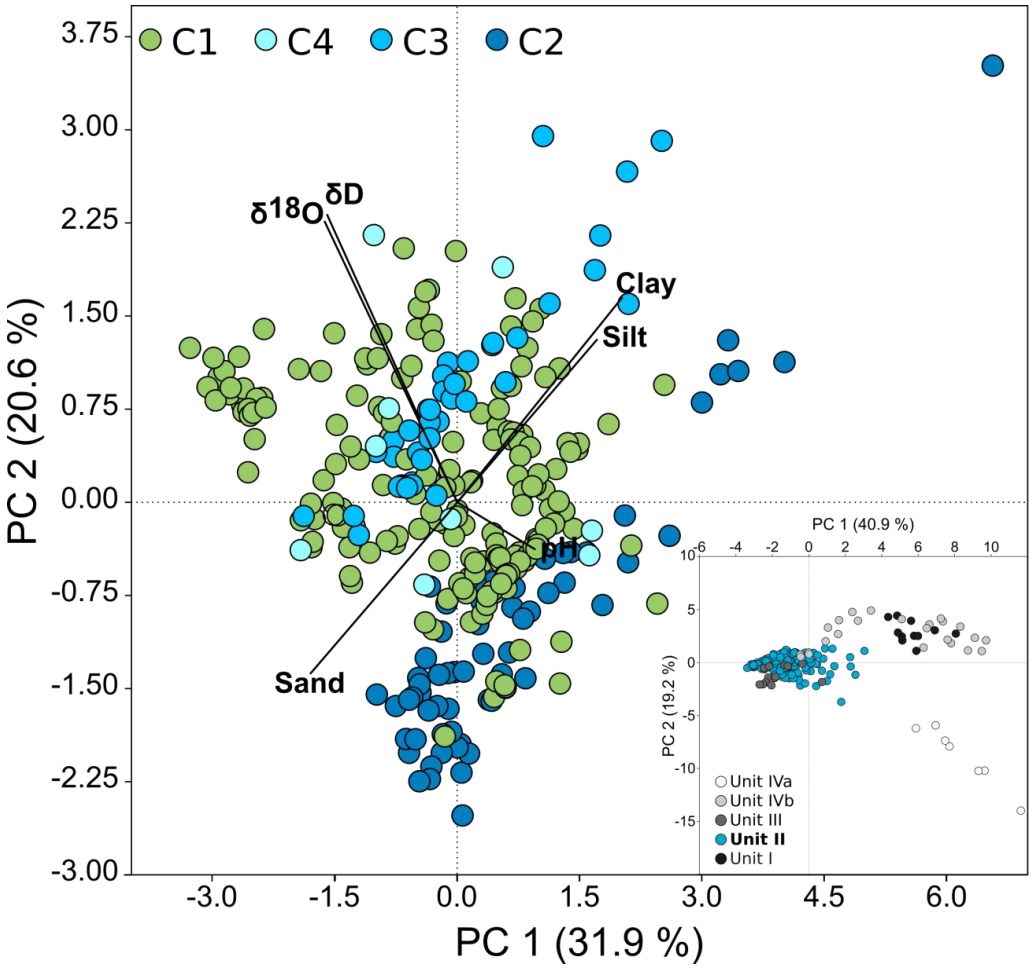

Figure 5-3: PCA of environmental, sedimentological and pore water data from Unit II of all four cores with PC 1 explaining 31.9% and PC 2 explaining 20.6 % of the variance between samples. Vectors show selected physicochemical factors that are mainly responsible for the variance between samples (see loadings plot Fig. C-4). C1: n = 183, C2: n = 66, C3: n = 38, C4: n = 9. Outliers located outside the 95% ellipses were removed. The insert presents all samples of the onshore-offshore transect coloured irrespective of the cores by Unit (n = 361).

For molecular analyses we took 6 replicate samples from each of the cores C1 (C1-1 – C1-6), C4 (C4-1 – C4-6) and C3 (C3-1 – C3-6) and 8 replicates from core C2 (C2-1, C2-2, C2-4, C2-5, C2-7, C2-8, C2-9, C2-10) (Fig. 5-2a). Those replicates were located at different depths within Unit II (Table C-4). Samples from C1 were located around 27 to 44 meters below surface, while samples from C4 were taken between 13 and 30 meters below the seafloor, samples from C3 between 9 and 25 m bsf, and samples from C2 between 40 and 58 m bsf. Unit II was mainly composed of sands with varying proportions of silt and to a minor extent of clay, and a frequent occurrence of wood fragments, plant detritus interlayers and small peat inclusions [*Winterfeld et al.*, 2011]. Both, sandy as well as organic-rich deposits were represented by three replicates

in C1, C4 and C3 and four replicates in C2 (Table C-4). Furthermore, to check for reproducibility we included samples from C2 retrieved in a previous study [*Mitzscherling et al.*, 2017] (sample names CK12xx). In order to prevent contamination caused by the drilling equipment we took the subsamples from the centre of the core. Subsampling was performed in a climate chamber under freezing conditions by using sterile tools. Thus, a contamination of the samples can be excluded.

Pore water and sediment analyses

Pore water of segregated ground ice was extracted from thawed subsamples of the sediment cores using rinsed Rhizons™ (0.15 µm pore diameter). Electrical conductivity, salinity, cation and anion concentrations, stable isotope concentrations ($\delta^{18}O$, δD), and pH were measured for 183 samples of C1, 67 samples of C2, 38 samples of C3 and 10 samples of C4 in Unit II (Table C-3). Electrical conductivity, salinity and pH were measured with a WTW MultiLab 540 using a TetraConTM 325 cell referenced to 20°C. Total dissolved element concentrations (Ba^{2+}, Ca^{2+}, K^{+}, Mg^{2+}, Na+, Si_{aq}) were determined by inductively coupled plasma optical emission spectrometry (ICP-OES, Optima 3000XL, Perkin-Elmer, Waltham) [*Boss and Frieden*, 1989]. Dissolved anion concentrations (Cl^{-}, SO_4^{2-}, Br^{-}, NO_3^{-}) were measured using a KOH eluent and a latex particle separation column on a Dionex DX-320 ion chromatographer [*Weiss*, 2001]. The pore water stable isotopes (δD and$\delta^{18}O$) of segregated ground ice were determined following [*Meyer et al.*, 2000] using a Finnigan MAT Delta-S mass spectrometer in combination with two equilibration units (MS Analysetechnik, Berlin).

Dissolved organic carbon (DOC) was measured as non-purgeable organic carbon via catalytic combustion at 680 °C using a total organic carbon analyzer (Shimadzu TOC-VCPH instrument) on samples treated with 20 µl of 30% supra-pure hydrochloric acid. The ice content was determined gravimetrically. Grain sizes were measured with a Coulter LS 200 laser particle size analyzer. The total organic carbon (TOC) was measured with the element analyser VARIO MAX C, while total carbon (TC), total nitrogen (TN) and total sulfur (TS) contents were determined with an elemental analyzer (Elementar Vario EL III).

DNA extraction

Core subsamples were homogenized in liquid nitrogen and DNA was extracted from ~5 g of sediment using a modified protocol of [*Zhou et al.*, 1996]. The method was described before [*Mitzscherling et al.*, 2017] and in the following we refer to these samples as molecular samples. Quality of the extracted genomic DNA was assessed via gel electrophoresis (Fig. C-1). DNA

concentration was quantified with the Qubit2 system (Invitrogen, HS-quant DNA) and the crude DNA was purified using the HiYield PCR Clean-Up & Gel-Extraction Kit (SLG) to reduce PCR inhibitors prior to PCR applications.

Quantification of the bacterial 16S rRNA gene

Quantitative PCR was performed using the CFX Connect™ Real-Time PCR Detection System (Bio-Rad Laboratories, Inc.) and the primers S-D-Bact-0341-b-S-17 and S-D-Bact-0517-a-A-18 targeting the bacterial 16S rRNA gene (Table C-5). Each reaction (20 µl) contained 2x concentrate of iTaq™ Universal SYBR® Green Supermix (Bio-Rad Laboratories), 0.5 µM of each the forward and reverse primer, sterile water and 2 µl of template DNA. The qPCR assays comprised the following steps: initial denaturation for 3 min at 95 °C, followed by 40 cycles of denaturation for 3 sec at 95 °C, annealing for 20 sec at 58.5 °C, elongation for 30 sec at 72 °C and a plate read step at 80 °C for 0.3 sec. Melt curve analysis from 65-95 °C with 0.5°C temperature increment per 0.5 sec cycle was conducted at the end of each run. The qPCR assay was calibrated using known amounts of PCR amplified gene fragments from a pure *Escherichia coli* culture. For each sample three technical replicates were analysed and DNA templates were diluted 5- to 100-fold prior to qPCR analysis. The PCR efficiencies based on standard curves were calculated using the BioRad CFX Manager software. They varied between 93 and 99%. All cycle data were collected using the single threshold C_q determination mode.

Total cell counts

Preparation and quantification of the total cell abundance per gram sediment were performed after [*Llobet-Brossa et al.*, 1998]. The modified protocol was described before by *Mitzscherling et al.* [2017]. Briefly, cells were fixed with 4% paraformaldehyde in phosphate-buffered saline (PBS). After incubation, the sediment was pelleted by centrifugation for 5 min at 9600 g and washed in sterile filtered PBS. Two subsamples of each sample were diluted in PBS and filtered onto a polycarbonate membrane filter (0.2 µm) by applying a vacuum. Total cell counts were determined by SYBR Green I. Fluorescence microscopy was performed with a Leica DM2000 fluorescence microscope using the FI/RH filter cube. A magnification of 100x was used to count cells of either 200 fields of view or until 1000 cells were counted. We counted two filters per sample.

High throughput Illumina16S rRNA gene sequencing and analysis

Sequencing of each sample was performed in two technical replicates. The sequencing primers that were used in this study only target bacteria and comprised different combinations of barcodes (Table C-6). PCR amplification was carried out with a T100™ Thermal Cycler (Bio-Rad Laboratories, CA, USA). The PCR mixtures (25 µl) contained 1.25 U of OptiTaq DNA Polymerase (Roboklon), 10x concentrate buffer C (Roboklon), 0.5 µM of the sequencing primers S-D-Bact-0341-b-S-17 and S-D-Bact-0785-a-A-21 (Table C-5), dNTP mix (0.2 mM each), additional 0.5 mM of $MgCl_2$ (Roboklon), PCR-grade water, and 2.5 µl of template DNA. PCR conditions comprised an initial denaturation at 95°C for 5 min, followed by 35 cycles of denaturation (95°C for 30 s), annealing (56°C for 30 s) and elongation (72°C for 1 min), and a final extension step of 72°C for 10 min. The PCR products were purified from agarose gel with the HiYieldPCR Clean-Up and Gel-Extraction Kit (Südlabor, Gauting, Germany) and were quantified with the QBIT2 system (Invitrogen, HS-Quant DNA). They were mixed in equimolar amounts and sequenced from both directions (GATC Biotech, Konstanz) based on the Illumina MiSeq technology. The library was prepared with the MiSeq Reagent Kit V3 for 2×300 bp paired-end reads. The 15% PhiX control v3 library was used for better performance due to different sequencing length.

Sequence analysis and bioinformatics

The data analysis of raw bacterial sequences started with the quality control of the sequencing library by the tool FastQC (quality control tool for high-throughput sequence data http://www.bioinformatics.babraham.ac.uk/projects/fastqc/ (last access: 10 Octover 2018) by Simon Andrews). The tool CutAdapt [*Martin*, 2011] was used to demultiplex the sequence reads according to their barcodes and to subsequently remove the barcodes. Forward and reverse sequenced fragments with overlapping sequence regions were merged using PEAR [*Zhang et al.*, 2014b], and the nucleotide sequence orientation was standardized. Low-quality sequences were filtered and trimmed by Trimmomatic [*Bolger et al.*, 2014], and chimeras were removed by Chimera. Slayer. Finally, the QIIME pipeline was used to cluster sequences into operational taxonomic units (OTUs) and to taxonomically assign them employing the SILVA database (release 123) with a cutoff value of 97% [*Caporaso et al.*, 2010].

Statistics

Prior to statistical analysis, absolute singletons and $OTU_{0.03}$ (operational taxonomic units of clustered sequences with 97% similarity level) not classified as bacteria or classified as

chloroplasts or mitochondria were removed. In addition, $OTU_{0.03}$ with reads <0.5% of total read counts in each sample were removed to reduce background noise. The background noise was estimated with the help of a positive control (*E. coli*), where the number of OTUs is known prior to sequencing. Absolute read counts were transformed into relative abundances in order to standardize the data and to make technical replicates comparable. Relative abundances of technical replicates were merged to mean relative abundances for bacterial community analysis i.e. the bubble plot and non-metric multidimensional scaling analysis (NMDS). Samples having < 15.000 raw reads were checked for divergent relative abundances within duplicates (Table C-7) and excluded from the calculation of mean relative abundances when the discrepancy was too big. Variation in $OTU_{0.03}$ composition, 16S rRNA gene and total cell abundance between samples and among drill sites, as well as correlations of the abundance and $OTU_{0.03}$ composition with environmental parameters were assessed using the Past 3.14 software [*Hammer et al.*, 2001] and R, especially the vegan and MASS packages. Principal component analyses (PCA) based on Euclidean distance were used to assess variation in environmental variables across the different sediment units and within Unit II. Prior to analysis, all environmental data were standardized by subtracting the mean and dividing by standard deviation. To assess the correlations of bacterial and microbial abundance with environmental parameters the rank-based Spearman correlation was calculated. The Bray-Curtis dissimilarity was used to assess the beta diversity of the microbial communities in a NMDS plot. Environmental factors that might influence its composition were determined by an environmental fit into the ordination. The significance of the variance introduced by the identified environmental factors was tested using a permutational approach as implemented in the adonis function of the vegan package. Factors were tested for auto-correlation as implemented in the corrplot package. A linear model of the remaining factors was subject to a redundancy analysis which was tested for signficance using the analysis of variance (ANOVA). ANOVA and the Tukey's pairwise post-hoc test were conducted to test whether DOC concentrations of the cores differed.

Results

Physicochemical pore water and sediment properties

Temperature (Fig. 5-2b) of Unit II was lowest in the terrestrial borehole (C1, constantly at around -12.4 °C at the time of drilling [*Junker et al.*, 2008] and between -12.0 and -12.5 °C recently measured over a 2 year period [*Kneier et al.*, 2018]) and increased with distance to the shore. According to [*Junker et al.*, 2008] C4 exhibited a temperature range from -7.1 to -5.8 °C.

Ground temperatures of C3 and C2 were similar with mean values of -1.4 and -1.5 °C, respectively, and showed marginal variation. C3 exhibited a slightly higher mean temperature than the longest inundated core C2.

Overall, the salinity of Unit II was low (Fig. 5-2b, [*Winterfeld et al.*, 2011]). In C4, the drill site located closest to the coast, Unit II had the highest pore water salinity (mean = 5.6 PSU) ranging from 0.9 to 17.6 PSU (Table C-2), which spans freshwater to mesohaline water but is much below seawater salinities. In comparison, bottom-water salinities at the drill sites ranged between 29.2 and 32.2 PSU [*Overduin et al.*, 2008]. Salinity in C3 reached a mean value of 1.1 PSU. The submarine core furthest offshore (C2) and the terrestrial core (C1) had a mean pore water salinity of around 0.8 and 0.5 PSU, respectively. The stable isotopes δD and $\delta^{18}O$ of the sediment cores C1 and C4 exhibited similar mean values of -22 ‰ for $\delta^{18}O$ and around -178 ‰ for δD, albeit a greater variance in C1 (Fig. 5-2c, Table C-2). Sediments of C3 were characterized by higher and constant isotope values of around -20 ‰ for $\delta^{18}O$ and -158 ‰ for δD. In core C2, the isotope values were smaller with mean values of -28 ‰ for $\delta^{18}O$ and -213 ‰ for δD (Table C-2).

DOC concentrations were lowest in Unit II of core C2, the core furthest offshore, and ranged from 4 to 41 mg C L^{-1}, with a mean value of 17 mg C L^{-1} (Fig. C-2). Towards the coast the DOC content increased to mean values of 43 mg C L^{-1} in C3 and 96 mg C L^{-1} in C4. The terrestrial core C1 had a mean DOC concentration of around 48 mg C L^{-1} with values ranging from 4 to 305 mg C L^{-1}, thereby having by far the highest measured DOC concentration of all cores. The TOC content in this Unit II was generally very low with mostly < 0.5 wt%. While C1 and C4 had lowest mean values of 0.17 wt%, the TOC content increased with distance to the coast to 0.22 wt% in C3 and 0.33 wt% in C2 (Table C-3). The pH of Unit II sediments ranged from slightly acidic to slightly alkaline values. In cores C1 and C4 the pH ranged from 5 to 7.9, whereas values of C2 and C3 were higher ranging from pH 6.5 to 8.0. Mean pH values of all cores were around pH 7 to 7.5. Other pore water data like anion and cation concentrations, conductivity, CNS, grain sizes and the gravimetrically determined water content can be found in Table C-3. The whole dataset is also deposited on PANGAEA [*Mitzscherling et al.*, 2018].

All environmental, sedimentological and pore water data (Table C-3) were used to conduct principal component analyses (PCA) to check for the level of similarity within Unit II. Unit II formed a dense cluster relative to the other sediment units (Fig. 5-3 Insert). Focusing on samples from Unit II only (Fig. 5-3) confirmed highly similar physicochemical characteristics of this unit in all cores even though C2 and C3 clustered along the axis PC2, while C1 and C4 were

more randomly scattered. Variance between samples was mainly explained by grain sizes, pore water stable isotope concentrations and to a lesser extent by pH.

Microbial abundance

Overall microbial abundance decreased from onshore to offshore (C1, C4, C3) and had increased again in the drill site located furthest from the coast (C2). The terrestrial permafrost core C1 and the submarine core C2 had highest DNA concentrations (Fig. C-2), total cell counts (TCC) (Fig. 5-4a) and bacterial 16S rRNA gene copy numbers of all cores (Fig. 5-4b). Lowest DNA concentrations and TCC were observed in core C3, whereas lowest numbers of bacterial 16S rRNA gene copies were found in core C4. All three abundance measures (DNA concentrations, TCC, and bacterial 16S rRNA gene copy numbers) significantly correlated with each other (Table C-8). DNA concentrations reached mean values of 141.6 ng g^{-1} and 106.9 ng g^{-1} in C1 and C2, respectively, whereas the mean DNA concentration in C4 and C3 were 88.5 and 19.8 ng g^{-1} (Table C-9). Mean TCC reached a value of 5 x 10^7 g^{-1} in C1. C4 and C2 had similar values of 1.3 x 10^7 g^{-1} and 1.5 x 10^7 g^{-1}, while cell numbers of C3 were one order of magnitude lower (1.5 x 10^6 g^{-1}). Bacterial 16S rRNA gene copy numbers usually exceeded TCC by an order of magnitude, with mean values of 1.6 x 10^8 g^{-1} and 2.9 x 10^8 g^{-1} in C1 and C2, but lower mean values of 3.6 x 10^7 g^{-1} and 1.7 x 10^7 g^{-1} in C4 and C3, respectively.

A correlation analysis (Table 5-1) revealed that microbial and bacterial abundance measures including DNA concentrations, 16S rRNA bacterial gene copies and TCC correlated with each other (Fig. 5-4c). They further showed a significant rank-based negative correlation with salinity ($p < 0.05$, Spearman $-0.63 \leq r_s \leq -0.35$), cations ($K^+$, Mg^{2+}, Na^+) and anions (Cl^-, Br^-) ($p < 0.05$, $-0.71 \leq r_s \leq -0.39$), and $\delta^{18}O$ ($p<0.05$, $-0.38 \leq r_s \leq -0.37$). Furthermore, DNA concentrations negatively correlated with temperature ($p < 0.05$, $r_s = -0.37$) and pH ($p < 0.05$, $r_s = -0.44$), while TCC negatively correlated with temperature ($p < 0.01$, $r_s = -0.64$) and 16S rRNA gene copies with pH ($p < 0.01$, $r_s = -0.24$). Positive correlations were found for DNA and 16S rRNA gene copies with total organic carbon (TOC, $p < 0.05$, $r_s > 0.34$) and the water content ($p < 0.01$, $r_s = 0.47$).

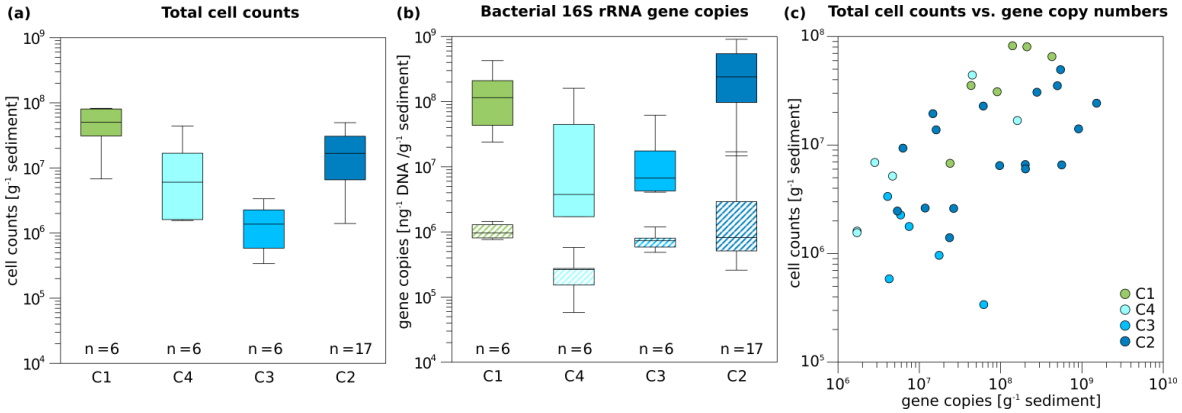

Figure 5-4: Boxplots of microbial and bacterial abundance in Unit II. a) Total cell counts and **b)** bacterial 16S rRNA gene copy numbers normalized to gram sediment wet weight (top, solid boxes) and to DNA concentration in ng (bottom, striped boxes) of the cores C1, C4, C3 and C2. Box plots contain the mean values obtained from two technical replicates of cell counts and three technical replicates of 16S rRNA gene copy numbers per biological replicate. Median lines are indicated within the boxes of which the size corresponds to ± 25% of the data, whereas the whiskers show the minimum and maximum of all data. Minimum, maximum and mean values, as well as standard deviation and sample numbers can be found in Table C-9. **c)** Correlation of total cell counts and bacterial 16S gene copy numbers g^{-1} sediment. Strength of the correlation is shown in table 1. Sample points were colored according to drill core.

Table 5-1: Spearman correlations of DNA concentration, 16S rRNA gene copy numbers normalized to gram sediment (16S Bacteria), 16S rRNA gene copy numbers normalized to ng DNA (16S/DNA) and total cell counts (TCC) with environmental and geochemical parameters. Presented is the correlation coefficient r_s. Significant negative correlations are highlighted in red and significant positive correlations are highlighted in green. Values in bold are significant (< 0.05) when omitting p-value corrections. Colour intensity represents the significance levels, from dark to light colour: $p < 0.001$; $p < 0.01$; $p < 0.05$. P-values and more data can be found in Table C-10.

	16S Bacteria	16S/DNA	TCC	Temp	Salinity	Depth [mbs/ mbsf]	Ba^{2+}	Ca^{2+}	K^{+}	Mg^{2+}	Na^{+}	Cl^{-}	SO_4^{2-}	Br^{-}	$\delta^{18}O$	δD	pH	TC	TOC	Grav. Water Content
DNA	**0.87**	**0.47**	**0.68**	**-0.37**	**-0.35**	0.30	-0.08	-0.09	**-0.39**	-0.32	**-0.39**	**-0.43**	-0.14	**-0.41**	**-0.37**	-0.33	**-0.44**	**0.40**	**0.34**	**0.47**
16S Bacteria		**0.79**	**0.61**	-0.24	**-0.48**	**0.51**	0.03	-0.20	**-0.49**	**-0.46**	**-0.57**	**-0.56**	-0.26	**-0.54**	**-0.38**	-0.33	**-0.52**	**0.44**	**0.39**	**0.47**
16S / DNA			**0.36**	-0.12	**-0.63**	**0.47**	0.04	**-0.47**	**-0.55**	**-0.60**	**-0.71**	**-0.67**	**-0.40**	**-0.66**	-0.16	-0.11	**-0.54**	0.21	0.19	0.26
TCC				**-0.64**	**-0.44**	0.26	**-0.38**	-0.23	**-0.42**	-0.37	**-0.50**	**-0.52**	-0.09	**-0.50**	**-0.37**	**-0.37**	-0.28	0.06	0.14	0.16

Bacterial community composition

The most abundant bacterial taxa were Actinobacteria (class), Chloroflexi (Gitt-GS-136, KD4-96), Clostridia (class), Gemmatimonadetes, and Proteobacteria (primarily Alpha- and Betaproteobacteria) (Fig. 5-5). *Candidatus* Aminicenantes (candidate phylum OP8) and *Candidatus* Atribacteria (candidate phylum OP9) were highly abundant in core C3, where Actinobacteria, Chloroflexi, and Gemmatimonadetes were almost absent.

Grouping patterns of the bacterial community based on the $OTU_{0.03}$ composition of the samples and the Bray-Curtis dissimilarity were visualized using a non-metric multidimensional scaling (NMDS, Fig. 5-5). The NMDS showed a clustering of samples according to their borehole location for C2 and C3, while communities of C1 and C4 were more scattered. We fitted environmental gradients with the NMDS ordination in order to test for correlation between the bacterial community compositions at each drill site with environmental parameters ($p < 0.05$). Samples located at the bottom left of the plot originated from a greater depth (C1 and C2) than samples to the top right (C3 and C4). Variance of samples from the bottom to the top was explained by rising pH, permafrost temperature and total sulphur content, while variance of samples from the left to the right side are likely explained by increasing values of Ba^{2+} and the pore water stable isotopes $\delta^{18}O$ and δD - a proxy for paleo-temperature and –climate. The bacterial community of C3 was most distinct and clustered furthest from communities of all other sites. It was linked with the pore water stable isotopes $\delta^{18}O$ and δD, Ba^{2+} and the sample depth. The variance between C1, C4 and C2 samples are explained by permafrost temperature differences across the cores (Fig. 5-2b). A subsequent permutational analysis of variance showed that depth, temperature, pH, TS, δD, $\delta^{18}O$, and Ba^{2+} contribute to the variance in the microbial community composition (Table C-11), whereof $\delta^{18}O$ and δD show a high auto-correlation. A redundancy analysis showed that the explanatory variables depth, temperature, pH and $\delta^{18}O$ significantly explain parts of the variance in the microbial composition ($p = 0.001$). Despite the overlaps within the NMDS ordination, a one-way PerMANOVA revealed that the variance between each of the clusters was significantly higher than within single clusters (Table C-12), i.e., the bacterial subpopulations of each drill site were significantly different from each other.

Figure 5-5: Relative abundance of bacterial classes from Unit II of the C1 - C4 cores. Coloured boxes and sample names below indicate the particular core. Sample names were explained earlier. Bubbles represent the mean value of relative abundances from two technical replicates.

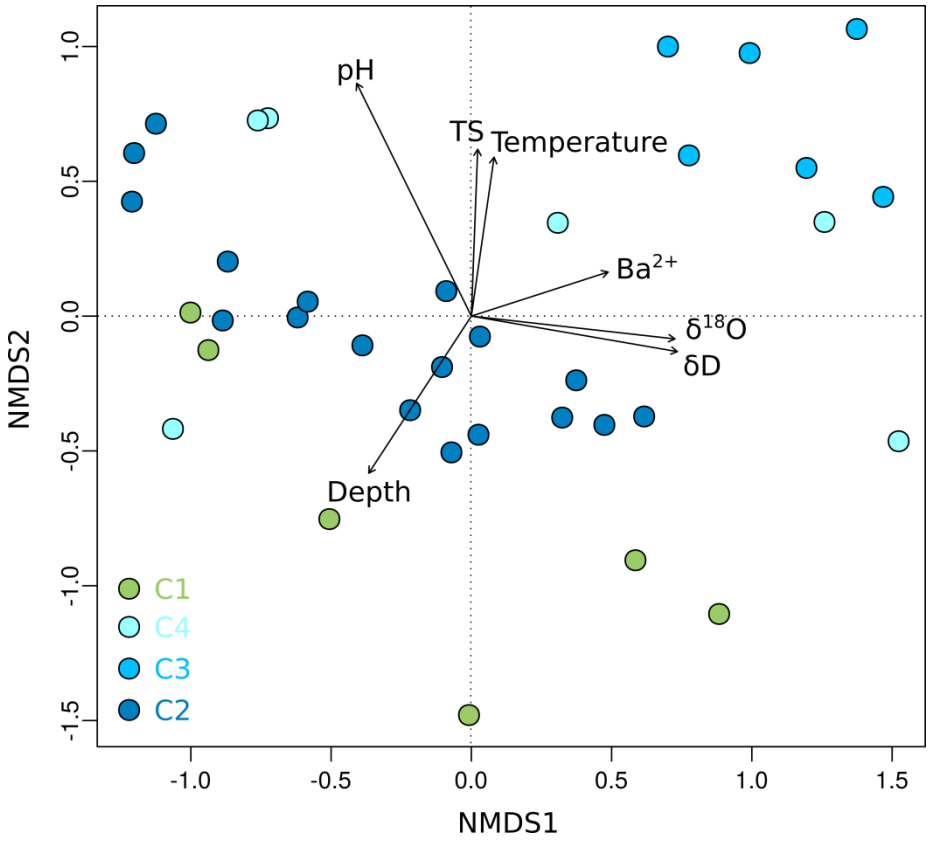

Figure 5-6: Non-metric multidimensional scaling (NMDS) plot of $OTU_{0.03}$ data from Unit II in dependence on environmental parameters. Shown are environmental factors that contribute significantly ($p < 0.05$) to the variance of the community data. The stress value of the NMDS plot is 0.13. Each dot represents the mean value of relative OTU abundances from two technical replicates. Sample depth is denoted as meters below the surface for terrestrial samples and meters below the seafloor for submarine samples.

Discussion

The present study aimed at understanding the effect of long-term permafrost warming independent of thaw on microbial community composition and abundance. The observed significant negative rank-based correlation between increasing temperature and total cell counts (TCC) contradicts our hypothesis that millennial-scale permafrost warming directly increases microbial abundance. It is, however, in line with related studies on arctic and subarctic soil microbial communities where a negative effect of increasing temperature on microbial abundance was assigned to freeze-thaw cycles [*Skogland et al.*, 1988; *Schimel et al.*, 2007] and substrate depletion [*Walker et al.*, 2018]. Both effects are, however, unlikely here. Firstly,

sample depths were always more than 10 m below surface and seafloor, respectively, and freeze-thaw cycles within the investigated Unit II can be excluded. Secondly, preservation, rather than depletion, of substrates was more likely in the two submarine cores C3 and C4, where DOC contents were comparable to that of the cold terrestrial permafrost of C1 (Fig. C-2). The degradation of DOC can be used as measure for microbial carbon turnover [*Seto and Yanagiya*, 1983] and the DOC concentration usually correlates with microbial abundance [*Smolander and Kitunen*, 2002; *Junge et al.*, 2004; *Vetter et al.*, 2010]. The cores C3 and C4 had significantly lower TCC and bacterial gene copy numbers (10^6 cells and 10^5 gene copies) than the onshore core C1 and the C2 core furthest offshore (10^7 cells and 10^6 gene copies). Thus, microbial activity and substrate utilization were likely low in C3 and C4. A negative influence of permafrost warming on microbial abundance is further challenged through some indication for microbial proliferation in core C2, which had experienced longest warming of all cores. In detail, TCC in C2 were higher than in the other submarine cores while DOC values were lower in C2, significantly different from C4 and C1 (Table C-13). Permafrost warming for more than two millennia may have enabled microbial communities to adapt to the new temperature regime and sediment properties as suggested before [*Mitzscherling et al.*, 2017]. Besides permafrost warming changing pore-water salinity had an effect on the microbial abundance. Rising permafrost temperature strongly correlates with TCC whereas salinity correlates strongest with bacterial gene copy numbers (Table 5-1). Bacterial 16S rRNA gene copy numbers were lowest in core C4 (10^5 gene copies), where pore-water salinities were elevated (electrical conductivity values >2000 µS cm^{-1}, Table C-3). Low gene copy numbers (10^5 gene copies) may result from osmotic stress that limits microbial growth [*Galinski*, 1995; *Rousk et al.*, 2011] and decreases microbial abundance in sediments [*Rietz and Haynes*, 2003; *Jiang et al.*, 2007; *Rath and Rousk*, 2015; *Wen et al.*, 2018]. We argue that the different levels of salinity are relicts of the paleo-climate and varying landscape types (e.g. thermokarst lakes and lagoons, fluvial, floodplain, Fig. C-5 and Table C-14) that formed Unit II during the last glacial cycle, i.e. the Weichselian glaciation 117 – 10 ka BP [*Svendsen et al.*, 2004]. According to the IR-OSL ages Unit II of C4 was deposited ~60 ka BP and earlier. Conductivity values in C4 that were higher than 2000 µS cm^{-1} could be the result of strong evaporation. The climate in the Laptev Sea region during the middle Weichselian (75 – 25 ka BP) was of extremely continental type characterized by low precipitation throughout the year and relative warm summers [*Hubberten et al.*, 2004]. Also, salinity values in Unit II of core C4 are lower than in the seafloor sediments of the same core but higher than in the sediment layer in between (Fig. 5-2b), supporting the idea that differences in salinity reflect the paleo-environment and climate,

and not an infiltration of seawater during the Holocene transgression. The presence of a temporary shallow thermokarst lake at the drilling site of C4 and following summer evaporation is one possible scenario leading to elevated salt concentrations [*Larry Lopez et al.*, 2007]. A strong influence of the paleo-climate on recent microbial abundance is further supported through a significant correlation between microbial abundance with $\delta^{18}O$ values (Table 5-1). The stable isotope composition of ground ice is widely used as an archive for paleo-climatic information and for the determination of ground ice genesis [*Vasil'chuk,* 1991; *Meyer et al.*, 2002a, 2002b]. Compared to the other cores, C3 for example was enriched in heavy isotope species of $\delta^{18}O$ (-20 to -15‰) and δD (-150 to -160‰), suggesting warmer temperatures at the time of deposition [*Meyer et al.*, 2002b]. As ground ice is mainly fed by summer and winter precipitation, its isotopic composition reflects the annual range of air temperatures. Isotope changes towards heavier values could also be the result of larger amounts of summer rain as well as less winter snow preserved in the ice. Assuming that IR-OSL ages of *Winterfeld et al.* [2011] are correct, sediments of C3 were deposited at around 50 ka BP and later. Thus, C3 sediments were probably deposited during a period where the extremely dry continental climate with relatively warm summers was especially pronounced (between 45 and 35 ka BP) [*Hubberten et al.*, 2004].

We suggest that microbial community composition like microbial abundance reflects the paleoclimate and sedimentation history and not a direct effect of permafrost warming. In detail, we observed a weak correlation between community composition with permafrost temperature and a strong correlation with pore water stable isotope values and depth, i.e. age. This suggestion is supported by similar findings in sea sediments as well as in lacustrine sediments. Microbial taxa of Arabian Sea sediments reflected past depositional conditions and exhibited paleo-environmental selection [*Orsi et al.*, 2017], while the microbial population in sediments of Laguna Potrok Aike in Argentina changed in response to both past environmental conditions and geochemical changes during burial [*Vuillemin et al.*, 2018]. The microbial communities in core C3 which were most distinct from the other locations (Fig. 5-6) may thus reflect the higher paleo-temperatures and different proportions of summer and winter precipitation discussed earlier. The strongest correlation of the bacterial community composition was, however, found with pH. Soil pH is a major factor controlling the bacterial diversity, richness and community composition on a continental scale [*Fierer and Jackson*, 2006; *Lauber et al.*, 2009]. On a global scale pH is also one of the major controls of archaeal communities [*Wen et al.*, 2017]. *Fierer and Jackson* [2006] showed that the richness and diversity of bacterial communities differed between ecosystem types, which could be explained by pH. This substantiates our suggestion

that Unit II and the bacterial community therein was formed under different paleo-climatic conditions and varying landscape types during the last glacial cycle. However, the limited number of environmental samples and the inference of other correlating environmental factors might decrease the statistical powers to see a more significant effect of temperature on the microbial community.

Independent of core C3, microbial community composition showed substantial site-specific differences. This local scale variation in community composition (β-diversity) likely results from the distance between the coring sites because β-diversity increases with increasing distance when environmental conditions differ [*Lindström and Langenheder*, 2012] and when dispersal is as limited as it is in permafrost environments [*Bottos et al.*, 2018]. Our data suggest that the bacterial community in submarine permafrost sediments has experienced a weak selection after deposition and mostly reflects the paleo-environmental and climatic conditions. Thereby this study joins a number of other studies reporting on microbial groups that are referred to as "the paleome". Those studies found correlations between the microbial diversity and past depositional conditions [*Lyra et al.*, 2013; *Vuillemin et al.*, 2016; *Orsi et al.*, 2017]. Marine communities were found in terrestrial settings or soil communities in (sub)seafloor sediments [*Inagaki and Nealson*, 2006; *Ciobanu et al.*, 2012; *Inagaki et al.*, 2015]. Like those, our study implies that the bacterial communities in permafrost soils under the seafloor underwent a weak selection pressure after burial either through dormancy or very low generation times under freezing conditions.

Irrespective of the effect of permafrost warming on microbial community composition and abundance, the cell counts and microbial taxa of this study expand our knowledge about microbial life in permafrost. The bacterial taxa dominating in the submarine permafrost samples were amongst the phyla that commonly occur in Artic permafrost and the active layer, like Proteobacteria, Firmicutes, Chloroflexi, Acidobacteria, Actinobacteria and Bacteroidetes [*Liebner et al.*, 2009; *Jansson and Taş*, 2014; *Mitzscherling et al.*, 2017; *Taş et al.*, 2018]. Furthermore, the most abundant taxa Actinobacteria, Chloroflexi, Firmicutes, Gemmatimonadetes and Proteobacteria (Fig. 5-5) are amongst the groups that were found to be active under frozen conditions in permafrost [*Tuorto et al.*, 2014; *Coolen and Orsi*, 2015]. The non-spore forming Actinobacteria were reported to dominate permafrost since they are well adapted to freezing conditions [*Johnson et al.*, 2007]. They are metabolically active at low temperatures and possess DNA-repair mechanisms. Firmicutes and Proteobacteria likely resist long-term exposure to subzero temperatures as they take advantage of nutrient and water availability [*Johnson et al.*, 2007; *Yergeau et al.*, 2010]. In addition, many members of the

Firmicutes are able to form spores. *Candidatus* Atribacteria, which dominated in the core C3, were recently described to harbor functions for survival under extreme conditions like high salinities and cold temperatures [*Glass et al.*, 2019]. They are further one of the cosmopolitan groups in the subseafloor and dominate the bacterial community in deep anoxic sediments with low organic carbon contents [*Orsi*, 2018]. This makes Atribacteria another candidate for activity under in situ conditions in submarine permafrost. Genome-based metabolic prediction shows that *Ca.* Atribacteria can ferment sugars and propionate producing H_2, which is a critical source of energy in anoxic settings, and they have the potential to polymerize carbohydrates and store them in shell proteins of bacterial microcompartments, thus increasing their fitness and leading to their selection [*Orsi*, 2018]. Besides subseafloor sediments *Ca.* Atribacteria were found to be abundant in lacustrine sediments in Argentina that were deposited under similar environmental conditions like C3, with permafrost and reduced vegetation in the catchment, an active hydrology reworking and dispersing the soils, and a very low organic carbon content. Also climatic conditions in the sedimentation period of the lacustrine sediments were similar to that of Unit II in C3, covering the driest period of the record and overall positive temperatures [*Vuillemin et al.*, 2018].

The TCC of the onshore permafrost core C1 were in the upper range of cell counts (10^6-10^7 cells g^{-1}) reported for other permafrost environments [*Steven et al.*, 2006; *Gilichinsky et al.*, 2008; *Jansson and Taş*, 2014] and TCC of the three submarine permafrost cores were comparable to microbial abundances from organic carbon rich sub-seafloor sediments (10^5-10^7 cells g^{-1}) [*Kallmeyer et al.*, 2012; *Parkes et al.*, 2014]. TCC and bacterial 16S rRNA gene abundance in cores C1 and C2, which were highest in this study, were at least one order of magnitude lower than values for the active layer, i.e. the seasonally thawed, upper permafrost layer [*Kobabe et al.*, 2004; *Liebner et al.*, 2008, 2015]. This is in line with modelling studies on generation times in the subsurface where cells were reported to divide only every ten to hundred years [*Jørgensen and Marshall*, 2016; *Starnawski et al.*, 2017]. It also underlines that the effect of warming on microbial abundance in the investigated submarine permafrost cores was likely poor as discussed earlier. The observation that 16S rRNA gene copies mostly exceeded TCC by an order of magnitude may reflect the long-term preservation of extracellular DNA due to low temperature conditions in permafrost [*Stokstad*, 2003; *Willerslev et al.*, 2004] and, to a lesser extent, the appearance of multiple 16S rRNA gene copies per cell [*Schmidt*, 1998]. Although qPCR is a good relative quantification method, it is only poorly related to cell counts [*Lloyd et al.*, 2013a]. In addition, cell counts might be slightly underestimated due to hidden cells below sediment particles [*Kallmeyer*, 2011].

Conclusions

Substantial permafrost warming is occurring throughout the Arctic today and the associated response of microbial communities driving the biogeochemical cycling and the formation of greenhouse gases is of general interest. Inundation by seawater accelerates permafrost warming and results in a steady state of temperature under the present conditions within a few centuries. This makes submarine permafrost a suitable natural laboratory to study the microbial response on climate relevant time-scales. Our results demonstrate that both microbial abundance and community composition even after millennia of submarine permafrost warming by more than 10 °C reflect the paleo-climate and sedimentation history. However, even though we could not finally prove that long-term permafrost warming directly affects microbial abundance and bacterial community composition we found indications for it especially in the core that had experienced longest warming. This deserves more attention, because a direct effect of permafrost warming on microbial abundance, composition and carbon turnover would alter our understanding of the permafrost carbon feedback, which to date only considers permafrost thaw. Based on our work we suggest that future work addresses the responsiveness of microbial communities to permafrost warming through the analysis of organic matter quality [*Fischer et al.*, 2002], chemical composition of permafrost DOM [*Sun et al.*, 1997; *Spencer et al.*, 2015; *Ward and Cory*, 2015], natural abundance isotope ratios of biomarkers [*Boschker and Middelburg*, 2002], metagenomics and metatranscriptomics [*Coolen and Orsi*, 2015; *Mackelprang et al.*, 2017]. Finally, in this study the length of the coring transect (~12 km), the age span within and between the cores and hence the comparatively long sedimentation period encompassed by our samples from Unit II had a stronger influence on recent microbial abundance and community than the large level of physicochemical similarity within this unit (Fig. 5-3 insert). Further studies on the microbial response to permafrost warming should focus on historically more similar samples without neglecting similar physicochemical properties.

Acknowledgments

Our thanks go to Aleksandr Maslov (SB RAS, Melnikov Permafrost Institute, Yakutsk, Russia), who provided indispensable drilling expertise. We thank Tiksi Hydrobase staff members Viktor Bayderin, Viktor Dobrobaba, Sergey Kamarin, Valery Kulikov, Dmitry Mashkov, Dmitry Melnichenko, Aleksandr Safin, and Aleksandr Shiyan for their field support and Dimitry Yu Bolshiyanov (Arctic Antarctic Research Institute, St. Petersburg) for logistical issues. Drilling was supported by the German Ministry for Education and Research, a Joint Russian German

Research Group (HGF-JRG100) of the Helmholtz Association of German Research Centres, and by the EU's INTAS program. Susanne Liebner is grateful for the funding of the Helmholtz Young Investigators Group (grant VH-NG-919). We further thank Anke Saborowski, Antje Eulenburg, Ute Bastian, and Katja Hockun for excellent laboratory support.

6 Synthesis

6.1 Introduction

Permafrost temperatures have increased by 0.4 °C within the last decade due to rapid warming of the Arctic [*Biskaborn et al.*, 2019]. This is critical since perennially frozen ground acts as a huge trap of organic carbon. Permafrost warming and thawing can result in the release of stored methane (CH_4) and is assumed to stimulate microorganisms and the turnover of stored organic carbon [*Waldrop et al.*, 2010; *Mackelprang et al.*, 2011; *Graham et al.*, 2012; *Schuur et al.*, 2015] leading to the release of the greenhouse gases CH_4 and CO_2 [*Graham.*, 2012; *Mackelprang et al.*, 2011]. This can accelerate global warming. However, the microbial response to permafrost warming and thawing on climate-relevant time scales remains unclear.
Submarine permafrost of the Arctic continental shelves, which is terrestrial permafrost under the seafloor, represents an analogue for permafrost warming that is presently occurring globally on land. Upon inundation hundreds to thousands of years ago submarine permafrost started to warm. Thus, it is a suitable natural laboratory to study the microbial response to permafrost warming on time-scales that are relevant for the global climate. Besides warming, submarine permafrost is affected by penetrating saline water into the upper sediment layers resulting in its degradation and thawing. Sediment temperatures in the Laptev Sea, the study area of this thesis, were observed to increase within a few hundred years after inundation. Temperatures were found to climax in a steady state at around -1 °C, the limit to maintain ice-bonded permafrost under submarine conditions [*Grigoriev*, 2008], and thus adapting to the annual average bottom-water temperature [*Wegner et al.*, 2005]. This warm permafrost is highly susceptible to any climate changes that would result in bottom-water warming as it would lead to immediate permafrost thawing.
Submarine permafrost covers an area of 605,006 km^2, almost half the size of the area of continuous land permafrost [*Ruppel*, 2015]. Although the amount of organic carbon that exists in submarine permafrost is still unquantified, it is most likely significant. In order to predict the microbial carbon turnover and release from submarine permafrost it is crucial to understand the effect of century-to-millennia-scale permafrost warming on the microorganisms and their response to seawater infiltration and permafrost degradation.
The infiltration of saline water into submarine permafrost provides suitable conditions for microorganisms that are capable of the anaerobic oxidation of methane (AOM). AOM could

mitigate the release of stored or produced methane. However, AOM in degrading submarine permafrost are poorly studied [*Overduin et al.*, 2015].

This thesis focusses on the investigation of the indigenous bacterial and archaeal communities in submarine permafrost from two sites in the Laptev Sea (core BK2 from Buor Khaya and cores C1-C4 from Mamontov Klyk), located on the East Siberian Arctic shelf. It is the first study using a systematic approach to describe the microbial response to permafrost warming and permafrost thawing in presence of seawater on different time scales (C4 ~ 220 yr, BK2 ~ 540 yr, C3 ~ 660 yr, C2 ~2500 yr). The thesis expands the results of a pilot study, which compared the methanogenic community in a cold terrestrial (core C1) and a warm submarine permafrost core (C2) at Cape Mamontov Klyk [*Feige*, 2009; *Koch et al.*, 2009], by using a higher number of biological replicates and more extensive analyses to assess the microbial community composition and abundance. In addition, this thesis reveals the controls of microbial community composition and abundance in permafrost under submarine conditions by analyzing them in the context of temperature, pore water chemistry and sediment physicochemical parameters. The detailed examination of those parameters is the second emphasis of this work and is consequently also part of the following discussion.

6.2 Microbial taxa in submarine permafrost

Deep below the seafloor, submarine permafrost represents an extreme habitat for microbial life characterized by low temperatures, the absence of oxygen, and changing thermal and chemical conditions. The penetration of seawater leads to elevated salt concentrations, which are known to cause osmotic stress on microorganisms. Elevated salinity can limit microbial growth [*Galinski*, 1995; *Rousk et al.*, 2011] and decrease microbial abundance in sediments [*Rietz and Haynes*, 2003; *Jiang et al.*, 2007; *Rath and Rousk*, 2015; *Wen et al.*, 2018]. Also, the microbial community is sensitive to changes in salinity resulting in shifts of the microbial composition [*Walsh et al.*, 2005; *Allison and Martiny*, 2008]. Therefore, the investigation of the submarine permafrost microbial community answers the basic question on the impact of seawater on the composition of a former terrestrial microbial community.

Despite millennial-scale seawater infiltration into the upper sediment layers (C2 at Cape Mamontov Klyk) the bacterial and archaeal communities in thawed permafrost sediments did not show any evidence of taxa commonly found in marine habitats. Only in the seabed sediments above typical marine taxa such as *Pirellulales* [*Duret et al.*, 2019], *Desulfobacterales*

[*Wang et al.*, 2012], *Thiotrichales* [*Anderson et al.*, 2017], and *Marinicellales* [*Anderson et al.*, 2017] as well as *Nitrosopumilus* (Thaumarchaeota) [*Könneke et al.*, 2005], MBG-B (Lokiarchaeota) and Izemarchaea/MBG-D (Euryarchaeota) [*Teske and Sorensen*, 2008] were discovered. Many of the observed bacterial taxonomic groups of the thawed permafrost below were found to comprise typical soil organisms such as Chloroflexi Gitt-GS 136 [*Delgado-Baquerizo et al.*, 2017], *Solirubrobacterales*, *Actinomycetales*, *Rhizobiales*, *Burkholeriales* [*Xiong et al.*, 2014; *Rui et al.*, 2015], or those that can live in both marine and terrestrial environments i.e. *Acidimicrobiales* [*Mizuno et al.*, 2015]. The archaeal community of the thawed permafrost also contained common terrestrial taxa like *Nitrososphaera* (Thaumarchaeota) or MCG-6 (Bathyarchaeota), and those that can be found in marine environments such as MCG-8 (Bathyarchaeota) [*Xiang et al.*, 2017]. A mixture of marine (Bathyarchaeota MCG-8, ANME-2a/b and ANME-2c) and terrestrial (Bathyarchaeota MCG-6) archaeal sequences was detected in the upper unfrozen part of the more recently inundated core BK2 (Buor Khaya). Thawed sediments harbored a different archaeal community than the ice-bonded sediments below the permafrost table, which was composed of ANME-2a/b, ANME-2d and *Methanosarcina*, and completely lacked the Bathyarchaeota MCG-6 or -8.

The ice-bonded permafrost population was generally found to resemble the communities from terrestrial permafrost. Bacterial taxa that dominate in the submarine permafrost of Cape Mamontov Klyk and Buor Khaya were amongst the phyla that commonly occur in Artic permafrost and the active layer, like Acidobacteria, Actinobacteria, Bacteroidetes Chloroflexi, Firmicutes and Proteobacteria [*Liebner et al.*, 2009; *Jansson and Taş*, 2014; *Mitzscherling et al.*, 2017; *Taş et al.*, 2018]. The most abundant orders within the thawed and unaffected submarine permafrost were *Actinomycetales* (Actinobacteria), Chloroflexi Gitt-GS 136, *Clostridiales* (Firmicutes), Gemm-1 Gemmatimonadetes, *Rhizobiales* (Alphaproteobacteria) and *Burkholderiales* (Betaproteobacteria), all of them are typical soil living bacteria. Firmicutes and Actinobacteria are the two major groups of gram-positive bacteria. *Actinomycetes* of the Actinobacteria are usually aerobic bacteria, but can also be facultative or obligate anaerobes, and are common inhabitants of soil and plant material. Most of them are able to form spores. Chloroflexi, also known as green non-sulfur bacteria, contain many members that are thermophilic and form thick microbial mats around hot springs. Non-thermophilic members can be found in marine microbial mats [*Madigan et al.*, 2011]. Other members prefer humid to dry ecosystems and have structural adaptations to desiccation. Chloroflexi Gitt-GS 136, were found in temperate semi-arid and dryland soils, have the ability to degrade cellulose and chitin [*Delgado-Baquerizo et al.*, 2017; *Zhang et al.*, 2018; *Zhou et al.*, 2019], and are resistant to

drying-rewetting cycles. *Clostridiales* belong to the endospore-forming Firmicutes and are primarily found in soils, where they live in anoxic "pockets" made by aerobes. The order of *Clostridiales* contains many fermentative species which can obtain energy from fermenting sugars, cellulose or amino acids [*Madigan et al.*, 2011]. *Rhizobiales* and *Burkholderiales* of the Proteobacteria can be found in diverse environments. The most abundant family of *Rhizobiales* found in submarine permafrost samples, namely *Bradyrhizobiaceae*, comprises organisms from different environments including soils or plant hosts, and their participation in biogeochemical cycles like nitrogen fixation is of extreme importance [*Marcondes de Souza et al.*, 2014]. The *Comamonadaceae* and *Oxalobacteraceae* of the *Burkholderiales* are also mostly found in soil or water habitats, or are plant-associated. Some of them can fix nitrogen [*Baldani et al.*, 2014; *Willems*, 2014].

Although bacterial phyla like Alphaproteobacteria, Chloroflexi, Firmicutes and Actinobacteria can be also found in other environments, such as Arctic seafloor basalts which have a completely different origin [*Lysnes et al.*, 2004], all of the bacterial orders in submarine permafrost described above, were typical soil organisms. Either they are dependent on hydrolyzing plant polymers as the first step of organic matter degradation (like *Burkholderiales*, *Actinomycetales*, *Chloroflexi* and *Clostridiales*) or are connected to plants in a symbiotic or pathogenic way (*Rhizobiales*). This indicates that submarine permafrost represents a typical soil habitat for bacteria that froze and did not drastically change upon inundation and warming.

Dominant archaeal taxa identified in ice-bonded submarine permafrost belonged to the domains of Euryarchaeota, Thaumarchaeota and Bathyarchaeota, the latter are both part of the TACK/Proteoarchaeota superphylum [*Adam et al.*, 2017]. Thaumarchaeota, initially classified as "mesophilic Crenarchaeota", were detected to form a deep branching separate phylum within the Archaea [*Brochier-Armanet et al.*, 2008]. This phylum comprises all known archaeal ammonia oxidizers, but also several unknown microorganisms with unknown energy metabolism. At both study sites of this work the Thaumarchaeota were comprised of *Nitrososphaera*, mainly detected in the terrestrial sediments, and *Nitrosopumilus* in the seabed. Both are important aerobic ammonia-oxidizing archaea of soil and marine environments, respectively [*Adam et al.*, 2017]. Since the conditions in permafrost under the seafloor are anoxic, *Nitrososphaera* may be a relict of original sedimentation. Bathyarchaeota (formerly Miscellaneous Crenarchaeota Group (MCG)), however, are one of the predominant groups in anoxic marine and terrestrial environments and are dominant in various soils and sediments [*Meng et al.*, 2014; *Xiang et al.*, 2017]. Furthermore, they are one of the most abundant groups in the subsurface sedimentary biosphere [*Meng et al.*, 2014] and in marine sediments [*Lloyd et*

al., 2013b]. Bathyarchaeota are phylogenetically divergent, forming 25 subgroups [*Zhou et al.*, 2018], and are adapted to a wide variety of marine and freshwater environments. Bathyarchaeota are able to anaerobically utilize detrital proteins, polymeric carbohydrates, fatty acids/aromatic compounds, methane or methylated compounds and/or potentially other organic matter such as recalcitrant components of bacterial cell walls [*Lloyd et al.*, 2013b] and the biopolymer lignin [*Yu et al.*, 2018]. They have a wide variety of metabolisms including acetongenesis, methane metabolism, dissimilatory nitrogen and sulfur reduction, and they potentially interact with anaerobic methane-oxidizing archaea, acetoclastic methanogens and heterotrophic bacteria [*Zhou et al.*, 2018]. Due to their ability to grow on a wide range of compounds Bathyarchaeota play significant roles in the global carbon cycle [*Adam et al.*, 2017]. The subgroups are adapted to specific habitat types with salinity being their main controlling factor [*Fillol et al.*, 2016]. The subgroups that were found in submarine permafrost of this study belong to MCG-6 and MCG-8. Both are part of the dominant MCG lineages. MCG-6 was described to be the indicator group of all lineages for soils and was one of the predominant groups in ice-bonded permafrost soils here. MCG-8 was discovered in various saline and marine sediments, such as lagoons, estuaries or mangroves [*Xiang et al.*, 2017], methane seeps and mud volcanoes [*Zhou et al.*, 2018] as well as in the seabed and upper thawed permafrost layers of this study. Due to the ability of Bathy-8/MCG-8 to degrade lignin this subgroup of Bathyarchaeota may play a role in degrading the recalcitrant carbon found in permafrost soils. Subgroup-8 furthermore has been suggested to be capable of methanogenesis [*Yu et al.*, 2018]. The presence of sulfate from penetrating seawater and the existence of trapped or produced methane make submarine permafrost sediments an ideal potential habitat for sulfate-dependent AOM, which usually can be found in the seabed [*Knittel and Boetius*, 2009]. In support of this hypothesis, ANME-2a/b and ANME-2c of the Euryarchaeota were detected amongst other marine archaeal clades in the thawed marine influenced layer of core BK2. Throughout the ice-bonded permafrost layer in core C2 at Cape Mamontov Klyk and right below the phase boundary (transition from ice-free to ice-bonded sediment) of core BK2 from Buor Khaya ANME-2d sequences were detected. While ANME-2a/b/c belong to the clusters that are responsible for sulfate-dependent AOM in marine environments [*Timmers et al.*, 2015, 2017], ANME-2d (also known as GoM-Arc I, AOM associated Archaea (AAA) or Methanoperedenaceae) can use nitrate (NO_3^-), iron (Fe^{3+}) and manganese (Mn^{4+}) as terminal electron acceptors [*Haroon et al.*, 2013; *Ettwig et al.*, 2016] and have been observed in diverse terrestrial environments [*Haroon et al.*, 2013]. Furthermore, in this study *Methanosarcina* of the Euryarchaeota were observed to co-occur with the ANME-2d clades, being exclusively

present in the ice-bonded permafrost. *Methanosarcina* are strictly anaerobic archaea that can produce methane from acetate, methanol, mono-, di- and trimethylamine as well as H_2+CO_2 and CO [*Boone and Mah*, 2015]. They prefer cold habitats and can be found in various environments such as marine and lake sediments, estuaries and soils [*Wen et al.*, 2017]. In this study, *Methanosarcina* were discovered to dominate the methanogenic community in submarine permafrost of the Laptev Sea shelf, thereby confirming previous findings [*Koch et al.*, 2009]. In addition, a so far unknown archaeal clade was detected to be predominant in the thawed sediments and in the frozen sediments that were infiltrated by seawater after millennia-scale inundation. The unknown archaeal clade and a sister clade were designated as Deep Submarine Permafrost Euryarchaeotal Group I (DSPEG I) and II (DSPEG II). Both groups had less than 82% sequence similarity values to the next cultured representative *Methanomassiliicoccus luminyensis*, which was isolated from human faeces [*Dridi et al.*, 2012] and belongs to the *Methanomassiliicoccales* of the superclass *Diaforarchaea*. *Methanomassiliicoccales* occur in various environments such as animal digestive systems but can also be found in marine and lake sediments, soils and sewers [*Adam et al.*, 2017; *Wen et al.*, 2017]. Based on their habitat preferences they can be subdivided in two different phylogenetic clades, a gastro-intestinal (GIT) clade and an environmental clade. Although *Methanomassiliicoccus luminyensis* was isolated from human faeces the strain is associated with the environmental group [*Söllinger et al.*, 2016]. Although *Methanomassiliicoccales* are unrelated to any previously known Class I and Class II methanogens, and are affiliated with a large clade of non-methanogenic lineages [*Adam et al.*, 2017] they form the seventh found order of methanogens [*Oren and Garrity*, 2013]. Members of the *Methanomassiliicoccales* display unique characteristics, as they lack genes coding for the methanogenesis from H_2+CO_2 pathway, and are therefore reliant on methyl-dependent hydrogenotrophic methanogenesis similar to the methylotrophic methanogenesis found in some members of the Bathyarchaeota [*Evans et al.*, 2015; *Adam et al.*, 2017]. In contrast, *Zinke et al.* [2018] described metagenome-assembled genomes (MAGs) from high latitude lake sediments, subsurface aquifers and estuary sediments with a similar sequence identity of 86% to *Methanomassiliicoccus luminyensis* that did not contain the canonical H_2/methylotrophic methanogenesis pathways. The MAGs were putatively heterotrophic and conserved energy through hydrogen production. Metagenomic or transcriptomic studies on submarine permafrost samples would shed further light on the functional potential of DSPEG I and II.

In summary, the archaeal community comprises organisms that are capable of performing a wide variety of processes for carbon degradation, including all different types of

methanogenesis, but are also able to oxidize methane anaerobically. The simultaneous occurrence of methanogenic and methanotrophic organisms suggests a feedback system of methane production and oxidation. Also, ammonia-oxidation is a fundamental core process of the biogeochemical cycling and plays a major role in greenhouse gas production.

In contrast to the microbial life found in the seabed and in ice-bonded permafrost sediments, the divergent bacterial and archaeal communities in thawed sediments may be a result of microorganisms being introduced by seawater infiltration into a relict terrestrial community and/or due to an active development of new microbial assemblages. Due to the large distance in C2 of around 18 m between samples of the seafloor and reworked permafrost sediments (PWI), it was not possible to assess how far into the thawed marine influenced permafrost sediments the typical seabed community persisted. In reworked permafrost, the absence of taxa that were found to be abundant in the seabed may be due to (i) dispersal limitation through the sediment (Bottos et al., 2018) and (ii) the selection of the subseafloor community from within the community present in seabed sediments. Due to the appearance of both, marine and terrestrial taxa the assemblages in thawed permafrost were different from those of the unaffected permafrost and the seabed, and thus from other marine and terrestrial habitats. Archaea appeared to form specific sub-communities, in accordance with the pore water units already within a few centuries (BK2), whereas the bacterial communities formed distinct sub-communities after 2500 years of seawater influence (C2). Archaea are known for their adaptation to extreme temperature and salinity [*Wilhelm et al.*, 2012] and are thus proposed to faster adapt to the changed thermal and chemical pore water conditions.

6.3 Permafrost microbial response to short-term seawater inundation

Submarine permafrost miccorganisms are expected to respond to salinty and termpertaure, as these two factors control seawater induced thawing and permafrost warming without thaw. The effect, salinity and temperature have on the microbial activity, was investigated on different time-scales. They reached from a few hundred years (C4 = 220 yr, BK2 = 540 yr, C3 = 660 yr) to several thousand years (~2500 yr, C2). In this thesis, hereafter scales of centuries are denoted as short-term, while scales of millennia are denoted as long-term. Changes in the microbial activity on those time-scales were measured by means of shifts in the community composition and changes in the microbial abundance. The microbial abundance was quantified by total cell

counts and copy numbers of the 16S rRNA gene as well as of functional genes. Shifts in the community composition were analyzed by amplicon sequencing of the 16S rRNA gene.

In order to look at the microbial community development in submarine permafrost in its entirety, physicochemical pore water and sediment characteristics in sediment cores from each study site (BK2 and C2) were extensively studied. Both sites were characterized by ice-free sediment deposits overlying ice-bonded permafrost unaffected by saline solution. However, the depth and thickness of the phase boundary differed between both sites as a result of differences in the inundation periods (C2 2500 years and BK2 540 years), the diffusive penetration of saline water into the seabed, and/or distinct sediment column properties that affect the penetration rate [*Ulyantsev et al.,* 2016]. While the core BK2 from Buor Khaya was characterized by a sharp transition from unfrozen to ice-bonded permafrost, the advanced stage of permafrost degradation in core C2 from Cape Mamontov Klyk was manifested in a gradual transition from thawed to ice-bonded permafrost with seawater that was detectable even in the frozen sediments.

Nevertheless, at both sites the submarine permafrost sediments could be classified into similar pore water units (PW units). According to their pore water chemical composition those units were described to represent the seawater influence and sedimentation history. PW I and II were found in permafrost of terrestrial origin that had been penetrated by seawater resulting in elevated salinity, conductivity, and ion concentrations. Differences between PW I and II were partly explained by postdepositional and posttransgression processes: wave and ice turbation of the seabed (PW I) and infiltration of saline seawater into the sediment (PW II). PW III was described to represent ice-bonded and warmed permafrost that was unaffected by the infiltration of seawater. Their similarity and occurrence at both sites suggest that pore water units are characteristic of submarine permafrost. They are a good indicator for submarine permafrost degradation and show that the response of permafrost pore water chemistry to inundation is already visible a few hundred years after inundation (BK2, after 540 years).

The bacterial community composition, however did not shift according to the observed pore water characteristics and thus showed no response to short-term seawater inundation and warming. Furthermore, unlike thawing of permafrost on land [*Steven et al.,* 2008b; *Coolen and Orsi,* 2015; *Schostag et al.,* 2019] thawing and warming under submarine conditions rather impaired the microbial communities on the time scale of centuries. This conclusion is based on a variety of different observations.

At first, cell counts in ice-bonded but warmed and in thawed, marine-influenced submarine permafrost were equal or even lower than in cold, terrestrial permafrost investigated in this

work (10^6-10^7 in sediment core C1 from Mamontov Klyk) and in other permafrost environments (10^3 to 10^8 cells $g^{-1)}$ [*Steven et al.*, 2006; *Gilichinsky et al.*, 2008; *Jansson and Taş*, 2014]. Moreover, cell abundances in the majority of submarine permafrost samples were at least one order of magnitude lower than those reported for the active layer (10^8-10^9 cells) [*Kobabe et al.*, 2004; *Liebner et al.*, 2008, 2015]. Abundanes were especially low in samples from post century-scale inundation cores (10^4-10^6 cells g^{-1} in BK2 warmed for 540 years; 10^5- 10^6 cells in C3 warmed for 660 years). This is in line with the lowest bacterial 16S rRNA gene copy numbers (10^5-10^6 copies g^{-1} in BK2 and 10^6 - 10^7 copies g^{-1} in C3 and C4, compared to up to 10^9 copies g^{-1} after warming for millennia in C2), and a low bacterial diversity observed at these sites (BK2). Also, the gene copy numbers of *mcrA*, the functional marker gene for methanogenic archaea, were low or even below detection limit in samples representing ice-bonded permafrost impacted by centuries of warming ($<10^4$ *mcrA* copies in BK2 compared to up to $>10^5$ copies g^{-1} in ice-bonded permafrost of C2).

Moreover, the microbial abundance was observed to decrease with rising temperatures and increasing salt concentrations in ice-bonded permafrost (along the transect). The elevated salinity in ice-bonded permafrost was most likely the result of climatic conditions or the habitat type at the time of sediment deposition. A negative effect of warming on the microbial abundance in ice-bonded permafrost could not be conclusively determined, but the osmotic stress caused by increasing salinity is known to impair microbial growth [*Galinski*, 1995; *Rousk et al.*, 2011] and decrease microbial abundance [*Rietz and Haynes*, 2003; *Jiang et al.*, 2007; *Rath and Rousk*, 2015; *Wen et al.*, 2018]. As bacteria represent the majority of the microbial community in permafrost and the active layer [*Kobabe et al.*, 2004; *Hoj et al.*, 2008], a decrease of the overall microbial abundance can be attributed to a decrease in the bacterial population. Archaeal abundance is likley to increase with increasing salinity [*Jiang et al.*, 2007]. Marine ANME communities benefited from seawater infiltration.

Finally, the low microbial abundance in submarine permafrost after century-scale warming was accompanied by high measured acetate concentrations (BK2) or high DOC contents (C3 and C4, Mamontov Klyk), indicating that microbial activity and substrate utilization were likely low or not yet stimulated.

Those results show that on short time scales seawater inundation and warming neither shifted the microbial community composition nor stimulated microbial activity.

6.4 Permafrost microbial response to long-term seawater inundation

The results of this thesis suggest that also millennia of warming could not displace the original microbial communities in ice-bonded permafrost. The paleo-environment (i.e. the paleo-climate and -habitat type) was the prevailing factor which shaped the microbial community composition, even centuries to millennia after inundation. Pore water stable isotopes and salinity, not a result of penetrating seawater, were used to reconstruct the paleo-environment. The conservation of the original bacterial communities during centuries to millennia of warming was found to be the reason for a strong variance between the cores. This finding is contradictory to *Koch et al.* [2009], who assigned the variance of the methanogenic community in ice-bonded terrestrial (C1) and submarine (C2) permafrost to environmental changes, i.e. temperature increase caused by flooding, and thus emphasizes the higher explanatory power of the combined approach used in the present study.

Only the microbial abundance is assumed to be positively correlated with millennia-scale temperature increase in ice-bonded submarine permafrost. Although microorganisms were found to be active in permafrost under submarine conditions regardless of inundation time (discussion on that is given in the following paragraph), only long-term warming resulted in the suggested stimulation. Cell abundances in ice-bonded permafrost unaffected by penetrating seawater that was subjected to 2500 years of permafrost warming (C2) were increased compared to seawater affected sediments of the same core and compared to ice-bonded sediments subjected to centuries of permafrost warming (C4, C3, BK2). Cell abundances were comparable to those reported in cold, terrestrial permafrost on land. Some sediment layers had cell abundances of up to 10^8 cells g^{-1}, similar to those found in the active layer of permafrost. This coincided with significantly lower DOC values. Since the degradation of DOC can be used as measure for microbial carbon turnover, permafrost warming for more than two millennia may have enabled microbial communities to adapt to the new temperature regime and sediment properties and to start cell proliferation. The diversity of this submarine permafrost site is thereby comparable to the permafrost active layer and permafrost thaw ponds [*Liebner et al.*, 2008; *Crevecoeur et al.*, 2015]. Finally, 2500 years of seawater influence led to changes in the bacterial community composition with depth and a stratification into sub-communities according to the chemical conditions of the described pore water units (in C2).

In conclusion, salinity of penetrating seawater and the paleo-climatic conditions had a stronger effect on shaping the microbial communities than rising temperature.

6.5 AOM in submarine permafrost

Although, the microbial abundance was low and the bacterial community not adapted to the pore water conditions after centuries of inundation and warming, several lines of evidence were found for microbial activity in submarine permafrost irrespective of inundation time.

The most promising indications for activity were the detection of ANME clades, low methane concentrations and $\delta^{13}C$-values of the methane that strongly indicate microbial oxidation. Marine ANME-2a/b affiliated with SEEP-SRB1/seep-associated *Desulfobacterium anilini*-group were detected in combination with low methane concentrations in the upper unfrozen sediments and in the sulfate-methane transition zone (SMTZ) of the core BK2, that underwent degradation for only 540 years. The SMTZ concurs with a sharp transition from unfrozen to ice-bonded permafrost. Furthermore, the relative abundance of methanogenic archaea and ANME (20-30%) as well as the gene copy numbers of *mcrA* were higher in thawed sediments (10^3-10^4 copies g^{-1}) but almost completely absent in the ice-bonded permafrost underneath. High ether lipid MI (methane index) values in the SMTZ further support a potential contribution of AOM communities to the consumption of methane.

At the drill site at Cape Mamontov Klyk, where warming and thawing occurred for about 2500 years (C2), the SMTZ was located in the upper part of ice-bonded permafrost and, thus, below the actual permafrost thaw front. Methane concentrations were generally low down into the ice-bonded permafrost, with the exception of elevated methane concentrations in the lower part of ice-bonded permafrost. Methane concentrations peaked at a depth of 52 m bsf. This methane peak coincided with an increase in *mcrA* gene copy numbers (from 10^2 to 10^5 copies g^{-1}) and the relative abundance of ANME-2d. Detected sulfate reducers were almost exclusively linked to *Desulfosporosinus* that have not been observed in AOM consortia so far. This suggests that sulfate-dependent AOM was likely not occurring. The concentrations of other potential terminal electron acceptors for AOM such as nitrate, iron and manganese [*Haroon et al.*, 2013; *Ettwig et al.*, 2016] correlated with the abundance of ANME-2d and were low in areas around the highest occurrence of ANME-2d sequences at 52 mbsf. It suggests that AOM by ANME-2d is possible in ice-bonded permafrost before it thaws.

Microbial activity in the upper part of ice-bonded permafrost was also supported by decreasing sulfate concentrations and increasing gene copy numbers of *dsrB*, the marker gene for sulfate reducing bacteria (SRB), pointing towards active sulfate reduction and organic matter decomposition independent of AOM at this depth.

6.6 Implications for the permafrost carbon feedback

Submarine permafrost unaffected of seawater penetration can be used as a natural laboratory to study the microbial response to permafrost warming on land, as the effect of warming in both, submarine and terrestrial settings is comparable. However, thawing of permafrost under submarine conditions is both caused and accompanied by seawater infiltration into a former terrestrial system. Therefore, the thawing process differs strongly from that in terrestrial permafrost.

Under frozen conditions microbial processes in terrestrial permafrost are dominated by stress responses, survival strategies and maintenance processes [*Coolen and Orsi*, 2015; *Mackelprang et al.*, 2017]. While warming does not have an effect on permafrost microbial communities across several days [*Schostag et al.*, 2019], thawing causes a rapid enzymatic response contributing to soil organic matter decomposing processess and a shift in the transcriptionally active community, but no changes in the abundance [*Coolen and Orsi*, 2015; *Schostag et al.*, 2019]. Transcripts that are enriched after permafrost thaw are indicative of heterotrophic methanogenic pathways utilizing acetate, methanol and methylamine, but also of acetogenesis, making acetogenic bacteria a potential source for acetoclastic methanogenesis [*Coolen and Orsi*, 2015]. The release of stored and microbially produced methane is thus a consequence of thawing permafrost on land. This particularly occurs when permafrost thaws beneath thermokarst lakes. Thawing of permafrost in thermokarst lakes follows a similar pattern as under the seafloor. It is more abrupt than the gradual thaw of near-surface permafrost [*Walter Anthony et al.*, 2018] and is not affected by freeze-thaw cycles occurring in the active layer, yet its bio-geochemical processes are very different. Methane production rates in thermokarst sediments increase with rising temperature [*de Jong et al.*, 2018]. Highest methane production potentials were observed in organic-rich and recently thawed lake sediments indicating that organic matter supply is important to methane production [*Heslop et al.*, 2015] and that thawing of permafrost beneath thermokarst lakes is beneficial for microbial carbon turnover. Although recent findings indicate that AOM also occurs in thermokarst environments mitigating the release of methane [*Winkel et al.*, 2019] thaw lakes emit huge quantities of methane to the atmosphere [*Walter et al.*, 2006, 2007]. Methane emissions from the land, especially from wetlands, are thus higher than those from the Arctic Ocean [*McGuire et al.*, 2009].

However, a microbial stimulation, in the form of higher growth rates and increasing abundance, was disproved for thawed permafrost at low positive temperatures. Permafrost microbial communities, which were hypothesized to be dominated by temperature depending specialists with a high functional potential and activity, were found to comprise mostly psychrotolerant

microorganisms. They do not have a higher metabolism and do not grow faster at low positive temperatures (1 °C) than microorganisms in soils from warmer climates [*Ernakovich and Wallenstein*, 2015]. This substantiates the result of this thesis that warming is accompanied with an increase in microbial abundance only after thousands of years.

In submarine permafrost, the exposure to a combination of warming and increasing pore water salinity was found to impair the bacterial community. Although microbial functions were not the focus of this work, stress response and adaptation are the supposed responses to thawing and warming of permafrost under submarine conditions. The relative abundances of acetogenic bacteria such as *Clostridia* or *Acidobacteria* were lower in thawed submarine permafrost compared to unaffected ice-bonded permafrost, demonstrating a reduced potential for acetoclastic methanogenesis upon thaw. Furthermore, Acetolcastic methanogenesis can only take place in sediment layers with low sulfate concentrations. Thus, in seawater affected sediments with high sulfate concentrations methanogenesis is known to be absent [*Jorgensen*, 1980] due to the inhibition of methanogenesis by sulfate [*Winfrey and Zeikus*, 1977]. In addition, the penetration of seawater supports sulfate-dependent AOM creating a methane filter for stored and produced methane. Also, the detection of terrestrial ANME-2d and their potential activity under subzero conditions may contribute to the mitigation of methane release from permafrost upon thawing. Consequently, the release of microbially produced greenhouse gases during permafrost thawing under submarine conditions and during permafrost warming without thaw is supposed to be low in comparison to thawing permafrost on land. In addition, carbon turnover in ice-bonded submarine permafrost is presumed to be very low.

6.7 Conclusions

The present study extends our knowledge about microbial communities in permafrost. In particular, it provides insights into the microbial response to permafrost warming and the effect of seawater infiltration into permafrost sediments on the pore water chemical conditions and on the indigenous microbial communities. The thesis further examines the existence and potential activity of AOM communities in terrestrial sediments under the seafloor, even under frozen conditions. The objectives of this work can be concluded as follows:

How does inundation of terrestrial permafrost change the pore water chemical conditions and physical state of permafrost?

- The infiltration of seawater into permafrost sediments leads to the formation of different pore water units, depending on the degree of seawater influence and on postdepositional and posttransgression processes. Pore water units can be used to distinguish sediments affected by reworking in the marine environment from the terrestrial permafrost thawed *in situ* beneath the seabed and from terrestrial permafrost that is unaffected by penetrating seawater.

Is submarine permafrost a suitable natural laboratory to study the response of microbial communities to permafrost warming and thaw ...?

- The effect of rising temperature on microbial communities is comparable in submarine and terrestrial permafrost, making submarine permafrost an ideal natural laboratory for predicting the temperature response of terrestrial permafrost microbial communities.
- Thawing under submarine conditions, however, differs strongly from thawing on land in its bio-geochemical processes. Unlike thawing below e.g. thermokarst lakes, which is beneficial for microbial carbon turnover and results in the highest methane production potentials in recently thawed sediments, thawing under submarine conditions impairs the microbial communities.

... and how do submarine permafrost communities differ from communities in onshore permafrost?

- Submarine permafrost sediments harbor a diverse bacterial community that resembles the community of terrestrial permafrost and soils containing dominant taxa that can be active under frozen conditions.
- Bacterial and archaeal assemblages in the seawater affected permafrost are different from the communities in unaffected permafrost and the seabed, and thus from other terrestrial and marine habitats. This shows a strong impact of salinity on the permafrost community composition.

What is the response of the indigenous microbial community to seawater infiltration and permafrost thaw?

- Century-scale warming and thawing under submarine conditions does not stimulate the permafrost microbial activity which was approximated by changes in the abundance and community composition. The exposure to a combination of warming and increasing

pore water salinity initially disturbs and probably decreases the bacterial community size and diversity.

- The formation of pore water units is already visible after centuries of inundation, while according to the pore water units the formation of new microbial assemblages was observed only after millennia-scale inundation.

Do microbial communities already respond to permafrost warming without thaw on climate relevant time-scales and how does this occur?

- The microbial communities in ice-bonded permafrost are mainly shaped by the paleo-climate and sedimentation history, showing that temperature had a subordinated effect on the bacterial community composition.
- A beneficial effect of temperature rise on the microbial population was only observed in ice-bonded permafrost after long-term i.e. millennia-scale warming. The warm submarine permafrost showed some indication for the stimulation of microbial growth such as increased microbial abundance and reduced amounts of substrate.

Is submarine permafrost a habitat for microbial assemblages involved in the anaerobic oxidation of methane and could they function as a filter for methane release?

- Archaeal communities are mainly composed of methanogenic members, but also include ANME clades and a putative new order, named DSPEG. ANME clades are composed of marine ANME clades in the seawater affected permafrost, and of terrestrial ANME clades in the unaffected permafrost.
- Irrespective of inundation time and seawater influence, submarine permafrost microbial communities are active. Indications for the anaerobic oxidation of methane, even at subzero temperatures, and sulfate reduction were found.
- Modelling suggests that potential AOM could mitigate the release of almost all stored or microbially produced methane from thawing submarine permafrost

The conclusions indicate that both, permafrost thawing under submarine conditions as well as permafrost warming without thaw have marginal effects on the microbial mobilization and turnover of the buried organic carbon. Thus, it is rather unlikely that microbial processes in permafrost under the seafloor substantially amplify the atmospheric methane budget.

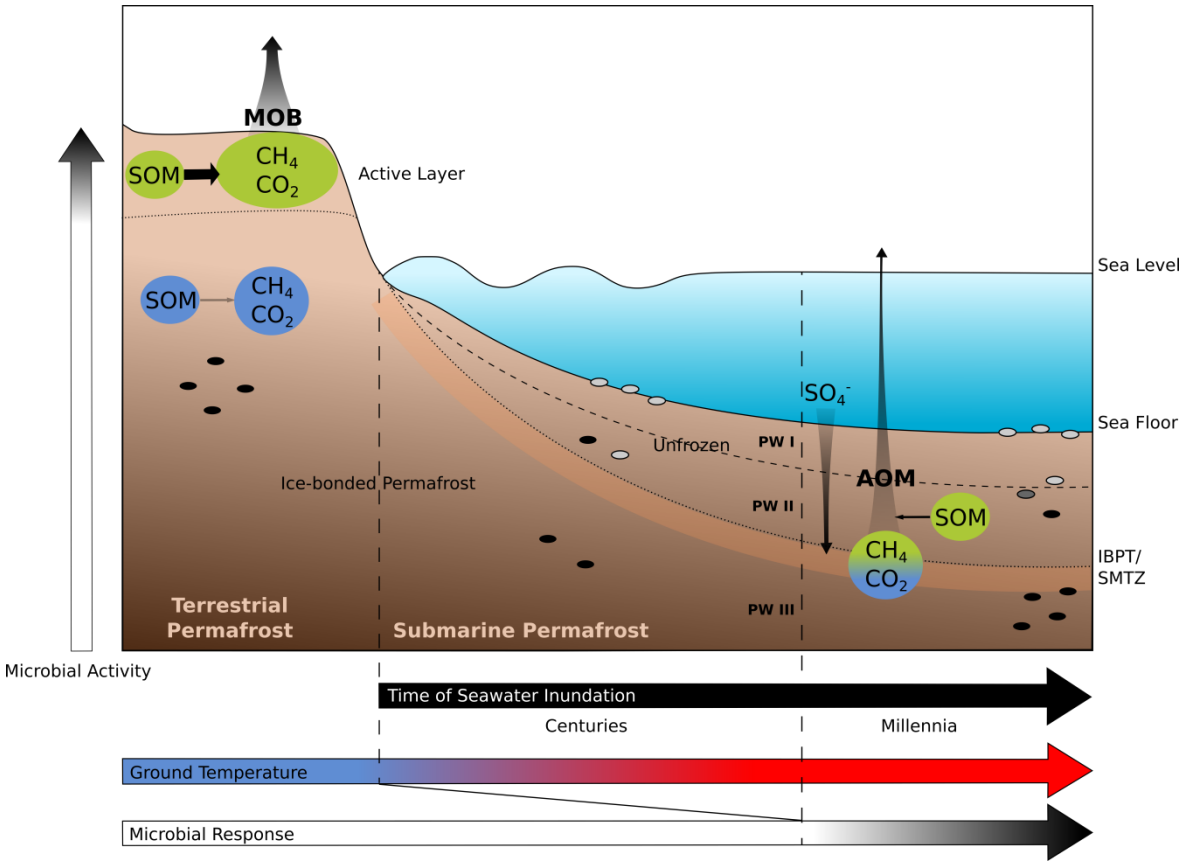

Figure 6-1: Schematic presentation of the results from this thesis including microbial activity, response to permafrost warming, abundance and community composition in dependence of seawater influence as well as carbon mobilization in terrestrial versus submarine permafrost. Blue and green colored circles represent either the soil organic matter or CH_4/CO_2 pools. Their color indicates if they are frozen/trapped (blue) or accessible to turnover and prone to release (green). Grey and black oval-shaped spheres illustrate microbial cells of different origin. SOM = soil organic matter; AOM = anaerobic oxidation of methane mediated by ANME; MOB = aerobic oxidation of methane mediated by methane oxidizing bacteria; PW = pore water unit; IBPT = ice-bonded permafrost table - the phase boundary between ice-free and ice-bonded sediment; SMTZ = sulfate-methane transition zone.

6.8 Critical remarks and Outlook

In this thesis, changes in the microbial abundance as well as in their community composition were used for estimating the responsiveness of microbial communities to permafrost warming. Those measures, however, may not be sensitive enough to investigate the microbial response. Microbial community composition and abundance were more strongly determined by the paleo-climate and -habitat type, and therefore varied significantly between drilling sites. Future work could address the analysis of organic matter quality [*Fischer et al.*, 2002], chemical composition of permafrost DOM [*Sun et al.*, 1997; *Spencer et al.*, 2015; *Ward and Cory*, 2015], natural

abundance isotope ratios of biomarkers [*Boschker and Middelburg*, 2002], metagenomics and metatranscriptomics [*Coolen and Orsi*, 2015; *Mackelprang et al.*, 2017]. Despite a large level of physicochemical similarity within the seawater unaffected submarine permafrost (Unit II) at Cape Mamontov Klyk the length of the coring transect (~12 km), the age span within and between the cores and hence the comparatively long sedimentation period encompassed by Unit II resulted in different origins of the microbial communities that strongly correlated with their abundance and composition. Further studies on the microbial response to permafrost warming should focus on historically more similar samples without neglecting similar physicochemical properties.

Although the enumeration of the total cell number is the best accepted method for determining the microbial abundance, the number of cells might have been slightly underestimated due to methodological issues during microscopy. Stacking of sediment particles on the filter is one factor that should be avoided. Hidden cells below sediment particles could further result in an underestimation. A simple way to approximate the true cell abundance is counting the free cells and the particle attached cells separately, and multiply the number of attached cells by two [*Kallmeyer*, 2011]. The possible underestimation of cell counts may have been one reason for the fact that 16S rRNA gene copies mostly exceeded TCC by an order of magnitude. In addition, the long-term preservation of extracellular DNA due to low temperature conditions in permafrost [*Stokstad*, 2003; *Willerslev et al.*, 2004] and, to a lesser extent, the appearance of multiple 16S rRNA gene copies per cell [*Schmidt*, 1998] may have resulted in higher gene copy numbers. Although qPCR is a good relative quantification method, it is only poorly related to cell counts [*Lloyd et al.*, 2013a] and was thus used for an evaluation and comparison of microbial gene abundance only between samples within this study.

Further work is also needed to clarify whether differences in the community size and structure between both study areas are a result of different inundation processes or spatial differences. Laboratory incubations with terrestrial permafrost samples under saline conditions could provide new insights into the true effect of seawater inundation on the indigenous microbial community.

The detection of ANME communities in thawed as well as in ice-bonded permafrost is one major result of this work that could help to improve climate models by incorporating predictions about the release of greenhouse gases from thawing submarine permafrost. However, the activity of those communities under *in situ* conditions remains to be proven. Future work on estimating the methane consumption could include the measurement of methane oxidation rates with isotopically labeled methane. This can be combined with secondary ion mass spectrometry

(SIMS) on ANME organisms detected with FISH for determining their stable isotope composition [*Orphan et al.*, 2001] or with the visualization of their translational activity [*Hatzenpichler et al.*, 2016]. When attempting to predict future greenhouse gas release it will also be critical to identify methanogenic activity and responsible microbial communities. In addition to ANME, a large diversity of potentially nitrogen cycling organisms was detected. Their role remains unknown and needs to be further investigated with the goal to understand their contribution in organic matter degradation of permafrost thaw processes.

The results obtained from core C2 at Cape Mamontov Klyk provide indicators for microbial proliferation and stimulation after millennia-scale permafrost warming. However, although several depths within this core were investigated the sediment core represents only one biological replicate for permafrost warming on timescales of millennia. For statistically significant results future studies should include a higher number of replicate cores ideally from different locations.

This thesis provides an important starting point for studying submarine permafrost as a climatically relevant and physicochemically unusual environment. More detailed studies are needed to fully understand the microbial impact on submarine permafrost carbon. Results should also be included in permafrost carbon feedback models.

Bibliography

ACIA. (2004). *ACIA (Arctic Climate Impact Assessment) Scientific Report; Arctic Climate - Past and Present*. (G. McBean, Ed.). Cambridge University Press.

Adam, P. S., Borrel, G., Brochier-Armanet, C., & Gribaldo, S. (2017). The growing tree of Archaea: new perspectives on their diversity, evolution and ecology. *The ISME Journal*, *11*(11), 2407–2425. https://doi.org/10.1038/ismej.2017.122

Alawi, M., Schneider, B., & Kallmeyer, J. (2014). A procedure for separate recovery of extra- and intracellular DNA from a single marine sediment sample. *Journal of Microbiological Methods*, *104*, 36–42. https://doi.org/10.1016/j.mimet.2014.06.009

Allison, S. D., & Martiny, J. B. H. (2008). Colloquium paper: resistance, resilience, and redundancy in microbial communities. *Proceedings of the National Academy of Sciences of the United States of America*, *105 Suppl*(Supplement_1), 11512–9. https://doi.org/10.1073/pnas.0801925105

Allison, S. D., McGuire, K. L., & Treseder, K. K. (2010). Resistance of microbial and soil properties to warming treatment seven years after boreal fire. *Soil Biology and Biochemistry*, *42*(10), 1872–1878. https://doi.org/10.1016/j.soilbio.2010.07.011

Altshuler, I., Goordial, J., & Whyte, L. G. (2017). Microbial Life in Permafrost. In *Psychrophiles: From Biodiversity to Biotechnology* (pp. 153–179). Cham: Springer International Publishing. https://doi.org/10.1007/978-3-319-57057-0_8

Anderson, M. J. (2001). A new method for non parametric multivariate analysis of variance. *Austral Ecology*, *26*, 32–46. https://doi.org/10.1111/j.1442-9993.2001.01070.pp.x

Anderson, R. E., Reveillaud, J., Reddington, E., Delmont, T. O., Eren, A. M., McDermott, J. M., et al. (2017). Genomic variation in microbial populations inhabiting the marine subseafloor at deep-sea hydrothermal vents. *Nature Communications*, *8*(1), 1114. https://doi.org/10.1038/s41467-017-01228-6

Anisimov, O. A. (2017). *Socio-economical impacts of thawing permafrost in Russia (Summary report - Impacts of Changing Climate in Permafrost Regions: the Russian Perspective)*. https://doi.org/10.13140/RG.2.2.27434.41920

Anthony, C. (1986). Bacterial Oxidation of Methane and Methanol. *Advances in Microbial Physiology*, *27*, 113–210. https://doi.org/10.1016/S0065-2911(08)60305-7

Are, F. (2003). Shoreface of the Arctic seas - A natural laboratory for subsea permafrost dynamics. In *Permafrost: Proceedings of the 8th International Conference on Permafrost*

(pp. 27–32). Zurich. Retrieved from http://research.iarc.uaf.edu/NICOP/DVD/ICOP 2003 Permafrost/Pdf/Chapter_006.pdf

Arshad, A., Speth, D. R., de Graaf, R. M., Op den Camp, H. J. M., Jetten, M. S. M., & Welte, C. U. (2015). A Metagenomics-Based Metabolic Model of Nitrate-Dependent Anaerobic Oxidation of Methane by Methanoperedens-Like Archaea. *Frontiers in Microbiology*, *6*, 1423. https://doi.org/10.3389/fmicb.2015.01423

Avery, G. B., Shannon, R. D., White, J. R., Martens, C. S., & Alperin, M. J. (1999). Effect of seasonal changes in the pathways of methanogenesis on the δ^{13}C values of pore water methane in a Michigan peatland. *Global Biogeochemical Cycles*, *13*(2), 475–484. https://doi.org/10.1029/1999GB900007

Ayala-del-Río, H. L., Chain, P. S., Grzymski, J. J., Ponder, M. A., Ivanova, N., Bergholz, P. W., et al. (2010). The Genome Sequence of Psychrobacter arcticus 273-4, a Psychroactive Siberian Permafrost Bacterium, Reveals Mechanisms for Adaptation to Low-Temperature Growth. *Applied and Environmental Microbiology*, *76*(7), 2304–2312. https://doi.org/10.1128/AEM.02101-09

Ayton, J., Aislabie, J., Barker, G. M., Saul, D., & Turner, S. (2010). *Crenarchaeota* affiliated with group 1.1b are prevalent in coastal mineral soils of the Ross Sea region of Antarctica. *Environmental Microbiology*, *12*(3), 689–703. https://doi.org/10.1111/j.1462-2920.2009.02111.x

Bakermans, C. (2017). Determining the limits of microbial life at subzero temperatures. In R. Margesi (Ed.), *Psychrophiles: from biodiversity to biotechnology* (pp. 21–38). Berlin: Springer, Berlin.

Bakermans, C., Bergholz, P. W., Ayala-del-Río, H., & Tiedje, J. (2009). Genomic Insights into Cold Adaptation of Permafrost Bacteria. In R. Margesin (Ed.), *Permafrost Soils. Soil Biology* (16th ed., pp. 159–168). Berlin, Heidelberg: Springer Berlin Heidelberg. https://doi.org/10.1007/978-3-540-69371-0_11

Bakermans, C., Skidmore, M. L., Douglas, S., & McKay, C. P. (2014). Molecular characterization of bacteria from permafrost of the Taylor Valley, Antarctica. *FEMS Microbiology Ecology*, *89*(2), 331–346. https://doi.org/10.1111/1574-6941.12310

Baldani, J. I., Rouws, L., Cruz, L. M., Olivares, F. L., Schmid, M., & Hartmann, A. (2014). The Family Oxalobacteraceae. In *The Prokaryotes* (pp. 919–974). Berlin, Heidelberg: Springer Berlin Heidelberg. https://doi.org/10.1007/978-3-642-30197-1_291

Bannert, A., Bogen, C., Esperschütz, J., Koubová, A., Buegger, F., Fischer, D., et al. (2012). Anaerobic oxidation of methane in grassland soils used for cattle husbandry.

Biogeosciences, *9*(10), 3891–3899. https://doi.org/10.5194/bg-9-3891-2012

Bauch, H. A., Mueller-Lupp, T., Taldenkova, E., Spielhagen, R. F., Kassens, H., Grootes, P. M., et al. (2001). Chronology of the holocene transgression at the north siberian margin. *Global and Planetary Change*, *31*(1–4), 125–139. https://doi.org/10.1016/S0921-8181(01)00116-3

Bauch, Henning A., & Kassens, H. (2005). Arctic Siberian shelf environments - An introduction. *Global and Planetary Change*, *48*(1-3 SPEC. ISS.), 1–8. https://doi.org/10.1016/j.gloplacha.2004.12.003

Beal, E. J., House, C. H., & Orphan, V. J. (2009). Manganese- and iron-dependent marine methane oxidation. *Science*, *325*(5937), 184–187. https://doi.org/325/5937/184 [pii] 10.1126/science.1169984

Berchet, A., Bousquet, P., Pison, I., Locatelli, R., Chevallier, F., Paris, J. D., et al. (2016). Atmospheric constraints on the methane emissions from the East Siberian Shelf. *Atmospheric Chemistry and Physics*, *16*(6), 4147–4157. https://doi.org/10.5194/acp-16-4147-2016

Bischoff, J., Mangelsdorf, K., Gattinger, A., Schloter, M., Kurchatova, A. N., Herzschuh, U., & Wagner, D. (2013). Response of methanogenic archaea to Late Pleistocene and Holocene climate changes in the Siberian Arctic. *Global Biogeochemical Cycles*, *27*(2), 305–317. https://doi.org/10.1029/2011GB004238

Bischoff, J., Mangelsdorf, K., Schwamborn, G., & Wagner, D. (2014). Impact of Lake-Level and Climate Changes on Microbial Communities in a Terrestrial Permafrost Sequence of the El'gygytgyn Crater, Far East Russian Arctic. *Permafrost and Periglacial Processes*, *25*(2), 107–116. https://doi.org/10.1002/ppp.1807

Biskaborn, B. K., Smith, S. L., Noetzli, J., Matthes, H., Vieira, G., Streletskiy, D. A., et al. (2019). Permafrost is warming at a global scale. *Nature Communications*, *10*(264), 1–11. https://doi.org/10.1038/s41467-018-08240-4

Boetius, A., & Wenzhöfer, F. (2013). Seafloor oxygen consumption fuelled by methane from cold seeps. *Nature Geoscience*, *6*(9), 725–734. https://doi.org/10.1038/ngeo1926

Boetius, A., Ravenschlag, K., Schubert, C. J., Rickert, D., Widdel, F., Gieseke, A., et al. (2000). A marine microbial consortium apparently mediating anaerobic oxidation of methane. *Nature*, *407*(6804), 623–626. https://doi.org/http://www.nature.com/nature/journal/v407/n6804/suppinfo/407623a0_S1.html

Bolger, A. M., Lohse, M., & Usadel, B. (2014). Trimmomatic: A flexible trimmer for Illumina

sequence data. *Bioinformatics*, *30*(15), 2114–2120. https://doi.org/10.1093/bioinformatics/btu170

Boone, D. R., & Mah, R. A. (2015). *Methanosarcina*. In *Bergey's Manual of Systematics of Archaea and Bacteria* (pp. 1–15). Chichester, UK: John Wiley & Sons, Ltd. https://doi.org/10.1002/9781118960608.gbm00519

Boschker, H. T. S., & Middelburg, J. J. (2002). Stable isotopes and biomarkers in microbial ecology. *FEMS Microbiology Ecology*, *40*(2), 85–95. https://doi.org/10.1111/j.1574-6941.2002.tb00940.x

Boss, C. B., & Frieden, K. J. (1989). *Concepts, instrumentation, and techniques in inductively coupled plasma atomic emission spectrometry. Handbook Perkin-Elmer*. USA: Perkin-Elmer Corporation.

Bottos, E. M., Kennedy, D. W., Romero, E. B., Fansler, S. J., Brown, J. M., Bramer, L. M., et al. (2018). Dispersal limitation and thermodynamic constraints govern spatial structure of permafrost microbial communities. *FEMS Microbiology Ecology*, *94*, 1–48. https://doi.org/10.1101/265132

Brochier-Armanet, C., Boussau, B., Gribaldo, S., & Forterre, P. (2008). Mesophilic crenarchaeota: proposal for a third archaeal phylum, the Thaumarchaeota. *Nature Reviews Microbiology*, *6*(3), 245–252. https://doi.org/10.1038/nrmicro1852

Brown, J., Ferrians, Jr, O. J., Heginbottom, J. A., & Melnikov, E. (1997). *Circum-Arctic map of permafrost and ground-ice conditions*. Washington DC: US Geological Survey.

Brown, J., Ferrians Jr., O. J., Heginbottom, J. A., & Melnikov, E. S. (2002). *Circum-Arctic Map of Permafrost and Ground-Ice Conditions, Version 2*. Boulder, Colo.: Natl. Snow and Ice Data Cent.

Buford Price, P., & Sowers, T. (2004). Temperature dependence of metabolic rates for microbial growth, maintenance and survival. *Proceedings of the National Academy of Sciences of the United States of America*, *101*(13), 4631–4636. https://doi.org/10.1073/pnas.95.12.6578

Campbell, B. B. J., & Kirchman, D. L. D. D. L. (2012). Bacterial diversity, community structure and potential growth rates along an estuarine salinity gradient. *The ISME Journal*, *7*(1), 210–220. https://doi.org/10.1038/ismej.2012.93

Canfield, D. E., Thamdrup, B., & Hansen, J. W. (1993). The anaerobic degradation of organic matter in Danish coastal sediments: Iron reduction, manganese reduction, and sulfate reduction. *Geochimica et Cosmochimica Acta*, *57*(16), 3867–3883. https://doi.org/10.1016/0016-7037(93)90340-3

Caporaso, J. G., Kuczynski, J., Stombaugh, J., Bittinger, K., Bushman, F. D., Costello, E. K., et al. (2010). QIIME allows analysis of high- throughput community sequencing data. *Nature Methods*, *7*(5), 335–336. https://doi.org/10.1038/nmeth0510-335

Castelle, C. J., Wrighton, K. C., Thomas, B. C., Hug, L. A., Brown, C. T., Wilkins, M. J., et al. (2015). Genomic expansion of domain archaea highlights roles for organisms from new phyla in anaerobic carbon cycling. *Current Biology*, *25*(6), 690–701. https://doi.org/10.1016/j.cub.2015.01.014

Cerqueira, T., Pinho, D., Egas, C., Froufe, H., Altermark, B., Candeias, C., et al. (2015). Microbial diversity in deep-sea sediments from the Menez Gwen hydrothermal vent system of the Mid-Atlantic Ridge. *Marine Genomics*, *24*, 343–355. https://doi.org/10.1016/j.margen.2015.09.001

Charkin, A. N., Dudarev, O. V., Semiletov, I. P., Kruhmalev, a. V., Vonk, J. E., Sánchez-García, L., et al. (2011). Seasonal and interannual variability of sedimentation and organic matter distribution in the Buor-Khaya Gulf: The primary recipient of input from Lena River and coastal erosion in the southeast Laptev Sea. *Biogeosciences*, *8*(9), 2581–2594. https://doi.org/10.5194/bg-8-2581-2011

Chattopadhyay, M. K. (2006). Mechanism of bacterial adaptation to low temperature. *Journal of Biosciences*, *31*(1), 157–165. https://doi.org/10.1007/BF02705244

Ciais, P., Sabine, C., Bala, G., Bopp, L., Brovkin, V., Canadell, J., et al. (2013). Carbon and other biogeochemical cycles. In T. F. Stocker, D. Qin, G.-K. Plattner, M. Tignor, S. K. Allen, J. Boschung, et al. (Eds.), *Climate change 2013: The physical science basis. Contribution of working group 1 to the fifth assessment report of the Intergovernmental Panel on Climate Change* (pp. 465–571). Cambridge University Press, Cambridge, United Kingdom and New York, NY, USA.

Ciobanu, M.-C., Rabineau, M., Droz, L., Révillon, S., Ghiglione, J.-F., Dennielou, B., et al. (2012). Sedimentological imprint on subseafloor microbial communities in Western Mediterranean Sea Quaternary sediments. *Biogeosciences*, *9*(9), 3491–3512. https://doi.org/10.5194/bg-9-3491-2012

Clarke, A. (2014). The thermal limits to life on Earth. *International Journal of Astrobiology*, *13*(02), 141–154. https://doi.org/10.1017/S1473550413000438

Coolen, M. J. L., & Orsi, W. D. (2015). The transcriptional response of microbial communities in thawing Alaskan permafrost soils. *Frontiers in Microbiology*, *6*(197), 1–14. https://doi.org/10.3389/fmicb.2015.00197

Corinaldesi, C., Danovaro, R., Anno, D., & Anno, A. D. (2005). Simultaneous Recovery of

Extracellular and Intracellular DNA Suitable for Molecular Studies from Marine Sediments Simultaneous Recovery of Extracellular and Intracellular DNA Suitable for Molecular Studies from Marine Sediments. *Society*, *71*(1), 46–50. https://doi.org/10.1128/AEM.71.1.46

Crevecoeur, S., Vincent, W. F., Comte, J., & Lovejoy, C. (2015). Bacterial community structure across environmental gradients in permafrost thaw ponds: Methanotroph-rich ecosystems. *Frontiers in Microbiology*, *6*(MAR), 1–15. https://doi.org/10.3389/fmicb.2015.00192

Crowe, S. A., Katsev, S., Leslie, K., Sturm, A., Magen, C., Nomosatryo, S., et al. (2011). The methane cycle in ferruginous Lake Matano. *Geobiology*, *9*(1), 61–78. https://doi.org/10.1111/j.1472-4669.2010.00257.x

D'Amico, S., Collins, T., Marx, J.-C., Feller, G., Gerday, C., & Gerday, C. (2006). Psychrophilic microorganisms: challenges for life. *EMBO Reports*, *7*(4), 385–389. https://doi.org/10.1038/sj.embor.7400662

D'Hondt, S., Jorgensen, B. B., Miller, D. J., Batzke, A., Blake, R., Cragg, B. A., et al. (2004). Distributions of Microbial Activities in Deep Subseafloor Sediments. *Science*, *306*(5705), 2216–2221. https://doi.org/10.1126/science.281.5379.978

Daae, F. L., Økland, I., Dahle, H., Jørgensen, S. L., Thorseth, I. H., & Pedersen, R. B. (2013). Microbial life associated with low-temperature alteration of ultramafic rocks in the Leka ophiolite complex. *Geobiology*, *11*(4), 318–339. https://doi.org/10.1111/gbi.12035

DeAngelis, K. M., Pold, G., Topçuoglu, B. D., van Diepen, L. T. a., Varney, R. M., Blanchard, J. L., et al. (2015). Long-term forest soil warming alters microbial communities in temperate forest soils. *Frontiers in Microbiology*, *6*(104), 1–13. https://doi.org/10.3389/fmicb.2015.00104

Dekas, A. E., Connon, S. A., Chadwick, G. L., Trembath-Reichert, E., & Orphan, V. J. (2016). Activity and interactions of methane seep microorganisms assessed by parallel transcription and FISH-NanoSIMS analyses. *The ISME Journal*, *10*(3), 678–692. https://doi.org/10.1038/ismej.2015.145

Delgado-Baquerizo, M., Eldridge, D. J., Ochoa, V., Gozalo, B., Singh, B. K., & Maestre, F. T. (2017). Soil microbial communities drive the resistance of ecosystem multifunctionality to global change in drylands across the globe. *Ecology Letters*, *20*(10), 1295–1305. https://doi.org/10.1111/ele.12826

DeLong, E. F. (1992). Archaea in coastal marine environments. *Proceedings of the National Academy of Sciences of the United States of America*, *89*(12), 5685–5689. https://doi.org/10.1073/PNAS.89.12.5685

Denich, T., Beaudette, L. ., Lee, H., & Trevors, J. . (2003). Effect of selected environmental and physico-chemical factors on bacterial cytoplasmic membranes. *Journal of Microbiological Methods*, *52*(2), 149–182. https://doi.org/10.1016/S0167-7012(02)00155-0

Dereviagin, A., & Kunitsky, V. (2004). Geographical and geological background. In L. Schirrmeister (Ed.), *Expeditions in Siberia in 2003. Reports on Polar and Marine Research 489* (pp. 63–66).

Dridi, B., Fardeau, M.-L., Ollivier, B., Raoult, D., & Drancourt, M. (2012). Methanomassiliicoccus luminyensis gen. nov., sp. nov., a methanogenic archaeon isolated from human faeces. *International Journal of Systematic and Evolutionary Microbiology*, *62*, 1902–1907. https://doi.org/10.1099/ijs.0.033712-0

Duret, M. T., Lampitt, R. S., & Lam, P. (2019). Prokaryotic niche partitioning between suspended and sinking marine particles. *Environmental Microbiology Reports*, *11*(3), 386–400. https://doi.org/10.1111/1758-2229.12692

Edgar, R. C. (2010). Search and clustering orders of magnitude faster than BLAST. *Bioinformatics*, *26*(19), 2460–2461. https://doi.org/10.1093/bioinformatics/btq461

Eicken, H., Dmitrenko, I., Tyshko, K., Darovskikh, A., Dierking, W., Blahak, U., et al. (2005). Zonation of the Laptev Sea landfast ice cover and its importance in a frozen estuary. *Global and Planetary Change*, *48*(1–3), 55–83. https://doi.org/10.1016/j.gloplacha.2004.12.005

Elberling, B., & Brandt, K. K. (2003). Uncoupling of microbial CO2 production and release in frozen soil and its implications for field studies of arctic C cycling. *Soil Biology and Biochemistry*, *35*(2), 263–272. https://doi.org/10.1016/S0038-0717(02)00258-4

Elvert, M., Boetius, A., Knittel, K., & Jørgensen, B. B. (2003). Characterization of Specific Membrane Fatty Acids as Chemotaxonomic Markers for Sulfate-Reducing Bacteria Involved in Anaerobic Oxidation of Methane. *Geomicrobiology Journal*, *20*(4), 403–419. https://doi.org/10.1080/01490450303894

Ernakovich, J. G., & Wallenstein, M. D. (2015). Permafrost microbial community traits and functional diversity indicate low activity at in situ thaw temperatures. *Soil Biology and Biochemistry*, *87*, 78–89. https://doi.org/10.1016/j.soilbio.2015.04.009

Ettwig, K. F., Zhu, B., Speth, D., Keltjens, J. T., Jetten, M. S. M., & Kartal, B. (2016). Archaea catalyze iron-dependent anaerobic oxidation of methane. *Proceedings of the National Academy of Sciences of the United States of America*, *113*(45), 12792–12796. https://doi.org/10.1073/pnas.1609534113

Evans, P. N., Parks, D. H., Chadwick, G. L., Robbins, S. J., Orphan, V. J., Golding, S. D., & Tyson, G. W. (2015). Methane metabolism in the archaeal phylum Bathyarchaeota revealed by genome-centric metagenomics. *Science*, *350*(6259), 434–438. https://doi.org/10.1126/science.aac7745

van Everdingen, R. O. (1998). *Multi-language glossary of permafrost and related ground-ice terms*. Boulder: National Snow and Ice Data Center/World Data Center for Glaciology.

Feige, K. (2009). *Molecular ecological analysis of methanogenic communities in terrestrial and submarine permafrost deposits of Siberian Laptev Sea area*. University of Potsdam.

Feller, G., & Gerday, C. (2003). Psychrophilic enzymes: Hot topics in cold adaptation. *Nature Reviews Microbiology*, *1*(3), 200–208. https://doi.org/10.1038/nrmicro773

Fierer, N., & Jackson, R. B. (2006). The diversity and biogeography of soil bacterial communities. *Proceedings of the National Academy of Sciences of the United States of America*, *103*(3), 626–631. https://doi.org/10.1073/pnas.0507535103

Fillol, M., Auguet, J.-C., Casamayor, E. O., & Borrego, C. M. (2016). Insights in the ecology and evolutionary history of the Miscellaneous Crenarchaeotic Group lineage. *The ISME Journal*, *10*(3), 665–677. https://doi.org/10.1038/ismej.2015.143

Fischer, H., Wanner, S. C., & Pusch, M. (2002). Bacterial abundance and production in river sediments as related to the biochemical composition of particulate organic matter (POM). *Biogeochemistry*, *61*(1), 37–55. https://doi.org/10.1023/A:1020298907014

Flynn, T. M., Sanford, R. A., Ryu, H., Bethke, C. M., Levine, A. D., Ashbolt, N. J., & Santo Domingo, J. W. (2013). Functional microbial diversity explains groundwater chemistry in a pristine aquifer. *BMC Microbiology*, *13*(146), 1–15. https://doi.org/10.1186/1471-2180-13-146

Frank-Fahle, B. A., Yergeau, É., Greer, C. W., Lantuit, H., & Wagner, D. (2014). Microbial functional potential and community composition in permafrost-affected soils of the NW Canadian Arctic. *PLoS ONE*, *9*(1). https://doi.org/10.1371/journal.pone.0084761

Franks, F. (2003). Nucleation of ice and its management in ecosystems. *Philosophical Transactions of the Royal Society of London. Series A: Mathematical, Physical and Engineering Sciences*, *361*(1804), 557–574. https://doi.org/10.1098/rsta.2002.1141

Fritz, M., Vonk, J. E., & Lantuit, H. (2017). Collapsing Arctic coastlines. *Nature Climate Change*, *7*(1), 6–7. https://doi.org/10.1038/nclimate3188

Fry, J. C., Parkes, R. J., Cragg, B. a., Weightman, A. J., & Webster, G. (2008). Prokaryotic biodiversity and activity in the deep subseafloor biosphere. *FEMS Microbiology Ecology*, *66*(2), 181–196. https://doi.org/10.1111/j.1574-6941.2008.00566.x

Galinski, E. A. (1995). Osmoadaptation in Bacteria. *Advances in Microbial Physiology*, *37*, 273–328. https://doi.org/10.1016/S0065-2911(08)60148-4

Ganzert, L., Bajerski, F., & Wagner, D. (2014). Bacterial community composition and diversity of five different permafrost-affected soils of Northeast Greenland. *FEMS Microbiology Ecology*, *89*(2), 426–441. https://doi.org/10.1111/1574-6941.12352

Gao, Y., Lee, J., Neufeld, J. D., Park, J., Rittmann, B. E., & Lee, H.-S. (2017). Anaerobic oxidation of methane coupled with extracellular electron transfer to electrodes. *Scientific Reports*, *7*(1), 5099. https://doi.org/10.1038/s41598-017-05180-9

Geets, J., Borremans, B., Diels, L., Springael, D., Vangronsveld, J., van der Lelie, D., & Vanbroekhoven, K. (2006). DsrB gene-based DGGE for community and diversity surveys of sulfate-reducing bacteria. *Journal of Microbiological Methods*, *66*(2), 194–205. https://doi.org/10.1016/j.mimet.2005.11.002

Ghabbour, E. A., & Davies, G. (Eds.). (2007). *Humic Substances: Structures, Models and Functions*. Royal Society of Chemistry.

Gilichinsky, D. A., Rivkina, E., Shcherbakova, V., Laurinavichuis, K., & Tiedje, J. (2003). Supercooled Water Brines Within Permafrost—An Unknown Ecological Niche for Microorganisms: A Model for Astrobiology. *Astrobiology*, *3*(2), 331–341. https://doi.org/10.1089/153110703769016424

Gilichinsky, D. A., Khlebnikova, G. M., Zvyagintsev, D. G., Fedorov-Davydov, D. G., & Kudryavtseva, N. N. (1989). Microbiology of Sedimentary Materials in the Permafrost Zone. *International Geology Review*, *31*(8), 847–858. https://doi.org/10.1080/00206818909465938

Gilichinsky, D. A., Vorobyova, E. A., Erokhina, L. G., Fyordorov-Dayvdov, D. G., & Chaikovskaya, N. R. (1992). Long-term preservation of microbial ecosystems in permafrost. *Advances in Space Research*, *12*(4), 255–263. https://doi.org/10.1016/0273-1177(92)90180-6

Gilichinsky, D. A. (2002). Permafrost. In G. Bitton (Ed.), *Encyclopedia of environmental microbiology* (pp. 2367–2385). New York: Wiley.

Gilichinsky, D. A., Vishnivetskaya, T., Petrova, M., Spirina, E., Mamykin, V., & Rivkina, E. (2008). Bacteria in permafrost. In R. Margesin (Ed.), *Psychrophiles: From Biodiversity to Biotechnology* (pp. 83–102). Berlin Heidelberg: Springer-Verlag. https://doi.org/10.1007/978-3-540-74335-4_6

Gilichinsky, D. A. (2008). Psychrophiles: from biodiversity to biotechnology. In R. Margesin, F. Schinner, J. C. Marx, & C. Gerday (Eds.), *Springer Science & Business Media* (pp. 83–

102).

Glass, J. B., Ranjan, P., Kretz, C. B., Nunn, B. L., Johnson, A. M., McManus, J., & Stewart, F. J. (2019). Adaptations of Atribacteria to life in methane hydrates: hot traits for cold life. *BioRxiv*, 1–26. https://doi.org/10.1101/536078

Graham, D. E., Wallenstein, M. D., Vishnivetskaya, T. A., Waldrop, M. P., Phelps, T. J., Pfiffner, S. M., et al. (2012). Microbes in thawing permafrost: The unknown variable in the climate change equation. *The ISME Journal*. https://doi.org/10.1038/ismej.2011.163

Grigoriev, M. N. (2008). *Kriomorphogenez i litodinamika pribrezhno-shelfovoi zony morei Vostochnoi Sibiri (Cryomorphogenesis and lithodynamics of the East Siberian near-shore shelf zone)*. Russian Academy of Sciences, Siberian Branch [in Russian], Yakutsk.

Grosse, G., Robinson, J., Bryant, R., Taylor, M. D., Harper, W., DeMasi, a., et al. (2013). Distribution of late Pleistocene ice-rich syngenetic permafrost of the Yedoma Suite in east and central Siberia, Russia. *Geological Survey Open File Report 2013-1078*, 37pp. Retrieved from http://epic.awi.de/33878/

Günther, F., Overduin, P. P., Makarov, A. S., & Grigoriev, M. N. (2013a). Russian-German Cooperation SYSTEM LAPTEV SEA: The Expeditions Laptev Sea—Mamontov Klyk 2011 & Buor Khaya 2012. In *Berichte zur Polar- und Meeresforschung = Reports on polar and marine research* (p. 664). https://doi.org/10.1016/S0376-7361(09)70018-4

Günther, F., Overduin, P. P., Sandakov, a. V., Grosse, G., & Grigoriev, M. N. (2013b). Short- and long-term thermo-erosion of ice-rich permafrost coasts in the Laptev Sea region. *Biogeosciences*, *10*(6), 4297–4318. https://doi.org/10.5194/bg-10-4297-2013

Günther, F., Overduin, P. P., Sandakov, A. V, Grosse, G., & Grigoriev, M. N. (2012). Thermo-erosion along the Yedoma Coast of the Buor Khaya Peninsula, Laptev Sea, East Siberia. *Tenth International Conference on Permafrost*, *2*, 137–142.

Haas, B. J., Gevers, D., Earl, A. M., Feldgarden, M., Ward, D. V, Giannoukos, G., et al. (2011). Chimeric 16S rRNA sequence formation and detection in Sanger and 454-pyrosequenced PCR amplicons. *Genome Research*, *21*(3), 494–504. https://doi.org/10.1101/gr.112730.110

Hammer, Ø., Harper, D. A. T., & Ryan, P. D. (2001). PAST: Paleontological Statistics Software Package for Education and Data Analysis. *Palaeontologia Electronica*, *4*(1), 1–9.

Hanson, C. A., Fuhrman, J. A., Horner-Devine, M. C., & Martiny, J. B. H. (2012). Beyond biogeographic patterns: processes shaping the microbial landscape. *Nature Reviews Microbiology*, *10*(May), 1–10. https://doi.org/10.1038/nrmicro2795

Hanson, R. S., & Hanson, T. E. (1996). Methanotrophic bacteria. *Microbiol. Rev.*, *60*(2), 439–

471. Retrieved from http://www.ncbi.nlm.nih.gov/pmc/articles/PMC239451/pdf/600439.pdf/?tool=pmcentrez

Haroon, M. F., Hu, S., Shi, Y., Imelfort, M., Keller, J., Hugenholtz, P., et al. (2013). Anaerobic oxidation of methane coupled to nitrate reduction in a novel archaeal lineage. *Nature*, *500*(7464), 567–570. https://doi.org/10.1038/nature12375

Harrison, W. D., & Osterkamp, T. E. (1982). Measurements of the electrical conductivity of interstitial water in subsea permafrost. In H. M. French (Ed.), *pPoceedings of the fourth Canadian Permafrost Conference* (pp. 229–237). Ottawa: National Research Council of Canada.

Hatzenpichler, R., Connon, S. A., Goudeau, D., Malmstrom, R. R., Woyke, T., & Orphan, V. J. (2016). Visualizing in situ translational activity for identifying and sorting slow-growing archaeal−bacterial consortia. *Proceedings of the National Academy of Sciences of the United States of America*, *113*(28), E4069–E4078. https://doi.org/10.1073/pnas.1603757113

Herlemann, D. P., Labrenz, M., Jürgens, K., Bertilsson, S., Waniek, J. J., & Andersson, A. F. (2011). Transitions in bacterial communities along the 2000 km salinity gradient of the Baltic Sea. *The ISME Journal*, *5*(10), 1571–9. https://doi.org/10.1038/ismej.2011.41

Heslop, J. K., Walter Anthony, K. M., Sepulveda-Jauregui, A., Martinez-Cruz, K., Bondurant, A., Grosse, G., & Jones, M. C. (2015). Thermokarst lake methanogenesis along a complete talik profile. *Biogeosciences*, *12*(14), 4317–4331. https://doi.org/10.5194/bg-12-4317-2015

Hinrichs, K.-U., & Boetius, A. (2002). The Anaerobic Oxidation of Methane: New Insights in Microbial Ecology and Biogeochemistry. In G. Wefer, D. Billett, D. Hebbeln, B. B. Jørgensen, M. Schlüter, & T. C. E. van Weering (Eds.), *Ocean Margin Systems* (pp. 457–477). Berlin, Heidelberg: Springer Berlin Heidelberg. https://doi.org/10.1007/978-3-662-05127-6_28

Hodgkins, S. B., Tfaily, M. M., McCalley, C. K., Logan, T. A., Crill, P. M., Saleska, S. R., et al. (2014). Changes in peat chemistry associated with permafrost thaw increase greenhouse gas production. *Proceedings of the National Academy of Sciences of the United States of America*, *111*(16), 5819–24. https://doi.org/10.1073/pnas.1314641111

Hoj, L., Olsen, R. A., & Torsvik, V. L. (2008). Effects of temperature on the diversity and community structure of known methanogenic groups and other archaea in high Arctic peat. *ISME J*, *2*(1), 37–48. https://doi.org/ismej200784 [pii] 10.1038/ismej.2007.84

Holler, T., Wegener, G., Knittel, K., Boetius, A., Brunner, B., Kuypers, M. M. M., & Widdel,

F. (2009). Substantial ^{13}C/ ^{12}C and D/H fractionation during anaerobic oxidation of methane by marine consortia enriched *in vitro*. *Environmental Microbiology Reports*, *1*(5), 370–376. https://doi.org/10.1111/j.1758-2229.2009.00074.x

Hopmans, E. C., Weijers, J. W. ., Schefuß, E., Herfort, L., Sinninghe Damsté, J. S., & Schouten, S. (2004). A novel proxy for terrestrial organic matter in sediments based on branched and isoprenoid tetraether lipids. *Earth and Planetary Science Letters*, *224*(1–2), 107–116. https://doi.org/10.1016/J.EPSL.2004.05.012

Hubberten, H. W., Andreev, A., Astakhov, V. I., Demidov, I., Dowdeswell, J. A., Henriksen, M., et al. (2004). The periglacial climate and environment in northern Eurasia during the Last Glaciation. *Quaternary Science Reviews*, *23*(11–13), 1333–1357. https://doi.org/10.1016/j.quascirev.2003.12.012

Hugelius, G., Strauss, J., Zubrzycki, S., Harden, J. W., Schuur, E. a. G., Ping, C. L., et al. (2014). Estimated stocks of circumpolar permafrost carbon with quantified uncertainty ranges and identified data gaps. *Biogeosciences*, *11*(23), 6573–6593. https://doi.org/10.5194/bg-11-6573-2014

Hultman, J., Waldrop, M. P., Mackelprang, R., David, M. M., McFarland, J., Blazewicz, S. J., et al. (2015). Multi-omics of permafrost, active layer and thermokarst bog soil microbiomes. *Nature*, *521*(7551), 208–212. https://doi.org/10.1038/nature14238

Hunger, S., Schmidt, O., Hilgarth, M., Horn, M. A., Kolb, S., Conrad, R., & Drake, H. L. (2011). Competing Formate- and Carbon Dioxide-Utilizing Prokaryotes in an Anoxic Methane-Emitting Fen Soil. *Applied and Environmental Microbiology*, *77*(11), 3773–3785. https://doi.org/10.1128/aem.00282-11

Inagaki, F, Hinrichs, K.-U., Kubo, Y., Bowles, M. W., Heuer, V. B., Hong, W.-L., et al. (2015). Exploring deep microbial life in coal-bearing sediment down to ~2.5 km below the ocean floor. *Science*, *349*(6246), 420–424. https://doi.org/10.1126/science.aaa6882

Inagaki, F., & Nealson, K. H. (2006). THE PALEOME: LETTERS FROM ANCIENT EARTH. In *Past and Present Water Column Anoxia* (pp. 21–39). Dordrecht: Kluwer Academic Publishers. https://doi.org/10.1007/1-4020-4297-3_02

IPCC in Climate Change 2013. (2013). The Physical Science Basis. Contribution of Working Group I to the Fifth Assessment Report of the Intergovernmental Panel on Climate Change. *Cambridge Univ. Press*, 1535.

Iversen, N., & Jør-gensen, B. B. (1985). Anaerobic methane oxidation rates at the sulfate-methane transition in marine sediments from Kattegat and Skagerrak (Denmark). *Limnology and Oceanography*, *30*(5), 944–955.

Jansson, J. K., & Taş, N. (2014). The microbial ecology of permafrost. *Nature Reviews. Microbiology*, *12*(6), 414–425. https://doi.org/10.1038/nrmicro3262

Jiang, H., Dong, H., Yu, B., Liu, X., Li, Y., Ji, S., & Zhang, C. L. (2007). Microbial response to salinity change in Lake Chaka, a hypersaline lake on Tibetan plateau. *Environmental Microbiology*, *9*(10), 2603–2621. https://doi.org/10.1111/j.1462-2920.2007.01377.x

Johnson, S. S., Hebsgaard, M. B., Christensen, T. R., Mastepanov, M., Nielsen, R., Munch, K., et al. (2007). Ancient bacteria show evidence of DNA repair. *Proceedings of the National Academy of Sciences*, *104*(36), 14401–14405. https://doi.org/10.1073/pnas.0706787104

Jones, B. M., Arp, C. D., Jorgenson, M. T., Hinkel, K. M., Schmutz, J. A., & Flint, P. L. (2009). Increase in the rate and uniformity of coastline erosion in Arctic Alaska. *Geophysical Research Letters*, *36*(3), 1–5. https://doi.org/10.1029/2008GL036205

de Jong, A. E. E., in 't Zandt, M. H., Meisel, O. H., Jetten, M. S. M., Dean, J. F., Rasigraf, O., & Welte, C. U. (2018). Increases in temperature and nutrient availability positively affect methane cycling mircoorganisms in arctic thermokarst lake sediments. *Environmental Microbiology*, *00*. https://doi.org/10.1111/1462-2920.14345

Jorgensen, B. B. (1980). Mineralization and the bacterial cycling of carbon, nitrogen and sulphur in marine sediments. In D. Ellwood, J. Hedger, M. Latham, J. Lynch, & J. Starer (Eds.), *Contemporary microbial ecology* (pp. 239–251). London, New York, Toronto, Sydney, San Francisco: Academic Press, 1980. Retrieved from http://agris.fao.org/agris-search/search.do?recordID=US201301302940

Jørgensen, B. B., & Marshall, I. P. G. (2016). Slow Microbial Life in the Seabed. *Annual Review of Marine Science*, *8*(1), 311–332. https://doi.org/10.1146/annurev-marine-010814-015535

Junge, K., Krembs, C., Deming, J., Stierle, A., & Eicken, H. (2001). A microscopic approach to investigate bacteria under in situ conditions in sea-ice samples. *Annals of Glaciology*, *33*, 304–310. https://doi.org/10.3189/172756401781818275

Junge, K., Eicken, H., & Deming, J. W. (2004). Bacterial Activity at -2 to -20 degrees C in Arctic wintertime sea ice. *Applied and Environmental Microbiology*, *70*(1), 550–557. https://doi.org/10.1128/AEM.70.1.550–557.2004

Junker, R., Grigoriev, M. N., & Kaul, N. (2008). Non-contact infrared temperature measurements in dry permafrost boreholes. *Journal of Geophysical Research: Soild Earth*, *113*(B4102), 1–10. https://doi.org/10.1029/2007JB004946

Kallmeyer, J. (2011). *Detection and Quantification of Microbial Cells in Subsurface Sediments*. *Advances in Applied Microbiology* (1st ed., Vol. 76). Elsevier Inc.

https://doi.org/10.1016/B978-0-12-387048-3.00003-9

Kallmeyer, J., Smith, D. C., Spivack, A. J., & D'Hondt, S. (2008). New cell extraction procedure applied to deep subsurface sediments. *Limnol. Oceanogr. Methods*, *6*, 236–245. https://doi.org/10.4319/lom.2008.6.236

Kallmeyer, J., Pockalny, R., Adhikari, R. R., Smith, D. C., & D'Hondt, S. (2012). Global distribution of microbial abundance and biomass in subseafloor sediment. *Proceedings of the National Academy of Sciences of the United States of America*, *109*(40), 16213–16216. https://doi.org/10.1073/pnas.1203849109

Kao-Kniffin, J., Woodcroft, B. J., Carver, S. M., Bockheim, J. G., Handelsman, J., Tyson, G. W., et al. (2015). Archaeal and bacterial communities across a chronosequence of drained lake basins in arctic alaska. *Scientific Reports*, *5*(1), srep18165. https://doi.org/10.1038/srep18165

Kattsov, V. M., Källén, E., Cattle, H., Christensen, J., Drange, H., Hanssen-bauer, I., et al. (2005). Future Climate Change: Modeling and Scenarios for the Arctic. In *Arctic Climate Impact Assessment* (pp. 99–150).

Khlebnikova, G. M., Gilichinskii, D. A., Fedorov-Davydov, D. G., & Vorob'eva, E. A. (1990). Quantitative Evaluation of Microorganisms in Permafrost Deposits and Buried Soils. *Microbiology (New York)*, *59*(1), 106–112. Retrieved from https://www.cabdirect.org/cabdirect/abstract/19911951870

Kirkpatrick, J. B., Walsh, E. a., & D'Hondt, S. (2016). Fossil DNA persistence and decay in marine sediment over hundred-thousand-year to million-year time scales. *Geology*, *44*(8), 615–618. https://doi.org/10.1130/G37933.1

Kneier, F., Overduin, P. P., Langer, M., Boike, J., & Grigoriev, M. N. (2018). Borehole temperature reconstructions reveal differences in past surface temperature trends for the permafrost in the Laptev Sea region, Russian Arctic. *Arktos*, *4*(7), 1–17. https://doi.org/10.1007/s41063-018-0041-3

Knittel, K, & Boetius, A. (2009). Anaerobic oxidation of methane: progress with an unknown process. *Annual Review of Microbiology*, *63*, 311–334. https://doi.org/10.1146/annurev.micro.61.080706.093130

Knittel, K., Lösekann, T., Boetius, A., Kort, R., & Amann, R. (2005). Diversity and Distribution of Methanotrophic Archaea at Cold Seeps. *Applied and Environmental Microbiology*, *71*(1), 467–479. https://doi.org/10.1128/aem.71.1.467-479.2005

Knoblauch, C., Spott, O., Evgrafova, S., Kutzbach, L., & Pfeiffer, E.-M. (2015). Regulation of methane production, oxidation, and emission by vascular plants and bryophytes in ponds

of the northeast Siberian polygonal tundra. *Journal of Geophysical Research: Biogeosciences*, *120*(12), 2525–2541. https://doi.org/10.1002/2015JG003053

Kobabe, S., Wagner, D., & Pfeiffer, E.-M. (2004). Characterisation of microbial community composition of a Siberian tundra soil by fluorescence in situ hybridisation. *FEMS Microbiology Ecology*, *50*(1), 13–23. https://doi.org/10.1016/j.femsec.2004.05.003

Koch, K., Knoblauch, C., & Wagner, D. (2009). Methanogenic community composition and anaerobic carbon turnover in submarine permafrost sediments of the Siberian Laptev Sea. *Environmental Microbiology*, *11*(3), 657–668. https://doi.org/10.1111/j.1462-2920.2008.01836.x

Kohnert, K., Serafimovich, A., Metzger, S., Hartmann, J., & Sachs, T. (2017). Strong geologic methane emissions from discontinuous terrestrial permafrost in the Mackenzie Delta, Canada. *Scientific Reports*, *7*(1), 5828. https://doi.org/10.1038/s41598-017-05783-2

Könneke, M., Bernhard, A. E., de la Torre, J. R., Walker, C. B., Waterbury, J. B., & Stahl, D. A. (2005). Isolation of an autotrophic ammonia-oxidizing marine archaeon. *Nature*, *437*(7058), 543–546. https://doi.org/10.1038/nature03911

Kousuke, I., Mußmann, M., MacGregor, B. J., & Amann, R. (2004). An improved fluorescence in situ hybridization protocol for the identification of bacteria and archaea in marine sediments. *FEMS Microbiology Ecology*, *50*(3), 203–212. Retrieved from http://www.sciencedirect.com/science/article/B6T2V-4D0GPPC-1/2/a9d8819380fb504b6f4970c30773a644

Krukenberg, V., Harding, K., Richter, M., Glöckner, F. O., Gruber-Vodicka, H. R., Adam, B., et al. (2016). *Candidatus* Desulfofervidus auxilii, a hydrogenotrophic sulfate-reducing bacterium involved in the thermophilic anaerobic oxidation of methane. *Environmental Microbiology*, *18*(9), 3073–3091. https://doi.org/10.1111/1462-2920.13283

Lantuit, H., Overduin, P. P., & Wetterich, S. (2013). Recent progress regarding permafrost coasts. *Permafrost and Periglacial Processes*, *24*(2), 120–130. https://doi.org/10.1002/ppp.1777

Lantuit, H., Overduin, P. P., Couture, N., Wetterich, S., Aré, F., Atkinson, D., et al. (2012). The Arctic Coastal Dynamics Database: A New Classification Scheme and Statistics on Arctic Permafrost Coastlines. *Estuaries and Coasts*, *35*(2), 383–400. https://doi.org/10.1007/s12237-010-9362-6

Larry Lopez, C. M., Brouchkov, A., Nakayama, H., Takakai, F., Federov, A. N., & Fukuda, M. (2007). Epigenetic salt accumulation and water movement in the active layer of central Yakutia in eastern Siberia. *Hydrological Processes*, *21*(1), 103–109.

https://doi.org/10.1002/hyp.6224

Lauber, C. L., Hamady, M., Knight, R., & Fierer, N. (2009). Pyrosequencing-Based Assessment of Soil pH as a Predictor of Soil Bacterial Community Structure at the Continental Scale. *Applied and Environmental Microbiology*, *75*(15), 5111–5120. https://doi.org/10.1128/aem.00335-09

Lazar, C. S., Baker, B. J., Seitz, K., Hyde, A. S., Dick, G. J., Hinrichs, K.-U., & Teske, A. P. (2016). Genomic evidence for distinct carbon substrate preferences and ecological niches of Bathyarchaeota in estuarine sediments. *Environmental Microbiology*, *18*(4), 1200–1211. https://doi.org/10.1111/1462-2920.13142

Lee, S. D., & Kim, S. J. (2007). Aeromicrobium tamlense sp. nov., isolated from dried seaweed. *International Journal of Systematic and Evolutionary Microbiology*, *57*(2), 337–341. https://doi.org/10.1099/ijs.0.64442-0

Liebner, S., Rublack, K., Stuehrmann, T., & Wagner, D. (2009). Diversity of aerobic methanotrophic bacteria in a permafrost active layer soil of the Lena Delta, Siberia. *Microbial Ecology*, *57*(1), 25–35. https://doi.org/10.1007/s00248-008-9411-x

Liebner, S., Harder, J., & Wagner, D. (2008). Bacterial diversity and community structure in polygonal tundra soils from Samoylov Island, Lena Delta, Siberia. *International Microbiology*, *11*(3), 195–202. https://doi.org/10.2436/20.1501.01.60

Liebner, S., Zeyer, J., Wagner, D., Schubert, C., Pfeiffer, E.-M., & Knoblauch, C. (2011). Methane oxidation associated with submerged brown mosses reduces methane emissions from Siberian polygonal tundra. *Journal of Ecology*, *99*, 914–922. https://doi.org/10.1111/j.1365-2745.2011.01823.x

Liebner, S., Ganzert, L., Kiss, A., Yang, S., Wagner, D., & Svenning, M. M. (2015). Shifts in methanogenic community composition and methane fluxes along the degradation of discontinuous permafrost. *Frontiers in Microbiology*, *6*(356), 1–10. https://doi.org/10.3389/fmicb.2015.00356

Lindström, E. S., & Langenheder, S. (2012). Local and regional factors influencing bacterial community assembly. *Environmental Microbiology Reports*, *4*(1), 1–9. https://doi.org/10.1111/j.1758-2229.2011.00257.x

Liptay, K., Chanton, J., Czepiel, P., & Mosher, B. (1998). Use of stable isotopes to determine methane oxidation in landfill cover soils. *Journal of Geophysical Research: Atmospheres*, *103*(D7), 8243–8250. https://doi.org/10.1029/97JD02630

Llobet-Brossa, E., Rossello-Mora, R., & Amann, R. (1998). Microbial Community Composition of Wadden Sea Sediments as Revealed by Fluorescence In Situ

Hybridization. *Applied and Environmental Microbiology*, *64*(7), 2691–2696.

Lloyd, K. G., May, M. K., Kevorkian, R. T., & Steen, A. D. (2013a). Meta-analysis of quantification methods shows that archaea and bacteria have similar abundances in the subseafloor. *Applied and Environmental Microbiology*, *79*(24), 7790–7799. https://doi.org/10.1128/AEM.02090-13

Lloyd, K. G., Schreiber, L., Petersen, D. G., Kjeldsen, K. U., Lever, M. A., Steen, A. D., et al. (2013b). Predominant archaea in marine sediments degrade detrital proteins. *Nature*, *496*(7444), 215–218. https://doi.org/10.1038/nature12033

Ludwig, W., Strunk, O., Westram, R., Richter, L., Meier, H., Yadhukumar, et al. (2004). ARB: a software environment for sequence data. *Nucleic Acids Research*, *32*(4), 1363–1371. https://doi.org/10.1093/nar/gkh293

Luo, C., Rodriguez-R, L. M., Johnston, E. R., Wu, L., Cheng, L., Xue, K., et al. (2014). Soil microbial community responses to a decade of warming as revealed by comparative metagenomics. *Applied and Environmental Microbiology*, *80*(5), 1777–1786. https://doi.org/10.1128/AEM.03712-13

Lyra, C., Sinkko, H., Rantanen, M., Paulin, L., & Kotilainen, A. (2013). Sediment Bacterial Communities Reflect the History of a Sea Basin. *PLoS ONE*, *8*(1), e54326. https://doi.org/10.1371/journal.pone.0054326

Lysnes, K., Thorseth, I. H., Steinsbu, B. O., Øvreås, L., Torsvik, T., & Pedersen, R. B. (2004). Microbial community diversity in seafloor basalt from the Arctic spreading ridges. *FEMS Microbiology Ecology*, *50*(3), 213–230. https://doi.org/10.1016/j.femsec.2004.06.014

Maayer, P. De, Anderson, D., Cary, C., & Cowan, D. A. (2014). Some like it cold : understanding the survival strategies of psychrophiles. *EMBO Reports*, *15*(5), 508–517.

Mackelprang, R., Waldrop, M. P., DeAngelis, K. M., David, M. M., Chavarria, K. L., Blazewicz, S. J., et al. (2011). Metagenomic analysis of a permafrost microbial community reveals a rapid response to thaw. *Nature*, *480*, 368–371. https://doi.org/10.1038/nature10576

Mackelprang, R., Burkert, A., Haw, M., Mahendrarajah, T., Conaway, C. H., Douglas, T. a., & Waldrop, M. P. (2017). Microbial survival strategies in ancient permafrost: Insights from metagenomics. *ISME Journal*, *11*(10), 2305–2318. https://doi.org/10.1038/ismej.2017.93

Madigan, M., Martinko, J., Stahl, D., & Clark, D. (2011). *Brock: Biology of Microorganisms*. (D. Espinoza, L. Dent, K. Cook, S. Cutt, E. Hutchinson, L. Southworth, et al., Eds.) (thirteenth). Pearson.

Männistö, M. K., Kurhela, E., Tiirola, M., & Häggblom, M. M. (2013). *Acidobacteria* dominate

the active bacterial communities of Arctic tundra with widely divergent winter-time snow accumulation and soil temperatures. *FEMS Microbiology Ecology*, *84*(1), 47–59. https://doi.org/10.1111/1574-6941.12035

Mantel, N. (1967). The Detection of Disease Clustering and a Generalized Regression Approach. *Cancer Research*, *27*(1), 209–220.

Manz, W., Eisenbrecher, M., Neu, T. R., & Szewzyk, U. (1998). Abundance and spatial organization of Gram-negative sulfate-reducing bacteria in activated sludge investigated by in situ probing with specific 16S rRNA targeted oligonucleotides. *FEMS Microbiology Ecology*, *25*(1), 43–61. https://doi.org/10.1111/j.1574-6941.1998.tb00459.x

Marcondes de Souza, J. A., Carareto Alves, L. M., de Mello Varani, A., & de Macedo Lemos, E. G. (2014). The Family Bradyrhizobiaceae. In *The Prokaryotes* (pp. 135–154). Berlin, Heidelberg: Springer Berlin Heidelberg. https://doi.org/10.1007/978-3-642-30197-1_253

Margesin, R., & Collins, T. (2019). Microbial ecology of the cryosphere (glacial and permafrost habitats): current knowledge. *Applied Microbiology and Biotechnology*, 1–13. https://doi.org/10.1007/s00253-019-09631-3

Martin, M. (2011). Cutadapt removes adapter sequences from high-throughput sequencing reads. *EMBnet.Journal*, *17*(1), 10–12. https://doi.org/10.14806/ej.17.1.200

Massana, R., Murray, A. E., Preston, C. M., & DeLong, E. F. (1997). Vertical distribution and phylogenetic characterization of marine planktonic Archaea in the Santa Barbara Channel. *Applied and Evironmental MMcrobiology*, *63*(1), 50–56. Retrieved from http://www.ncbi.nlm.nih.gov/pubmed/8979338

Mastepanov, M., Sigsgaard, C., Dlugokencky, E. J., Houweling, S., Strom, L., Tamstorf, M. P., & Christensen, T. R. (2008). Large tundra methane burst during onset of freezing. *Nature*, *456*(7222), 628–630. https://doi.org/nature07464 [pii]10.1038/nature07464

Mayeux, B., Fardeau, M.-L., Bartoli-Joseph, M., Casalot, L., Vinsot, A., & Labat, M. (2013). Desulfosporosinus burensis sp. nov., a spore-forming, mesophilic, sulfate-reducing bacterium isolated from a deep clay environment. *INTERNATIONAL JOURNAL OF SYSTEMATIC AND EVOLUTIONARY MICROBIOLOGY*, *63*(Pt 2), 593–598. https://doi.org/10.1099/ijs.0.035238-0

McDonald, D., Price, M. N., Goodrich, J., Nawrocki, E. P., DeSantis, T. Z., Probst, A., et al. (2012). An improved Greengenes taxonomy with explicit ranks for ecological and evolutionary analyses of bacteria and archaea. *ISME J*, *6*(3), 610–618. https://doi.org/http://www.nature.com/ismej/journal/v6/n3/suppinfo/ismej2011139s1.html

McGuire, A. D., Anderson, L. G., Christensen, T. R., Dallimore, S., Guo, L. D., Hayes, D. J., et al. (2009). Sensitivity of the carbon cycle in the Arctic to climate change. *Ecological Monographs*, *79*(4), 523–555.

Meng, J., Xu, J., Qin, D., He, Y., Xiao, X., & Wang, F. (2014). Genetic and functional properties of uncultivated MCG archaea assessed by metagenome and gene expression analyses. *The ISME Journal*, *8*(3), 650–659. https://doi.org/10.1038/ismej.2013.174

Meyer, H., Schönicke, L., Wand, U., Hubberten, H. W., & Friedrichsen, H. (2000). Isotope studies of hydrogen and oxygen in ground ice - Experiences with the equilibration technique. *Isotopes in Environmental and Health Studies*, *36*(2), 133–149. https://doi.org/10.1080/10256010008032939

Meyer, H., Dereviagin, A., Siegert, C., Schirrmeister, L., & Hubberten, H. W. (2002a). Palaeoclimate reconstruction on Big Lyakhovsky Island, North Siberia - Hydrogen and oxygen isotopes in ice wedges. *Permafrost and Periglacial Processes*, *13*(2), 91–105. https://doi.org/10.1002/ppp.416

Meyer, H., Dereviagin, A., Siegert, C., & Hubberten, H.-W. (2002b). Paleoclimatic Studies on Bykovsky Peninsula, North Siberia - Hydrogen and Oxygen Isotopes in Ground Ice. *Polarforschung*, *70*, 37–51.

Mitzscherling, J., Horn, F., Winterfeld, M., Mahler, L., Kallmeyer, J., Overduin, P. P., et al. (2018). Pore water chemistry, grain sizes and sediment temperature of 4 sediment cores from submarine permafrost at Mamontov Klyk Cape, Laptev Sea shelf. *PANGAEA*. https://doi.org/https://doi.org/10.1594/PANGAEA.895292

Mitzscherling, J., Winkel, M., Winterfeld, M., Horn, F., Yang, S., Grigoriev, M. N., et al. (2017). The development of permafrost bacterial communities under submarine conditions. *Journal of Geophysical Research: Biogeosciences*, *122*(7), 1689–1704. https://doi.org/10.1002/2017JG003859

Mizuno, C. M., Rodriguez-Valera, F., & Ghai, R. (2015). Genomes of planktonic acidimicrobiales: Widening horizons for marine actinobacteria by metagenomics. *MBio*, *6*(1), 1–11. https://doi.org/10.1128/mBio.02083-14

Moss, R., Babiker, M., Brinkman, S., Calvo, E., Carter, T., Edmonds, J., et al. (2011). *Towards New Scenarios for Analysis of Emissions, Climate Change, Impacts, and Response Strategies*. *Intergovernmental Panel on Climate Change*. Geneva. Retrieved from https://gisclimatechange.ucar.edu/inspector

Müller, K.-D., Husmann, H., & Nalik, H. P. (1990). A New and Rapid Method for the Assay of Bacterial Fatty Acids Using High Resolution Capillary Gas Chromatography and

Trimethylsulfonium Hydroxide. *Zentralblatt Für Bakteriologie*, *274*(2), 174–182. https://doi.org/10.1016/S0934-8840(11)80100-3

Müller, S., Bobrov, A. A., Schirrmeister, L., Andreev, A. A., & Tarasov, P. E. (2009). Testate amoebae record from the Laptev Sea coast and its implication for the reconstruction of Late Pleistocene and Holocene environments in the Arctic Siberia. *Palaeogeography, Palaeoclimatology, Palaeoecology*, *271*(3–4), 301–315. https://doi.org/10.1016/J.PALAEO.2008.11.003

Muyzer, G., De Waal, E. C., & Uitterlinden, A. G. (1993). Profiling of complex microbial populations by denaturing gradient gel electrophoresis analysis of polymerase chain reaction-amplified genes coding for 16S rRNA. *Applied and Environmental Microbiology*, *59*(3), 695–700.

Mykytczuk, N. C. S., Foote, S. J., Omelon, C. R., Southam, G., Greer, C. W., & Whyte, L. G. (2013). Bacterial growth at -15 °C; molecular insights from the permafrost bacterium Planococcus halocryophilus Or1. *The ISME Journal*, *7*(6), 1211–1226. https://doi.org/10.1038/ismej.2013.8

Narrowe, A. B., Angle, J. C., Daly, R. A., Stefanik, K. C., Wrighton, K. C., & Miller, C. S. (2017). High-resolution sequencing reveals unexplored archaeal diversity in freshwater wetland soils. *Environmental Microbiology*, *19*(6), 2192–2209. https://doi.org/10.1111/1462-2920.13703

Nicolsky, D. J., Romanovsky, V. E., Romanovskii, N. N., Kholodov, a. L., Shakhova, N. E., & Semiletov, I. P. (2012). Modeling sub-sea permafrost in the East Siberian Arctic Shelf: The Laptev Sea region. *Journal of Geophysical Research: Earth Surface*, *117*(3), 1–22. https://doi.org/10.1029/2012JF002358

Niemann, H., Lösekann, T., de Beer, D., Elvert, M., Nadalig, T., Knittel, K., et al. (2006). Novel microbial communities of the Haakon Mosby mud volcano and their role as a methane sink. *Nature*, *443*, 854–858. https://doi.org/10.1038/nature05227

Nikrad, M. P., Kerkhof, L. J., & Häggblom, M. M. (2016). The subzero microbiome: microbial activity in frozen and thawing soils. *FEMS Microbiology Ecology*, *92*(6), fiw081. https://doi.org/10.1093/femsec/fiw081

Nobu, M. K., Dodsworth, J. a, Murugapiran, S. K., Rinke, C., Gies, E. a, Webster, G., et al. (2016). Phylogeny and physiology of candidate phylum 'Atribacteria' (OP9/JS1) inferred from cultivation-independent genomics. *The ISME Journal*, *10*(2), 273–286. https://doi.org/10.1038/ismej.2015.97

Nordi, K. Á., Thamdrup, B., & Schubert, C. J. (2013). Anaerobic oxidation of methane in an

iron-rich Danish freshwater lake sediment. *Limnology and Oceanography*, *58*(2), 546–554. https://doi.org/10.4319/lo.2013.58.2.0546

Nordi, K. Á. & Thamdrup, B. (2014). Nitrate-dependent anaerobic methane oxidation in a freshwater sediment. *Geochimica et Cosmochimica Acta*, *132*, 141–150. https://doi.org/10.1016/J.GCA.2014.01.032

Normand, P., Daffonchio, D., & Gtari, M. (2014). The Family Geodermatophilaceae. In *The Prokaryotes* (pp. 361–379). Berlin, Heidelberg: Springer Berlin Heidelberg. https://doi.org/10.1007/978-3-642-30138-4_180

Oni, O., Miyatake, T., Kasten, S., Richter-Heitmann, T., Fischer, D., Wagenknecht, L., et al. (2015). Distinct microbial populations are tightly linked to the profile of dissolved iron in the methanic sediments of the Helgoland mud area, North Sea. *Frontiers in Microbiology*, *06*, 365. https://doi.org/10.3389/fmicb.2015.00365

Oren, A., & Garrity, G. M. (2013). List of new names and new combinations previously effectively, but not validly, published. *International Journal of Systematic and Evolutionary Microbiology*, *63*, 3931–34.

Oren, A., & Xu, X.-W. (2014). The Family Hyphomicrobiaceae. In *The Prokaryotes* (pp. 247–281). Berlin, Heidelberg: Springer Berlin Heidelberg. https://doi.org/10.1007/978-3-642-30197-1_257

Orphan, V. J., House, C. H., Hinrichs, K. U., McKeegan, K. D., & DeLong, E. F. (2001). Methane-consuming archaea revealed by directly coupled isotopic and phylogenetic analysis. *Science (New York, N.Y.)*, *293*(5529), 484–487. https://doi.org/10.1126/science.1061338

Orsi, W. D. (2018). Ecology and evolution of seafloor and subseafloor microbial communities. *Nature Reviews Microbiology*, *16*(11), 671–683. https://doi.org/10.1038/s41579-018-0046-8

Orsi, W. D., Coolen, M. J. L., Wuchter, C., He, L., More, K. D., Irigoien, X., et al. (2017). Climate oscillations reflected within the microbiome of Arabian Sea sediments. *Scientific Reports*, *7*(1), 1–12. https://doi.org/10.1038/s41598-017-05590-9

Osterkamp, T. E. (2001). Sub-sea Permafrost. In J. H. Steele, S. A. Thorpe, & K. K. Turekian (Eds.), *Encyclopedia of Ocean Science* (Vol. 5, pp. 2902–2912). New York, London: Academic Press. https://doi.org/10.1016/B978-012374473-9.00008-4

Overduin, P. P., Hubberten, H. W., Rachold, V., Romanovskii, N., Grigoriev, M. N., & Kasymskaya, M. (2007). The evolution and degradation of coastal and offshore permafrost in the Laptev and East Siberian Seas during the last climatic cycle. In *Coastline changes:*

interrelation of climate and geological processes (Vol. 426, pp. 97–111).

Overduin, P. P., Rachold, V., & Grigoriev, M. N. (2008). The State of Subsea Permafrost in the Western Laptev Nearshore Zone. In *Proceedings of the Ninth International Conference on Permafrost, Fairbanks, Alaska* (pp. 1345–1350).

Overduin, P. P. (2007a). Russian-German Cooperation SYSTEM LAPTEV SEA: The expedition COAST I. In Lutz Schirrmeister (Ed.), *Expeditions in Siberia 2005* (pp. 1–40). Reports on Polar and Marine Research.

Overduin, P. P. (2007b). *The Expedition COAST I.* (Lutz Schirrmeister, Ed.), *Expeditions in Siberia in 2005*.

Overduin, P. P., Westermann, S., Yoshikawa, K., Haberlau, T., Romanovsky, V., & Wetterich, S. (2012). Geoelectric observations of the degradation of nearshore submarine permafrost at Barrow (Alaskan Beaufort Sea). *Journal of Geophysical Research: Earth Surface*, *117*(2), 1–9. https://doi.org/10.1029/2011JF002088

Overduin, P. P., Liebner, S., Knoblauch, C., Günther, F., Wetterich, S., Schirrmeister, L., et al. (2015). Methane oxidation following submarine permafrost degradation: Measurements from a central Laptev Sea shelf borehole. *Journal of Geophysical Research G: Biogeosciences*, *120*(5), 965–978. https://doi.org/10.1002/2014JG002862

Overduin, P. P., Wetterich, S., Günther, F., Grigoriev, M. N., Grosse, G., Schirrmeister, L., et al. (2016). Coastal dynamics and submarine permafrost in shallow water of the central Laptev Sea, East Siberia. *The Cryosphere*, *10*(4), 1449–1462. https://doi.org/10.5194/tc-10-1449-2016

Panikov, N. S., Flanagan, P. W., Oechel, W. C., Mastepanov, M. A., & Christensen, T. R. (2006). Microbial activity in soils frozen to below −39 °C. *Soil Biology and Biochemistry*, *38*(4), 785–794. https://doi.org/10.1016/J.SOILBIO.2005.07.004

Parkes, R. J., Sass, H., Cragg, B. A., Webster, G., Roussel, E. G. P., & Weightman, A. J. (2014). Studies on prokaryotic populations and processes in subseafloor sediments - an update. In J. Kallmeyer & D. Wagner (Eds.), *Microbial Life of the Deep Biosphere* (pp. 1–27). Berlin: de Gruyter.

Pester, M., Bittner, N., Deevong, P., Wagner, M., & Loy, A. (2010). A 'rare biosphere' microorganism contributes to sulfate reduction in a peatland. *The ISME Journal*, *4*(12), 1591–1602. https://doi.org/10.1038/ismej.2010.75

Petrescu, A. M. R., Lohila, A., Tuovinen, J.-P., Baldocchi, D. D., Desai, A. R., Roulet, N. T., et al. (2015). The uncertain climate footprint of wetlands under human pressure. *Proceedings of the National Academy of Sciences of the United States of America*, *112*(15),

4594–4599. https://doi.org/10.1073/pnas.1416267112

Pointing, S. B., Chan, Y., Lacap, D. C., Lau, M. C. Y., Jurgens, J. A., & Farrell, R. L. (2009). Highly specialized microbial diversity in hyper-arid polar desert. *Proceedings of the National Academy of Sciences of the United States of America*, *106*(47), 19964–9. https://doi.org/10.1073/pnas.0908274106

Portnov, A., Smith, A. J., Mienert, J., Cherkashov, G., Rekant, P., Semenov, P., et al. (2013). Offshore permafrost decay and massive seabed methane escape in water depths >20 m at the South Kara Sea shelf. *Geophysical Research Letters*, *40*(15), 3962–3967. https://doi.org/10.1002/grl.50735

Preuss, I., Knoblauch, C., Gebert, J., & Pfeiffer, E.-M. (2013). Improved quantification of microbial CH4 oxidation efficiency in arctic wetland soils using carbon isotope fractionation. *Biogeosciences*, *10*(4), 2539–2552. https://doi.org/10.5194/bg-10-2539-2013

Pruitt, K. D., Tatusova, T., & Maglott, D. R. (2005). NCBI Reference Sequence (RefSeq): a curated non-redundant sequence database of genomes, transcripts and proteins. *Nucleic Acids Research*, *33*(Database issue), D501–D504. https://doi.org/10.1093/nar/gki025

Quast, C., Pruesse, E., Yilmaz, P., Gerken, J., Schweer, T., Yarza, P., et al. (2012). The SILVA ribosomal RNA gene database project: improved data processing and web-based tools. *Nucleic Acids Research*, *41*(D1), D590–D596. https://doi.org/10.1093/nar/gks1219

Rachold, V., Bolshiyanov, D. Y., Grigoriev, M. N., Hubberten, H.-W., Junker, R., Kunitsky, V. V., et al. (2007). Nearshore arctic subsea permafrost in transition. *Eos, Transactions American Geophysical Union*, *88*(13), 149–150. https://doi.org/10.1029/2007EO130001

Radujković, D., Verbruggen, E., Sigurdsson, B. D., Leblans, N. I. W., Janssens, I. A., Vicca, S., & Weedon, J. T. (2018). Prolonged exposure does not increase soil microbial community compositional response to warming along geothermal gradients. *FEMS Microbiology Ecology*, *94*(2), 1–10. https://doi.org/10.1093/femsec/fix174

Raghoebarsing, A. A., Pol, A., van de Pas-Schoonen, K. T., Smolders, A. J. P., Ettwig, K. F., Rijpstra, W. I. C., et al. (2006). A microbial consortium couples anaerobic methane oxidation to denitrification. *Nature*, *440*(7086), 918–921. https://doi.org/Doi 10.1038/Nature04617

Rath, K. M., & Rousk, J. (2015). Salt effects on the soil microbial decomposer community and their role in organic carbon cycling : A review. *Soil Biology and Biochemistry*, *81*, 108–123. https://doi.org/10.1016/j.soilbio.2014.11.001

Raymond-Bouchard, I., Chourey, K., Altshuler, I., Iyer, R., Hettich, R. L., & Whyte, L. G.

(2017). Mechanisms of subzero growth in the cryophile *Planococcus halocryophilus* determined through proteomic analysis. *Environmental Microbiology*, *19*(11), 4460–4479. https://doi.org/10.1111/1462-2920.13893

Reeburgh, W. S. (2007). Oceanic methane biogeochemistry. *American Chemical Society*, *107*(2), 486–513. https://doi.org/10.1021/cr050362v

Richter-Menge, J., Overland, J. E., & Mathis, J. T. (2016). Arctic Report Card. Retrieved February 28, 2017, from http://www.arctic.noaa.gov/Report-Card

Rietz, D. N., & Haynes, R. J. (2003). Effects of irrigation-induced salinity and sodicity on soil microbial activity. *Soil Biology and Biochemistry*, *35*(6), 845–854. https://doi.org/10.1016/S0038-0717(03)00125-1

Riley, M., Staley, J. T., Danchin, A., Wang, T. Z., Brettin, T. S., Hauser, L. J., et al. (2008). Genomics of an extreme psychrophile, Psychromonas ingrahamii. *BMC Genomics*, *9*(210), 1–19. https://doi.org/10.1186/1471-2164-9-210

Rinke, C., Schwientek, P., Sczyrba, A., Ivanova, N. N., Anderson, I. J., Cheng, J.-F., et al. (2013). Insights into the phylogeny and coding potential of microbial dark matter. *Nature*, *499*(7459), 431–437. https://doi.org/10.1038/nature12352

Rinnan, R., Michelsen, A., Baath, E., & Jonasson, S. (2007). Fifteen years of climate change manipulations alter soil microbial communities in a subarctic heath ecosystem. *Global Change Biology*, *13*(1), 28–39. https://doi.org/DOI 10.1111/j.1365-2486.2006.01263.x

Rivkina, E., Shcherbakova, V., Laurinavichius, K., Petrovskaya, L., Krivushin, K., Kraev, G., et al. (2007). Biogeochemistry of methane and methanogenic archaea in permafrost. *FEMS Microbiology Ecology*, *61*(1), 1–15. https://doi.org/DOI 10.1111/j.1574-6941.2007.00315.x

Rivkina, E. M., Friedmann, E. I., & Mckay, C. P. (2000). Metabolic Activity of Permafrost Bacteria below the Freezing Point. *Applied and Environmental Microbiology*, *66*(8), 3230–3233. https://doi.org/10.1128/AEM.66.8.3230-3233.2000

Romanovskii, N. N., Hubberten, H.-W., Gavrilov, A. V., Tumskoy, V. E., Tipenko, G. S., Grigoriev, M. N., & Siegert, C. (2000). Thermokarst and land-ocean interactions, Laptev Sea Region, Russia. *Permafrost and Periglacial Processes*, *11*, 137–152.

Romanovskii, N. N., Hubberten, H. W., Gavrilov, A. V., Eliseeva, A. A., & Tipenko, G. S. (2005). Offshore permafrost and gas hydrate stability zone on the shelf of East Siberian Seas. *Geo-Marine Letters*, *25*, 167–182. https://doi.org/10.1007/s00367-004-0198-6

Romanovskii, N N, Hubberten, H. W., Gavrilov, A. V, Tumskoy, V. E., & Kholodov, A. L. (2004). Permafrost of the east Siberian Arctic shelf and coastal lowlands. *Quaternary*

Science Reviews, *23*(11–13), 1359–1369. https://doi.org/http://dx.doi.org/10.1016/j.quascirev.2003.12.014

Romanovskii, N. N, & Hubberten, H. W. (2001). Results of permafrost modelling of the lowlands and shelf of the Laptev Sea Region, Russia. *Permafrost and Periglacial Processes*, *12*(2), 191–202. https://doi.org/10.1002/ppp.387

Romanovsky, V. E., Smith, S. L., & Christiansen, H. H. (2010). Permafrost thermal state in the polar Northern Hemisphere during the international polar year 2007-2009: a synthesis. *Permafrost and Periglacial Processes*, *21*(2), 106–116. https://doi.org/10.1002/ppp.689

Rousk, J., Elyaagubi, F. K., Jones, D. L., & Godbold, D. L. (2011). Bacterial salt tolerance is unrelated to soil salinity across an arid agroecosystem salinity gradient. *Soil Biology and Biochemistry*, *43*(9), 1881–1887. https://doi.org/10.1016/j.soilbio.2011.05.007

Ruff, S. E., Biddle, J. F., Teske, A. P., Knittel, K., Boetius, A., & Ramette, A. (2015). Global dispersion and local diversification of the methane seep microbiome. *Proceedings of the National Academy of Sciences of the United States of America*, *112*(13), 4015–4020. https://doi.org/10.1073/pnas.1421865112

Rui, J., Li, J., Wang, S., An, J., Liu, W., Lin, Q., et al. (2015). Responses of Bacterial Communities to Simulated Climate Changes in Alpine Meadow Soil of the Qinghai-Tibet Plateau. *Applied and Environmental Microbiology*, *81*(17), 6070–6077. https://doi.org/10.1128/AEM.00557-15

Ruppel, C. (2015). Permafrost-associated gas hydrate: Is it really approximately 1 % of the global system? *Journal of Chemical and Engineering Data*, *60*(2), 429–436. https://doi.org/10.1021/je500770m

Ruppel, C. D., & Kessler, J. D. (2017). The interaction of climate change and methane hydrates. *Reviews of Geophysics*, *55*(1), 126–168. https://doi.org/10.1002/2016RG000534

Sapart, C. J., Shakhova, N., Semiletov, I., Jansen, J., Szidat, S., Kosmach, D., et al. (2017). The origin of methane in the East Siberian Arctic Shelf unraveled with triple isotope analysis. *Biogeosciences*, *14*(9), 2283–2292. https://doi.org/10.5194/bg-14-2283-2017

Saunois, M., Bousquet, P., Poulter, B., Peregon, A., Ciais, P., Canadell, J. G., et al. (2016). The global methane budget 2000–2012. *Earth System Science Data*, *8*(2), 697–751. https://doi.org/10.5194/essd-8-697-2016

Scheller, S., Yu, H., Chadwick, G. L., McGlynn, S. E., & Orphan, V. J. (2016). Artificial electron acceptors decouple archaeal methane oxidation from sulfate reduction. *Science*, *351*(6274), 703–707. https://doi.org/10.1126/science.aad7154

Schimel, J., Balser, T. C., & Wallenstein, M. (2007). Microbial Stress-Response Physiology

and Its Implications for Ecosystem Function. *Ecology*, *88*(6), 1386–1394. https://doi.org/10.1890/06-0219

Schindlbacher, A., Rodler, A., Kuffner, M., Kitzler, B., Sessitsch, A., & Zechmeister-Boltenstern, S. (2011). Experimental warming effects on the microbial community of a temperate mountain forest soil. *Soil Biology and Biochemistry*, *43*(7), 1417–1425. https://doi.org/10.1016/j.soilbio.2011.03.005

Schirrmeister, L., Grosse, G., Kunitsky, V., Magens, D., Meyer, H., Dereviagin, A., et al. (2008). Periglacial landscape evolution and environmental changes of Arctic lowland areas for the last 60000 years (western Laptev Sea coast, Cape Mamontov Klyk). *Polar Research*, *27*(2), 249–272. https://doi.org/10.1111/j.1751-8369.2008.00067.x

Schirrmeister, L., Schwamborn, G., Overduin, P. P., Strauss, J., Fuchs, M. C., Grigoriev, M., et al. (2016). Yedoma Ice Complex of the Buor Khaya Peninsula (southern Laptev Sea). *Biogeosciences Discussions*, *0*(August), 1–36. https://doi.org/10.5194/bg-2016-283

Schloss, P. D., Westcott, S. L., Ryabin, T., Hall, J. R., Hartmann, M., Hollister, E. B., et al. (2009). Introducing mothur: Open-Source, Platform-Independent, Community-Supported Software for Describing and Comparing Microbial Communities. *Applied and Environmental Microbiology*, *75*(23), 7537–7541. https://doi.org/Doi 10.1128/Aem.01541-09

Schmidt, T. M. (1998). Multiplicity of Ribosomal RNA Operons in Prokaryotic Genomes. In *Bacterial Genomes* (pp. 221–229). Boston, MA: Springer US. https://doi.org/10.1007/978-1-4615-6369-3_21

Schostag, M., Priemé, A., Jacquiod, S., Russel, J., Ekelund, F., & Jacobsen, C. S. (2019). Bacterial and protozoan dynamics upon thawing and freezing of an active layer permafrost soil. *The ISME Journal*, 1. https://doi.org/10.1038/s41396-019-0351-x

Schouten, S., Huguet, C., Hopmans, E. C., Kienhuis, M. V. M., & Damsté, J. S. S. (2007). Analytical Methodology for TEX86 Paleothermometry by High-Performance Liquid Chromatography/Atmospheric Pressure Chemical Ionization-Mass Spectrometry. *Analytical Chemistry*, *79*(7), 2940–2944. https://doi.org/10.1021/AC062339V

Schreiber, L., Holler, T., Knittel, K., Meyerdierks, A., & Amann, R. (2010). Identification of the dominant sulfate-reducing bacterial partner of anaerobic methanotrophs of the ANME-2 clade. *Environmental Microbiology*, *12*(8), no-no. https://doi.org/10.1111/j.1462-2920.2010.02275.x

Schubert, C. J., Vazquez, F., Losekann-Behrens, T., Knittel, K., Tonolla, M., & Boetius, A. (2011). Evidence for anaerobic oxidation of methane in sediments of a freshwater system

(Lago di Cadagno). *FEMS Microbiology Ecology*, *76*(1), 26–38. https://doi.org/DOI 10.1111/j.1574-6941.2010.01036.x

Schuur, E. A. G., McGuire, A. D., Grosse, G., Harden, J. W., Hayes, D. J., Hugelius, G., et al. (2015). Climate change and the permafrost carbon feedback. *Nature*, *520*, 171–179. https://doi.org/10.1038/nature14338

Schuur, E A G, Vogel, J. G., Crummer, K. G., Lee, H., Sickman, J. O., & Osterkamp, T. E. (2009). The effect of permafrost thaw on old carbon release and net carbon exchange from tundra. *Nature*, *459*, 556–559. https://doi.org/10.1038/Nature08031

Schuur, E. A G, Bockheim, J., Canadell, J. G., Euskirchen, E., Field, C. B., Goryachkin, S. V, et al. (2008). Vulnerability of permafrost carbon to climate change: Implications for the global carbon cycle. *Bioscience*, *58*(8), 701–714. https://doi.org/10.1641/B580807

Segarra, K. E. A., Schubotz, F., Samarkin, V., Yoshinaga, M. Y., Hinrichs, K.-U., & Joye, S. B. (2015). High rates of anaerobic methane oxidation in freshwater wetlands reduce potential atmospheric methane emissions. *Nature Communications*, *6*(1), 7477. https://doi.org/10.1038/ncomms8477

Seto, M., & Yanagiya, K. (1983). Rate of CO2 evolution from soil in relation to temperature and amount of dissolved organic carbon. *Japanese Journal of Ecology*, *33*, 199–205.

Shakhova, N., & Semiletov, I. (2007). Methane release and coastal environment in the East Siberian Arctic shelf. *Journal of Marine Systems*, *66*(1–4), 227–243. https://doi.org/10.1016/J.JMARSYS.2006.06.006

Shakhova, N. E., Alekseev, V. A., & Semiletov, I. P. (2010). Predicted methane emission on the East Siberian shelf. *Doklady Earth Sciences*, *430*(2), 190–193.

Shakhova, N., Semiletov, I., Salyuk, A., Yusupov, V., Kosmach, D., & Gustafsson, Ö. (2010). Extensive Methane Venting to the Atmosphere from Sediments of the East Siberian Arctic Shelf. *Science*, *327*, 1246–1250. https://doi.org/10.1126/science.1229223

Shakhova, N., Semiletov, I., Leifer, I., Sergienko, V., Salyuk, A., Kosmach, D., et al. (2014). Ebullition and storm-induced methane release from the East Siberian Arctic Shelf. *Nature Geoscience*, *7*, 64–70. https://doi.org/10.1038/ngeo2007

Shcherbakova, V., Yoshimura, Y., Ryzhmanova, Y., Taguchi, Y., Segawa, T., Oshurkova, V., & Rivkina, E. (2016). Archaeal communities of Arctic methane-containing permafrost. *FEMS Microbiology Ecology*, *92*(10), fiw135. https://doi.org/10.1093/femsec/fiw135

Shi, T., Reeves, R. H., Gilichinsky, D. A., & Friedmann, E. I. (1997). Characterization of Viable Bacteria from Siberian Permafrost by 16S rDNA Sequencing. *Microbial Ecology*, *33*, 169–179.

Shur, Y. L., & Jorgenson, M. T. (2007). Patterns of permafrost formation and degradation in relation to climate and ecosystems. *Permafrost and Periglacial Processes*, *18*(1), 7–19. https://doi.org/10.1002/ppp.582

Skogland, T., Lomeland, S., & Goksøyr, J. (1988). Respiratory burst after freezing and thawing of soil: Experiments with soil bacteria. *Soil Biology and Biochemistry*, *20*(6), 851–856. https://doi.org/10.1016/0038-0717(88)90092-2

Smemo, K. A., & Yavitt, J. B. (2011). Anaerobic oxidation of methane: an underappreciated aspect of methane cycling in peatland ecosystems? *Biogeosciences*, *8*(3), 779–793. https://doi.org/10.5194/bg-8-779-2011

Smolander, A., & Kitunen, V. (2002). Soil microbial activities and characteristics of dissolved organic C and N in relation to tree species. *Soil Biology & Biochemistry*, *34*, 651–660. https://doi.org/10.1016/S0038-0717(01)00227-9

Söllinger, A., Schwab, C., Weinmaier, T., Loy, A., Tveit, A. T., Schleper, C., & Urich, T. (2016). Phylogenetic and genomic analysis of Methanomassiliicoccales in wetlands and animal intestinal tracts reveals clade-specific habitat. *FEMS Microbiology Ecology*, *92*(1), 1–12. https://doi.org/10.1093/femsec/fiv149

Spencer, R. G. M., Mann, P. J., Dittmar, T., Eglinton, T. I., McIntyre, C., Holmes, R. M., et al. (2015). Detecting the signature of permafrost thaw in Arctic rivers. *Geophysical Research Letters*, *42*(8), 1–6. https://doi.org/https://doi.org/10.1002/2015GL063498

Stapel, J. G., Schirrmeister, L., Overduin, P. P., Wetterich, S., Strauss, J., Horsfield, B., & Mangelsdorf, K. (2016). Microbial lipid signatures and substrate potential of organic matter in permafrost deposits: Implications for future greenhouse gas production. *Journal of Geophysical Research: Biogeosciences*, *121*(10), 2652–2666. https://doi.org/10.1002/2016JG003483

Starnawski, P., Bataillon, T., Ettema, T. J. G., Jochum, L. M., Schreiber, L., Chen, X., et al. (2017). Microbial community assembly and evolution in subseafloor sediment. *Proceedings of the National Academy of Sciences*, *114*(11), 2940–2945. https://doi.org/10.1073/pnas.1614190114

Steinberg, L. M., & Regan, J. M. (2008). Phylogenetic Comparison of the Methanogenic Communities from an Acidic, Oligotrophic Fen and an Anaerobic Digester Treating Municipal Wastewater Sludge. *Applied and Environmental Microbiology*, *74*(21), 6663–6671. https://doi.org/10.1128/aem.00553-08

Steven, B., Léveillé, R., Pollard, W. H., & Whyte, L. G. (2006). Microbial ecology and biodiversity in permafrost. *Extremophiles*, *10*(4), 259–267.

https://doi.org/10.1007/s00792-006-0506-3

Steven, B., Briggs, G., McKay, C. P., Pollard, W. H., Greer, C. W., & Whyte, L. G. (2007a). Characterization of the microbial diversity in a permafrost sample from the Canadian high Arctic using culture-dependent and culture-independent methods. *FEMS Microbiology Ecology*, *59*(2), 513–523. https://doi.org/10.1111/j.1574-6941.2006.00247.x

Steven, B., Niederberger, T. D., Bottos, E. M., Dyen, M. R., & Whyte, L. G. (2007b). Development of a sensitive radiorespiration method for detecting microbial activity at subzero temperatures. *Journal of Microbiological Methods*, *71*(3), 275–280. https://doi.org/10.1016/J.MIMET.2007.09.009

Steven, B., Pollard, W. H., Greer, C. W., & Whyte, L. G. (2008). Microbial diversity and activity through a permafrost/ground ice core profile from the Canadian high Arctic. *Environmental Microbiology*, *10*(12), 3388–3403. https://doi.org/10.1111/j.1462-2920.2008.01746.x

Steven, B., Niederberger. T. D., & Whyte, L. G. (2009). Bacterial and Archaeal Diversity in Permafrost. In Rosa Margesin (Ed.), *Permafrost Soils. Soil Biology* (Vol. 16, pp. 59–72). Springer Berlin / Heidelberg. https://doi.org/10.1007/978-3-540-69371-0

Stokstad, E. (2003). Ancient DNA Pulled From Soil. *Science*, *300*(5618), 407a – 407. https://doi.org/10.1126/science.300.5618.407a

Strauss, J. (2014). *Organic carbon in ice-rich permafrost : Characteristics, quantity, and availability*. Alfred-Wegener-Institut Helmholtz Centre for Polar and Marine Research.

Strauss, J., Schirrmeister, L., Grosse, G., Wetterich, S., Ulrich, M., Herzschuh, U., & Hubberten, H.-W. (2013). The deep permafrost carbon pool of the Yedoma region in Siberia and Alaska. *Geophysical Research Letters*, *40*(23), 6165–6170. https://doi.org/10.1002/2013GL058088

Stroeve, J., Serreze, M., Drobot, S., Gearheard, S., Holland, M., Masalink, J., et al. (2008). Arctic sea ice extent plummets in 2007. *Eos*, *89*(2), 13–20. https://doi.org/10.1029/2007GL029703.The

Sun, L., Perdue, E. M., Meyer, J. L., & Weis, J. (1997). Use of elemental composition to predict bioavailability of dissolved organic matter in a Georgia river. *Limnology and Oceanography*, *42*(4), 714–721. https://doi.org/10.4319/lo.1997.42.4.0714

Svendsen, J. I., Alexanderson, H., Astakhov, V. I., Demidov, I., Dowdeswell, J. a., Funder, S., et al. (2004). Late Quaternary ice sheet history of northern Eurasia. *Quaternary Science Reviews*, *23*(11–13), 1229–1271. https://doi.org/10.1016/j.quascirev.2003.12.008

Takai, K., Horikoshi, K., & Takai, K. E. N. (2000). Rapid Detection and Quantification of

Members of the Archaeal Community by Quantitative PCR Using Fluorogenic Probes Rapid Detection and Quantification of Members of the Archaeal Community by Quantitative PCR Using Fluorogenic Probes. *Applied and Environmental Microbiology*, *66*(11), 5066–5072. https://doi.org/10.1128/AEM.66.11.5066-5072.2000.Updated

Tarnocai, C., Canadell, J. G., Schuur, E. A. G., Kuhry, P., Mazhitova, G., & Zimov, S. (2009). Soil organic carbon pools in the northern circumpolar permafrost region. *Global Biogeochemical Cycles*, *23*(2), GB2023. https://doi.org/10.1029/2008gb003327

Taş, N., Prestat, E., McFarland, J. W., Wickland, K. P., Knight, R., Berhe, A. A., et al. (2014). Impact of fire on active layer and permafrost microbial communities and metagenomes in an upland Alaskan boreal forest. *The ISME Journal*, *8*(9), 1904–1919. https://doi.org/10.1038/ismej.2014.36

Taş, N., Prestat, E., Wang, S., Wu, Y., Ulrich, C., Kneafsey, T., et al. (2018). Landscape topography structures the soil microbiome in arctic polygonal tundra. *Nature Communications*, *9*(777), 1–13. https://doi.org/10.1038/s41467-018-03089-z

Taylor, J. P., Wilson, B., Mills, M. S., & Burns, R. G. (2002). Comparison of microbial numbers and enzymatic activities in surface soils and subsoils using various techniques. *Soil Biology and Biochemistry*, *34*(3), 387–401. https://doi.org/10.1016/S0038-0717(01)00199-7

Teira, E., Reinthaler, T., Pernthaler, A., Pernthaler, J., & Herndl, G. J. (2004). Combining catalyzed reporter deposition-fluorescence in situ hybridization and microautoradiography to detect substrate utilization by bacteria and Archaea in the deep ocean. *Applied and Environmental Microbiology*, *70*(7), 4411–4444. https://doi.org/10.1128/AEM.70.7.4411-4414.2004

Teske, A., & Sorensen, K. B. (2008). Uncultured archaea in deep marine subsurface sediments: have we caught them all? *ISME J*, *2*(1), 3–18. https://doi.org/ismej200790 [pii] 10.1038/ismej.2007.90

Teske, A., Hinrichs, K.-U., Edgcomb, V., de Vera Gomez, A., Kysela, D., Sylva, S. P., et al. (2002). Microbial diversity of hydrothermal sediments in the Guaymas Basin: evidence for anaerobic methanotrophic communities. *Applied and Environonmental Microbiology*, *68*(4), 1994–2007. https://doi.org/10.1128/AEM.68.4.1994-2007.2002

Thornton, B. F., & Crill, P. (2015). Arctic permafrost: Microbial lid on subsea methane. *Nature Climate Change*, *5*(8), 723–724. https://doi.org/10.1038/nclimate2740

Thornton, B. F., Geibel, M. C., Crill, P. M., Humborg, C., & Mörth, C. M. (2016). Methane fluxes from the sea to the atmosphere across the Siberian shelf seas. *Geophysical Research*

Letters, *43*(11), 5869–5877. https://doi.org/10.1002/2016GL068977

Timmers, P. H. A., Widjaja-Greefkes, H. C. A., Ramiro-Garcia, J., Plugge, C. M., & Stams, A. J. M. (2015). Growth and activity of ANME clades with different sulfate and sulfide concentrations in the presence of methane. *Frontiers in Microbiology*, *6*, 988. https://doi.org/10.3389/fmicb.2015.00988

Timmers, P. H. A., Welte, C. U., Koehorst, J. J., Plugge, C. M., Jetten, M. S. M., & Stams, A. J. M. (2017). Reverse Methanogenesis and Respiration in Methanotrophic Archaea. *Archaea*, *2017*, 1–22. https://doi.org/10.1155/2017/1654237

Tuorto, S. J., Darias, P., Mcguinness, L. R., Panikov, N., Zhang, T., Häggblom, M. M., & Kerhof, L. J. (2014). Bacterial genome replication at subzero temperatures in permafrost. *The ISME Journal*, *8*, 139–149. https://doi.org/10.1038/ismej.2013.140

Ulyantsev, A. S., Polyakova, N. V., Romankevich, E. A., Semiletov, I. P., & Sergienko, V. I. (2016). Ionic composition of pore water in shallow shelf deposits of the Laptev Sea. *Doklady Earth Sciences*, *467*(1), 308–313. https://doi.org/10.1134/S1028334X16030211

Unell, M., Kabelitz, N., Jansson, J. K., & Heipieper, H. J. (2007). Adaptation of the psychrotroph *Arthrobacter chlorophenolicus* A6 to growth temperature and the presence of phenols by changes in the anteiso/iso ratio of branched fatty acids. *FEMS Microbiology Letters*, *266*(2), 138–143. https://doi.org/10.1111/j.1574-6968.2006.00502.x

Vaksmaa, A., Jetten, M. S. M., Ettwig, K. F., & Lüke, C. (2017). McrA primers for the detection and quantification of the anaerobic archaeal methanotroph 'Candidatus Methanoperedens nitroreducens.' *Applied Microbiology and Biotechnology*, *101*(4), 1631–1641. https://doi.org/10.1007/s00253-016-8065-8

Vasil'chuk, Y. K. (1991). Reconstruction of the paleoclimate of the Late Pleistocene and Holocene of the basis of isotope studies of subsurface ice and waters of the permafrost zone. *Water Resources*, *17*(6), 640–647.

Vetter, A., Vieth, A., Mangelsdorf, K., Lerm, S., Alawi, M., Wolfgramm, M., et al. (2010). Biogeochemical Characterisation of Geothermally Used Groundwater in Germany. In *Proceedings World Geothermal Congress* (pp. 1–6). Bali.

Vieira, G., Bockheim, J., Guglielmin, M., Balks, M., Abramov, A. A., Boelhouwers, J., et al. (2010). Thermal state of permafrost and active-layer monitoring in the antarctic: Advances during the international polar year 2007-2009. *Permafrost and Periglacial Processes*, *21*(2), 182–197. https://doi.org/10.1002/ppp.685

Vishnivetskaya, T., Kathariou, S., McGrath, J., Gilichinsky, D., & Tiedje, J. M. (2000). Low-temperature recovery strategies for the isolation of bacteria from ancient permafrost

sediments. *Extremophiles*, *4*(3), 165–173. https://doi.org/10.1007/s007920070031

Vishnivetskaya, T. A, Petrova, M. a, Urbance, J., Ponder, M., Moyer, C. L., Gilichinsky, D. a, & Tiedje, J. M. (2006). Bacterial community in ancient Siberian permafrost as characterized by culture and culture-independent methods. *Astrobiology*, *6*(3), 400–414. https://doi.org/10.1089/ast.2006.6.400

Vorobyova, E., Soina, V., Gorlenko, M., Minkovskaya, N., Zalinova, N., Mamukelashvili, A., et al. (1997). The deep cold biosphere : facts and hypothesis. *FEMS Microbiology Reviews*, *20*, 277–290.

Vuillemin, A., Ariztegui, D., Leavitt, P. R., & Bunting, L. (2016). Recording of climate and diagenesis through sedimentary DNA and fossil pigments at Laguna Potrok Aike, Argentina. *Biogeosciences*, *13*(8), 2475–2492. https://doi.org/10.5194/bg-13-2475-2016

Vuillemin, A., Ariztegui, D., Horn, F., Kallmeyer, J., Orsi, W. D., Anselmetti, F., et al. (2018). Microbial community composition along a 50 000-year lacustrine sediment sequence. *FEMS Microbiology Ecology*, *94*(4), 1–14. https://doi.org/10.1093/femsec/fiy029

Wagner, D., Gattinger, A., Embacher, A., Pfeiffer, E.-M., Schloter, M., & Lipski, A. (2007). Methanogenic activity and biomass in Holocene permafrost deposits of the Lena Delta, Siberian Arctic and its implication for the global methane budget. *Global Change Biology*, *13*(5), 1089–1099. https://doi.org/10.1111/j.1365-2486.2007.01331.x

Wagner, M., Roger, A. J., Flax, J. L., Gregory, A., Stahl, D. A., & Brusseau, G. A. (1998). Phylogeny of Dissimilatory Sulfite Reductases Supports an Early Origin of Sulfate Respiration Phylogeny of Dissimilatory Sulfite Reductases Supports an Early Origin of Sulfate Respiration. *Journal of Bacteriology*, *180*(11), 2975–2982.

Walczowski, W., & Piechura, J. (2006). New evidence of warming propagating toward the Arctic Ocean. *Geophysical Research Letters*, *33*(12), 1–5. https://doi.org/10.1029/2006GL025872

Waldrop, M. P., Wickland, K. P., White, R., Berhe, a. a., Harden, J. W., & Romanovsky, V. E. (2010). Molecular investigations into a globally important carbon pool: Permafrost-protected carbon in Alaskan soils. *Global Change Biology*, *16*(9), 2543–2554. https://doi.org/10.1111/j.1365-2486.2009.02141.x

Walker, T. W. N., Kaiser, C., Strasser, F., Herbold, C. W., Leblans, N. I. W., Woebken, D., et al. (2018). Microbial temperature sensitivity and biomass change explain soil carbon loss with warming. *Nature Climate Change*, *8*, 885–889. https://doi.org/10.1038/s41558-018-0259-x

Walsh, D. A., Papke, R. T., & Doolittle, W. F. (2005). Archaeal diversity along a soil salinity

gradient prone to disturbance. *Environmental Microbiology*, *7*(10), 1655–1666. https://doi.org/10.1111/j.1462-2920.2005.00864.x

Walter Anthony, K., Schneider von Deimling, T., Nitze, I., Frolking, S., Emond, A., Daanen, R., et al. (2018). 21St-Century Modeled Permafrost Carbon Emissions Accelerated By Abrupt Thaw Beneath Lakes. *Nature Communications*, *9*(1). https://doi.org/10.1038/s41467-018-05738-9

Walter, K. M., Zimov, S. A., Chanton, J. P., Verbyla, D., & Chapin, F. S. (2006). Methane bubbling from Siberian thaw lakes as a positive feedback to climate warming. *Nature*, *443*(7107), 71–75. https://doi.org/Doi 10.1038/Nature05040

Walter, K. M., Smith, L. C., & Chapin, F. S. (2007). Methane bubbling from northern lakes: present and future contributions to the global methane budget. *Philosophical Transactions of the Royal Society A-Mathematical Physical and Engineering Sciences*, *365*(1856), 1657–1676. https://doi.org/DOI 10.1098/rsta.2007.2036

Wang, Y., Sheng, H. F., He, Y., Wu, J. Y., Jiang, Y. X., Tam, N. F. Y., & Zhou, H. W. (2012). Comparison of the levels of bacterial diversity in freshwater, intertidal wetland, and marine sediments by using millions of illumina tags. *Applied and Environmental Microbiology*, *78*(23), 8264–8271. https://doi.org/10.1128/AEM.01821-12

Ward, C. P., & Cory, R. M. (2015). Chemical composition of dissolved organic matter draining permafrost soils. *Geochimica et Cosmochimica Acta*, *167*, 63–79. https://doi.org/10.1016/j.gca.2015.07.001

Watanabe, K., & Mizoguchi, M. (2002). Amount of unfrozen water in frozen porous media saturated with solution. *Cold Regions Science and Technology*, *34*(2), 103–110. https://doi.org/10.1016/S0165-232X(01)00063-5

Weber, H. S., Habicht, K. S., & Thamdrup, B. (2017). Anaerobic Methanotrophic Archaea of the ANME-2d Cluster Are Active in a Low-sulfate, Iron-rich Freshwater Sediment. *Frontiers in Microbiology*, *8*(Article 619), 1–13. https://doi.org/10.3389/fmicb.2017.00619

Weedon, J. T., Kowalchuk, G. A., Aerts, R., van Hal, J., van Logtestijn, R., Taş, N., et al. (2012). Summer warming accelerates sub-arctic peatland nitrogen cycling without changing enzyme pools or microbial community structure. *Global Change Biology*, *18*(1), 138–150. https://doi.org/10.1111/j.1365-2486.2011.02548.x

Weedon, J. T., Kowalchuk, G. A., Aerts, R., Freriks, S., Röling, W. F. M., & van Bodegom, P. M. (2017). Compositional stability of the bacterial community in a climate-sensitive Sub-Arctic Peatland. *Frontiers in Microbiology*, *8*(317), 1–11.

https://doi.org/10.3389/fmicb.2017.00317

Wegner, C., Hölemann, J. A., Dmitrenko, I., Kirillov, S., & Kassens, H. (2005). Seasonal variations in Arctic sediment dynamics - Evidence from 1-year records in the Laptev Sea (Siberian Arctic). *Global and Planetary Change*, *48*, 126–140. https://doi.org/10.1016/j.gloplacha.2004.12.009

Wei, S., Cui, H., Zhu, Y., Lu, Z., Pang, S., Zhang, S., et al. (2018). Shifts of methanogenic communities in response to permafrost thaw results in rising methane emissions and soil property changes. *Extremophiles*, *22*(3), 447–459. https://doi.org/10.1007/s00792-018-1007-x

Weijers, J. W. H., Lim, K. L. H., Aquilina, A., Sinninghe Damsté, J. S., & Pancost, R. D. (2011). Biogeochemical controls on glycerol dialkyl glycerol tetraether lipid distributions in sediments characterized by diffusive methane flux. *Geochemistry, Geophysics, Geosystems*, *12*(10), 1–15. https://doi.org/10.1029/2011gc003724

Weiss, J. (2001). *Ionenchromatographie* (3rd ed.). Weinheim: Wiley-VHC.

Wen, X., Yang, S., Horn, F., Winkel, M., & Wagner, D. (2017). Global Biogeographic Analysis of Methanogenic Archaea Identifies Community-Shaping Environmental Factors of Natural Environments. *Frontiers in Microbiology*, *8*(July), Article 1339. https://doi.org/10.3389/fmicb.2017.01339

Wen, X., Unger, V., Jurasinski, G., Koebsch, F., Horn, F., Rehder, G., et al. (2018). Predominance of methanogens over methanotrophs contributes to high methane emissions in rewetted fens. *Biogeosciences Discussions*, *15*(21), 6519–6536. https://doi.org/10.5194/bg-2018-184

Wik, M., Varner, R. K., Anthony, K. W., MacIntyre, S., & Bastviken, D. (2016). Climate-sensitive northern lakes and ponds are critical components of methane release. *Nature Geoscience*, *9*(2), 99–105. https://doi.org/10.1038/ngeo2578

Wilhelm, R. C., Radtke, K. J., Mykytczuk, N. C. S., Greer, C. W., & Whyte, L. G. (2012). Life at the Wedge: the Activity and Diversity of Arctic Ice Wedge Microbial Communities. *Astrobiology*, *12*(4), 347–360. https://doi.org/10.1089/ast.2011.0730

Willems, A. (2014). The Family Comamonadaceae. In *The Prokaryotes* (pp. 777–851). Berlin, Heidelberg: Springer Berlin Heidelberg. https://doi.org/10.1007/978-3-642-30197-1_238

Willerslev, E., Hansen, A. J., Rønn, R., Brand, T. B., Barnes, I., Wiuf, C., et al. (2004). Long-term persistence of bacterial DNA. *Current Biology*, *14*(1), 13–14. https://doi.org/10.1016/j.cub.2003.12.012

Winfrey, M. R., & Zeikus, J. G. (1977). Effect of sulfate on carbon and electron flow during

microbial methanogenesis in freshwater sediments. *Applied and Environmental Microbiology*, *33*(2), 275–281. Retrieved from https://aem.asm.org/content/33/2/275.short

Winkel, M., Sepulveda-Jauregui, A., Martinez-Cruz, K., Heslop, J. K., Rijkers, R., Horn, F., et al. (2019). First evidence for cold-adapted anaerobic oxidation of methane in deep sediments of thermokarst lakes. *Environmental Research Communications*, *1*(2), 021002. https://doi.org/10.1088/2515-7620/ab1042

Winkel, M., de Beer, D., Lavik, G., Peplies, J., & Mußmann, M. (2014). Close association of active nitrifiers with Beggiatoa mats covering deep-sea hydrothermal sediments. *Environmental Microbiology*, *16*(6), 1612–1626. https://doi.org/10.1111/1462-2920.12316

Winkel, M., Mitzscherling, J., Overduin, P. P., Horn, F., Winterfeld, M., Rijkers, R., et al. (2018). Anaerobic methanotrophic communities thrive in deep submarine permafrost. *Scientific Reports*, *8*(1), 1–13. https://doi.org/10.1038/s41598-018-19505-9

Winterfeld, M. (2009). *Characterisation of terrestrial permafrost affected by inundation and Late Quaternary landscape evolution (Western Laptev Sea , Siberia)*. Ernst Moritz Arndt Universität Greifswald.

Winterfeld, M., Schirrmeister, L., Grigoriev, M. N., Kunitsky, V. V., Andreev, A., Murray, A., & Overduin, P. P. (2011). Coastal permafrost landscape development since the Late Pleistocene in the western Laptev Sea, Siberia. *Boreas*, *40*(4), 697–713. https://doi.org/10.1111/j.1502-3885.2011.00203.x

Woodgate, R. a., Aagaard, K., & Weingartner, T. J. (2006). Interannual changes in the Bering Strait fluxes of volume, heat and freshwater between 1991 and 2004. *Geophysical Research Letters*, *33*(15), 2–6. https://doi.org/10.1029/2006GL026931

Xiang, X., Wang, R., Wang, H., Gong, L., Man, B., & Xu, Y. (2017). Distribution of Bathyarchaeota Communities Across Different Terrestrial Settings and Their Potential Ecological Functions. *Scientific Reports*, *7*(1), 45028. https://doi.org/10.1038/srep45028

Xiong, J., Sun, H., Peng, F., Zhang, H., Xue, X., Gibbons, S. M., et al. (2014). Characterizing changes in soil bacterial community structure in response to short-term warming. *FEMS Microbiology Ecology*, *89*(2), 281–292. https://doi.org/10.1111/1574-6941.12289

Xu, G., Chen, J., Berninger, F., Pumpanen, J., Bai, J., Yu, L., & Duan, B. (2015). Labile, recalcitrant, microbial carbon and nitrogen and the microbial community composition at two Abies faxoniana forest elevations under elevated temperatures. *Soil Biology and Biochemistry*, *91*, 1–13. https://doi.org/10.1016/J.SOILBIO.2015.08.016

Yang, S., Liebner, S., Alawi, M., Ebenhöh, O., & Wagner, D. (2014). Taxonomic database and cut-off value for processing mcrA gene 454 pyrosequencing data by MOTHUR. *Journal of Microbiological Methods*, *103*, 3–5. https://doi.org/10.1016/J.MIMET.2014.05.006

Yergeau, E, Kang, S., He, Z., Zhou, J., & Kowalchuk, G. A. (2007). Functional microarray analysis of nitrogen and carbon cycling genes across an Antarctic latitudinal transect. *ISME J*, *1*(2), 163–179. https://doi.org/ismej200724 [pii]10.1038/ismej.2007.24

Yergeau, E., Arbour, M., Brousseau, R., Juck, D., Lawrence, J. R., Masson, L., et al. (2009). Microarray and real-time PCR analyses of the responses of high-arctic soil bacteria to hydrocarbon pollution and bioremediation treatments. *Applied and Environmental Microbiology*, *75*(19), 6258–67. https://doi.org/10.1128/AEM.01029-09

Yergeau, E., Hogues, H., Whyte, L. G., & Greer, C. W. (2010). The functional potential of high Arctic permafrost revealed by metagenomic sequencing, qPCR and microarray analyses. *The ISME Journal*, *4*(9), 1206–1214. https://doi.org/10.1038/ismej.2010.41

Yi, H., & Chun, J. (2004). Nocardioides aestuarii sp. nov., isolated from tidal flat sediment. *International Journal of Systematic and Evolutionary Microbiology*, *54*(6), 2151–2154. https://doi.org/10.1099/ijs.0.63192-0

Yu, T., Wu, W., Liang, W., Lever, M. A., Hinrichs, K.-U., & Wang, F. (2018). Growth of sedimentary Bathyarchaeota on lignin as an energy source . *Proceedings of the National Academy of Sciences*, *115*(23), 6022–6027. https://doi.org/10.1073/pnas.1718854115

Zeglin, L. H., Sinsabaugh, R. L., Barrett, J. E., Gooseff, M. N., & Takacs-Vesbach, C. D. (2009). Landscape Distribution of Microbial Activity in the McMurdo Dry Valleys: Linked Biotic Processes, Hydrology, and Geochemistry in a Cold Desert Ecosystem. *Ecosystems*, *12*(4), 562–573. https://doi.org/10.1007/s10021-009-9242-8

Zhang, D. F., Zhong, J. M., Zhang, X. M., Jiang, Z., Zhou, E. M., Tian, X. P., et al. (2014a). Nocardioides nanhaiensis sp. nov., an actinobacterium isolated from a marine sediment sample. *International Journal of Systematic and Evolutionary Microbiology*, *64*(PART 8), 2718–2722. https://doi.org/10.1099/ijs.0.062851-0

Zhang, J., Kobert, K., Flouri, T., & Stamatakis, A. (2014b). PEAR: A fast and accurate Illumina Paired-End reAd mergeR. *Bioinformatics*, *30*(5), 614–620. https://doi.org/10.1093/bioinformatics/btt593

Zhang, K., Shi, Y., Jing, X., He, J. S., Sun, R., Yang, Y., et al. (2016). Effects of short-term warming and altered precipitation on soil microbial communities in alpine grassland of the tibetan plateau. *Frontiers in Microbiology*, *7*(1032), 1–11. https://doi.org/10.3389/fmicb.2016.01032

Zhang, T., Barry, R. G., Knowles, K., Heginbottom, J. A., & Brown, J. (1999). Statistics and characteristics of permafrost and ground-ice distribution in the Northern Hemisphere. *Polar Geography*, *23*(2), 132–154. https://doi.org/10.1080/10889379909377670

Zhang, T., Barry, R. G., Knowles, K., Ling, F., & Armstrong, R. L. (2003). Distribution of seasonally and perennially frozen ground in the Northern Hemisphere. In A. Phillips, Springman (Ed.), *Proceedings of the 8th International Conference on Permafrost* (pp. 1289–1294). Zürich: Permafrost.

Zhang, W., Parker, K. M., Luo, Y., Wan, S., Wallace, L. L., & Hu, S. (2005). Soil microbial responses to experimental warming and clipping in a tallgrass prairie. *Global Change Biology*, *11*(2), 266–277. https://doi.org/10.1111/j.1365-2486.2005.00902.x

Zhang, Y., Hao, X., Alexander, T. W., Thomas, B. W., Shi, X., & Lupwayi, N. Z. (2018). Long-term and legacy effects of manure application on soil microbial community composition. *Biology and Fertility of Soils*, *54*(2), 269–283. https://doi.org/10.1007/s00374-017-1257-2

Zhang, Y. G., Zhang, C. L., Liu, X.-L., Li, L., Hinrichs, K.-U., & Noakes, J. E. (2011). Methane Index: A tetraether archaeal lipid biomarker indicator for detecting the instability of marine gas hydrates. *Earth and Planetary Science Letters*, *307*(3–4), 525–534. https://doi.org/10.1016/J.EPSL.2011.05.031

Zhigarev, L. A. (1997). *Submarine cryolithozone (okeanicheskaya kriolitozna)*. MSU Publishing, Moscow (in Russian).

Zhou, D., Feng, H., Schuelke, T., De Santiago, A., Zhang, Q., Zhang, J., et al. (2019). Rhizosphere Microbiomes from Root Knot Nematode Non-infested Plants Suppress Nematode Infection. *Microbial Ecology*, 1–12. https://doi.org/10.1007/s00248-019-01319-5

Zhou, J., Bruns, M. A., & Tiedje, J. M. (1996). DNA recovery from soils of diverse composition. *Applied and Environmental Microbiology*, *62*(2), 316–322.

Zhou, Z., Pan, J., Wang, F., Gu, J. D., & Li, M. (2018). Bathyarchaeota: Globally distributed metabolic generalists in anoxic environments. *FEMS Microbiology Reviews*, *42*(5), 639–655. https://doi.org/10.1093/femsre/fuy023

Zimov, S. A., Schuur, E. A., & Chapin 3rd, F. S. (2006). Permafrost and the global carbon budget. *Science*, *312*(5780), 1612–1613. https://doi.org/10.1126/science.1128908

Zink, K.-G., & Mangelsdorf, K. (2004). Efficient and rapid method for extraction of intact phospholipids from sediments combined with molecular structure elucidation using LC-ESI-MS-MS analysis. *Analytical and Bioanalytical Chemistry*, *380*(5–6), 798–812.

https://doi.org/10.1007/s00216-004-2828-2

Zinke, L. A. ., Evans, P. N. ., Parks, D. ., Varner, R. K. ., Rich, V. I. ., Tyson, G. W. ., & Emerson, J. B. (2018). An Archaeal Clade Grouped Closely to Methanomassiliicoccales Lacks the Canonical Methanogenesis Pathway. In *American Geophysical Union, Fall Meeting 2018* (pp. B11C-2162).

Zogg, G. P., Zak, D. R., Ringelberg, D. B., White, D. C., MacDonald, N. W., & Pregitzer, K. S. (1997). Compositional and Functional Shifts in Microbial Communities Due to Soil Warming. *Soil Science Society of America Journal*, *61*(2), 475–481. https://doi.org/10.2136/sssaj1997.03615995006100020015x

A. Appendix Manuscript I

AGU PUBLICATIONS

JGR

Journal of Geophysical Research: Biogeosciences

RESEARCH ARTICLE
10.1002/2017JG003859

Special Section:
The Arctic: An AGU Joint Special Collection

The development of permafrost bacterial communities under submarine conditions

Julia Mitzscherling[1], Matthias Winkel[1], Maria Winterfeld[2,3], Fabian Horn[1], Sizhong Yang[1], Mikhail N. Grigoriev[4], Dirk Wagner[1], Pier P. Overduin[2], and Susanne Liebner[1]

[1]GFZ German Research Centre for Geosciences, Section 5.3 Geomicrobiology, Potsdam, Germany, [2]Helmholtz Centre for Polar and Marine Research, Research Department Potsdam, Alfred Wegener Institute, Potsdam, Brandenburg, Germany, [3]Now at Helmholtz Centre for Polar and Marine Research, Research Department Bremerhaven, Alfred Wegener Institute, Bremerhaven, Bremen, Germany, [4]Melnikov Permafrost Institute, Siberian Branch, Russian Academy of Sciences, Yakutsk, Russia

Key Points:
- Submarine permafrost is an extreme habitat for microbial life deep below the seafloor with changing thermal and chemical conditions
- Millennia after inundation by seawater, bacteria stratify into communities in permafrost, marine-affected permafrost, and seabed sediments
- Permafrost pore water chemistry changes in response to inundation before permafrost thaws; it can be used to detect the marine influence

Supporting Information:
- Supporting Information S1
- Table S1

Correspondence to:
J. Mitzscherling,
jmagritz@gfz-potsdam.de

Citation:
Mitzscherling, J., M. Winkel, M. Winterfeld, F. Horn, S. Yang, M. N. Grigoriev, D. Wagner, P. P. Overduin, and S. Liebner (2017), The development of permafrost bacterial communities under submarine conditions, *J. Geophys. Res. Biogeosci.*, *122*, 1689–1704, doi:10.1002/2017JG003859.

Received 23 MAR 2017
Accepted 16 JUN 2017
Accepted article online 21 JUN 2017
Published online 17 JUL 2017

©2017. American Geophysical Union. All Rights Reserved.

Abstract Submarine permafrost is more vulnerable to thawing than permafrost on land. Besides increased heat transfer from the ocean water, the penetration of salt lowers the freezing temperature and accelerates permafrost degradation. Microbial communities in thawing permafrost are expected to be stimulated by warming, but how they develop under submarine conditions is completely unknown. We used the unique records of two submarine permafrost cores from the Laptev Sea on the East Siberian Arctic Shelf, inundated about 540 and 2500 years ago, to trace how bacterial communities develop depending on duration of the marine influence and pore water chemistry. Combined with geochemical analysis, we quantified total cell numbers and bacterial gene copies and determined the community structure of bacteria using deep sequencing of the bacterial 16S rRNA gene. We show that submarine permafrost is an extreme habitat for microbial life deep below the seafloor with changing thermal and chemical conditions. Pore water chemistry revealed different pore water units reflecting the degree of marine influence and stages of permafrost thaw. Millennia after inundation by seawater, bacteria stratify into communities in permafrost, marine-affected permafrost, and seabed sediments. In contrast to pore water chemistry, the development of bacterial community structure, diversity, and abundance in submarine permafrost appears site specific, showing that both sedimentation and permafrost thaw histories strongly affect bacteria. Finally, highest microbial abundance was observed in the ice-bonded seawater unaffected but warmed permafrost of the longer inundated core, suggesting that permafrost bacterial communities exposed to submarine conditions start to proliferate millennia after warming.

1. Introduction

Extensive shallow water areas of the Arctic continental shelf are underlain by submarine permafrost [*Zhang et al.*, 1999; *Rachold et al.*, 2007]. The shallowest and most spacious shelf of the World Ocean is the East Siberian Arctic Shelf encompassed by the Laptev, East Siberian, and the Russian part of the Chukchi Seas. It comprises more than 80% of the potential submarine permafrost in the Arctic [*Overduin et al.*, 2015].

Submarine permafrost is relict terrestrial permafrost that developed on land and was subsequently inundated by postglacial sea level rise during the Holocene, 7 to 15 ka ago [*Romanovskii and Hubberten*, 2001]. Even today, especially Arctic permafrost coasts, which account for 34% of the coasts worldwide [*Lantuit et al.*, 2012], are vulnerable to sea level rise, declining sea ice cover, and longer and warmer thawing seasons [*Fritz et al.*, 2017]. Resulting coastline collapses, with mean modern erosion rates of 1 to 2 m yr^{-1} [*Lantuit et al.*, 2012] and local erosion rates of up to 25 m y^{-1} [*Jones et al.*, 2009], lead to an annual formation of about 10 km^2 of submarine permafrost on the East Siberian Arctic Shelf alone [*Grigoriev*, 2008]. This erosion of permafrost coasts is an abrupt form of permafrost degradation and results in yet unquantified fluxes of carbon and nutrients from thawing permafrost with presumably large consequences for the biogeochemical cycling of the shelf area [*Fritz et al.*, 2017].

The seawater inundation and infiltration cause drastic changes in the thermal regime and geochemical composition of submarine permafrost [*Ulyantsev et al.*, 2016]. With annual average bottom water temperatures of −1.8°C to −1°C [*Wegner et al.*, 2005], it is 12 to 17°C warmer than the annual average surface temperature over on-land permafrost [*Romanovskii et al.*, 2005]. As temperatures in high latitudes have been rising faster than the global average over the past decades [*IPCC*, 2013], bottom water warming further increases

AGU Journal of Geophysical Research: Biogeosciences 10.1002/2017JG003859

the degradation rates of submarine permafrost in the Laptev and East Siberian Seas. Besides top-down seawater heat and salt fluxes, bottom-up geothermal heat fluxes are responsible for the degradation of submarine permafrost [*Osterkamp*, 2001; *Shakhova et al.*, 2010]. The seabed temperature of much of the Arctic shelf seas is cryotic (<0°C). In coastal waters, submarine permafrost temperature is around −1°C [*Overduin et al.*, 2015], the limit to maintain ice-bonded permafrost under submarine conditions [*Grigoriev*, 2008]. Warming and destabilization of submarine permafrost increase sediment permeability. On the one hand, this can result in the release of long preserved methane (CH_4) into the water column and atmosphere [*Shakhova et al.*, 2010; *Portnov et al.*, 2013; *Shakhova et al.*, 2014, *Thornton et al.*, 2016]. On the other hand, trapped organic material becomes more accessible to microorganisms after thawing, potentially inducing the decomposition of soil organic matter and transforming complex organic compounds to soluble metabolites and gases, such as CH_4, CO_2, and N_2O [*Graham et al.*, 2012; *Mackelprang et al.*, 2011]. Its release is potentially relevant to global climate, since terrestrial and submarine permafrost store twice as much carbon as is currently in the atmosphere [*Schuur et al.*, 2009].

Microbial life in thawing permafrost is expected to be stimulated before permafrost thaws completely [*Schuur et al.*, 2015]; i.e., activity and abundance should increase [*Waldrop et al.*, 2010; *Graham et al.*, 2012; *Mackelprang et al.*, 2011]. Submarine permafrost is thereby affected not only by rising temperatures but also by elevated salt concentrations [*Harrison and Osterkamp*, 1982]. In particular, during the first decades of inundation, there may be an active layer at the seabed that thaws and freezes seasonally [*Osterkamp*, 2001]. Brine drainage from the growing sea ice increases water salinity and decreases temperatures of the bottom-water in fall and winter. Brines can infiltrate the seabed, even when it is frozen. They are responsible for thawing the underlying submarine permafrost at negative sediment temperatures. In contrast to rising temperatures and the release of substrate, the evolution of submarine permafrost with salt infiltration as the main process has been disregarded in assumptions how microbial life responds to submarine permafrost thaw. Osmotic stress is known to limit microbial growth and activity [*Galinski*, 1995]. Although microbes have a number of features (fast growth rates, physiological flexibility, and a rapid evolution, i.e., mutation or horizontal gene transfer) to acclimate, adapt, and recover, several studies showed that microbial community composition is sensitive to disturbances [reviewed by *Allison and Martiny*, 2008]. These studies observed shifts and no resilience in the microbial community composition within a few years. Therefore, we hypothesize that increasing salinity in terrestrial permafrost deposits might impair the indigenous microbial community before it is stimulated through rising temperatures. We expect the terrestrial community to change its composition in response to seawater infiltration. Assuming limited microbial growth and activity due to osmotic stress, as mentioned above, the community is initially expected to decrease in population size. To test this, we studied the pore water chemistry and bacterial community composition, diversity, and abundance by means of the bacterial 16S rRNA gene copy numbers, total cell counts, and deep sequencing of the bacterial 16S rRNA gene of two submarine permafrost cores from the Western and Central Laptev Sea Shelf inundated for different time periods.

2. Materials and Methods

2.1. Regional Setting and Study Areas

The Laptev Sea, bordered by the Taymyr Peninsula to the west and the New Siberian Island to the east, has an average water depth of less than 60 m. During the Weichselian glaciation (Late Pleistocene), large areas of the nonglaciated arctic continental shelf were exposed to climatic conditions which led to the formation of cold, thick, and continuous permafrost [*Svendsen et al.*, 2004]. Subsequently, a large portion of the ice-rich terrestrial permafrost that developed was inundated by a combination of the Holocene marine transgression and coastal thermoerosion [*Winterfeld et al.*, 2011].

The first study area at Cape Mamontov Klyk (supporting information Figure S1) was described by *Winterfeld et al.* [2011]. Cape Mamontov Klyk (~73°60′N, 117°18′E) is situated in the Western Laptev Sea. During a campaign in 2005 [*Rachold et al.*, 2007; *Schirrmeister*, 2007], a submarine core (C2) was drilled about 11.5 km offshore. Assuming a mean annual coastal erosion rate of 4.5 m yr^{-1} [*Grigoriev*, 2008], the drill site was inundated 2500 years ago [*Rachold et al.*, 2007]. The core was retrieved in approximately 6 m water depth with a sea ice thickness of 1.35 m and bottom-water salinity of 29.2 practical salinity unit (psu). Core material was retrieved between 6 and 77 m bsl (meters below sea level). Temperature measurements at the site of C2

AGU Journal of Geophysical Research: Biogeosciences 10.1002/2017JG003859

were performed 1 to 11 days after drilling and are described and published elsewhere [*Junker et al.*, 2008; *Overduin et al.*, 2008]. Temperatures of the C2 borehole ranged between −1.5 and −0.8°C.

The second study area is located in the Buor Khaya Bay (supporting information Figure S1). Within the framework of the Drilling Expedition Buor Khaya in 2012 [*Günther et al.*, 2013], the submarine sediment core BK2 was retrieved about 750 m off the coast west of the Buor Khaya Peninsula, in the Central Laptev Sea. Drilling was performed in 4.3 m deep water with a sea ice cover of 2.09 m and a bottom-water salinity of 5.9 psu [*Günther et al.*, 2013]. Core material was retrieved between 6 and 51 m bsl. Borehole temperature of BK2 was recorded for 4 days after drilling. Measurement and temperature data of BK2 were published by *Overduin et al.* [2015]. Borehole temperatures ranged between 0.4 and −0.9°C. Based on the distance of the borehole from the modern coastline and on the mean annual erosion rate of 1.4 ± 0.8 m yr^{-1} [*Günther et al.*, 2012], the location of BK2 was flooded around 540 years ago [*Overduin et al.*, 2015]. Since the Buor Khaya Peninsula is covered by thermokarst depressions and characterized by an eroding Ice Complex coastal bluff, it is likely that the drill site was affected by Holocene thermokarst or thermokarst lake development prior to erosion and that it was frozen at the time of inundation.

2.2. Geochemical Analyses

Pore water was extracted from thawed subsamples of the sediment cores using Rhizons™ (0.2 μm pore diameter). Electrical conductivity, salinity, cation (Ba^{2+}, Ca^{2+}, K^{+}, Mg^{2+}, Na^{+}, and Si_{aq}) and anion (Cl^{-}, SO_4^{2-}, Br^{-}, NO_3^{-}) concentrations, stable isotope concentrations ($\delta^{18}O$ and δD), and pH were measured for 94 samples of C2 (Cape Mamontov Klyk) and for 80 samples of BK2 (Buor Khaya Bay; supporting information Tables S1 and S2). Electrical conductivity and salinity were measured with a WTW MultiLab 540 by using a standard conductivity cell (TetraConR 325) with four graphite electrodes. Total dissolved element concentration was determined via the analytical technique of inductively coupled plasma optical emission spectrometry using a Perkin-Elmer ICP-OES Optima 3000XL. In order to measure the concentration (mg/L) of dissolved anions, an ion chromatograph (Dionex DX-320), a latex-particle separation column, and KOH as eluent were used. Values below detection limit were assigned values of half the detection limit for inclusion in principal component analyses (PCAs). The determination of deuterium (δD) and oxygen isotope ($\delta^{18}O$) ratios was performed using a Finnigan MAT Delta-S mass spectrometer in combination with two equilibration units (MS Analysetechnik, Berlin).

2.3. Extraction of Nucleic Acids

Total nucleic acids were extracted as described by *Zhou et al.* [1996] in a slightly modified way. Sediment samples from 5 to 10 g were homogenized in liquid nitrogen and mixed with 13.5 mL of DNA extraction buffer (100 m*M* Tris-HCl [pH 8.0], 100 m*M* sodium EDTA [pH 8.0], 100 m*M* sodium phosphate [pH 8.0], and 1.5 *M* NaCl, 1% CTAB) and 100 μL of proteinase K (10 mg/mL) in 50 mL centrifuge tubes. They were incubated with horizontal shaking for 1 h at 37°C and 225 rpm. After the addition of 1.5 mL of 20% sodium dodecyl sulfate, the samples were incubated in a water bath at 65°C for 2 h with gentle inversions every 20 min. Supernatants were recovered by centrifugation at 6000 *g* for 10 min at room temperature and collected in fresh 50 mL centrifuge tubes. The sediment pellets were extracted two more times as follows: addition of 4.5 mL of extraction buffer and 0.5 mL of 20% sodium dodecyl sulfate, vortexing the tubes for 10 s, incubation at 65°C for 10 min, and centrifugation as described before. Supernatants of the three extraction cycles were combined and mixed with an equal volume of chloroform-isoamyl alcohol (24:1 vol/vol) and the coprecipitant GlycoBlue™ (1:300). After recovery of the aqueous phase by centrifugation, the DNA was precipitated with 0.6 volumes of isopropanol at room temperature for 1 h and pelleted by centrifugation at 16,000 *g* for 20 min. Finally, the DNA pellet was washed three times with 1 mL of ice-cold 70% ethanol and resuspended in a final volume of 500 μL of sterile deionized water.

Genomic DNA was quantified with the QBIT2 system (Invitrogen, HS-quant DNA) and calculated per gram sediment wet weight. The crude DNA was purified using the HiYield PCR Clean-Up and Gel-Extraction Kit (Südlabor, Gauting, Germany) to reduce polymerase chain reaction (PCR) inhibitors and the necessity to dilute the DNA extracts prior to PCR applications.

2.4. Quantification of the Bacterial 16S rRNA Genes

Quantitative PCR was performed using the CFX Connect™ Real-Time PCR Detection System (Bio-Rad Laboratories, Inc., Hercules, USA) and the following primer set: Eub341F and Eub534R [*Muyzer et al.*, 1993].

AGU Journal of Geophysical Research: Biogeosciences 10.1002/2017JG003859

Each reaction (25 μL) contained 2× concentrate of iTaq™ Universal SYBR® Green Supermix (Bio-Rad Laboratories, Inc., Hercules, USA), 0.4 μ*M* of the forward and reverse primer, sterile water, and 5 μL of DNA template. The environmental DNA samples were diluted 5- to 100-fold and run in three technical replicates. The PCR reactions comprised an initial denaturation (5 min at 95°C), followed by 40 cycles of 0.5 s at 95°C, 30 s at an annealing temperature of 55.7°C, 10 s at 72°C, and a plate read step at 80°C for 0.3 s. Melt curve analysis from 65 to 95°C with 0.5°C temperature increment per 0.5 s cycle and gel electrophoresis on the PCR products were conducted at the end of each run to identify nonspecific amplification of DNA. The qPCR assay was calibrated using known amounts of PCR amplified and cloned gene fragments from a pure *Escherichia coli* culture. Genomic standards were included in each qPCR run to ensure linearity and expected slope values of the Ct/log curves. PCR efficiency, based on the standard curve, was calculated using the BioRad CFX Manager software and varied between 95 and 100%. All cycle data were collected using the single threshold Cq determination mode. Abundances of the bacterial 16S rRNA gene and of cells were calculated per gram sediment wet weight.

2.5. Amplification and Illumina MiSeq Sequencing of the Bacterial 16S rRNA Gene

We sequenced 19 samples from the core C2 and 10 samples from BK2. From BK2, two samples right above and below the ice-bonded permafrost table were pooled. The sampling depths are illustrated in Figure 2. PCR and sequencing were performed in two technical replicates for each sample. Bacterial 16S rRNA genes were amplified using the sequencing primers S-D-Bact-0341-b-S-17 and S-D-Bact-0785-a-A-21 (supporting information Table S3) comprising different combinations of barcodes (supporting information Table S4). Preparation and sequencing was performed in two technical replicates.

The PCR amplification was carried out with a T100™ Thermal Cycler (Bio-Rad Laboratories, CA, USA), and the PCR mixture of 25 μL contained 0.025 U μL^{-1} of HotStarTaq DNA Polymerase (Qiagen), 1× PCR buffer (Tris-Cl, KCl, $(NH_4)_2SO_4$, 15 m*M* $MgCl_2$; pH 8.7, Qiagen), 0.4 μ*M* of forward and reverse primer (supporting information Table S3), dNTP mix (0.2 m*M* each; Thermo Fisher Scientific, Darmstadt, Germany), 2 μ*M* of $MgCl_2$ (Qiagen), RNase-free water (EURx), and 2.5 μL of DNA extract. PCR conditions were as follows: initial denaturation at 95°C for 5 min, followed by 30 cycles of denaturation (95°C for 30 s), annealing (55°C for 30 s) and elongation (72°C for 1 min), and a final extension step of 72°C for 10 min.

The PCR products were purified from agarose gel with the HiYieldPCR Clean-Up and Gel-Extraction Kit (Südlabor, Gauting, Germany). Amplicons were quantified with the QBIT2 system (Invitrogen, HS-Quant DNA), mixed in equimolar amounts and sequenced from both directions (GATC Biotech, Konstanz) based on the Illumina MiSeq technology. The library was prepared with the MiSeq Reagent Kit V3 for 2× 300 bp paired-end reads according to the manufacturer's protocols. For better performance due to different sequencing length, 15% PhiX control v3 library was used.

2.6. Sequence Analyses and Bioinformatics

The acquired raw data of bacterial sequences were analyzed starting with the quality control of the sequencing library by the tool FastQC (Quality Control tool for High Throughput Sequence Data http://www.bioinformatics.babraham.ac.uk/projects/fastqc/ by S. Andrews). Demultiplexing of the sequence reads according to their barcodes and subsequent removal of the barcodes were performed with the CutAdapt tool [*Martin*, 2011]. Using PEAR [*J. Zhang et al.*, 2014], forward and reverse sequenced fragments with overlapping sequence regions were merged, and the nucleotide sequence orientation was standardized. Low-quality sequences were filtered and trimmed by Trimmomatic [*Bolger et al.*, 2014], and chimeras were removed by Chimera.Slayer. Finally, the QIIME pipeline was used to cluster sequences into operational taxonomic units (OTUs) and to taxonomically assign them employing the Greengenes database with a cutoff value of 97% [*Caporaso et al.*, 2010]. Older taxonomic assignments for bacteria were corrected manually after *Rinke et al.* [2013] and *Nobu et al.* [2016]. OP9 and JS1 were renamed to *Atribacteria*, OD1 to *Parcubacteria*, and CD12 to *Aerophobetes*.

2.7. Statistical Analyses

$OTU_{0.03}$ with reads <0.1% of the total read counts per sample, $OTU_{0.03}$ not classified as bacteria or classified as chloroplasts, and absolute singletons were removed prior to statistical analysis. Absolute read counts were transformed to relative abundances in order to standardize the data and to account for different sequencing

AGU Journal of Geophysical Research: Biogeosciences 10.1002/2017JG003859

depths. Variation in pore water and $OTU_{0.03}$ composition between samples and among pore water units, as well as correlations of the $OTU_{0.03}$ composition structure with pore water parameters, and determination of diversity were assessed using the Past 3.12 software [*Hammer et al.*, 2001]. Diversity indices and richness were calculated based on the mean relative abundance of all $OTU_{0.03}$ of duplicates. To visualize the grouping patterns of sediment samples based on pore water data, principal component analyses based on the Euclidean distance of standardized ($(x - \text{mean})/\text{stdev}$) pore water variables were used. Grouping patterns based on the $OTU_{0.03}$ composition of samples were determined by nonmetric multidimensional scaling (NMDS) based on the Bray-Curtis distance measure. To test whether pore water units and their communities, as well as the total communities of the two study sites, were significantly different, a nonparametric multivariate analysis of variance (MANOVA)/permutational MANOVA (PerMANOVA) was conducted [*Anderson*, 2001]. Mantel tests were used to study the relationship between pore water units and community structuring effects [*Mantel*, 1967].

Determination of the core community of $OTU_{0.03}$ in two different pore water units was performed using a custom R script. We filtered specialist $OTU_{0.03}$, which were present in all samples of one unit but not in the other.

2.8. Total Cell Counts

Fixation, sonication, and filtration of sediment were performed as previously described [*Llobet-Brossa et al.*, 1998]. In order to prevent lysis of the cells during the hybridization process, macromolecules and cytoskeletal structures were stabilized by fixation with formaldehyde. At the same time, the fixation makes the cell walls permeable. An amount of 0.5 g of sediment was fixed with 1.5 mL 4% paraformaldedhyde-phosphate-buffered saline (PBS; composed of 137 m*M* NaCl, 2.7 m*M* KCl, 15 m*M* Na_2HPO_4, and 1.7 m*M* KH_2PO_4 [pH 7.6 in water]) for 1 h at room temperature or at 4°C overnight. After incubation, the sediment was pelleted by centrifugation at 9600 *g* for 5 min, and the supernatant was discarded. The paraformaldehyde fixed samples were washed twice in freshly sterile filtered 1.5 mL PBS and stored in 1.5 mL of PBS/ethanol (1:1) at −20°C until further processing. The following sonication, according to *Ishii et al.* [2004], was performed to relieve cells attached to sediment particles. A volume of 200 μL of the fixed sample was diluted sixfold in PBS/ethanol (1:1), placed on ice, and treated by low intensity sonication with a Sonotrode MS73 probe (Sonopuls HD3100, Bandelin, Berlin, Germany) for 30 s at a setting of 1.5 s sonication pulses (on/off 0.5 s/1.0 s) and an amplitude of 20%. Sonication was repeated two times. After each sonication step, the sample was resuspended. Of the supernatant, 200 μL was transferred to a fresh tube and replaced by 200 μL of PBS/ethanol. The collected supernatant was chilled on ice for 2 min or stored at −20°C until further processing. The sonicated supernatant was diluted in PBS and filtered through a polycarbonate membrane filter. The filtration was performed by applying a vacuum and a pressure of around −5 mbar. Finally, the filters were air dried at room temperature and stored at −20°C until further processing [*Ishii et al.*, 2004].

Total cell counts were determined by SYBR Green I. Filters were placed on a glass slide, mounted with 3 μL of SBYR Green I staining solution (1 volume of 1:40 SYBR Green I, 1 volume of 0.1% *p*-phenylenediamine, and 1 volume of 4:1 Citifluor/Vecta Shield) and covered with a cover slip [*Kallmeyer et al.*, 2008]. Fluorescence microscopy was performed with a Leica DM2000 fluorescence microscope using the filter cube FI/RH for SYBR Green I.

3. Results

3.1. Pore Water Chemistry

According to the PCA of C2 and BK2 (Figure 1), variance between the samples on the horizontal axis (PC1) is explained by the seawater influence represented by salinity, conductivity, and most of the ion concentrations (Br^-, Cl^-, Na^+, Mg^{2+}), with nonsaline sediments to the left and saline sediments to the right side. In each plot, different clusters contained samples of consecutive depth, thus defining pore water units in the sediment. Pore water unit I (PW I) represented samples in the upper meters of both cores and is characterized by elevated salinity, conductivity, and ion concentrations. Pore water unit II (PW II) represented samples located below PW I. These sediments showed a rapid decline of cations, anions, salinity, and conductivity. The parameters mentioned before were lower than in PW I but still elevated in comparison to the underlying samples,

AGU Journal of Geophysical Research: Biogeosciences 10.1002/2017JG003859

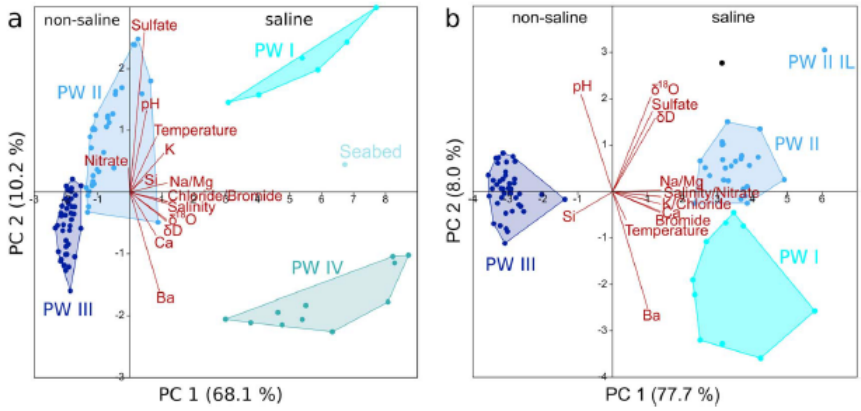

Figure 1. Principal component analyses show the variation of sediment samples based on standardized pore water and temperature data (Euclidean distance). Pore water units (PW) were defined based on cluster analysis and are represented by different colors. The percentage of variation between samples described by principal components 1 and 2 (PC 1 and 2) is indicated on the axes. (a) In total, PC 1 and PC 2 explained 78.3% of the variance between samples of C2 (inundated ~2500 years ago). (b) PC 1 and PC 2 explained 85.7% of variance between samples of BK2 (inundated 540 years ago). Environmental variables are projected as dark red vectors.

which represented the pore water unit III (PW III). These were not influenced by seawater: salinity was less than 1 psu for most samples.

In C2, clusters of PW II and PW III are not very distinct from each other (Figure 1a), as the influence of the saline water (concentration of ions, etc.) decreased gradually with depth, leading to a smooth transition from one unit to the other. Furthermore, an additional cluster formed (PW IV), representing samples in the unfrozen sediments below PW III, located deepest in the core. Although clustering apart from PW I on the vertical axis, parameters were comparable (high salinity and ion concentrations). Pore water stable isotope signatures in PW I and IV laid in the range of −9 to −20‰ ($\delta^{18}O$) and −75 to −150‰ (δD), where increasing marine influence was shown by a tendency toward heavier values. PW III had values consistent with a glacial origin of pore water, with values from −30 to −20‰ ($\delta^{18}O$) and −150 to −230‰ (δD). A one-way PerMANOVA still revealed that the variance between each of the clusters was significantly higher than within single clusters ($p = 0.0001$, supporting information Table S5). One single sample was located between the clusters of PW I and PW IV (Figure 1a), representing the uppermost centimeters of sediment, namely the seabed.

In contrast to C2, the separation of PW II and PW III in BK2 was very clear (Figure 1b). Salinity, conductivity, and the concentrations of all ions showed a sudden drop at the depth of 28.75 m bsl, the same depth at which the ice-bonded permafrost table occurred. The seawater penetration abruptly stopped at this depth, leaving the underlying sediments (PW III) unaffected. In BK2, PW I and PW II clustered close together as both were comparably strongly influenced by seawater. Variations in pore water stable isotope signature for the Buor Khaya borehole were discussed in *Overduin et al.* [2015] and suggest a terrestrial cold climate origin not yet affected by the infiltration of seawater in PW III. Together with pH and barium and sulfate concentrations, isotopes were important in differentiating PW I from PW II sediments in BK2. However, the difference between all three clusters determined by one-way PerMANOVA was significant ($p = 0.0001$, supporting information Table S6). Two samples were located apart from any cluster. One of them originated from the first few centimeters of sediment recovered (6 m bsl, black). However, the most deviant sample (PW II IL) originated from 12.35 m bsl depth, most closely located to PW II.

Analyses of samples from both cores in one principal component analysis (supporting information Figure S2) revealed that the PW III of both cores and PW II of C2 clustered together. Furthermore, the PW I of both cores, PW IV in C2, and PW II in BK2 clustered on the opposite site of the plot with increased influence of the salt water. PW II of C2 scattered between the PW I/PW II and PW III with most of the samples clustering close to PW III. In terms of pore water parameters, one-way PerMANOVA revealed no significant difference between both sediment cores ($p = 0.9999$; $F = -0.0005$).

AGU Journal of Geophysical Research: Biogeosciences 10.1002/2017JG003859

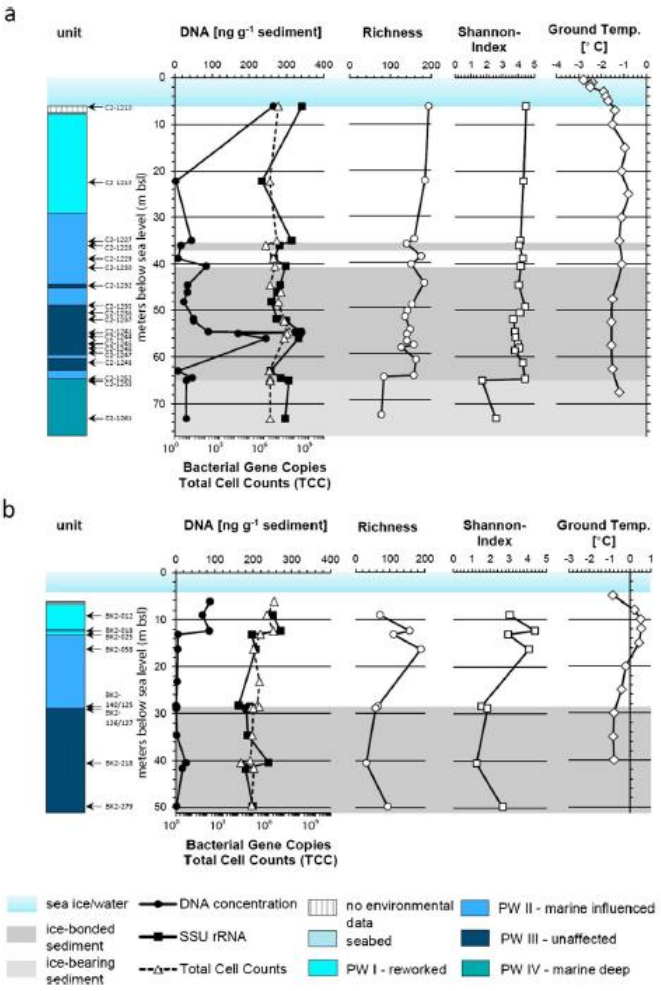

Figure 2. Sediment characteristics: (left to right) pore water units, depth of samples chosen for sequencing, DNA concentration (filled dots), bacterial 16S rRNA gene copy number (filled squares) and total cell counts (TCC, triangles) per gram sediment wet weight, richness (no. of $OTU_{0.03}$, dots), Shannon Index (diversity, squares), and ground temperature (diamond) of (a) C2 (inundated ~2500 years ago) and (b) BK2 (inundated 540 years ago). Sea ice/water thickness is indicated at the top of the figures; ice-bonded permafrost is shown in the graphs.

3.2. Stratification of Pore Water Units

Grouping the samples according to the previously shown clusters resulted in a clear separation of the PW I and II in the PCA, which was reflected in the stratigraphy of C2 (Figure 2a). PW I reached down to a depth of 29 m without interruption, whereas PW II and III showed some alternating layering effects in some depths. PW II reached down to a depth of 48.8 m bsl and was interrupted by PW III at between 44.7 and 45.2 m bsl. The largest zone of PW III extended to more than 10 m from 48.8 to 62.3 m bsl with an interlayer of PW II at 60.5 m bsl. Below PW III, again a layer of PW II occurred and reached down to a depth of 64.5 m bsl. This was followed by sediments which were similar to the PW I, namely pore water unit IV (PW IV).

Journal of Geophysical Research: Biogeosciences 10.1002/2017JG003859

The PW I in BK2 reached down to a depth of 13.65 m bsl (Figure 2b). An interlayer at the depth of 12.35 m bsl, resulting from the sample clustering far apart of any cluster (PW II IL in Figure 1b), divided this unit into upper and lower parts. PW II reached down to a depth of 28.75 m bsl. Frozen sediment below the permafrost table, unaffected of marine waters, formed the PW III.

3.3. Microbial Abundance in Submarine Permafrost

DNA concentrations of C2 are illustrated in Figure 2a and showed a high value of 265.2 ng g^{-1} in the upper centimeters right below the seafloor. A small DNA peak of 84.3 ng g^{-1} was found in the PW II sediment at a depth of 40.4 m bsl. But the highest DNA concentrations with maxima between 89.9 and 341.5 ng g^{-1} were found at the depth interval of 54.6 to 56.1 m bsl in the frozen PW III. The depth profile of the microbial abundance showed the same trend. The uppermost sample just below the seafloor revealed high numbers of 9.2×10^6 cells and 3.5×10^8 gene copies, but total cell counts and bacterial 16S rRNA gene abundance peaked again between 54.6 to 56.1 m bsl, with ~5×10^7 cells g^{-1} and 2.7×10^8 gene copies.

In comparison, BK2 (Figure 2b) exhibited three to four times lower DNA concentrations than C2 (Figure 2a). Cell counts were 20 to 70 times lower, and the abundance of the bacterial 16S rRNA gene was even 50 to 250 times lower than in C2. In contrast to C2, the highest biomass here was found in the upper meters of the sediment core. In PW I and the thin interlayer of PW II, DNA concentrations reached values of 68.3 to 87.9 ng g^{-1}. The lower part of PW II was characterized by very low values not exceeding 6 ng g^{-1}. Lowest DNA concentrations were obtained at the transition of frozen to unfrozen sediment with minimum values of 1.0 ng g^{-1} right above the ice-bonded permafrost table (IBPT). In the unaffected frozen unit (PW III), DNA concentrations peaked at a depth of 40.5 m bsl with 25.9 ng g^{-1}. Depth profiles of both bacterial gene copies and total cell counts were similar. Highest values in BK2 were obtained in the PW I and its interlayer with up to 2.4×10^6 cells and 6.2×10^6 gene copies. The second highest value of 1.1×10^6 gene copies was found in the ice-bonded part at a depth of around 40.5 m bsl, but generally cell counts in BK2 decreased with depth.

3.4. Diversity

The richness and diversity of C2 (Figure 2a) were quite constant from the seabed to PW III, with the highest values in the marine sample and a slightly decreasing trend. Here mean $OTU_{0.03}$ numbers of duplicates ranged between 127 and 194, in contrast to $OTU_{0.03}$ numbers of 78 to 84 in PW IV (supporting information Table S7). Diversity indices behaved very similar (Shannon index 3.7 to 4.5; Simpson index >0.9 in PW I–III and Shannon index 1.7 to 2.6; Simpson index 0.5 to 0.8 in PW IV).

In BK2, values of the Shannon index and the richness of $OTU_{0.03}$ showed a similar trend (Figure 2b). Both were highest in the unfrozen part (PW I and II) of BK2 and lowest in the permafrost unit PW III. Mean $OTU_{0.03}$ numbers of duplicates ranged between 31 and 189 per sample (supporting information Table S7). A decrease could be observed right above the phase boundary and in the ice-bonded PW III. Those depths were highly dominated by a few taxa.

3.5. Structure of the Bacterial Community

Using the relative abundances of $OTU_{0.03}$ and the Bray-Curtis distance measure, ordination plots were created (NMDS). The NMDS ordination of all samples from both cores showed some level of clustering of the bacterial communities in accordance with the separation by regional properties and environmental factors (supporting information Figure S3). Bacterial communities of both study sites formed two significant clusters (supporting information Table S8).

Individually, C2 exhibited distinct microbial communities according to the pore water units (Figure 3a). The NMDS plot showed an arrangement of the communities according to the depth location of pore water units. The community of the deep PW II was located between the PW II and PW III clusters showing the similarity to both of them. The microbial communities on the $OTU_{0.03}$ level differed significantly between the units (supporting information Table S9). A Mantel test with the total community and pore water data, including temperature, revealed a significant correlation ($p = 0.001$, correlation $R = 0.46$). Mantel tests with the total community and single pore water parameters at the corresponding depths showed that there was no correlation with calcium, silicon, and nitrate, and only a weak correlation with sulfate ($R < 0.25$; supporting information Table S10).

AGU Journal of Geophysical Research: Biogeosciences 10.1002/2017JG003859

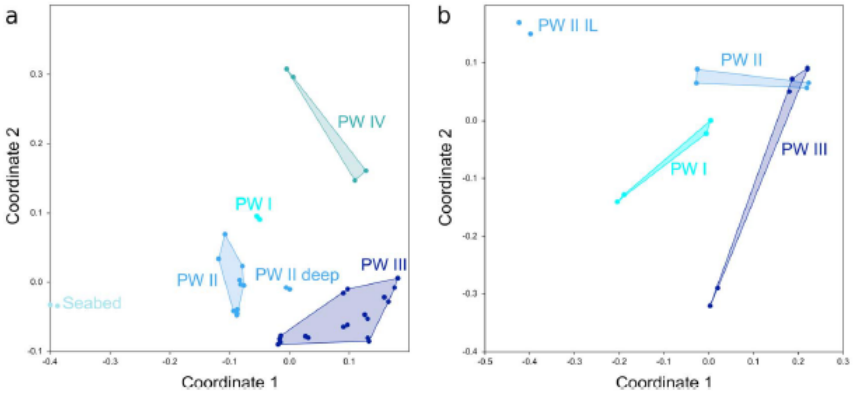

Figure 3. Nonmetrical multidimensional scaling of the microbial community structure based on relative abundances of $OTU_{0.03}$ (Bray-Curtis dissimilarity). Colors represent the pore water units from which the $OTU_{0.03}$ originate. (a) NMDS of bacterial communities found in C2 (inundated ~2500 years ago). The seabed is not defined by pore water but by the shallow depth location of the sample. Stress: 0.12. (b) NMDS of bacterial communities found in BK2 (inundated 540 years ago). PW II IL means the interlayer of pore water unit II within PW I. Stress: 0.07.

In BK2, we did not observe bacterial community structures that were specific for any pore water unit (Figure 3b). In addition to the corresponding pore water data, the bacterial community of the sample at 12.35 m depth (PW II IL) differed from the others. Grouping the samples according to the pore water units showed an overall significant difference between those groups, but not when considered pairwise (supporting information Table S11). Furthermore, there was no correlation of the overall community composition of BK2 to pore water parameters ($p = 0.357$, $R = 0.07$).

The most abundant phyla of C2 and BK2 on the order level are shown in Figures 4a and 4b and supporting information Tables S12 and S13. In BK2, 90 orders were identified (supporting information Table S14), but only 17 had >3% abundance. The bacterial community of C2 consisted of 138 identified orders with 34 exceeding a relative abundance of 3%, twice the number of BK2.

The composition and distribution of the most frequent orders (>3%) of both sediment cores showed few similarities. Only *Clostridiales* were found to be abundant in several units of both cores. *Atribacteria* SB-45 was abundant in units with elevated salt concentrations (PW IV in C2 and PW I and II in BK2), *Burkholderiales* in units with low salinity, and *Rhizobiales* throughout all PW units (Figure 4).

In C2, no clear marine or terrestrial community was observed, except for the uppermost sample of C2 representing the seabed, because many of the observed taxonomic groups can be found in both marine and terrestrial environments. The seabed was characterized by many marine-related orders which were unique for that horizon, such as *Pirellulales* and orders of the *Deltaproteobacteria* (*Desulfobacterales*, MBNT15, *Myxococcales*) and *Gammaproteobacteria* (*Chromatiales*, *Thiotrichales*, *Marinicellales*). In regard to the dominant orders, PW I to PW III showed a quite similar community composition. Community characteristics of PW units and differences between them are described in the following. PW I mainly contained groups that could be found elsewhere in PW II or PW III sediments (*Acidimicrobiales*, *Actinomycetales*, *Gaiellales*, *Solirubrobacterales*, *Chloroflexi* Gitt-GS-136, *Gemmatimonadetes* Gemm-1, *Rhizobiales*, *Sphingomonadales*) and that were mostly absent from the shallowest and deepest layers (seabed and PW IV). Abundant groups, such as *Actinomycetales* and Gitt-GS-136, were found in all PW I to PW III. Both underwent a shift on family level from PW II to PW III. *Actinomycetales* in PW II were dominated by *Nocardioidiaceae*, whereas *Intrasporangiaceae* and *Actinotalea* dominated in PW III. Further, *Chloroflexi* Gitt-GS-136 was abundant in PW II, while in PW III, *Chloroflexi* Ellin6529 was more abundant. Besides *Actinomycetales* and *Chloroflexi*, *Clostridiales* was among the most abundant orders in PW III. In addition, PW III contained numerous taxa that were unique for this pore water unit (for example, *Acidobacteria* iii1–15, *Gaiellales*, *Bacteriodales*, or *Gemmatimonadetes* N1423WL). The deepest unit PW IV was highly dominated by *Clostridiales* and SB-45 of the phylum *Atribacteria*. Due to the high dominance of *Clostridia*, there were only two other taxa

AGU Journal of Geophysical Research: Biogeosciences 10.1002/2017JG003859

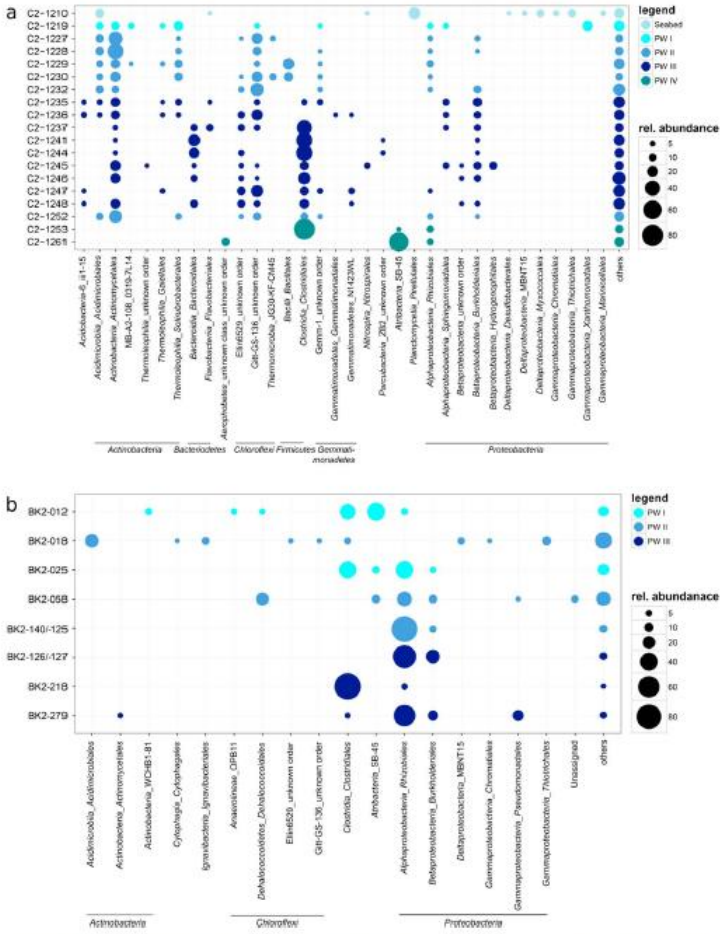

Figure 4. Relative abundance of bacterial orders of samples from (a) C2 (inundated ~2500 years ago) and (b) BK2 (inundated 540 years ago). Orders with an abundance of more than 3% are shown. The remaining orders are categorized as "others." Colors indicate the pore water unit.

(*Aerophobetes* and *Rhizobiales*) with a sequence abundance above 3%. In general, PW IV comprised less taxa, reflected in a lower diversity and richness compared to the other units (see supporting information Table S7).

In BK2, a few taxa such as *Clostridiales* and *Rhizobiales* were highly abundant especially within PW III and right above the permafrost table. The bacterial community of the sample BK2-018 was very different from that of all other samples (Figure 4b) coinciding with the pore water data (Figure 1b, PW II IL) and the $OTU_{0.03}$ data (Figure 3b, PW II IL). Except for *Clostridiales*, all other taxa (for example *Acidimicrobiales*, *Cytophagales*, *Ignavibacteriales*, *Chromatiales*, and *Thiotrichales*) were only observed in BK2-018. Core groups of BK2 were *Clostridiales*, *Rhizobiales*, and *Burkholderiales* and were found in all three pore water units of BK2.

In addition to the general community composition, we investigated the core communities of PW II and PW III in C2 (supporting information Table S15). We excluded PW I due to the low sample number. Given the overall low sample number in BK2, a determination of the core communities was not reasonable. The core community of PW II in C2 was much more diverse than that of PW III, counting 28 $OTU_{0.03}$. In contrast, the

AGU Journal of Geophysical Research: Biogeosciences 10.1002/2017JG003859

community of PW III in C2 contained only eight shared $OTU_{0.03}$. Taxa such as *Acidimicrobia*, *Actinobacteria*, and *Thermoleophilia* were represented by several $OTU_{0.03}$ in PW II but completely absent in the core community of PW III. In contrast to the seabed, a clear marine origin of PW II taxa was not evident. Some taxa such as *Acidimicrobiales* (*Acidimicrobia*), *Nocardioidaceae* and *Geodermatophilaceae* (*Actinomycetales*), and *Hyphomicrobiaceae* (*Rhizobiales*) were, however, reported to be successful in marine environments [*Yi and Chun*, 2004; *Lee and Kim*, 2007; *Normand et al.*, 2014; *Oren and Xu*, 2014; *D. F. Zhang et al.*, 2014; *Mizuno et al.*, 2015].

4. Discussion

Bacterial communities in two submarine permafrost settings from the East Siberian Arctic Shelf (BK2 and C2) were exposed to permafrost warming and thaw and the infiltration of seawater by inundation for about 540 and 2500 years, respectively. The inundation period was thereby based on recent rates of coastal retreat. Although the rate at which the sea transgresses over land is determined by many different factors, the degradation of permafrost in the nearshore zone is at least partially controlled by the coastal erosion rates [*Are*, 2003; *Overduin et al.*, 2016]. Due to a high mean annual coastal erosion rate of 4.5 m yr^{-1} over the past decades at the C2 site [*Grigoriev*, 2008], we assume an initially rapid submergence relative to BK2. The more rapid erosion at the C2 site leads to shorter times for seawater penetration for a particular distance from the coast, all other factors being equal. In contrast, the comparably low mean annual coastal erosion rate over the past decades of 1.4 m yr^{-1} means that inundation occurred more slowly at BK2. The proximity of BK2 to the coast and the shallower water suggests that seasonal changes in salinity and temperature are probably still large due to this proximity and that wave action will penetrate more deeply into the sediment [*Overduin et al.*, 2015]. The marine influence, characterized by a constant salinity in the unfrozen sediment of BK2, extended down to the ice-bonded permafrost table, suggesting convective downward transport of salt [*Overduin et al.*, 2015]. The coupling of heat with convective transport [*Osterkamp*, 2001] and higher terrestrial permafrost and geothermal heat fluxes in this region [*Nicolsky et al.*, 2012] likely also explain high sediment temperatures (−0.8 to 0.5°C) of BK2.

Although both coring sites belong to the ice-rich syngenetic permafrost deposits called Yedoma or Ice Complex [*Schirrmeister et al.*, 2008, 2016; *Grosse et al.*, 2013], C2 is located 250 km westward and 550 northward of BK2. Despite their spatial separation and differing glacial sediment source regions, the sub-Yedoma terrestrial sandy sediment at both sites was deposited in similar local fluvial-alluvial environments with intermittent organic layers of woody and fibrous detritus [*Winterfeld et al.*, 2011; *Overduin et al.*, 2015]. The portions of the two cores undergoing submarine degradation have similar ages [*Winterfeld et al.*, 2011; *Schirrmeister et al.*, 2016]. Permafrost at the C2 site has a temperature close to −12°C at the damping depth for annual temperature fluctuations; at BK2, the temperature is similar though closer to −10°C, probably due to differences in regional climate. There were similarities between how pore water chemistry varied over depth in both cores, which reflected similar stages of permafrost degradation. PW III represents ice-bonded and warmed permafrost that was unaffected by the infiltration of seawater. PW I and II were found in permafrost of terrestrial origin that had been influenced by seawater. PW IV was only observed in one of the cores, where drilling penetrated through the frozen permafrost into a partially frozen marine layer. *Winterfeld et al.* [2011] suggested that the corresponding sediment layer was Eemian and marine in origin. The similarity of pore water units at the two sites suggests that they are characteristic of submarine permafrost. They can be partly explained by postdepositional and posttransgression processes: wave and ice turbation of the seabed (PW I) and infiltration of saline seawater into the sediment (PW II). In addition to warming of the sediment by the overlying seawater, these processes contribute to thawing of permafrost below the seabed after inundation. In C2, for example, PCA strongly suggests that seawater infiltrates into ice-bonded permafrost before thawing is complete. Higher solute concentrations decrease the temperature of freezing of the pore water and increase the liquid water content of the sediment [*Overduin et al.*, 2008]. Since freezing affects the volume of the habitable space in the sediment and the concentration of solutes in that habitable space, depending on temperature and salinity, freezing is an important control on microbial activity. Determination of the in situ ice and liquid water content in the sediment at the time of sampling or during the period of warming following inundation is difficult for samples at or close to freezing temperature. Based on the measured pore water salinities, pore water solutions had freezing points of between −1.76 and −0.6°C for PW I and IV and −0.9 and 0°C for PW II and III. The almost isothermal temperature profile in

AGU Journal of Geophysical Research: Biogeosciences 10.1002/2017JG003859

supporting information Table S1, for example, showed sediment at or near the freezing point, especially in PW IV. Permafrost dynamics and pore water composition in particular thus expand the bacterial habitat and have the potential to influence bacterial community composition.

The stratification of bacterial subcommunities at C2 (Figure 3a) coincides with changes in the bacterial community composition (Figure 4a). For example, the shallowest sample of C2, a few centimeters below the seafloor, harbored the highest number of unique phyla and predominantly those typical for marine conditions such as *Pirellulales*, *Desulfobacterales*, *Thiotrichales*, and *Marinicellales* [*Wang et al.*, 2012; *Campbell and Kirchman*, 2012]. The bacterial community composition of this layer thus shows a marine origin, so that we refer to it as the seabed. The underlying subcommunities of PW I and II lack an imprint of clearly marine taxa despite seawater infiltration and even though parameters such as salinity and stable water isotopes largely serve to explain their community patterns (supporting information Table S10). At the same time, they have evolved into subcommunities significantly different from those of the unaffected permafrost unit PW III (supporting information Table S9). The separation into individual subcommunities of PW II and III is further manifested through different core groups of both layers (supporting information Table S15). So, although the bacterial community composition has changed in response to seawater infiltration, it reflects the bacterial assemblages of terrestrial permafrost even after centuries to millennia of exposure to submarine conditions. In C2, bacterial communities can consequently be classified as belonging to terrestrial permafrost, marine-affected permafrost, reworked permafrost sediments, or seabed. Continuing permafrost thaw will eventually lead to the complete loss of the original permafrost bacterial assemblages. They will probably shift to new assemblages like those of PW II but remain distinct in their composition from bacterial communities at the seabed. In contrast to C2, no significant correlation between community and environmental data along the BK2 core was observed, meaning that an assignment of bacterial communities consistent with pore water units was not possible. The statistical lack of significance may have been the result of low biomass in BK2.

With total cell counts of 10^3–10^7 cells g^{-1} sediment, the microbial abundances of both submarine permafrost cores were within the range of cell counts found in terrestrial long-term cryogenic formations such as frozen ground and buried soils [*Gilichinsky*, 2008]. Cell numbers of C2 were comparable with microbial abundances from subseafloor sediments (10^6–10^7 cells mL^{-1} sediment) [*Parkes et al.*, 2014]. The depth profiles of total DNA concentration, bacterial gene copy numbers, and total cell counts in both cores followed a similar trend. Still, in C2 the abundance of the bacterial 16S rRNA gene often exceeded that of the total cell counts by at least an order of magnitude (supporting information Tables S16 and S17). This cannot be solely due to multiple 16S rRNA gene copies per cell [*Schmidt*, 1998] but reflects the long-term preservation of extracellular DNA (up to 400,000 years) due to low temperature conditions in permafrost [*Stokstad*, 2003; *Willerslev et al.*, 2004]. A large proportion of external DNA has frequently been observed in marine sediments as well [*Corinaldesi et al.*, 2005; *Alawi et al.*, 2014; *Kirkpatrick et al.*, 2016]. Future cell separation approaches will shed light on the extent and distribution of external DNA versus DNA of intact cells. In subseafloor sediments, the microbial abundance usually shows an exponential decrease with depth [*Kallmeyer et al.*, 2012]. In C2, however, maximum microbial abundances, bacterial gene copy numbers, and DNA concentrations occurred in the unaffected permafrost unit, which confirms that even in frozen sediments microbial cells can be conserved and survive within thin brine veins [*Steven et al.*, 2007; *Wagner et al.*, 2007; *Bischoff et al.*, 2013]. C2 also exhibited a quite constant diversity and richness in all pore water units except for PW IV. The diversity of this submarine permafrost site is thereby comparable with the permafrost active layer and permafrost thaw ponds [*Liebner et al.*, 2008; *Crevecoeur et al.*, 2015], though lower than in marine and deep-sea hydrothermal sediments [*Wang et al.*, 2012; *Cerqueira et al.*, 2015]. Recalling the clear stratification of bacterial assemblages according to the degree of marine influence, C2 displays thus a very unusual subseafloor habitat where permafrost table depth, stage of permafrost degradation, and time of inundation are constraints for the abundance and structure of bacteria and where permafrost is a bottom-up source for subseafloor life. "Bottom-up" refers in this case to its vertical position and the fact that, due to permafrost thaw, it is being continuously released at the lower boundary of the thawed sediment layer. Since C2 can be considered representative for submarine permafrost after millennia of exposure to submarine conditions, its unique features as a subsurface habitat are likely applicable to large areas of the Siberian Arctic Shelf.

The origin and development of bacterial community structure and diversity differ between the two submarine permafrost cores. β-diversity, the variation in community composition, increases with distance and

AGU Journal of Geophysical Research: Biogeosciences 10.1002/2017JG003859

when local environmental conditions differ [*Lindström and Langenheder*, 2012]. Given that the terrestrial sediment at both sites was deposited in similar local fluvial-alluvial environments, we assign the high β-diversity of the bacterial communities to the large spatial distance and different glacial sediment source regions. Not even the infiltration of seawater into the units PW I and II resulted in similar bacterial community structure of C2 and BK2 (supporting information Figure S3 and Table S8) even though dispersal, i.e., the movement of an individual taxon from one location to another by passive or active mechanisms [*Hanson et al.*, 2012], through seawater should be high [*Lindström and Langenheder*, 2012]. For example, abundant taxa of PW II in BK2 were *Rhizobiales* and *Burkholederiales*, whereas PW II in C2 harbored predominantly *Acidimicrobiales*, *Actinomycetales*, and *Chloroflexi* Gitt-GS-136. The heterogeneity of bacterial communities in shelf sediments of the Laptev Sea is in line with a substantial β-diversity of bacterial communities in deep marine subsurface sediments from different continental margin sites in the Pacific Ocean [*Fry et al.*, 2008]. A large β-diversity even in sediment layers influenced by seawater for decades and hundreds of years could reflect (i) that marine bacterial taxa did not establish in the new location of formerly terrestrial sediment, (ii) the movement of seawater through the sediment matrix is too slow, or (iii) the movement of seawater through the sediment matrix occurs at very different rates in C2 compared to BK2. Our results indeed show that sediments of terrestrial origin in C2 are less influenced by marine inundation than sediments in BK2. The more gradual transition between PW II and PW III (Figure 1a) in C2, compared to BK2, indicates that the penetration of seawater into the sediment takes place more slowly in C2. This can be due to different seabed conditions caused by wave and sea ice action, which drive the diffusive penetration into the seabed, and/or distinct sediment column properties that affect the penetration rate [*Ulyantsev et al.*, 2016]. As a consequence of the relatively deep water column and the low sea ice thickness, seasonal changes in seabed temperature and salinity were likely lower in amplitude at the C2 site. Still, bottom water salinity in the western part of the Laptev Sea is higher than in the central Laptev Sea, which is influenced by fluvial discharge [*Schirrmeister*, 2007; *Charkin et al.*, 2011; *Günther et al.*, 2013]. The concentration profile in C2 [*Winterfeld et al.*, 2011] suggests a predominantly diffusive transport of dissolved constituents of the pore water through the sediment column, whereas the BK2 profile suggests either more rapid diffusion and/or advective transport [*Osterkamp*, 2001].

C2 furthermore appears to host bacterial communities that have been stimulated by warming and started to proliferate, an assumption that was made before in the context with submarine permafrost [*Koch et al.*, 2009] and that is generally associated with the development of microbes in thawing permafrost [*Graham et al.*, 2012; *Schuur et al.*, 2015]. Thereby, stimulation of the microbes may be facilitated by a rising water content in warming permafrost [*Overduin et al.*, 2008]. This is supported by highest total cell counts, DNA concentrations, and bacterial gene copy numbers of all units in the ice-bonded unaffected permafrost unit of C2, when neglecting the seabed sample. We cannot, however, rule out that cell numbers were high before transgression. The drop in microbial abundance between the unaffected permafrost unit (PW III) and the terrestrial units that are marine-influenced (PW I and II) further indicate that in C2 the microbial community was disturbed by seawater infiltration. This would be in line with observed decreases in soil microbial abundance after exposure to elevated salt concentrations [*Rietz and Haynes*, 2003]. In BK2, microbial cell numbers decrease with depth which is typical for subseafloor habitats. In addition, the microbial data along BK2, for example, the lowest microbial abundance in the seawater-unaffected permafrost sediments, do not show any indication for proliferation due to warming. The ice-bonded permafrost is still characterized by subzero temperatures, an environment where water activity, rates of nutrient exchange, and growth rates are low [*Rivkina et al.*, 2000]. Microorganisms must resist exposure to subzero temperatures for prolonged periods of time [*Wagner et al.*, 2007]. This is highly selective for cells and may be the reason for the small bacterial diversity and population size (10^4 cells g^{-1} sediment) in BK2. In addition, a high mean acetate concentration of 132.6 μM in the unaffected sediments (supporting information Figure S4) indicate that despite the temperature increase, bacterial activity and growth in the permafrost unit were not yet stimulated. In fact, three orders of magnitude less microbial cells in PW III of BK2 compared to C2 suggest that the reaction of the permafrost bacterial community in BK2 to inundation is more strongly determined by disturbance than by the beneficial increase in temperature. As a corollary, this would suggest that bacterial communities in C2 reflect a later stage in the reaction of permafrost bacterial communities to marine transgression of permafrost.

AGU Journal of Geophysical Research: Biogeosciences 10.1002/2017JG003859

5. Conclusions

This study highlights that submarine permafrost is a suitable natural laboratory for studying the response of permafrost bacterial communities both to temperature and salinity increase on geological timescales. It shows that concentrations and stable isotopes of pore water solutes can be used to distinguish sediments affected by reworking in the marine environment from the terrestrial permafrost thawed in situ beneath the seabed. Further, we show that seawater infiltrates into frozen ice-bonded permafrost before thawing is complete. The effect of these processes is also reflected in the bacterial communities found in thawed and frozen submarine permafrost. Submarine permafrost originates as terrestrial permafrost but is warmer and has more saline pore water as a result of inundation by seawater. These differences change bacterial community structure, abundance, and diversity, but the communities themselves remain terrestrial. The exposure to warming and increasing pore water salinity is a disturbance that probably results in a decrease of the community size followed by increasing proliferation on a timescale of millennia. Further work is needed to clarify whether differences in the community size and structure are a result of different inundation processes or spatial differences and whether microbes in unaffected sediments exposed to warming are actively proliferating.

Acknowledgments
Sequences of the submarine permafrost communities presented in this work were deposited at the NCBI Sequence Read Archive (SRA) with the Project number BioProject ID# PRJNA352907. Bacterial 16S rRNA gene sequences have the accession numbers SRR5184420-SRR5184446 and are available from Genbank, EMBL, and DDBJ. Pore water data for the C2 and BK2 cores are available at https://doi.pangaea.de/10.1594/PANGAEA.873837. Coring was supported by the German Ministry for Education and Research, a Joint Russian German Research Group (HGF-JRG100) of the Helmholtz Association of German Research Centres, and by the EU's INTAS program. Susanne Liebner is grateful for the funding of the Helmholtz Young Investigators Group (grant VH-NG-919). Our thanks go to Anke Saborowski, Monique Thiele, Linda Mahler, Antje Eulenburg, Ute Bastian, and Katja Hockun for excellent laboratory support, André Friese for acetate and formate measurements, and Jens Kallmeyer for sharing his knowledge in the field of cell counts. We further thank Aleksandr Maslov (SB RAS, Melnikov Permafrost Institute, Yakutsk, Russia), who provided indispensable drilling expertise, and we thank Tiksi Hydrobase staff members Viktor Bayderin, Viktor Dobrobaba, Sergey Kamarin, Valery Kulikov, Dmitry Mashkov, Dmitry Melnichenko, Aleksandr Safin, and Aleksandr Shiyan for their field support.

Supporting information Manuscript I

Figures

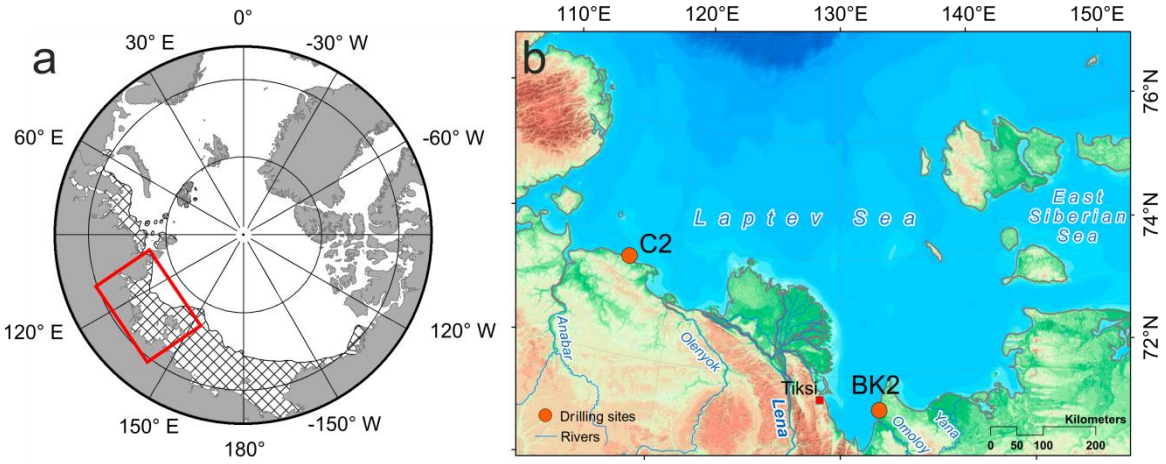

Figure A-1: see Figure 2-2

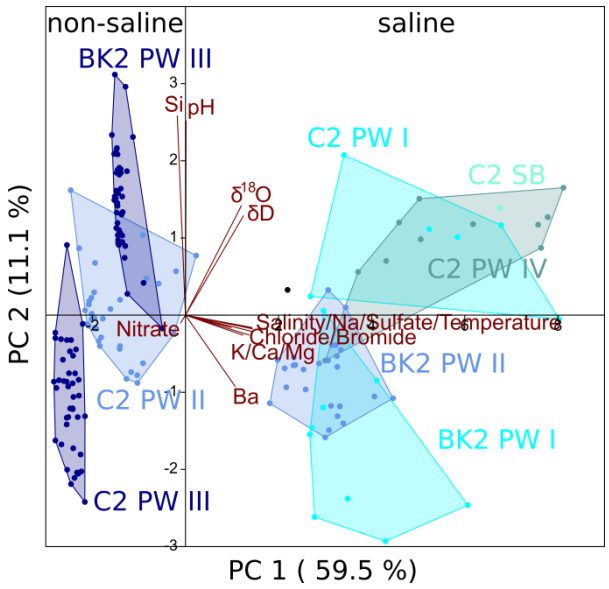

Figure A-2: Principal component analysis (PCA) showing the variation of sediment depths from both cores based on standardized environmental variables (Euclidean distance). Pore water units (PW) were defined based on cluster analysis and are shown by different colors. C2 SB means C2 seabed. The percentage of variation between samples described by principal components 1 and 2 (PC 1 and 2) is indicated on the axes. 72.8% variance between samples of both cores were explained by PC1 and PC2. Environmental variables are projected as dark red vectors.

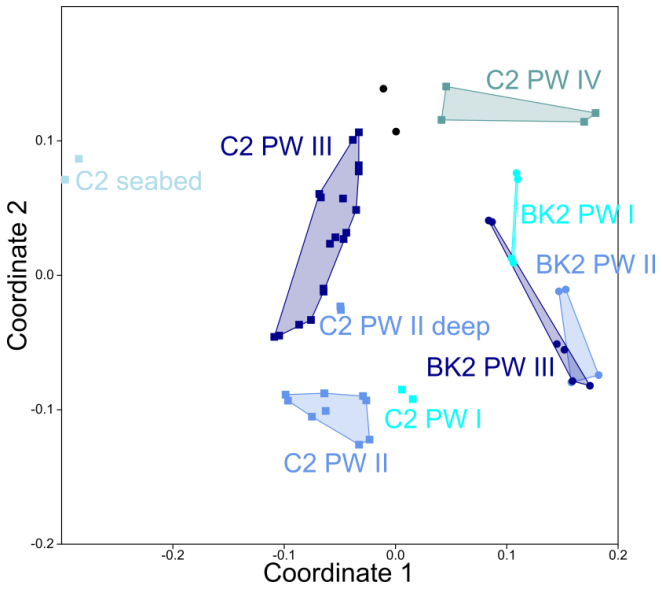

Figure A-3: Non-metrical multidimensional scaling (NMDS) of the microbial community structure based on the relative abundance of OTUs0.03 (Bray-Curtis dissimilarity). Colors represent the pore water units from which the OTUs0.03 originate. The seabed was not defined by pore water but by the shallow depth location. Shown are samples from both study sites. Filled squares represent samples of C2 and dots represent samples of BK2.

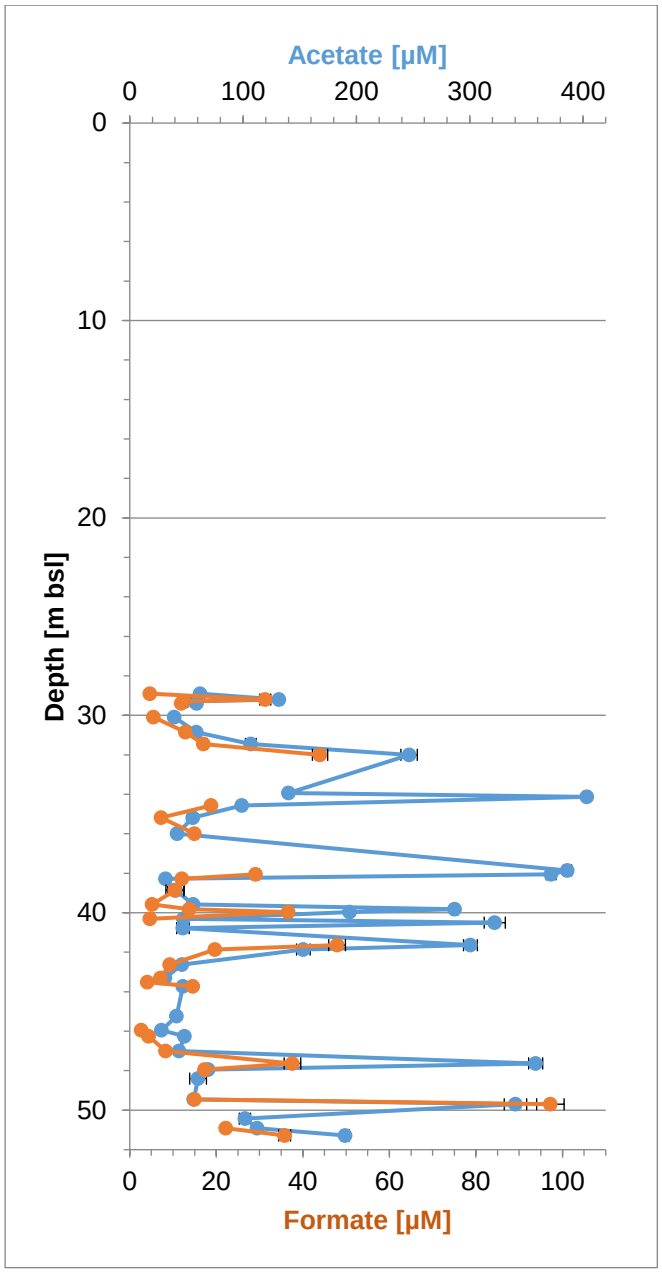

Figure A-4: Volatile fatty acids were measured in the frozen part of BK2. Detection limit of acetate was 25 µM and of formate 3 µM.

Tables

Table A-1: Pore water data of core C2.

This table was provided as a separate excel file.

Table A-2: Pore water data of core BK2.

This table was provided as a separate excel file.

Table A-3: Oligonucleotide primers used in this study.

Target		Primers	Primer sequence (5'-3')	Size [bp]	T [°C]	No. of PCR cycles	Reference
sequencing Illumina MiSeq							
Bacteria	16S rRNA	S-D-Bact-0341-b-S-17	CCT ACG GGA GGC AGC AG	464	55	30	[*Muyzer et al.*. 1993]
		S-D-Bact-0785-a-A-21	GAC TAC HVG GGT ATC TAA TCC				[*Herlemann et al.*. 2011]
quantitative PCR							
Bacteria	16S rRNA	S-D-Bact-0341-b-S-17	CCT ACG GGA GGC AGC AG	193	55.7	40	[*Muyzer et al.*. 1993]
		S-D-Bact-0517-a-A-18	ATT ACC GCG GCT GCT GG				[*Muyzer et al.*. 1993]

Table A-4: Barcode sequences for Illumina MiSeq sequencing used in this study.

Barcode ID forward primer	Barcode sequence	Barcode ID reverse primer	Barcode sequence
SfiA-MW00	ACACGT	SfiB-MW10	CAGTCA
SfiA-MW07	ATCGAT	SfiB-MW11	CATGAC
SfiA-MW08	ATGCTA	SfiB-MW12	GACTAG
SfiA-MW09	CACAGT	SfiB-MW13	GAGATC
Bac-26-For	ACATACGCGT	SfiB-MW14	GATCGA
Bac-27-For	ACGCGAGTAT	SfiB-MW17	GTGTGT
Bac-28-For	ACTACTATGT	SfiB-MW18	TCAGAG
Bac-31-For	AGCGTCGTCT	SfiB-MW19	TCGAGA
Bac-33-For	ATAGAGTACT	Bac-02-Rev	ACGCGATCGA
Bac-34-For	CACGCTACGT	Bac-04-Rev	TGACGTATGT
Bac-35-For	CAGTAGACGT	Bac-05-Rev	TCTATACTAT
Bac-36-For	CGACGTGACT	Bac-06-Rev	TCTAGCGACT
Bac-38-For	TACACGTGAT	Bac-07-Rev	TAGTGTAGAT
Bac-39-For	TACAGATCGT	Bac-08-Rev	TACGCTGTCT
Bac-40-For	TACGCTGTCT	Bac-11-Rev	TACAGATCGT
Bac-41-For	TAGTGTAGAT	Bac-13-Rev	TACACGTGAT
Bac-42-For	TCGATCACGT	Bac-14-Rev	TACACACACT
Bac-44-For	TCTAGCGACT	Bac-17-Rev	CGACGTGACT

Bac-45-For	TCTATACTAT	Bac-18-Rev	CAGTAGACGT
Bac-47-For	TGTGAGTAGT	Bac-19-Rev	CACGCTACGT
Bac-49-For	ACGCGATCGA	Bac-22-Rev	ATAGAGTACT
Bac-50-For	ACTAGCAGTA	Bac-23-Rev	AGCGTCGTCT
Bac-03-For	AGACGCACTC	Bac-25-Rev	ACATACGCGT
Bac-16-For	TCACGTACTA	Bac-26-Rev	ACTACTATGT
Bac-25-For	TCGTCGCTCG	Bac-28-Rev	TCGTCGCTCG
Bac-37-For	TACACACACT	Bac-30-Rev	TAGAGACGAG
		Bac-31-Rev	TACGAGTATG
		Bac-33-Rev	TACTCTCGTG

Table A-5: One-way PerMANOVA of pore water units in C2. Summary presents the overall test statistics. Pairwise analysis shows Bonferroni corrected p-values above the diagonal and F-values below.

Summary	
Permutation N:	9999
Total sum of squares:	1287
Within-group sum of squares:	295
F:	74.8
p (same):	0.0001

Pairwise

	PW I	**PW II**	**PW III**	**PW IV**
PW I		**0.001**	**0.001**	**0.002**
PW II	65.45		**0.001**	**0.001**
PW III	129.9	42.86		**0.001**
PW IV	9.858	108.5	192.9	

Table A-6: One-way PerMANOVA of pore water units in BK2. Summary presents the overall test statistics. Pairwise analysis shows Bonferroni corrected p-values above the diagonal and F-values below.

Summary	
Permutation N:	9999
Total sum of squares:	1118
Within-group sum of squares:	191.8
F:	122.3
p (same):	0.0001

Pairwise

	PW I	**PW II**	**PW III**
PW I		**0.0006**	**0.0006**
PW II	15		**0.0006**
PW III	158	365	

Table A-7: Statistics of sequencing analysis and representative taxa.

Sample Site	Sample ID	PW unit	Depth [mbsl]	Raw reads	Quality reads	Observed $OTU_{0.03}$	Simpson (1-D)	Shannon (H)	Most frequent class	Most frequent order
Buor Khaya	BK2-012	I	9.02	158,997	94,222	71	0.9024	3.031	*Atribacteria*	SB-45
	BK2-018	II	12.40	63,474	33,913	156	0.9763	4.393	*Acidimicrobiia*	*Acidimicrobiales*
	BK2-025	I	13.16	226,250	158,585	110	0.873	2.968	*Alphaproteo-bacteria*	*Rhizobiales*
	BK2-058	II	16.30	175,215	98,057	189	0.9295	4.062	*Alphaproteo-bacteria*	*Rhizobiales*
	BK2-140/ BK2-125	II	28.46	37,598	29,656	64	0.4959	1.517	*Alphaproteo-bacteria*	*Rhizobiales*
	BK2-126/ BK2-127	III	28.9	81,673	65,527	58	0.6568	1.841	*Alphaproteo-bacteria*	*Rhizobiales*
	BK2-218	III	40.53	73,705	70,634	31	0.4663	1.25	*Clostridia*	*Clostridiales*
	BK2-279	III	49.76	79,883	70,653	93	0.7698	2.657	*Alphaproteo-bacteria*	*Rhizobiales*
Mamon-tov Klyk	C2-1210	Sea-bed	6.05	31,699	18,820	194	0.9769	4.485	*Planctomycetia*	*Pirellulales*
	C2-1219	I	22.20	62,458	38,318	185	0.9674	4.326	*Thermoleophilia*	*Xanthomonadales*
	C2-1227	II	34.95	22,207	14,552	159	0.9653	4.137	*Actinobacteria*	*Actinomycetales*
	C2-1228	II	36.00	47,770	34,974	140	0.9658	4.059	*Actinobacteria*	*Actinomycetales*
	C2-1229	II	38.75	74,729	70,653	176	0.9579	4.29	*Bacilli*	*Bacillales*
	C2-1230	II	40.43	50,698	32,102	151	0.9658	4.144	Gitt-GS-136	Gitt-GS-136-_unknown order
	C2-1232	II	44.48	144,563	110,923	183	0.9478	4.024	Gitt-GS-136	Gitt-GS-136_unknown order
	C2-1235	III	49.31	140,433	75,465	153	0.98	4.434	*Betaproteo-bacteria*	*Actinomycetales*
	C2-1236	III	50.65	38,105	23,949	142	0.9615	4.107	Gitt-GS-136	Gitt-GS-136-_unknown order
	C2-1237	III	51.95	120,970	68,153	136	0.9105	3.689	*Clostridia*	*Clostridiales*
	C2-1241	III	54.71	160,212	92,619	148	0.9115	3.782	*Clostridia*	*Clostridiales*
	C2-1244	III	55.80	57,911	36,158	141	0.932	3.826	*Clostridia*	*Clostridiales*
	C2-1245	III	57.25	65,588	42,383	141	0.9591	3.976	*Betaproteo-bacteria*	*Actinomycetales*
	C2-1246	III	58.10	61,136	37,742	158	0.9504	4.075	*Clostridia*	*Clostridiales*
	C2-1247	III	58.65	27,173	19,359	127	0.9517	3.775	Gitt-GS-136	Gitt-GS-136-_unknown order
	C2-1248	III	61.30	37,247	22,047	163	0.9681	4.272	*Actinobacteria*	*Actinomycetales*
	C2-1252	II	64.70	58,088	31,080	158	0.9776	4.418	*Actinobacteria*	*Actinomycetales*
	C2-1253	IV	65.00	119,492	88,514	84	0.4808	1.706	*Clostridia*	*Clostridiales*
	C2-1261	IV	73.25	207,746	152,301	78	0.8306	2.583	*Atribacteria*	SB-45

Table A-8: One-way PerMANOVA of total bacterial communities in C2 and BK2.

Permutation N:	9999
Total sum of squares:	20,42
Within-group sum of squares:	16,93
F:	10,72
p (same):	0,0001

Table A-9: One-way PerMANOVA of bacterial communities in different pore water units and an extra defined sample (seabed) for the upper layer of the core C2. Summary presents the overall test statistics. Pairwise analysis shows Bonferroni corrected p-values above the diagonal and F-values below.

Summary

Permutation N:	9999
Total sum of squares:	12.62
Within-group sum of squares:	6.085
F:	6.874
p (same):	0.0001

Pairwise

	Seabed	**PW I**	**PW II**	**PW III**	**PW II deep**	**PW IV**
Seabed		1.000	0.2415	0.0930	1.000	0.9930
PW I	38.01		0.228	0.0945	1.000	1.000
PW II	8.064	3.831		**0.0015**	0.6420	**0.0120**
PW III	6.967	5.512	12.7		0.5085	**0.0015**
PW II deep	60.43	30.26	2.479	2.536		1.000
PW IV	5.241	4.731	8.414	7.642	4.274	

Table A-10: Testing the correlation of the bacterial community with single pore water parameters in C2 and BK2 with the Mantel Test.

	C2		**BK2**	
	p-value	**Correlation R**	**p-value**	**Correlation R**
Barium	**0.0053**	0.4255	0.7911	-0.2143
Calcium	0.1945	0.0953	0.8419	-0.1940
Potassium	**0.0121**	0.3771	0.9858	-0.3580
Magnesium	**0.0058**	0.3676	0.3394	0.0559
Sodium	**0.0056**	0.4523	0.6703	-0.0933
Silicon	0.8249	-0.1008	0.5685	-0.0761
Chloride	**0.0020**	0.4767	0.7058	-0.1076
Sulfate	**0.0458**	0.2355	0.1386	0.3659
Bromide	**0.0013**	0.4587	0.7493	-0.1294
Nitrate	0.9487	-0.1630	0.4473	-0.0085
Salinity	**0.0007**	0.4903	0.6853	-0.1035
$\delta^{18}O$	**0.0008**	0.4979	0.1649	0.3530
δD	**0.0007**	0.4830	0.1172	0.4019
pH	**0.0007**	0.3859	0.2368	0.1844
Temperature	**0.0001**	0.5909	0.0806	0.2630

Table A-11: One-way PerMANOVA of bacterial communties in different pore water units in BK2. Summary presents the overall test statistics. Pairwise analysis shows Bonferroni corrected p-values above the diagonal and F-values below.

Summary

Permutation N:	9999
Total sum of squares:	4.307
Within-group sum of squares:	2.1
F:	4.203
p (same):	0.0009

Pairwise

	PW I	PW II	PW III
PW I		0.1716	0.3826
PW II	4.524		1.000
PW III	3.180	1.413	

Table A-12: Most frequent order with > 3% relative abundance of samples in C2.

Class	Order	C2-1210	C2-1219	C2-1227	C2-1228	C2-1229	C2-1230	C2-1232	C2-1235	C2-1236	C2-1237	C2-1241	C2-1244	C2-1245	C2-1246	C2-1247	C2-1248	C2-1252	C2-1253	C2-1261
Acidobacteria-6	iii1-15	-	-	-	-	-	-	-	4.5	6.2	-	-	-	-	-	4.3	4.6	-	-	-
Acidimicrobia	*Acidimicrobiales*	13.2	8.2	11.6	12.1	7.6	7.2	10.6	5.1	4.2	-	-	-	-	-	-	-	8.8	-	-
Actinobacteria	*Actinomycetales*	-	10.6	33.6	44.0	14.3	17.8	9.2	14.7	12.8	4.6	3.5	3.9	18.8	16.5	-	15.7	28.2	-	-
MB-A2-1-8	319-7L14	-	6.3	-	-	3.2	-	-	-	-	-	-	-	-	-	-	-	-	-	-
Thermoleophi-lia	*unkown order*	-	-	--	-	-	-	-	-	-	-	-	-	3.3	-	-	-	-	-	-
Thermoleophi-lia	*Gaiellales*	-	4.5	-	-	4.1	-	-	3.2	3.9	-	-	-	-	-	5.2	-	-	-	-
Thermoleophi-lia	*Solirubrobacterales*	-	14.6	4.0	6.9	11.1	12.1	-	7.2	4.4	-	-	-	-	-	-	-	7.1	-	-
Bacteroidia	*Bacteroidales*	-	-	-	-	-	-	-	-	-	8.2	24.2	19.2	4.0	7.8	-	10.8	-	-	-
Flavobacteriia	*Flavobacteriales*	3.4	-	-	-	-	-	-	3.7	-	8.7	-	-	-	-	-	-	-	-	-
*Aerophobetes*_unknown class	unknown order	-	-	-	-	-	-	-	-	-	-	-	-	-	-	-	-	-	-	11.2
Ellin6529	unknown order	-	-	3.0	-	-	3.2	6.2	-	8.5	8.0	-	6.5	4.6	5.4	11.9	10.5	4.2	-	-
Gitt-GS-136	unknown order	-	5.1	19.6	12.4	5.9	19.1	29.8	5.7	20.2	6.2	-	-	3.4	3.3	24.1	7.3	10.1	-	-
Thermomicro-bia	JG3--KF-CM45	-	-	5.5	-	-	8.1	-	-	-	-	-	-	-	-	-	-	-	-	-
Bacilli	*Bacillales*	-	-	-	-	22.0	14.4	-	-	-	-	-	-	-	-	-	-	-	-	-
Clostridia	*Clostridiales*	-	-	-	-	-	-	-	6.1	-	38.9	44.6	46.4	13.2	25.3	12.7	15.2	9.8	76.4	-
Gemm-1	unknown order	-	3.9	-	3.2	3.5	4.5	4.7	5.8	-	-	-	-	-	-	5.9	-	4.2	-	-
Gemmatimonadetes	*Gemmatimonadales*	-	-	-	-	-	-	-	-	3.3	-	-	-	-	-	-	-	-	-	-
Gemmatimonadetes	N1423WL	-	-	-	-	-	-	-	-	3.2	-	-	-	-	-	7.5	4.1	-	-	-
Nitrospira	*Nitrospirales*	3.3	-	-	-	-	-	-	-	-	-	-	-	6.7	-	-	-	-	-	-
Parcubacteria	ZB2_o	-	-	-	-	-	-	-	-	-	-	3.1	4.4	-	-	-	-	-	-	-
Atribacteria	SB-45	-	-	-	-	-	-	-	-	-	-	-	-	-	-	-	-	-	3.6	65.6
Planctomycetia	*Pirellulales*	24.0	-	-	-	-	-	-	-	-	-	-	-	-	-	-	-	-	-	-
Alphaproteobacteria	*Rhizobiales*	-	6.4	5.9	5.3	8.5	4.7	4.9	-	-	-	-	-	-	-	4.2	-	6.6	8.6	7.5
Alphaproteobacteria	*Sphingomonadales*	-	5.4	-	-	-	-	-	7.8	6.0	5.1	-	-	7.4	-	-	-	-	-	-
Betaproteobacteria	*unknown order*	-	-	-	-	-	-	-	-	-	-	-	-	3.1	4.1	-	3.7	-	-	-
Betaproteobacteria	*Burkholderiales*	-	-	6.1	3.9	-	-	9.9	13.3	8.8	7.4	4.1	3.9	10.3	8.0	-	5.2	4.2	-	-
Betaproteobacteria	*Hydrogenophilales*	-	-	-	-	-	-	-	-	-	-	-	-	10.8	-	-	-	-	-	-
Deltaproteobacteria	*Desulfobacterales*	3.3	-	-	-	-	-	-	-	-	-	-	-	-	-	-	-	-	-	-
Deltaproteobacteria	*MBNT15*	4.7	-	-	-	-	-	-	-	-	-	-	-	-	-	-	-	-	-	-
Deltaproteobacteria	*Myxococcales*	9.3	-	-	-	-	-	-	-	-	-	-	-	-	-	-	-	-	-	-
Gammaproteo-bacteria	*Chromatiales*	5.9	-	-	-	-	-	-	-	-	-	-	-	-	-	-	-	-	-	-
Gammaproteo-bacteria	*Thiotrichales*	10.5	-	-	-	-	-	-	-	-	-	-	-	-	-	-	-	-	-	-
Gammaproteo-bacteria	*Xanthomonadales*	-	16.8	-	-	-	-	-	-	-	-	-	-	-	-	-	-	-	-	-
Gammaproteo-bacteria	*Marinicellales*	5.3	-	-	-	-	-	-	-	-	-	-	-	-	-	-	-	-	-	-
others < 3%		17.1	18.2	10.6	12.2	20.0	9.1	24.7	22.9	18.5	12.8	20.6	15.8	14.2	29.5	24.1	22.9	16.8	11.4	15.7

Table A-13: Most frequent order with > 3% relative abundance of samples in BK2.

Class	Order	BK2012	BK2018	BK2025	BK2058	BK2126 - 2127	BK2140 - 2125	BK2218	BK2279
Unassigned		-	-	-	6.7	-	-	-	-
Acidimicrobiia	*Acidimicrobiales*	-	23.1	-	-	-	-	-	-
Actinobacteria	*Actinomycetales*	-	-	-	-	-	-	-	3.3
Actinobacteria	WCHB1-81	5.3	-	-	-	-	-	-	-
Cytophagia	*Cytophagales*	-	3.1	-	-	-	-	-	-
Ignavibacteria	*Ignavibacteriales*	-	7.4	-	-	-	-	-	-
Anaerolineae	OPB11	4.2	-	-	-	-	-	-	-
Dehalococcoidetes	*Dehalococcoidales*	3.9	-	-	20.5	-	-	-	-
Ellin6529	unknown order	-	3.6	-	-	-	-	-	-
Gitt-GS-136	unknown order	-	3.2	-	-	-	-	-	-
Clostridia	*Clostridiales*	29.4	5.6	36.1	-	-	-	92.1	3.6
Atribacteria	SB-45	40.3	-	6.2	8.9	-	-	-	-
Alphaproteobacteria	*Rhizobiales*	5.4	-	38.4	27.2	69.6	87.0	4.9	61.2
Betaproteobacteria	*Burkholderiales*	-	-	4.4	8.7	23.9	6.0	-	12.4
Deltaproteobacteria	MBNT15	-	6.4	-	-	-	-	-	-
Gammaproteobacteria	*Chromatiales*	-	3.1	-	-	-	-	-	-
Gammaproteobacteria	*Pseudomonadales*	-	-	-	3.4	-	-	-	14.3
Gammaproteobacteria	*Thiotrichales*	-	9.7	-	-	-	-	-	-
others < 3%		11.4	34.8	14.8	24.6	6.4	7.0	3.0	5.3

Table A-14: Total number of identified taxa on different levels in each core.

	C2	BK2
OTUs	1193	496
Phylum	26	27
Class	76	55
Order	138	90
Family	217	126
Genus	296	159

Table A-15: Core $OTU_{0.03}$ found in each sample of the pore water unit II or III of C2. OTU ID SP_B_OTU# stands for Submarine Permafrost Bacteria OTU#.

PW unit	OTU ID	Phylum	Class	Order	Family	Genus
PW II	SP_B_OTU83	*Actinobacteria*	*Acidimicrobiia*	*Acidimicrobiales*		
	SP_B_OTU84	*Actinobacteria*	*Acidimicrobiia*	*Acidimicrobiales*		
	SP_B_OTU100	*Actinobacteria*	*Acidimicrobiia*	*Acidimicrobiales*	C111	
	SP_B_OTU114	*Actinobacteria*	*Acidimicrobiia*	*Acidimicrobiales*	*Iamiaceae*	*Iamia*
	SP_B_OTU143	*Actinobacteria*	*Actinobacteria*	*Actinomycetales*		
	SP_B_OTU148	*Actinobacteria*	*Actinobacteria*	*Actinomycetales*		
	SP_B_OTU149	*Actinobacteria*	*Actinobacteria*	*Actinomycetales*		
	SP_B_OTU168	*Actinobacteria*	*Actinobacteria*	*Actinomycetales*	*Geodermatophilaceae*	
	SP_B_OTU214	*Actinobacteria*	*Actinobacteria*	*Actinomycetales*	*Nocardioidaceae*	
	SP_B_OTU217	*Actinobacteria*	*Actinobacteria*	*Actinomycetales*	*Nocardioidaceae*	
	SP_B_OTU220	*Actinobacteria*	*Actinobacteria*	*Actinomycetales*	*Nocardioidaceae*	
	SP_B_OTU251	*Actinobacteria*	MB-A2-108	0319-7L14		
	SP_B_OTU291	*Actinobacteria*	*Thermoleophilia*	*Gaiellales*	*Gaiellaceae*	
	SP_B_OTU339	*Actinobacteria*	*Thermoleophilia*	*Solirubrobacterales*		
	SP_B_OTU346	*Actinobacteria*	*Thermoleophilia*	*Solirubrobacterales*		
	SP_B_OTU347	*Actinobacteria*	*Thermoleophilia*	*Solirubrobacterales*		
	SP_B_OTU641	*Chloroflexi*	Ellin6529			
	SP_B_OTU652	*Chloroflexi*	Gitt-GS-136			
	SP_B_OTU785	*Gemmatimonadetes*	Gemm-1			
	SP_B_OTU786	*Gemmatimonadetes*	Gemm-1			
	SP_B_OTU787	*Gemmatimonadetes*	Gemm-1			
	SP_B_OTU788	*Gemmatimonadetes*	Gemm-1			
	SP_B_OTU834	*Nitrospirae*	*Nitrospira*	*Nitrospirales*	*Nitrospiraceae*	*Nitrospira*
	SP_B_OTU1052	*Proteobacteria*	*Alphaproteobacteria*	*Rhizobiales*	*Hyphomicrobiaceae*	
	SP_B_OTU1053	*Proteobacteria*	*Alphaproteobacteria*	*Rhizobiales*	*Hyphomicrobiaceae*	
	SP_B_OTU1065	*Proteobacteria*	*Alphaproteobacteria*	*Rhizobiales*	*Hyphomicrobiaceae*	*Hyphomicrobium*
	SP_B_OTU1145	*Proteobacteria*	*Alphaproteobacteria*	*Sphingomonadales*	*Sphingomonadaceae*	*Kaistobacter*
	SP_B_OTU1183	*Proteobacteria*	*Betaproteobacteria*	*Burkholderiales*	*Alcaligenaceae*	
PW III	SP_B_OTU640	*Chloroflexi*	Ellin6529			
	SP_B_OTU651	*Chloroflexi*	Gitt-GS-136			
	SP_B_OTU766	*Firmicutes*	*Clostridia*	*Clostridiales*	*Peptococcaceae*	*Desulfosporosinus*
	SP_B_OTU817	*Gemmatimonadetes*	*Gemmatimonadetes*	N1423WL		
	SP_B_OTU1146	*Proteobacteria*	*Alphaproteobacteria*	*Sphingomonadales*	*Sphingomonadaceae*	*Kaistobacter*
	SP_B_OTU1205	*Proteobacteria*	*Betaproteobacteria*	*Burkholderiales*	*Comamonadaceae*	
	SP_B_OTU1206	*Proteobacteria*	*Betaproteobacteria*	*Burkholderiales*	*Comamonadaceae*	
	SP_B_OTU1207	*Proteobacteria*	*Betaproteobacteria*	*Burkholderiales*	*Comamonadaceae*	

Table A-16: Mean values of cell counts, bacterial 16S rRNA gene copies [cells g^{-1}], DNA concentrations [ng g^{-1}] and Shannon indices for each pore water unit in both cores.

Sample Site	PW unit	Ø TCC	Stdev	n	Ø 16S gene copies	Stdev	n	Ø DNA	Stdev	n	Ø Shannon	Stdev	n
Mamontov Klyk	Seabed	9.20E+06		1	3.52E+08		1	265.22		1	4.485		1
	PW I	2.46E+06		1	7.32E+05		1	3.20		1	4.326		1
	PW II	3.63E+06	2.11E+06	6	2.31E+07	2.39E+07	5	39.40	26.66	5	4.179	0.15	5
	PW III	2.29E+07	1.42E+07	9	1.01E+08	1.14E+08	9	112.80	115.37	9	3.993	0.25	9
	PW IV	1.97E+06	1.08E+06	2	3.58E+07	1.36E+07	2	69.13	5.83	2	2.145	0.62	2
Buor Khaya	PW I	1.17E+06	1.11E+06	3	9.80E+05	1.27E+06	2	54.01	42.78	3	3.000	0.04	2
	PW II	5.74E+05	8.35E+05	5	1.61E+06	3.08E+06	4	19.97	37.18	5	3.324	1.57	3
	PW III	7.69E+04	3.12E+04	7	2.22E+05	4.07E+05	6	8.87	10.37	6	1.916	0.71	3

Table A-17: Mann-Whitney Test for equal medians of 16S rRNA gene copy numbers and Total Cell Counts in C2.

16S		**TCC**	
N:	19	N:	20
Mean rank:	11.923	Mean rank:	80.769
Mann-Whitney U :	105		
z :	-23.742	**p (same med.):**	**0.017585**
Monte Carlo permutation:		**p (same med.):**	**0.0159**

Table A-18: Mann-Whitney Test for equal medians of 16S rRNA gene copy numbers and Total Cell Counts in BK2.

TCC		**16S Bacteria**	
N:	15	N:	12
Mean rank:	87.037	Mean rank:	52.963
Mann-Whitney U :	65		
z :	-11.955	**p (same med.):**	**0.2319**
Monte Carlo permutation:		**p (same med.):**	**0.2367**

B. Appendix Manuscript II

www.nature.com/scientificreports

SCIENTIFIC REPORTS

OPEN

Anaerobic methanotrophic communities thrive in deep submarine permafrost

Received: 12 September 2017
Accepted: 22 December 2017
Published online: 22 January 2018

Matthias Winkel[1], Julia Mitzscherling[1], Pier P. Overduin[2], Fabian Horn[1], Maria Winterfeld[3], Ruud Rijkers[1], Mikhail N. Grigoriev[4], Christian Knoblauch[5], Kai Mangelsdorf[6], Dirk Wagner[1] & Susanne Liebner[1]

Thawing submarine permafrost is a source of methane to the subsurface biosphere. Methane oxidation in submarine permafrost sediments has been proposed, but the responsible microorganisms remain uncharacterized. We analyzed archaeal communities and identified distinct anaerobic methanotrophic assemblages of marine and terrestrial origin (ANME-2a/b, ANME-2d) both in frozen and completely thawed submarine permafrost sediments. Besides archaea potentially involved in anaerobic oxidation of methane (AOM) we found a large diversity of archaea mainly belonging to *Bathyarchaeota*, *Thaumarchaeota*, and *Euryarchaeota*. Methane concentrations and δ^{13}C-methane signatures distinguish horizons of potential AOM coupled either to sulfate reduction in a sulfate-methane transition zone (SMTZ) or to the reduction of other electron acceptors, such as iron, manganese or nitrate. Analysis of functional marker genes (*mcrA*) and fluorescence *in situ* hybridization (FISH) corroborate potential activity of AOM communities in submarine permafrost sediments at low temperatures. Modeled potential AOM consumes 72–100% of submarine permafrost methane and up to 1.2 Tg of carbon per year for the total expected area of submarine permafrost. This is comparable with AOM habitats such as cold seeps. We thus propose that AOM is active where submarine permafrost thaws, which should be included in global methane budgets.

Terrestrial permafrost landscapes, which developed during glacial cold periods, are known to be a large reservoir of organic carbon (~1300 Pg)[1]. Permafrost thaw and the following microbial production of carbon dioxide and methane from liberated organic matter may act as a positive feedback to climate warming[2]. Methane has 34 times higher global warming potential over a 100 year period[3] and is a more critical greenhouse gas than carbon dioxide. The amount and the release rates of methane are not well constrained although they are critical for evaluating future climate change.

Several Arctic sources of methane have been identified, including methane bursts during soil freezing[4], thermokarst lakes[5], lakes and ponds[6], wetlands[7], gas hydrates[8] and submarine permafrost[9]. Submarine permafrost on continental shelves of the Arctic Ocean is a consequence of the inundation of terrestrial permafrost by sea water during the Holocene marine transgression[10,11]. Coastal submarine permafrost froze under subaerial terrestrial conditions in alluvial/fluvial settings and has remained frozen since then[12,13]. Submarine permafrost is much more susceptible to thawing than permafrost on land, because of overlying warm marine water causing diffusion of salt water into the sediments from the top, and because of geothermal heat flux from below[9]. Based on thermal modeling of permafrost development over glacial/interglacial cycles, submarine permafrost is likely to have persisted in deep sediment layers for hundreds of millennia[14]. Over those millennial timescales submarine permafrost reaches its freezing point, between −2 and −1 °C, after which it slowly starts degrading due to the influence of high salt concentration[10,15]. Our knowledge of evolving carbon pools and carbon turnover in submarine permafrost is, however, scarce.

[1]GFZ German Research Centre for Geosciences, Helmholtz Centre Potsdam, Section 5.3 Geomicrobiology, 14473, Potsdam, Germany. [2]Alfred Wegener Institute, Helmholtz Centre for Polar and Marine Research, Periglacial Research, 14473, Potsdam, Germany. [3]Alfred Wegener Institute, Helmholtz Centre for Polar and Marine Research, Marine Geochemistry, 27570, Bremerhaven, Germany. [4]Mel'nikov Permafrost Institute, SB RAS, Yakutsk, 677010, Russia. [5]Institute of Soil Science, Universität Hamburg, 20146, Hamburg, Germany. [6]GFZ German Research Centre for Geosciences, Helmholtz Centre Potsdam, Section 3.2 Organic Geochemistry, 14473, Potsdam, Germany. Correspondence and requests for materials should be addressed to M.W. (email: mwinkel@gfz-potsdam.de)

Arctic submarine permafrost regions have the potential to emit large amounts of methane to the atmosphere[16], however flux measurements are controversial. First estimates suggest a release of 8.0 Tg of methane per year from the East Siberian Arctic Shelf (comprising Laptev Sea, East Siberian Sea and the Russian part of the Chukchi Sea), which would equal the release of methane from the entire world ocean[9]. In contrast, recent estimates for the Laptev and East Siberian Seas are almost three times lower (2.9 Tg y^{-1})[17]. Methane is mainly released from the sediment but the source is undear[18]. It is expected that permafrost degradation can create pathways for the release of gas captured within submarine permafrost sediment or within gas hydrates underneath[16]. Low δ^{13}C-CH_4 values indicate a biogenic or thermogenic origin of methane released from submarine permafrost[13,19]. A previous study demonstrated a drop of methane concentrations at the permafrost thaw front deep inside the sediments, which coincided with increasing δ^{13}C-CH_4 values from −70‰ to −35‰ that points to anaerobic oxidation of methane (AOM)[13]. Sulfate penetrating from the seabed into the sediment created a deep sulfate-methane transition zone (SMTZ) similar to other geological formations in the subsurface[20], with sulfate being a potential electron acceptor for AOM[21].

Most studies on AOM in the marine system have focused on ANME archaea that couple the oxidation of methane to the reduction of sulfate via a syntrophic lifestyle with sulfate-reducing bacteria (SRB)[22–24]. Three main marine clades, ANME-1a/b, ANME-2a/b/c, and ANME-3 have been identified so far[25]. These clades are associated with sulfate-reducing bacteria of the genera *Desulfosarcina*, *Desulfococcus*, *Desulfobulbus* and *Desulfofervidus*, which belong to the class *Deltaproteobacteria*[25] and of the phylum *Thermodesulfobacteria*[26]. Besides the marine ANMEs there is evidence of terrestrial AOM driven by the ANME-2d clade[27,28]. ANME-2d sequences were detected in wetland and permafrost habitats[29–31] so they might mitigate the release of methane in these environments. A recent study on wetlands showed that even low amounts of sulfate (µM) are sufficient to couple AOM with sulfate reduction in terrestrial environments[32]. In addition, alternative electron acceptors for AOM such as iron[33,34], manganese[33] as well as nitrate[27,35] and humic substances[36,37] have been suggested. To date, the microbial mitigation of methane emissions from permafrost environments is only evident in aerobic soils and sediments[38,39], while communities that oxidize methane anaerobically in thawing permafrost in the deep subsurface remain unexplored[8]. We hypothesize that active marine and terrestrial ANME clades exist in thawing submarine permafrost similar to microorganisms found in terrestrial enrichments[27,35] or marine SMTZ[40,41], and that these clades could function as an efficient methane filter for a diffusive methane release.

We investigated AOM in two deep submarine permafrost cores (48 m and 71 m) from the Siberian Shelf with different stages of submarine permafrost thaw[42] that were inundated for about 540 and 2,500 years, respectively[11,13]. To identify microbial assemblages involved in AOM, we performed high-throughput sequencing of archaeal and bacterial 16S rRNA genes and of the functional marker gene methyl co-enzyme reductase (*mcrA*) that is encoded by both methanogens and anaerobic methanotrophs. We quantified *mcrA* and dissimilatory sulfate reductase (*dsrB*) gene markers by quantitative PCR (qPCR) and correlated their abundance with the 16S rRNA gene abundance of AOM-related microorganisms. We visualized AOM-related microorganisms by catalyzed reporter deposition fluorescence *in situ* hybridization (CARD-FISH) and constructed ANME-specific 16S rRNA gene clone libraries to resolve their diversity in submarine permafrost sediments. Pore water geochemistry i. e., concentrations of methane, nitrate, sulfate, iron, and manganese, was analyzed to verify potential horizons of methane consumption. Analysis of stable carbon isotope geochemistry of methane and microbial membrane lipid biomarker were performed to evaluate the activity of AOM communities *in situ*.

Results

Isotopic evidence of AOM and potential electron acceptors. Methane concentrations were low (average 48 µM) in the ice-bonded permafrost section of the Cape Mamontov Klyk core (hereafter C2) inundated for ~2,500 years[13] and peaked at approximately 52 m below seafloor (bsf) with a concentration of 990 µM (Fig. 1A). In contrast, methane concentrations in the ice-bonded permafrost section of the Buor Khaya core (hereafter BK2) were on average 8 times higher than in C2 (Fig. 2A). δ^{13}C values of methane in the ice-bonded permafrost of BK2 showed values between −71 and −53‰ typical for a biological origin[43] (Fig. 2A). Above the ice-bonded permafrost, δ^{13}C values of methane ranged from −37 to −30‰ within a few meters on top of the thaw front and stayed constant to a depth of about 12 mbsf[13]. Above 12 mbsf δ^{13}C-values of methane showed high dynamics with values ranging between −67 to −32‰ (Fig. 2A). δ^{13}C values of methane in the C2 core were only measurable in parts of the ice-bonded permafrost and showed ^{13}C values between −72‰ to −37‰ (Fig. 1A). Independently of one another, both cores showed opposing dynamics of methane concentration and δ^{13}C values with a clear signal of AOM at the SMTZ of BK2. Estimated release rates of methane from the ice-bonded permafrost of BK2 together with the modeled fraction of methane that was oxidized yielded potential AOM rates of 1.7–2.1 nmol cm^{-3} d^{-1} ± 0.9–1.2 nmol cm^{-3} d^{-1}[13] in the SMTZ.

Sulfate from sea water penetrated into the ice-bonded permafrost section of core C2 and into the thaw front of core BK2 indicating the presence of a SMTZ (Figs 1B and 2B). Sulfate concentrations of 12 to 24 mM in the unfrozen part of the C2 core decreased with depth and penetrated almost 10 m into the ice-bonded permafrost. Here, sulfate concentrations were still high with up to 12.5 mM. Below 40 mbsf sulfate concentrations were low (<0.4 mM) with the exception of ~52 mbsf (~1.5–2 mM) and the lower permafrost thaw front at ~58 mbsf (2.3 to 5.5 mM). Sulfate in the marine-affected layers of BK2 showed low concentrations (<0.5 mM) in the first 5 mbsf and brackish concentration of 2 to 7 mM between 5 mbsf and the ice-bonded permafrost. Inside the ice-bonded permafrost sulfate concentrations were low (average 0.08 mM) (Fig. 2B). In core C2, other potential terminal electron acceptors (TEA) such as nitrate, manganese, and iron were detected in the permafrost sediment layers (Fig. 1B). The latter two were only detected as total ions with no information on the oxidative state. Nitrate and manganese concentrations displayed high fluctuations in ice-bonded layers showing marine influence[42] in the sediment i.e. between 29 and 43 mbsf. A high concentration of nitrate and manganese was also observed at the lower boundary of the ice-bonded permafrost (58.5 mbsf). In the ice-bonded permafrost part of BK2, manganese,

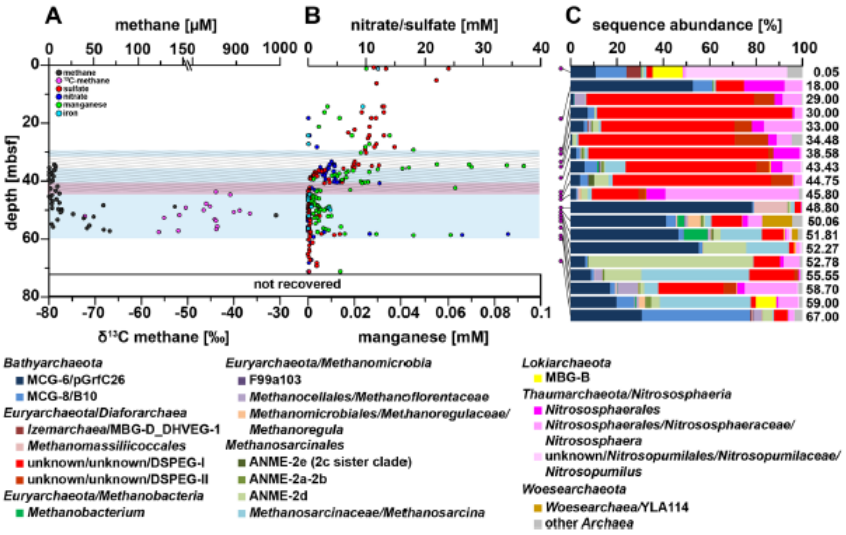

Figure 1. Pore water profiles of methane, nitrate, sulfate, manganese and relative archaeal abundance in the Mamontov Klyk core C2. (**A**) Methane concentrations are shown in black and corresponding $\delta^{13}C$-values in magenta[19]. (**B**) Nitrate concentrations are shown in blue, sulfate concentrations in red, manganese concentrations in green, and iron concentrations in light blue. (**C**) Purple dots on the left show depth location in the core. Relative abundance of archaeal 16S rRNA gene sequences are shown as bar plots. Colors of bars refer to the taxa in the legend below figure. Numbers on the right refer to the exact depth in the core. ANME = ANaerobic MEthanotrophic archaea, DHVEG-1 = Deep Hydrothermal Vent Euryarchaeotal Group 1, DSPEG = Deep Submarine Permafrost Euryarchaeotal Group, MBG-B = Marine Benthic Group B, MBG-D = Marine Benthic Group D, MCG = Miscellaneous Crenarchaeotal Group. The shaded area represents the permafrost degradation zone, the red area a sulfate-methane transition zone, and the light blue areas ice-bonded permafrost. All uncolored areas of the plots correspond to unfrozen submarine permafrost and marine sediments.

iron and nitrate were close to or even below the detection limit. In the unfrozen part, manganese and iron concentrations were an order of magnitude higher and iron concentrations showed an increase towards the surface (Fig. 2B).

Archaeal community structures of degrading permafrost. The upper layer of core C2, inundated for 2,500 years, was dominated by sequences of typical marine archaeal taxa. They were represented by aerobic ammonia-oxidizing *Thaumarchaeota* of the genus *Nitrosopumilus* (~44%), *Lokiarchaeota* found at hydrothermal vents (~15%), marine benthic group D (6%) and other marine taxa such as marine group II (~2%, Fig. 1C). At 18 mbsf *Bathyarchaeota* sequences of the MCG-6/pGrfC26 clade dominated (~53%) the archaeal community. This clade includes members able to degrade polymeric carbohydrates in the sulfate reduction zone[44]. In the same depth a shift towards taxa that are commonly found in terrestrial environments such as the ammonia-oxidizing *Nitrososphaerales* (~25%) was observed. Here we also detected a so far unknown clade, which we designated as **D**eep **S**ubmarine **P**ermafrost **E**uryarchaeotal **G**roup I (DSPEG I, ~12%). This new clade is closely related to *Methanomassiliicoccales* of the superclass *Diaforarchaea*. DSPEG I increased in relative sequence abundance with depth (Figs 1C and 3). DSPEG I and a sister clade (designated DSPEG II) were most dominant in the sediment horizons between 29 and 44.8 mbsf, where they represented between 62 to 84% of all archaeal sequences (Fig. 1C). Both groups showed less than 82% sequence similarity values to the next cultured representative *Methanomassiliicoccus luminyensis*[45] placing them in a putative new order. Other abundant sequences belong to *Methanoflorentaceae* (~0.1–5%), ANME-2d (~0.2–6%), *Methanosarcina* (~0.2–9%), *Bathyarchaeota* MCG-6 and MCG-8 (~0.8–11%), as well as *Nitrososphaerales* (~3.7–22%). At 45 mbsf there was a pronounced shift towards *Nitrososphaerales* sequences (~65%). In the sediment layers between 49–52 mbsf, where most of the electron acceptors showed low concentrations, *Bathyarchaeota* of the MCG-6/pGrfC26 clade dominated (~41–78%). In these sediment horizons, many methanogen-related sequences appeared, such as *Methanoregula* (~0.1–6% between 50.1–52.3 mbsf), *Methanosarcina* (~2–18%), *Methanobacterium* (~3–10% 50.1–52.3 mbsf) and *Methanomassiliicoccaceae* (0.7–14% between 48.8–50.6 mbsf). Between 50.1 and 51.8 mbsf *Woesearchaeota* of the YLA114 clade were present (~3–13%). In core C2 ANME-2d sequences increased in relative abundance from less than 1% at 48.80 mbsf to 18% at 52.3 mbsf and up to 70% at 52.8 mbsf. The high abundance of anaerobic methane-oxidizers coincides around the highest peak of the methane concentration profile in the ice-bonded permafrost (284 µM) at 52 mbsf (Fig. 1). In the same depth, about 1.1% of sequences are related to *Methanosarcinaceae*/ANME-3 as described by reference[24] (Table S1). A second, much smaller peak of the methane

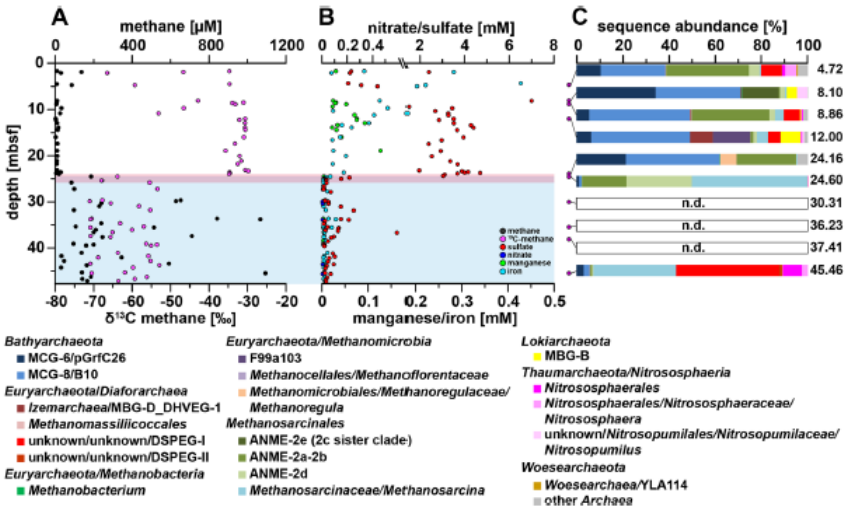

Figure 2. Pore water profiles of methane, nitrate, sulfate, iron, manganese and relative archaeal abundance in the Buor Khaya core BK2. (**A**) Methane concentrations are shown in black and corresponding δ13C-values in magenta[13]. (**B**) Nitrate concentrations are shown in blue, sulfate concentrations in red, manganese concentrations in green, and iron concentrations in light blue. (**C**) Purple dots on the left show depth location in the core. Relative abundance of archaeal 16S rRNA gene sequences are shown as bar plots. Colors of bars refer to the taxa in the legend below figure. Numbers on the right refer to the exact depth in the core. ANME = ANaerobic MEthanotrophic archaea, DHVEG-1 = Deep Hydrothermal Vent Euryarchaeotal Group 1, DSPEG = Deep Submarine Permafrost Euryarchaeotal Group, MBG-B = Marine Benthic Group B, MBG-D = Marine Benthic Group D, MCG = Miscellaneous Crenarchaeotal Group. The red area represents a sulfate-methane transition zone and the light blue area ice-bonded permafrost. All uncolored areas of the plots correspond to unfrozen submarine permafrost and marine sediments. n.d. – not detected.

concentration profile (10 µM) at 55.6 mbsf showed 16% ANME-2d sequences. At the same depth *Methanosarcina* represented the most abundant group (~47% of all archaeal sequences) and DSPEG I and II related sequences were the second most abundant (~21%, Fig. 1C). Towards the lower boundary of the ice-bonded permafrost at 58.7 mbsf, the DSPEG I and II increased again in sequence abundance (~33%). The sediment horizon directly underneath the permafrost contained some sequences related to marine environments, such as *Lokiarchaeota* (~9%), and ANME-2a/b (2.5%). The deepest sediment sample showed mostly *Bathyarchaeota* sequences of subgroups MCG-6 and MCG-8 (~77%) and DSPEG I and II, ANME-2d, *Methanoflorentaceae* and *Nitrososphaerales* (~6%, 4%, 3% and 2%, respectively) sequences.

The more recently inundated core BK2 contained a mixture of marine and terrestrial archaeal sequences in the depth between 4.7 and 12 mbsf. Marine clades were represented by ANME-2a/2b (~0.5–35%), *Methanomicrobia* of clade F99a103 (~0.1–16%) that were first discovered at a hydrothermal chimney, ANME-2c sister clade (~16%, 8.1 mbsf), Marine Benthic Group D (~0.1–10%), *Lokiarchaeota* (~0.7–9), and *Nitrosopumilales* (~0.3–4%). Terrestrial clades were represented by *Methanosarcinales*/*Methanosarcina* (~0.7–15%), DSPEG I and II (~0.1–9%), and *Nitrososphaerales* (~0.2–5%). The high numbers of ANME-2a/b sequences (Fig. 2C) at depths of ~5 and ~9 mbsf correlated with highest δ^{13}C-methane values in the uppermost 12 m that were characterized by highly variable methane δ^{13}C-values (−67 to −31‰, Fig. 2C). Still, *Bathyarchaeota*-related sequences of the clades MCG-6 and MCG-8 (~40–71%) dominated throughout the layers above the ice-bonded permafrost. In contrast, they drastically decreased (~2%) in the upper layer of the ice-bonded permafrost. The sediment horizon between 24.0 and 24.7 mbsf was characterized by opposing gradients of sulfate and methane. In the upper part of this layer that is strongly marine influenced ANME-2a/b made up about 26% of all archaeal sequences while in the lower and still partially ice-bonded part of the permafrost thaw front both ANME-2a/b and ANME-2d clades were detected in high abundances (19% and 28%, respectively, Fig. 2C). In the ice-bonded permafrost of core BK2, archaea were only detected in about 45.46 mbsf. Here, *Methanosarcina* (~37%) and DSPEG I and II (~46%) related sequences dominated. A detailed description of the bacterial community structure and diversity of both cores was described elsewhere[42].

Diversity of ANME-related groups in degrading permafrost. Both cores displayed layers where ANME sequences dominated the archaeal community. The two major groups, ANME-2a/b and ANME-2d showed a remarkably high diversity with 23 and 17 operational taxonomic units (OTUs), respectively (Figs 3 and 4A). ANME-2d separated into 4 different clusters (Fig. 4B), with the majority of all sequences falling into cluster 1. This cluster also contained *Candidatus* Methanoperedens nitroreducens BLZ1[46], known to either use nitrate[27]

Figure 3. Phylogenetic affiliation of submarine permafrost archaeal sequences based on 16S rRNA gene. Taxonomic cluster in red contain sequences of submarine permafrost. Numbers in brackets show the number of OTUs per cluster. The scale bar represents 10 percent sequence divergence. The tree was rooted with the DPANN superphylyum.

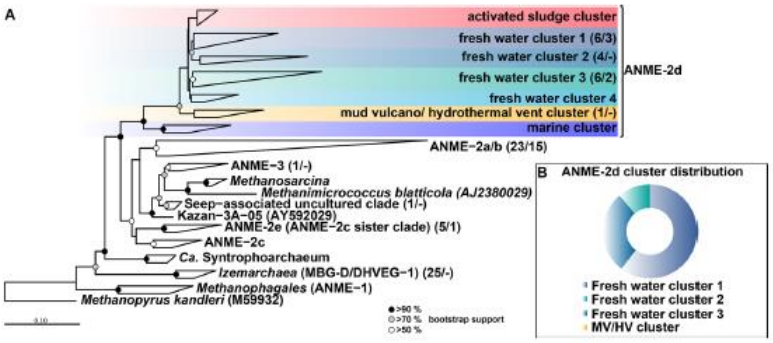

Figure 4. Phylogenetic affiliation of ANME sequences based on 16S rRNA gene. (**A**) The first number in the parenthesis represents the number of OTUs from the Illumina sequencing, while the second number represents the number of sequences of the clone library with ANME-specific primers. *Methanopyrus kandleri* was used as outgroup. The scale bar represents 10 percent sequence divergence. (**B**) The ring diagram represents the whole relative abundance of all ANME-2d sequences in both submarine permafrost cores.

or iron[47] as electron acceptor for methane oxidation. Besides the two dominant ANME-groups, we also detected sequences in a sister clade of ANME-2c (designated ANME-2e) with 5 OTUs (Figs 3 and 4 for details see also Figs S1 and S2). Other sequences of this group were retrieved from cold seep sites and mud volcanoes. Moreover, we detected 1 OTU that fell into the ANME-3 cluster (Figs 3 and 4, for details see also Fig. S2). Clone libraries of the SMTZ, using specific ANME-2a primers revealed mainly ANME-2a/b sequences but also ANME-2d as well as one sequence of the ANME-2e cluster (Fig. 4A, for details see also Fig. S1). Corroborative CARD-FISH analysis

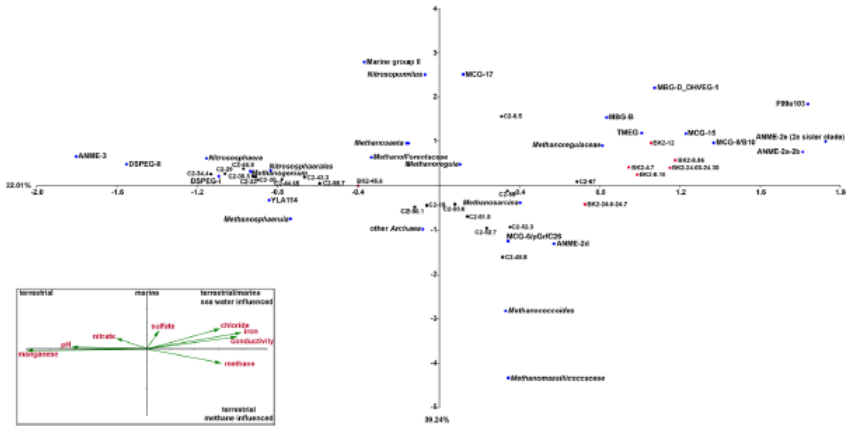

Figure 5. Canonical correspondence analysis (CCA) of environmental factors and archaeal taxa that contributed with more than 1% in any of the depth. Inlet: Environmental factors are plotted as triplot with scaling 3. Samples of core C2 are projected as black dots and samples of BK2 as red dots. The archaeal taxa are shown as blue dots. Percentages at axes represent the 'Eigenvalues' that explain the variability for the first two axes.

of the SMTZ detected ANME-2a consortia with the specific ANME-2a-647 probe (Fig. S3), while detection with a specific probe for *Desulfosarcina/Desulfococcus* showed no signal in any consortium.

Canonical correspondence analysis (CCA) illustrated that ANME-2a/b and ANME-2e clustered with other marine-related archaea and are mainly influenced by salinity, iron and sulfate (Fig. 5). Spearman rank correlations revealed that the abundance of ANME-2a/b significantly correlated with iron concentrations ($R = 0.65$, $p < 0.03$). ANME-2d sequences clustered together with sequences of *Methanosarcina* and *Bathyarchaeota* of the MCG-6/pGrfC26 clade and fall in the terrestrial methane-influenced quadrant of the plot. However Spearman correlation revealed no significant correlation.

Functional groups responsible for methane cycling. Quantitative detection of the methyl co-enzyme reductase subunit A (*mcrA*) as functional marker for methane production (methanogens) and AOM (ANME) showed a decrease with depth in the unfrozen permafrost of both cores (0 to 29 mbsf for C2, and 0 to 24 mbsf for BK2, respectively, Fig. S4A and B). In the ice-bonded permafrost of core C2 we detected an increase in *mcrA* copy numbers with the highest copy numbers ($0.3–1.2 \times 10^5 \pm 0.4$ - $\times 10^5$ g^{-1} wet weight) between ~45 and 52 mbsf. At 53 mbsf total *mcrA* copy numbers decreased, while 16S rRNA gene sequences at the same depth were almost exclusively affiliated with ANME-2d (Figs 1C and S4A). 454 amplicon analyses of the *mcrA* sequences showed a relative increase of ANME-2d-related *mcrA* genes towards the layers with highest ANME-2d-related 16S rRNA gene sequences between 52.3 and 55.6 mbsf (Figs 2C and S5). Quantification of ANME-2d with recently designed *mcrA* primers in the ice-bonded permafrost[48] showed up to $1.2 \pm 0.5 \times 10^5$ copy numbers g^{-1} wet weight at approximately 57 mbsf and an average copy number of $5.1 \pm 1.5 \times 10^4$ g^{-1} wet weight over the whole core (Fig. S6).

Analysis of the dissimilatory sulfate reductase subunit B (*dsrB*) for SRB mainly followed the depth distribution of *Desulfosporosinus* 16S rRNA sequences in the C2 core, with a few exceptions (29.0, 30.0, 34.4 and 38.5 mbsf) where an increase in the *dsrB* could not be related to any known sulfate-reducers (Fig. S7A).

McrA copy numbers in BK2 slightly increased at the SMTZ and may be underestimated due to a primer bias against ANME *mcrA* genes[48], while 16S rRNA gene sequences showed 25–47% ANME-related sequences at the SMTZ (Fig. S4B). The *dsrB* copy numbers slightly increased at the SMTZ, although SRB represented < 1% of the total bacterial 16S rRNA gene sequences (Fig. S7B). Phylogenetic reconstruction of SRB at the SMTZ indicated that all sequences of the upper part belonged to typical marine clades SEEP-SRB1 and another seep-associated *Desulfobacterium anilini*-group (red OTUs, Fig. S8). In the lower part of the SMTZ that is dominated by ANME-2d sequences, seep-associated SRB were below detection limit, while only *Desulfosporosinus*-related sequences (blue OTU, Fig. S8) could be observed.

Lipid biomarker measurements revealed very low concentrations that prevented a precise isotopic analysis to conclude activity of AOM microbial communities. However, calculated branched and isoprenoid tetraether (BIT) indices showed values of terrestrial origin ranging from 0.99 to 1[49]. Moreover calculated methane indices (MI) for isoprenoid glycerol dialkyl glycerol tetraethers (GDGTs) showed values between 0.85 to 0.99 in the unfrozen sediment layer and 1 at the SMTZ[50]. The ratio of archaeal to bacterial ether lipids showed dominant archaeal values in the SMTZ (Fig. S9). For further discussion on lipid biomarker see supplementary material.

Methane oxidation rates in submarine permafrost. The fraction of produced methane that, based on carbon isotopic signature change, was oxidized varied between 72–86% for the C2 core and 79–100% for the BK2 core, respectively. Methane release rates depend on the permafrost degradation rate and the methane concentration in the pore space of the core section. Assuming that our cores are representative for the whole submarine

permafrost area with an estimated distribution of 3 million square kilometer[2], modeling for the C2 core resulted in 0.0001–0.0984 Tg C y^{-1} (average 0.004–0.005 Tg C y^{-1}, highest and lowest oxidation, respectively) and 0.0242–1.1889 Tg C y^{-1} (average 0.1712–0.2167 Tg C y^{-1}, highest and lowest oxidation, respectively) for the BK2 core.

Discussion

Atmospheric methane concentration has been increasing again for the last decade, but the sources and mechanisms for this increase are not fully understood[51]. One potentially large but highly controversial source of methane is submarine permafrost, which faces drastic changes due to global temperature increase and associated Arctic sea ice reduction[52]. Our study provides multiple lines of evidence that ANME communities are present in submarine permafrost layers where methane is being consumed. We thus propose the microbial mitigation of methane release from thawing deep submarine permafrost on the Siberian Arctic Shelf. We detected both marine and terrestrial ANME clades likely involved in the AOM process at various depths, not only at the permafrost thaw front, but also in still ice-bonded permafrost that undergoes degradation. Our study indicates that AOM occur at temperatures below 0 °C[42] (Table S2).

Pore water methane concentrations in the two cores were in the typical range of deep sediments and soils[20,53]. The permafrost thaw front at the BK2 site, inundated about 540 years ago reflects a deep SMTZ. We identified a steep decline of methane concentration above the SMTZ. This is in accordance with core (IID-13)[54] in close proximity that also showed a large decrease (10^6 to 10^3 nM) in methane concentrations at the thaw boundary while δ^{13}C-values of methane from unfrozen layers above (~15 to 4 m) of this core are not reported. Altogether the study of Sapart *et al.*, (2017)[54] finds no evidence for AOM, which might be due to regional influences such as river water, land surface run off and warming by river discharge. Our δ^{13}C-values of methane in the unfrozen part clearly show a large shift that can only be explained by microbial oxidation. The calculated potential rates based on methane release and the fraction of methane oxidized (1.7–2.1 nmol cm^{-3} d^{-1} ± 0.9–1.2 nmol cm^{-3} d^{-1} [13])[13] are typical for margin SMTZ and exceed those of subsurface SMTZ[25].

At the permafrost thaw front of BK2, we detected marine and terrestrial ANME clades that potentially mitigate the methane release into overlying sediment layers. The upper unfrozen part of the SMTZ represents a typical marine sulfate-dependent AOM community of ANME-2a/b (Fig. 2C) affiliated with SEEP-SRB1/seep-associated *Desulfobacterium anilini*-group (Fig. S7A). These sulfate-dependent AOM communities are of marine origin and are often found in mud vulcanoes, and in methane and hydrocarbon seeps[55]. Visualization of ANME-2a *in situ* using CARD-FISH further supports their occurrence at the permafrost thaw front of BK2. The molecular detection of associated SRB is, however, not conclusive. This might be due to SEEP-SRB partners that are not targeted by the DSS685 probe[56] or by yet unidentified bacterial partners[57]. The lower part of the SMTZ was characterized by a clear transition to a terrestrial AOM community closely related to *Candidatus* Methanoperedens nitroreducens (ANME-2d) that might be capable of using alternative TEA such as nitrate and iron[27,47], although no information on the oxidative state of iron is available. A recent genomic study proposed that these organisms have the genetic repertoire for an independent AOM process without a bacterial partner[46]. Besides the analysis of AOM assemblages via a DNA approach we also found high ether lipid MI values in the SMTZ of BK2 that further supports a potential involvement of AOM communities[50]. The high abundances of marine-derived ANME-2a/b sequences in several depths above the SMTZ of BK2 with BIT indices towards an exclusively terrestrial origin show that terrestrial and marine sediments were only slightly mixed in the upper meters of BK2 (Fig. 2). The terrestrial sediments were thus influenced by sea water penetrating down to the permafrost table and thereby transport of marine organisms into deeper layers occurred (Fig. 2). This is consistent with profiles of other environmental parameters (pH, temperature, isotopes and ion concentrations) and the stratification and composition of the bacterial communities[42].

In core C2, the layer between 29 and 43 mbsf is characterized by alternating frozen and partly thawed sediments (Fig. 1) and showed high fluctuations in the concentrations of nitrate and manganese. These fluctuations indicate degradation of thawing permafrost (shaded area, Fig. 1) and an increase in microbial activity resulting in the consumption of labile carbon pools[58]. Active processes in ice-bonded permafrost close to thawing (mean temperature: −1.2 ± 0.2 °C, Table S2) can occur in liquid water films surrounding mineral particles, which form a network in which microbial activity is expected[59]. Microbial activity may thereby be supported through sulfate as additional electron acceptor[60] penetrating into the ice-bonded sediment. Indeed, sulfate concentrations decreased and *dsrB* copy numbers increased with depth pointing towards active sulfate reduction and effective anaerobic organic matter decomposition[61]. In C2, the SMTZ occurred below the actual permafrost thaw front but inside the ice-bonded permafrost and was characterized by high manganese and nitrate concentration. Nitrate and manganese concentrations at the SMTZ and in the lower thaw boundary were in the higher µM to mM ranges that exceeded those typically reported for subsurface environments[20] by an order of magnitude (http://publications.iodp.org/). So far it is not clear why nitrate as favorable electron acceptor is not quickly consumed under anaerobic conditions. Nevertheless, the high concentrations of nitrate and manganese could promote AOM with alternative TEA[33,35] and shows ongoing degradation of ice-bonded permafrost. Also, the detection of ANME-2a/b in this layer shows their migration into permafrost by downward marine water intrusion[42]. Unlike in core BK2, the ice-bonded layer of C2 was almost free of methane. At the same time ANME-2d occurred almost entirely throughout this layer. The relatively low copy numbers of ANME-2d detected with specific *mcrA* primers and compared with total cell counts[42] are still in the range of North Sea and River sediment[48]. The highest abundance of ANME-2d coincided with the highest methane concentration, which we consistently detected by several molecular approaches (16S rRNA, *mcrA* and ANME-2d-specific *mcrA*). Taken all this together we suggest that ANME-2d members are responsible for AOM in the ice-bonded permafrost before it completely thaws. An alternative explanation for the low methane concentrations and the low abundance of ANMEs in most of the ice-bonded layers are a relic of AOM communities that were active under different environmental conditions in

the past. Whether methane was trapped in the permafrost during freezing or it was produced by microbial degradation of organic matter under recent *in situ* conditions cannot be resolved since radiocarbon analysis would give similar results in both cases.

Even though sulfate reduction might be relevant for organic matter mineralization[61], links to sulfate-dependent AOM were not observed in the core C2. While C2 exhibited high copy numbers of *dsrB* and of SRB-related sequences, sulfate reducers were almost exclusively linked to *Desulfosporosinus* that have not been observed in AOM consortia so far. This genus belongs to the phylum *Firmicutes* and has been found in natural terrestrial environments such as peatlands, aquifer and permafrost[62,63]. Other TEA than sulfate, such as nitrate, iron and manganese, could also be related to AOM, and showed relatively low concentrations at the highest occurrence of ANME-2d sequences at 52 mbsf. This serves further as an indication of methane consumption during the process of AOM as known from physiological studies of ANME-2d enrichments[27,47] but direct evidence is missing. Finally, besides the detected electron acceptors, other TEA such as humic acids could serve in the AOM process. Humic acids were shown to be involved in AOM[36,37] in peatlands where they were detected in high concentrations. Humic acids are produced during organic matter degradation and soil formation[64] and could thus play a role in thawing permafrost, too.

Two clades, which we named DSPEG I and DSPEG II, mainly occurred in submarine permafrost layers that showed relatively high concentrations of iron and manganese in the pore water (Fig. 1B,C). This could point towards an involvement in iron (III) and manganese (IV) reduction within the anaerobic oxidation of organic matter, in addition to sulfate reduction[62]. Since the oxidative state of both metals has not been determined it is not clear whether these metals are used as TEA. Future analysis should focus on oxidative states of metals in these environments to further clarify a potential role in organic matter degradation and AOM. Nevertheless, Spearman rank analysis showed significant correlations between DSPEG I and DSPEG II and manganese concentrations ($R = 0.58$, $p < 0.006$ and $R = 0.53$, $p < 0.02$, respectively) and negative correlations with methane concentrations ($R = -0.57$, $p < 0.02$ and $R = -0.64$, $p < 0.004$, respectively) as illustrated in the CCA (Fig. 5). We propose that these two groups reflect indicator taxa (Table S3) for degrading permafrost. This is also supported by high occurrence of DSPEG I and DSPEG II (~19 to 28%, Fig. 1C) at the lower boundary of the ice-bonded permafrost, representing bottom-up permafrost thaw. Here, high concentrations of sulfate, nitrate, and manganese show an upwardly directed thaw process (Fig. 1B). Both groups were also dominant (47%) in the deepest sample of BK2, while degradation and an upward thaw cannot be concluded from our data. Environmental sequences affiliated with the DSPEG groups were mainly retrieved from cold environments[65,66] and pristine aquifers[67], which further support an active role in low temperature habitats.

Taken together our molecular and biogeochemical data from two submarine permafrost cores indicate several microbial assemblages that have the potential to prevent the release of trapped or recently produced methane into the overlying unfrozen sediment following submarine permafrost thaw. Therefore, we challenge the assumption that high methane emissions reported for the Siberian Arctic Shelves originate from degrading submarine permafrost itself[9] and suggest different mechanisms to be responsible, such as diffusion or ebullition through discontinuities in permafrost or the release from gas hydrates[8,68] at a limited spatial scale. Microbial assemblages in deep permafrost environments are usually associated with slow growth rates[69] and low abundances[70], and their activity is difficult to measure. New approaches such as BONCAT-FISH[57] have the potential for more direct detection of active microorganism and the analysis of their genomic potential.

The calculated fraction of methane that was oxidized in the SMTZ of BK2 showed high efficiencies, pointing towards an effective biological methane filter. While methane oxidation within the intact ice-bonded permafrost section of BK2 is unlikely, C2 showed several layers with heavier stable isotopes (≥ -45‰) and high fractions (72 to 86%) of methane that were oxidized. Actual methane oxidation rates may be even higher, since methane production of freshly available organic material is not taken into account. Still, on a global scale the estimated submarine permafrost area (~3 million km²)[2], could consume 0.0001 to 1.1889 Tg y^{-1} of methane from newly degraded permafrost assuming AOM activities similar to those in our cores. This only account for the methane released, since it is difficult to determine the total sediment volume in which AOM activity takes place. Submarine permafrost is thus comparable to AOM in other environments with high methane fluxes such as seep sites (<10 Tg C y^{-1})[71], while AOM in wetlands (200 Tg C y^{-1})[32] and marine SMTZ (<50 Tg C y^{-1})[71] clearly show higher consumption rates. The latter two span areas that are 6 to 40 times larger than those of submarine permafrost.

Our study provides first molecular evidence of microbial communities in thawing submarine permafrost that are likely involved in AOM processes. In addition, many archaeal taxa such as the newly designated DSPEG groups, a large diversity of *Bathyarchaeota*, and *Thaumarchaeota* closely related to nitrogen cycling organisms are detected. Their function is unknown and need further investment to understand their contribution in organic matter degradation of permafrost thaw processes.

Materials and Methods

Site description and sampling. Sediment cores were drilled along two transects from terrestrial permafrost to offshore, submarine permafrost in the Siberian Laptev Sea: Mamontov Klyk (2005) and Buor Khaya (2012) (Table S2). The outermost submarine permafrost cores influenced longest by inundation were chosen for chemical and microbial investigation. The Mamontov Klyk study site was located in the western Laptev Sea (Fig. S10). The core drilled 11.5 km offshore is characterized by three different lithostratigraphical units and contains two ice-bonded permafrost layers between 29.5–30.4 mbsf and 34.3–58.7 mbsf, respectively[12]. The core had a total length of 71 m and contained sandy loam sediment with on average 0.38% organic carbon and an average C/N ratio of 14.

The study site of Buor Khaya is located in the central Laptev Sea on the western part of the Buor Khaya peninsula (Fig. S10). The submarine core contained again three lithological units with an ice-bonded permafrost layer

between 24.7–47.6 mbsf[13]. The core had a total length of 47.7 m. The retrieved sediment material consisted of fine sand and contained about 1% organic carbon with a C/N ratio of 14.

The drilling was performed with a mobile drilling rig (URB-2A-2/ URB-4T) and is described elsewhere[12,13]. Cores were kept frozen at −20 °C and transported to the laboratories in Germany under frozen conditions. The frozen cores were split along the vertical axis under aseptic conditions. One half was used as an archive, whereas the other half was split into quarters for microbiological and for geochemical, sedimentological and micropalaeontological analyses.

Geochemical analysis. The cores were sectioned at different intervals. The core of the Mamontov Klyk site (C2) was separated into 118 horizons that were used for pore water analyses in 2007, 2 years after the drilling took place. The core was constantly stored at −20 °C between drilling and subsampling. The Buor Khaya site (BK2) was divided into 80 horizons. After thawing of subsamples in 2013, one year after the drilling, pore water was collected using Rhizones© with an effective pore diameter of 0.1 µm. The concentrations of sulfate and nitrate were determined via a KOH eluent and a latex particle separation column on a Dionex DX-320 ion chromatograph. Total manganese and iron ions were measured by a Perkin-Elmer 'Inductively Coupled Plasma Optical Emission Spectrometry' (ICP-OES) Optima 3000 XL.

For methane measurements, 3 g of frozen material were retrieved with ice screws and immediately immersed in 20 ml serum vials containing a saturated NaCl solution (315 g l^{-1}). Serum vials were sealed with butyl-rubber stoppers and a crimp seal. Headspace gas was measured in triplicates with different setups. In brief, gas was analyzed with an Agilent 6890[19] or 7890A[13] gas chromatograph equipped with a flame ionization detector and with a carbon plot capillary column or HP-Plot Q (Porapak-Q) column. The temperature of the oven, injector and detector were 40, 120, and 160 °C, respectively. In both cases, helium was used as carrier gas. The amount of gas in the vials was calculated from headspace concentrations, gas pressure and solubility, and the volume of liquid in the bottles. Methane concentrations are reported relative to sediment pore water volume, regardless of whether present as ice or water, based on calculated total sediment water content. The $\delta^{13}C$-CH_4 was determined with an isotope ratio mass spectrometer (Finnigan Delta Plus) equipped with a PreCon and a GC/C III interface (Thermo Fisher Scientific). The precision of replicated measurements was better than 0.5‰ VPDB. Methane $\delta^{13}C$-signatures were linked to the VPDB scale using internal (−43.8‰ VPDB) and external (RM8561; −73.27‰ VPDB) standards measured at least every 10 analyses.

DNA extraction, 16S rRNA Illumina sequencing and analysis. In 2014, genomic DNA of 4.7–13 g homogenized sediment from different depth (C2: 19 samples and BK2: 10 samples, Table S2) was extracted after the protocol of Zhou *et al.*, 1996[72]. DNA concentrations were quantified with Nanophotometer® P360 (Implen GmbH) and Qubit® 2.0 Flurometer (Thermo Fisher Scientific).

The 16S rRNA gene for bacteria was amplified with the primer combination S-D-Bact-0341-b-S-17 and S-D-Bact-0785-a-A-21. The 16S rRNA gene for archaea was amplified in a nested approach with the primer combination S-D-Arch-0020-a-S-19 and S-D-Arch-0958-a-A-19 in the first PCR for 40 cycles and S-D-Arch-0349-a-S-17 and S-D-Arch-0786-a-A-20 in the second PCR for 35 cycles, respectively. The primers were labelled with different combinations of barcodes that are listed together with primer sequences in Tables S4 and S5. The PCR mix contained 1 × PCR buffer (Tris•Cl, KCl, $(NH_4)_2SO_4$, 15 mM $MgCl_2$; pH 8.7) (QIAGEN), 0.5 µM of each primer (Biomers), 0.2 mM of each deoxynucleoside (Thermo Fisher Scientific), and 0.025 U μl^{-1} hot start polymerase (QIAGEN). The thermocycler conditions were 95 °C for 5 min (denaturation), followed by 40 cycles of 95 °C for 1 min (denaturation), 56 °C for 45 sec (annealing) and 72 °C for 1 minute and 30 sec (elongation), concluded with a final elongation step at 72 °C for 10 min. PCR products were purified with a Hi Yield® Gel/PCR DNA fragment extraction kit (Süd-Laborbedarf). We performed technical duplicates of one DNA sample and PCR products of 3 individual runs per sample were combined. PCR products of different samples were pooled in equimolar concentrations and reduced to a final volume of 10 µl with a concentration of 200 ng μl^{-1} in a vacuum centrifuge Concentrator plus (Eppendorf).

Illumina sequencing has been performed by GATC Biotech AG using 300 bp paired-end mode. For better performance due to different sequencing lengths, we used 15% PhiX control v3 library.

The quality and taxonomic classification of the Illumina sequences were analyzed with a customized QIIME pipeline[73]. For details see Supplementary material and methods.

Construction of ANME-specific clone libraries. DNA of permafrost thaw horizons with methane peaks were investigated to amplify ANME communities with specific primers. Therefore we used an ANME-specific probe as reverse primer and a universal archaeal primer as forward primer (Table S4). PCR mixes (25 µl) contained 1 × PCR buffer, 0.2 mM dNTP's, 2 mM $MgCl_2$, 0.08 mg ml^{-1} bovine serum albumin, and 0.02 units HotStart Taq Plus Polymerase (QIAGEN) and were performed under the following conditions: initial denaturation 94 °C for 10 min, 30 cycles of denaturation 94 °C for 30 sec, annealing 59 °C for 1 min, extension 72 °C for 3 min, and a final elongation at 72 °C for 10 min. PCR amplicons were purified with the HiYield® Gel/PCR DNA Extraction Kit (Süd-Laborbedarf). Purified PCR products were cloned with the TOPO® TA Cloning® Kit (Invitrogen). Positive clones were directly sequenced by Sanger sequencing (GATC Biotech).

Phylogenetic reconstruction. For phylogenetic analyses of 16S rRNA gene of archaeal and bacterial sequences, the ARB software package was used[74]. After manual refinement of representative sequences of OTUs achieved by the Illumina sequencing and partial sequences of clone libraries against the alignment of the SILVA 16S rRNA gene SSU reference database release 115[75], phylogenetic trees were calculated. Phylogenetic reconstructions were based on the maximum-likelihood algorithm (PHYLIP-ML, 100 bootstraps) implemented in ARB with reference sequences (>1400 bp for bacteria and >850 bp for archaea) and the implement archaeal or

bacterial position variability filters. Our own partial sequences were added to the tree using the maximum parsimony algorithm without allowing changes in tree topology.

454 pyrosequencing of functional genes and analysis. The *mcrA* fragment was amplified using the primer set mlas and mcrA-rev (Table S4). In a touchdown PCR denaturation, annealing and elongation time was set at 1 min. The PCR conditions were as follows: initial denaturation at 95 °C for 3 min, 15 cycles with a stepwise temperature decrement from 65 °C to 50 °C, followed by 15 cycles with an annealing temperature of 55 °C and a final elongation at 72 °C for 10 min. Tagging of amplicons with unique multiple identifier (MID) tags (Table S6) for 454 sequencing was conducted in a second PCR using amplicons from the touchdown PCR as template and 15 cycles with a constant annealing temperature of 55 °C. PCR reactions were performed in several separate reactions and pooled until reaching at least 150 ng final product. We used the same chemicals as for 16S rRNA gene amplifications. PCR products were purified with a Hi Yield® Gel/PCR DNA fragment extraction kit (Süd-Laborbedarf). Amplicons were quantified with the Qubit 2.0 system using the ds DNA HS assay kit (Invitrogen), mixed in equimolar amounts and sequenced from both directions by Eurofins Genomics using Roche/454 GS FLX++ technology.

454 mcrA sequences were analyzed with the mothur software[76] by a customized standard operating procedure. For details see Supplementary material and methods.

Quantification of functional genes. Quantitative PCR was performed using the CFX Connect™ Real-Time PCR Detection System (Bio-Rad Laboratories). Each reaction contained iTaq™ Universal SYBR® Green Supermix (12.5 µl per reaction of 2× concentrate, Bio-Rad Laboratories), PCR primers (0.5 µl containing 20 µM each), sterile water (6.5 µl) and DNA template (5 µl) added to a final volume of 25 µl. Primers targeting the functional genes *mcrA* and *dsrB* were used (Table S4). The PCR reactions comprised an initial denaturation (5 min at 95 °C), followed by 40 cycles of 5 sec at 95 °C, 30 s at the specific annealing temperature (see Table S4), 10 sec at 72 °C and a plate read step at 80 °C for 3 s. Melt curve analysis from 65 to 95 °C with a 0.5 °C temperature increment per cycle (5 sec) was conducted at the end of each run to check for non-specific amplification of DNA. The qPCR assays were calibrated using known amounts of PCR amplified and cloned gene fragments from corresponding taxa (standards of pure cultures) in the range of 10^6–101 copies μl^{-1}. Prior to qPCR analysis, DNA templates were diluted 5- to 100-fold and triplicates were analyzed for each sample. The PCR efficiency based on the standard curve was calculated using the Bio Rad CFX Manager software and varied between 88 and 100%, depending on the standard. All cycle data were collected using the single threshold cq determination mode.

Quantification of ANME-2d. The DNA was diluted 1:100 to prevent inhibition of amplification by environmental compounds, e.g. humic acids, and to keep the cq value of the samples within detectable limits. The abundance of ANME-2d archaea was quantified by qPCR with specific *mcrA* primers (Table S4). The PCR mix consisted of 10 µl KAPA HiFi SYBR green mix (KAPA Biosystems), primers (0.04 µl containing 100 mM each), $MgCl_2$ solution (0.5 µl of 50 mM), bovine serum albumin (BSA) (0.3 µl), sterile water (9.02 µl) and 1 µl DNA template. qPCR amplifications were performed by 10 min 98 °C initialization; 40 cycles of 5 sec denaturation at 95 °C, 30 sec of annealing at 60 °C, 1 min of elongation at 72 °C, 2 sec at 82 °C for fluorescence detection; and finally a melting curve from 55 °C to 95 °C with a 0.5 °C increment every 5 sec. For quantification, a tenfold dilution series of mcrA156F/mcrA345R product cloned into a pGEM-T easy plasmid of a known copy number was used as a standard[48]. The PCR product specificity was checked by melt analysis and compared to the standard with a melting temperature of 82 °C.

Microbial lipid biomarker extraction. Different fractions of lipids were extracted from sediment of the SMTZ. For a detailed method description see supplementary material.

Catalyzed reporter deposition fluorescence *in situ* hybridization (CARD-FISH). For CARD-FISH, sediments were fixed for 1 h at room temperature with 4% formaldehyde (Fluka). For amplification, a fluorescine-labelled tyramide was used. The protocol for CARD-FISH followed the description published earlier[77]. For details see supplementary material and methods.

Statistical analysis of archaeal community. Statistical analysis was performed with the PAST 3.14 software[78]. Canonical correlation analysis (CCA) was performed with 7 environmental parameters (chloride, pH, conductivity, methane, sulfate, manganese, iron, and nitrate) as explanatory variables and relative abundance of archaeal genera to families. Explanatory variables were standardized by log10 transformation prior to computation, with the exception of pH and conductivity. Chloride, pH and conductivity were used to account for the marine influence of seawater penetration into the permafrost. The significance of canonical axes was tested via permutation computed for N = 999. Spearman correlation analysis was performed with the implemented tools in PAST 3.14.

Modeling of methane oxidation rates in submarine permafrost. We used the highest change in stable isotope signature of dissolved methane in both cores to calculate the fraction of produce CH_4 that got oxidized ($f_{ox,i}$). For that we used the formula[79]:

$$f_{ox,i} = \frac{\delta_o - \delta_p}{1000 * (\propto_{ox} - \propto_{trans})} \quad (1)$$

δ_o and δ_p are the $\delta^{13}C$ values (in ‰) of CH_4 in the oxidized submarine permafrost layers (>−37‰) and of CH_4 produced or trapped in subjacent submarine permafrost layers (<−52‰), respectively. α_{ox} and α_{trans} are the fractionation factors for anaerobic oxidation of CH_4 and CH_4 transport, respectively.

We assumed that CH_4 is transported by diffusion and used a fractionation factor for soil of $\alpha_{trans} = 1.001$[80]. Fractionation factors (α_{ox}) for sulfate-dependent (S-)AOM in marine enrichments range between 1.009–1.039[81]. Therefore, we used the highest and lowest value for calculations. Since the submarine permafrost is a former freshwater system we also used fractionation factors for S-AOM ($\alpha_{ox} = 1.030$)[82], iron-dependent (Fe-) AOM ($\alpha_{ox} = 1.031$)[83], nitrate-dependent (N-) AOM ($\alpha_{ox} = 1.032$)[84] and extracellular electron transfer (EEL-) AOM ($\alpha_{ox} = 1.0174$)[85], latter likely reflecting humic acids as potential electron acceptor. Calculated fractions of oxidized methane for the low marine S-AOM and the EEL-AOM revealed values over 1 and seems to not represent suitable AOM fractionation factors and were not considered further.

To compare the AOM activity of submarine permafrost to that of other habitats, we took the lowest, highest and average methane concentration of ice-bonded permafrost for both cores and calculated the methane release rate due to permafrost degradation rate for the cores. The permafrost degradation rate is calculated by the mean coastal erosion rate and the permafrost table depth[12,13] and gave values of 0.6 cm per year for C2, and 5.3 cm per year for BK2[86], respectively. Assuming the AOM activity of our cores to be representative for submarine permafrost, we further extrapolated methane concentration to the whole area of submarine permafrost (3 million square kilometers)[2]. As last step we used the highest and lowest fraction of methane that got oxidized to calculate specific rates for both cores.

Data deposition. Sequences of the submarine permafrost metagenome have been deposited at the NCBI Sequence Read Archive (SRA) with the Project number BioProject ID# PRJNA352907, under the accession numbers SRR5183846-SRR5183871 for archaeal 16S rRNA gene sequences, SRR5184420-SRR5184446 for bacterial 16S rRNA gene sequences, and SRR5019811-SRR5019818 for *mcrA* sequences. ANME-specific, partial 16S rRNA gene sequences of clone libraries are available in Genbank, EMBL and DDBJ under the accession numbers KY613956-KY613991.

Acknowledgements

We thank Antje Eulenburg, Ute Bastian, Katja Hockun, Cornelia Karger, Maria Bade and Anke Saborowski for excellent laboratory support. We further thank Aleksandr Maslov (SB RAS, Mel'nikov Permafrost Institute, Yakutsk, Russia) who provided indispensable drilling expertise. We further thank Annika Vaksmaa of Radboud University, Nijmegen to kindly provide an ANME-2d mcrA standard. We thank Tiksi Hydrobase staff members Viktor Bayderin, Viktor Dobrobaba, Sergey Kamarin, Valery Kulikov, Dmitry Mashkov, Dmitry Melnichenko, Aleksandr Safin, and Aleksandr Shiyan for their field support and Birgit Schwinge (Universität Hamburg) for her help with the methane isotope measurements. We further thank Aurèle Vuillemin for helpful discussion on the manuscript and two anonymous reviewers for good comments and suggestions to improve the manuscript. This study was supported by the Helmholtz Gemeinschaft (HGF) by funding the Helmholtz Young Investigators Group of S.L. (VH-NG-919).

Author Contributions

M.W., P.O. and S.L. planned the research. P.O. and M.G. conducted the field work. M.W.J.M. and R.R. conducted the molecular work. M.W. and F.H. analyzed the sequences. P.O., M.Wf. conducted the chemical measurements. C.K. analyzed the isotopic measurements of methane. M.W. and K.M. performed lipid analysis. M.W. carried out statistics. D.W. facilitated laboratory work and contributed to the discussion; M.W. and S.L. wrote the manuscript with input from all authors.

Additional Information

Supplementary information accompanies this paper at https://doi.org/10.1038/s41598-018-19505-9.

Competing Interests: The authors declare that they have no competing interests.

Publisher's note: Springer Nature remains neutral with regard to jurisdictional claims in published maps and institutional affiliations.

Open Access This article is licensed under a Creative Commons Attribution 4.0 International License, which permits use, sharing, adaptation, distribution and reproduction in any medium or format, as long as you give appropriate credit to the original author(s) and the source, provide a link to the Creative Commons license, and indicate if changes were made. The images or other third party material in this article are included in the article's Creative Commons license, unless indicated otherwise in a credit line to the material. If material is not included in the article's Creative Commons license and your intended use is not permitted by statutory regulation or exceeds the permitted use, you will need to obtain permission directly from the copyright holder. To view a copy of this license, visit http://creativecommons.org/licenses/by/4.0/.

© The Author(s) 2018

Supporting Information Manuscript II

Methods

Illumina Sequence analysis. The quality of the sequences was checked using the fastqc tool. (FastQC A Quality Control tool for High Throughput Sequence Data http://www.bioinformatics.babraham.ac.uk/projects/fastqc/ by S. Andrews). Sequence raw reads were demultiplexed (Table B-3) and barcodes were removed with the CutAdapt tool [trim-n; e 0.1; only consider exact barcodes for mapping] [*Martin*, 2011]. The subsequent steps included merging of reads using overlapping sequence regions using PEAR [Q 25; p 0.0001; v 20] [*Zhang et al.*, 2014b], standardizing the nucleotide sequence orientation, and trimming and filtering of low quality sequences using Trimmomatic [SE; LEADING Q25; TRAILING Q25; SLIDINGWINDOW 5:25; MINLEN 200] [*Bolger et al.*, 2014]. After trimming we performed a chimera check with ChimeraSlayer [*Haas et al.*, 2011] and removed sequences from the dataset. Subsequently sequences were clustered into operational taxonomic units (OTU) by usearch v6.1 [*Edgar*, 2010] at a nucleotide cutoff level of 97% similarity and taxonomically assigned employing the GreenGenes database 13.05 [*McDonald et al.*, 2012] using the pick_open_reference approach of the QIIME pipeline [*Caporaso et al.*, 2010]. The OTU table was filtered for singletons, chloroplasts, mitochondrial and bacterial sequences. Older taxonomic assignments for archaea were corrected manually after [*Rinke et al.*, 2013; *Castelle et al.*, 2015; *Adam et al.*, 2017] e.g. Micellaneous Crenarchaeal Group (MCG) was renamed to *Bathyarchaeota*. OTUs with relative abundance lower than 0.1% for the individual libraries were not analyzed. Statistics of the sequence pipeline plus representative taxa are listed in Table B-3. The full diversity of all archaeal sequences are listed in the Table B-1.

Analysis of 454 functional sequences. Raw sequences were processed by the mothur software package (v.1.34.4) [*Schloss et al.*, 2009] by a modified standard operating procedure (SOP). Sequences were quality filtered by removing sequences with barcode or primer errors, homopolymers longer than 8, and or average quality scores less than 25. Afterwards unique sequences were aligned against an in-house reference *mcrA* database [*Yang et al.*, 2014] on a nulceotide alignment. A chimera check using the processed sequences as own reference let to a detection of up to 20% chimeras but manual reviewing against the non-redundant RefSeq NCBI database [*Pruitt et al.*, 2005] showed no chimeric blast hits and therefore sequences were not excluded from the analysis. Sequences were clustered using the furthest neighbor method

and OTUs were assigned at a cutoff value of 0.16[13]. OUT sequences were checked for translation errors in the ARB environment [*Ludwig et al.*, 2004], aligned and taxonomical classified by a manually curated ARB database on amino acid level with clustering at 85.7% and 75.4% amino acid similarity after [*Hunger et al.*, 2011].

CARD-FISH. PFA fixed samples were washed twice in 1× phosphate-buffered saline (PBS) and stored in PBS/ethanol (1:1, vol/vol) at −20°C. Sediments were filtered on polycarbonate membranes (0.2 μm pore size; 25 mm diameter; Millipore) and CARD-FISH on all samples was performed according to *Ishii et al.* [2004] using an fluorescin-labelled tyramide. Archaeal cells were permeabilized using proteinase K according to *Teira et al.* [2004]. Filter sections were embedded with a mix of Citifluor : VECTASHIELD [4:1] (VECTASHIELD® Mounting Medium H-1000, Vector Laboratories and Citifluor) containing 4′,6′-diamidino-2-phenylindole at a final concentration of 1 μg ml^{-1}. Preparations were examined under a fluorescent microscope Leica DM 2000 with camera DFC 420C and filter systemFI/RH (Leica). Image stacks were merged with the 'Picolay' software (www.picolay.de) to get focused images of the consortia.

Microbial lipid biomarker extraction. Sediment samples were freeze-dried and ground. Between 4.3-9.5 g of ground sediment was mixed with 50 ml of the extraction mixture composed of methanol/dichloromethane/ammonium acetate buffer (2:1:0.8, pH 7.6) and extracted by ultra-sonication for 15 min. Afterwards, samples were centrifuged at 2500 rpm for 10 min. The solvent was transferred to a separation funnel. As internal standard, 50 μg of 1-myristyl-(D27)-2-hydroxy-*sn*-glycerol-3-phosphocholine was added. The remaining sediment was extracted another 2 times with 50 ml of the extraction mixture. For phase separation, the combined three supernatants were adjusted with dichlormethane and water to achieve a ratio of 1:1:0.9. Afterwards the organic phase was transferred into a TurboVap® 500 system (Biotage) and the remaining water phase was re-extracted 2 times with 10 ml dichloromethane. The combined organic phases were evaporated and finally dried with a gentle stream of nitrogen. Subsequently, the obtained sediment extract was separated into fractions of different polarity (low polar lipids, free FAs, glycolipids, and phospholipid PLs) by using different columns. The first column was a pure silica column (1 g silica gel 63–200 μm) combined with a downstream Florisil® column (1g magnesium silica gel 150-250 μm). According to the method described by *Zink and Mangelsdorf* [2004], the low polar fraction was eluted with 20 mL of chloroform, the free FAs with 50 mL of methyl formate blended with 12.5 μL of glacial acetic acid and the

glycolipid fraction with 20 mL of acetone. After removal of the Florisil® column, the PLs were eluted with 25 mL of methanol from the silica column. To improve the recovery of PLs, the silica column was rinsed with 25 mL of a methanol/water mixture (60:40) and the extract was captured in a separation funnel. Dichloromethane and water were added for phase separation (methanol/dichloromethane/water, 1:1:0.9); the organic phase was removed, and the water phase was re-extracted 2 times with dichloromethane. Finally, the organic phases were combined with the PL fraction and all fractions were evaporated to dryness and stored at -20°C until analysis.

Detection of Phospholipid Fatty Acids (PLFA), Glycerol Dialkyl Glycerol Tetraethers (GDGT) and Archaeol. For the detection of glycerol dialkyl glycerol tetraethers (GDGT) and archaeol, the low polar lipid fraction was dissolved in 250 µl dichloromethane/methanol (99:1), and a 40-fold excess of *n*-hexane (10 ml) was added to precipitate asphaltenes. Asphaltenes were removed via filtration over sodium sulfate. The extract was separated into an aliphatic/alicyclic and an aromatic hydrocarbon fraction as well as into a polar fraction containing nitrogen, sulphur, and oxygen (NSO) bearing compounds using a medium-pressure liquid chromatography (MPLC). Subsequently, all fractions were evaporated to dryness and stored at -20°C until analysis and directly used for measurements.

Half of the PL fraction was used for PLFA analysis by a mild alkaline hydrolysis via ester cleavage [*Müller et al.*, 1990]. For identification of the resulting fatty acids, a gas chromatograph (Trace GC Ultra, Thermo Electron Corporation) equipped with a cold injection system (Thermo Electron Corporation) and a 50 m × 0.22 mm × 0.25 µm BPX5 (SGE) column coupled to a DSQ Mass Spectrometer (Thermo Finnigan Quadrupole MS, Thermo Electron Corporation) were used. The gas chromatograph were run in splitless mode with the following setup: initial oven temperature 50 °C (1 min isothermal), heating rate 3 °C/min to 310 °C (held for 30 min) and injection temperature from 50 to 300 °C at a rate of 10 °C/s. Helium was used as carrier gas with a constant flow of 1 ml min^{-1}. The mass spectrometer operated in the electron impact mode at 70 eV. Full-scan mass spectra were recorded from m/z 50–650 at a scan rate of 1.5 scans s^{-1}. The measurement of GDGTs were performed with a Shimadzu LC20AD HPLC instrument coupled to a Finnigan TSQ 7000 triple quadrupole MS with an atmospheric pressure chemical ionization (APCI) interface following a method described by *Schouten et al.* [2007].

Results

In the SMTZ, the concentrations of archaeal lipids (archaeol and isoprenoid glycerol dialkyl glycerol tetraether, iGDGTs) and bacterial lipids (branched GDGTs and phospholipid fatty acids, PLFAs) were in the lower range typically observed in subsurface sediments (ng g^{-1} sediment for ether lipids and µg g^{-1} for PLFAs) [*Bischoff et al.*, 2014]. These reflect globally observed cell abundances in the subsurface that can be very low beneath 10 mbsf (10^3 to 10^8 per cm^3) [*Kallmeyer et al.*, 2012]. Unfortunately, concentrations were too low to determine $\delta^{13}C$ isotope values of specific lipids. Nevertheless, the ratio of archaeal (archaeol + isoprenoid GDGTs) ether lipids to bacterial branched GDGT showed almost exclusively archaeal lipids in the SMTZ, whereas ratios in layers above the SMTZ showed significantly lower ratios (Fig. B-9). Moreover, we detected some PLFAs such as $C_{16:1\omega7c}$, $C_{18:1\omega9}$ and $C_{18:1\omega7c}$ in significant proportions (2.64 to 10.7%, Table B-7) that have been shown to be related to bacteria involved in or influenced by AOM processes in coastal wetlands and grasslands [*Bannert et al.*, 2012; *Segarra et al.*, 2015]. However, the concentrations of these specific PLFAs were also too low to determine their carbon isotope signature.

Discussion

The absence of PLFAs such $C_{16:1\omega5}$, cy$C_{17:0\omega5,6}$ and $C_{17:1\omega6c}$ (Table B-7) known to represent *Desulfosarcina/Desulfococcus* SRB in AOM consortia of methane seep sediments [*Elvert et al.*, 2003] can be explained by a low biomass typical for such deep habitats. Alternatively, the seep-associated *Desulfobacterium anilini*-group may have a different lipid biomarker pattern or unknown bacterial partner are associated with ANMEs at submarine permafrost thaw fronts. The presence and partly enrichment of PLFAs $C_{16:1\omega7c}$, $C_{18:1\omega9}$ and $C_{18:1\omega7c}$ (Table B-7), which were shown to be related to AOM in peatland environments [*Bannert et al.*, 2012; *Segarra et al.*, 2015], likely reflect other SRB communities responsible in this untypical SMTZ in deep submarine permafrost.

The ether-lipid ratios of the SMTZ were untypical for permafrost (Fig. B-9), since analyses of terrestrial and lacustrine permafrost showed most of the time higher concentrations for branched GDGTs over archaeol and isoprenoid GDGTs in the same sediment horizons [*Bischoff et al.*, 2014; *Stapel et al.*, 2016].

Figures

Figure B-1: Phylogenetic affiliation of ANME sequences based on 16S rRNA. Sequences in bold represent OTUs from the Illumina sequencing and clone library sequences. *Methanopyrus kandleri* was used as outgroup. The scale bar represents 10 percent sequence divergence.

This figure was provided as separate .pdf file.

Figure B-2: Phylogenetic affiliation of archaeal sequences based on 16S rRNA. Sequences in bold represent OTUs from the Illumina sequencing and clone library sequences. *Escherichia coli* was used as outgroup. The scale bar represents 10 percent sequence divergence.

This figure was provided as separate .pdf file.

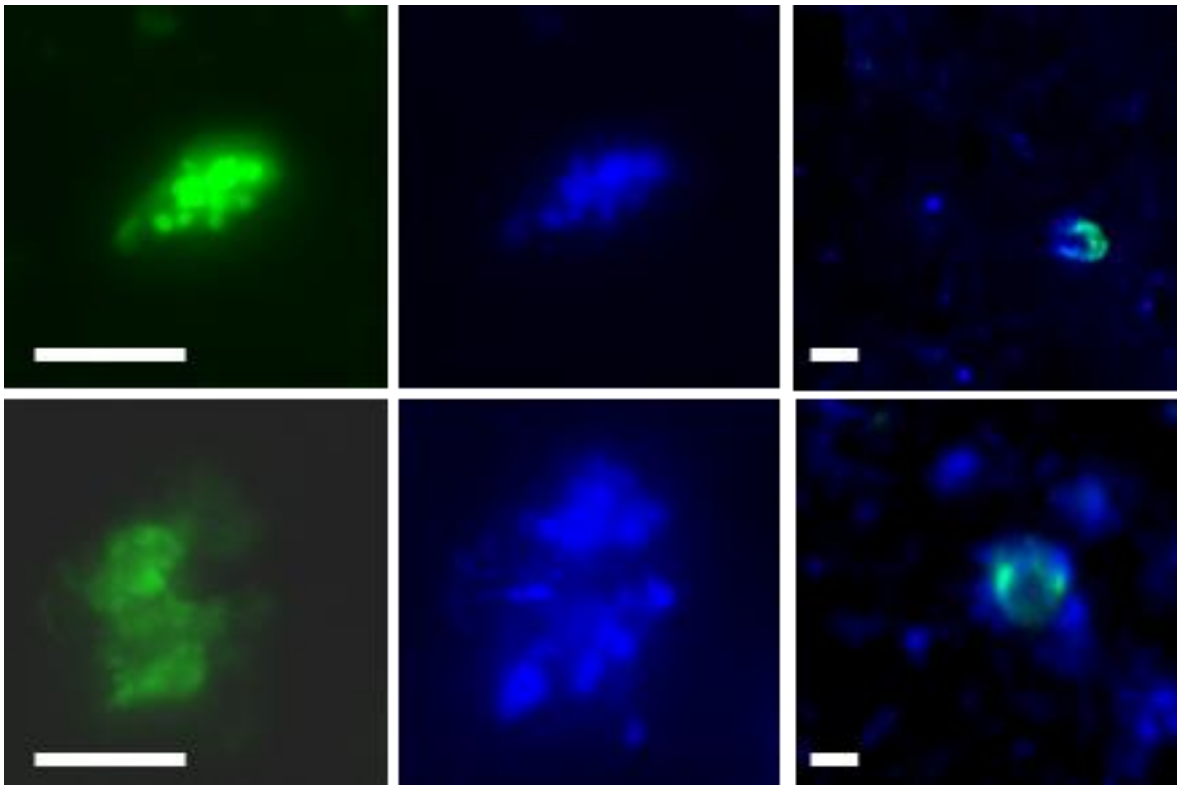

Figure B-3: Micrographs of ANME-2a consortia at the SMTZ of submarine permafrost core BK2. Anaerobic methanotrophic cells of the 2a clade were detected by CARD-FISH (probe: ANME-2a-647 - green) first column and corresponding counterstaining with DAPI (blue) second column. The third column shows overlays of ANME-2a (green) and DAPI (blue). The scale bar represents 5 µm. The first two image columns were created by Picolay (http://www.picolay.de/, © Herbiert Cypionka)

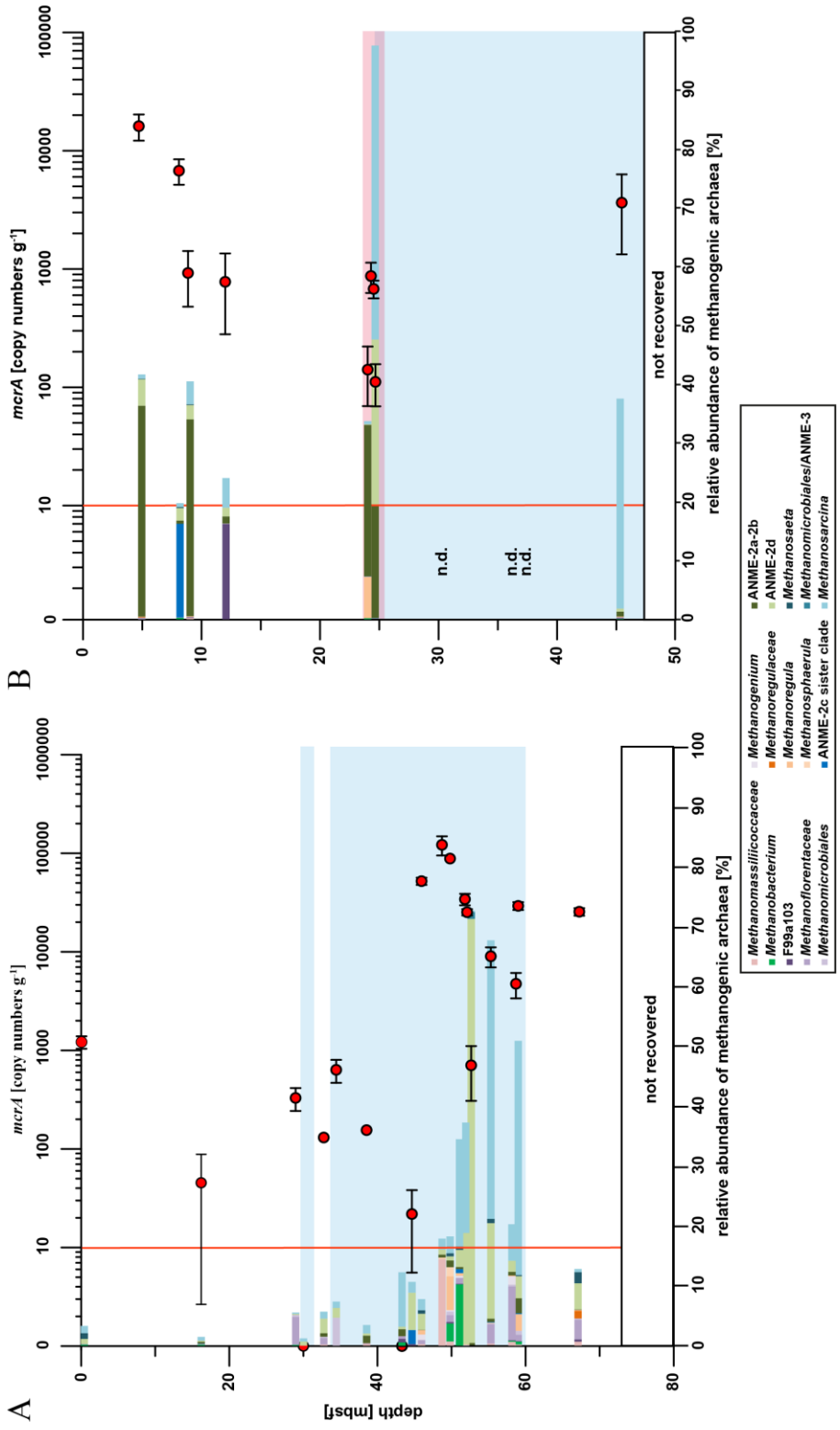

Figure B-4: Methanogenic/ANME communities of core C2 (A) and BK2 (B). Red circles show *mcrA* copy numbers per gram sediment wet weight as detected by quantitative PCR. The red line represents the detection limit of the qPCR related to the lowest standard. Bar charts show relative abundance of archaeal 16S rRNA sequences related to known methanogenic and methanotrophic archaea. The blue shaded area represents ice-bonded permafrost, the red area the SMTZ. All uncolored areas of the plots correspond to unfrozen submarine permafrost and marine sediments. n. d. - no detection.

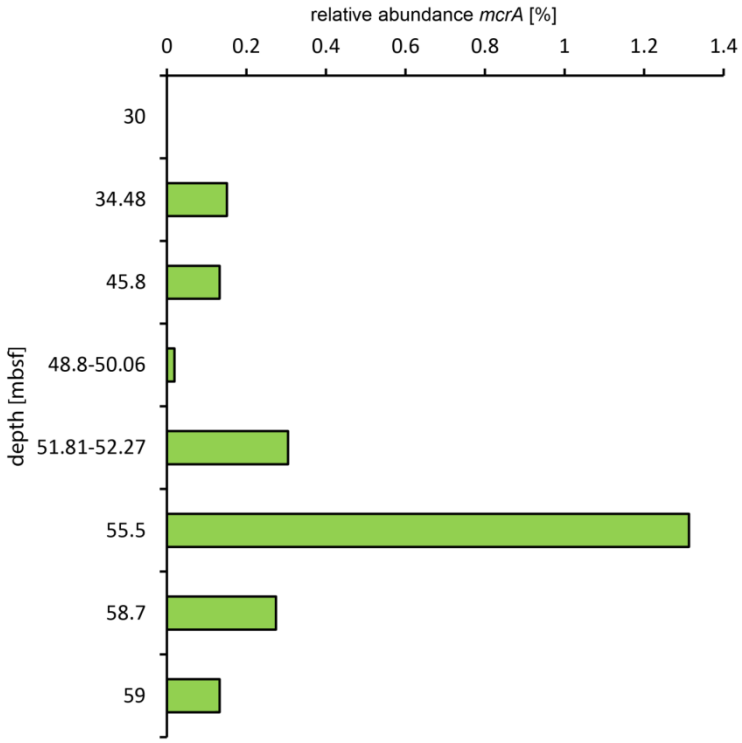

Figure B-5: Relative abundance of ANME-2d-related *mcrA* sequences in submarine core C2. *McrA* sequences are based on 454 sequencing.

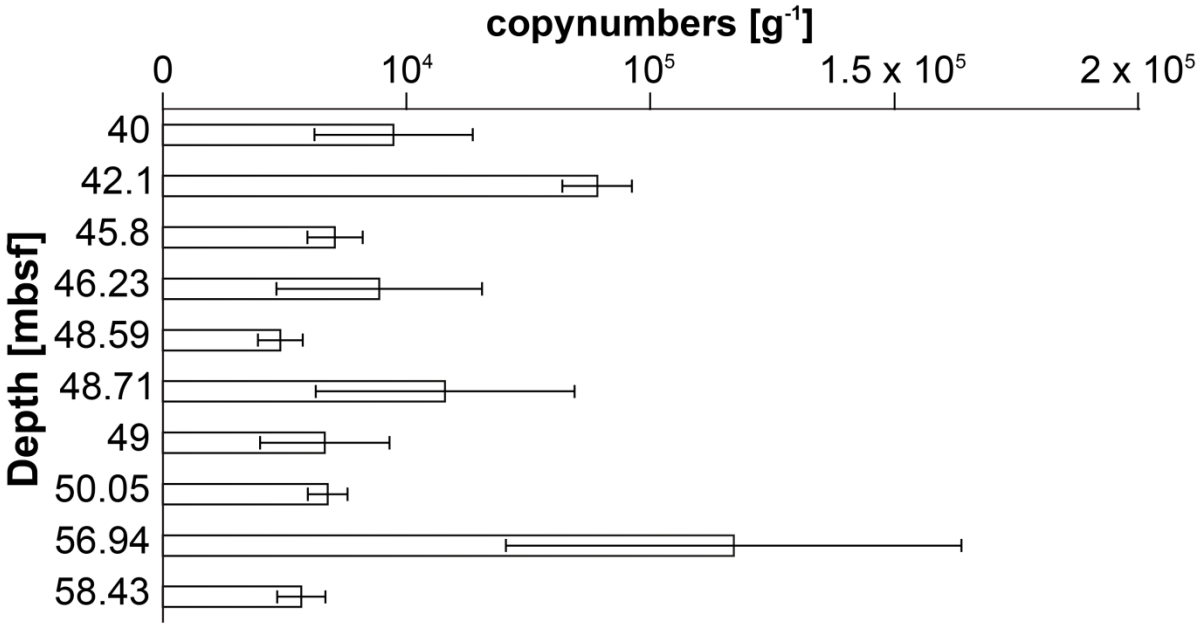

Figure B-6: ANME-2d specific *mcrA* copy numbers of core C2. The sampling scheme along the depth is not identical for the *mcrA* quantification and the next-generation sequencing.

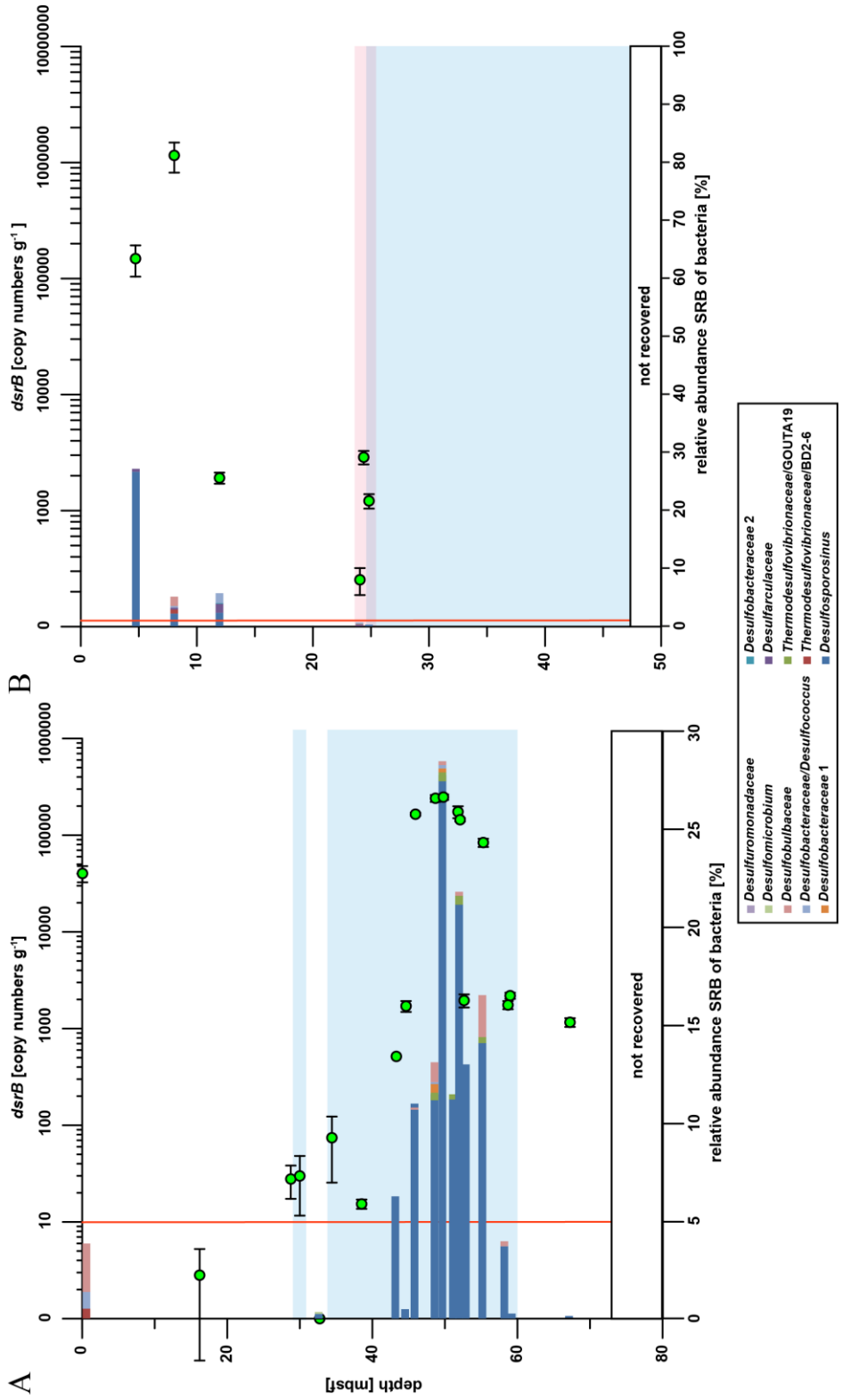

Figure B-7: Sulfate-reducing bacteria of core C2 (A) and BK2 (B). Green circles show *dsrB* copy numbers per gram sediment wet weight as detected by quantitative PCR. The red line represents the detection limit of the qPCR related to the lowest standard. Bar charts show relative abundance of bacterial 16S rRNA sequences related to known sulfate reducers. The blue shaded areas represent ice-bonded permafrost and the red area the SMTZ. All uncolored areas of the plots correspond to unfrozen (ice-free) submarine permafrost and marine sediments.

Figure B-8: Phylogenetic reconstruction of 16S rRNA sequences related to sulfate-reducing bacteria. Operational taxonomic units belonging to the upper part of the SMTZ are shown in bold-red, of the lower part in bold-blue and all other submarine permafrost in bold-black. The scale bar represents 10% sequence divergence. The colored boxes highlight cluster of SRB in submarine permafrost.

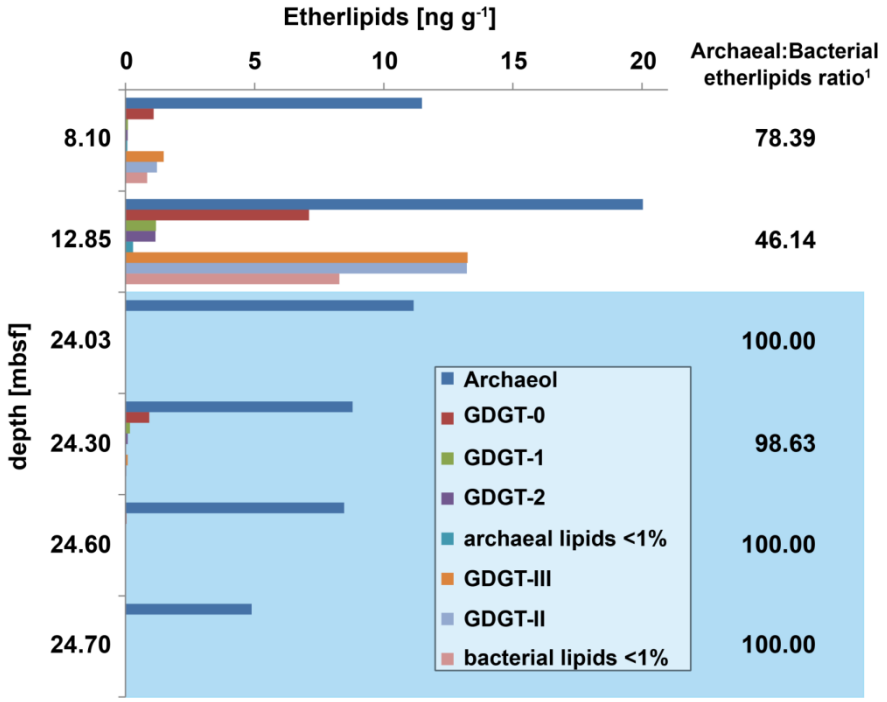

Figure B-9: Concentrations of archaeal and bacterial ether-lipids in submarine permafrost core BK2. The upper two samples represent marine-influenced submarine permafrost layers. While the lower four samples represent SMTZ layers (light blure rectangle). Ratios of total archaeal vs. total bacterial ether-lipids for each sediment horizon are shown on the right side.

[1] Calculation of ratio (total archaeal ether lipids/(total archaeal + bacterial ether lipids)*100), whereas total archaeal ether lipids comprise archaeol and isoprenoid glycerol dialkyl glycerol tetraethers with non to 2 cyclopentyl rings (GDGT-0 to 2). Bacterial ether lipids represent branched GDGT-II and –III, for structures see [*Weijers et al.*, 2011].

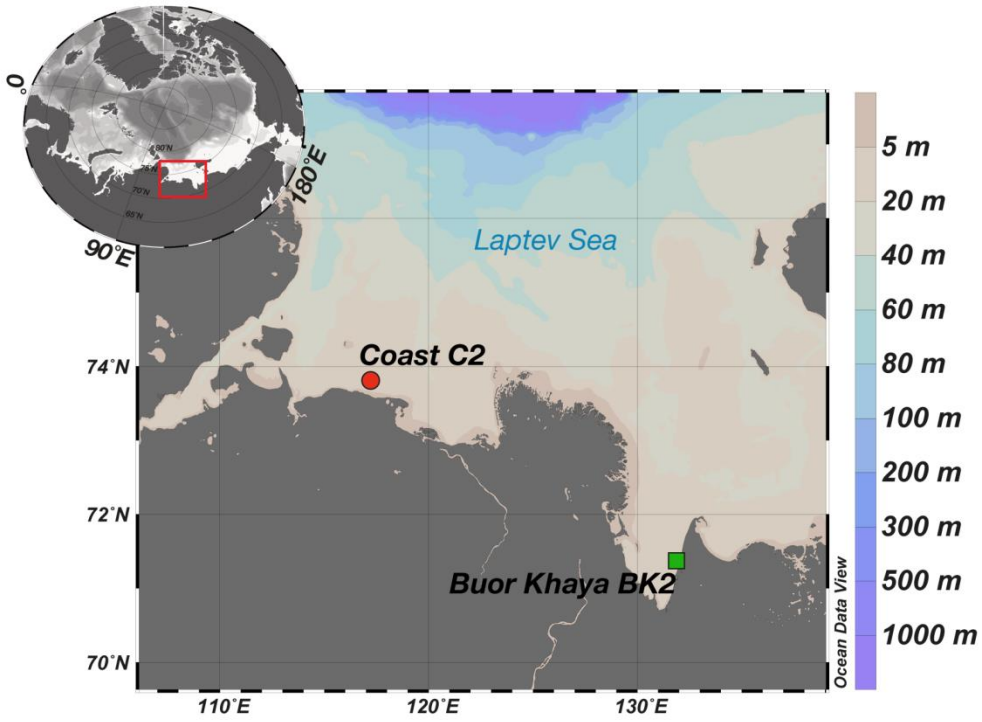

Figure B-10: Geographical location of sampling sites. Globe in the upper left corner shows the arctic region with the red rectangle showing the large map. Large map shows the geographical locations of the submarine permafrost cores C2 (red dot) and BK2 (green square) with ocean depth in meter according to the color code on the right-hand side. The map was produced with the free software Ocean Data View version 4.7.8 (Schlitzer, R., Ocean Data View, odv.awi.de, 2017).

Tables

Table B-1: Relative abundance of archaeal sequences in both submarine permafrost cores C2 and BK2.

This table was provided as separate .pdf file.

Table B-2: Characteristics of submarine permafrost cores

	Mamontov Klyk (C2)	Buor Khaya (BK2)
number of samples	18	10 (for DNA), 6 (for lipid analysis)
estimate time of inundation [years]	~2,500	~540
maximum depth [m bsl]	77	51.7
water depth [m]	6	4.3
sea ice cover [m]	1.35	2.09
permafrost boundary [mbsf]	29.5	24.45
mean temperature [°C]	-1.2±0.2	-0.5±0.4
distance to coast [km]	11.5	0.8
latitude	73° 36' 21.5" N	71° 25' 20.3" N
longitude	117° 10' 01.1" E	132° 05' 05.3" E

Table B-3: Statistics of sequence analysis pipeline and representative taxa.

Sample site	Depth [m]	Raw reads	Quality reads	Observed $OTU_{0.03}$	Inverse Simpson	Shannon	Most frequent class*	Most frequent order*
Mamontov Klyk	0.50	266,820	245,919	85	11.94	3.24	unknown *Thaumarchaeota*	*Nitrosopumilus*
	18.00	97,307	92,379	44	4.26	1.97	unknown *Bathyarchaeota*	MCG-6
	29.00	159,157	146,155	63	2.72	1.97	*Diaforarchaea*	DSPEG-I
	30.00	199,727	189,569	38	2.00	1.49	*Diaforarchaea*	DSPEG-I
	33.00	72,724	68,147	52	2.97	1.99	*Diaforarchaea*	DSPEG-I
	34.43	115,192	105,217	44	2.45	1.77	*Diaforarchaea*	DSPEG-I
	38.53	170,804	161,167	45	1.82	1.25	*Diaforarchaea*	DSPEG-I
	43.31	213,945	141,103	51	3.27	2.07	*Diaforarchaea*	DSPEG-I
	44.65	182,186	162,813	59	2.38	1.84	*Diaforarchaea*	DSPEG-I
	45.80	286,328	258,712	64	4.63	2.35	*Nitrosospheria*	*Nitrososphaerales*
	48.71	130,327	126,630	25	3.29	1.58	unknown *Bathyarchaeota*	MCG-6
	50.06	132,523	83,306	84	9.21	3.12	unknown *Bathyarchaeota*	MCG-6
	51.81	151,919	125,190	84	8.21	2.79	unknown *Bathyarchaeota*	MCG-6
	52.27	325,097	307,942	53	4.53	2.32	unknown *Bathyarchaeota*	MCG-6
	52.69	269,218	258,031	27	4.05	1.91	*Methanomicrobia*	*Methanosarcinales* (ANME2d)
	55.55	127,461	121,361	56	3.99	2.13	*Methanomicrobia*	*Methanosarcinales* (*Methanosarcina*)
	58.70	159,324	145,886	78	8.53	2.88	*Diaforarchaea*	DSPEG-I
	59.00	145,000	132,862	85	6.95	2.90	*Methanomicrobia*	*Methanosarcinales* (*Methanosarcina*)
	67.00	285,525	262,655	78	4.59	2.50	unknown *Bathyarchaeota*	MCG-8
Buor Khaya	4.72	94,240	84,493	69	5.67	2.42	*Methanomicrobia*	*Methanosarcinales* (ANME2a-b)
	8.10	71,752	61,673	69	6.01	2.51	unknown *Bathyarchaeota*	MCG-8
	8.86	265,732	246,799	62	4.25	2.13	unknown *Bathyarchaeota*	MCG-8
	12.00	148,222	129,665	99	5.33	2.73	unknown *Bathyarchaeota*	MCG-8
	24.03-24.30	85,366	81,216	47	6.95	2.52	unknown *Bathyarchaeota*	MCG-8
	24.53-24.68	136,400	131,025	32	3.64	1.76	*Methanomicrobia*	*Methanosarcinales* (*Methanosarcina*)
	30.31	n.d.	n.d.	n.d.	n.d.	n.d.	n.d.	n.d.
	36.23	n.d.	n.d.	n.d.	n.d.	n.d.	n.d.	n.d.
	37.41	n.d.	n.d.	n.d.	n.d.	n.d.	n.d.	n.d.
	45.46	249,600	233,141	35	3.38	1.68	*Diaforarchaea*	DSPEG-I

***** Based on relative abundance of 16S rRNA sequences

n.d. not detected

Table B-4: Oligonucleotides primer and probes used in this study.

Target gene	Primers	Sequence (5'-3')	Size [bp]	T (°C)	FA [%]	No. of PCR Cycles	Reference
Sequencing Illumina MiSeq							
Bacteria 16S rRNA	S-D-Bact-0341-b-S-17	CCT ACG GGA GGC AGC AG	464	55		30	(Muyzer et al., 1993)
	S-D-Bact-0785-a-A-21	GAC TAC HVG GGT ATC TAA TCC					(Herlemann et al., 2011)
Archaea 16S rRNA	D-Arch-0020-a-S-19	TTC CGG TTG ATC CYG CCR G	956	55		40	(Massana et al., 1997)
	S-D-Arch-0958-a-A-19	YCC GGC GTT GAV TCC AAT T					(DeLong, 1992)
Archaea 16S rRNA	S-D-Arch-0349-a-S-17	GYG CAS CAG KCG MGA AW	457	56		35	(Takai et al., 2000)
	S-D-Arch-0786-a-A-20	GGA CTA CVS GGG TAT CTA AT					
Sequencing 454/ quantitative PCR							
Methanogens and ANME	mlas	GGT GGT GTM GGD TTC ACM CAR TA	469	65-50 (touchdown)/ 55 (final); 57 (qPCR)		15/ 15; 40 (qPCR)	(Steinberg & Regan, 2008)
	mcrA-rev	CGT TCA TBG CGT AGT TVG GRT AGT					
quantitative PCR							
sulfate-reducing *Bacteria*	DSRp2060F	CAA CAT CGT YCA YAC CCA GGG	350	60		40	(Geets et al., 2006)
	DSR4R	GTG TAG CAG TTA CCG CA					(M. Wagner et al., 1998)
ANME-2d	*mcrA*159F	AAA GTG CGG AGC AGC AAT CAC C	186	60		40	(Vaksmaa et al., 2017)
	*mcrA*345R	TCG TCC CAT TCC TGC TGC ATT GC					
16S rRNA clone libraries							
Archaea 16S rRNA	S-D-Arch-0008-a-S-16	TCC GGT TGA TCC TGC C	638	59		30	(Andreas Teske et al., 2002)
ANME-2a 16S rRNA	ANME-2a-647	TCT TCC GGT CCC AAG CCT					(Katrin Knittel et al., 2005)
16S rRNA probes							
ANME-2a	ANME-2a-647	TCT TCC GGT CCC AAG CCT			50		(Katrin Knittel et al., 2005)
Desulfosarcina-Desulfococcus	DSS658	TCC ACT TCC CTC TCC CAT			50		(Manz et al., 1998)

Table B-5: Barcode sequences for Illumina MiSeq sequencing used in this study.

Barcode_ID	Barcode sequence
00	ACACGT
01	ACGTAC
02	ACTGCA
03	AGAGTC
04	AGCTGA
05	AGTCAG
06	ATATCG
07	ATCGAT
08	ATGCTA
09	CACAGT
10	CGATAT
11	CATGAC
12	GACTAG
13	GAGATC
14	GATCGA
15	TATACG
16	TCTCTC
17	TGCATG
18	TGACGT
19	TGTGAC

Table B-6: Barcode sequences of 454 sequencing used in this study.

MID_ID	MID sequence
MID-01	ACGAGTGCGT
MID-02	ACGCTCGACA
MID-03	AGACGCACTC
MID-04	AGCACTGTAG
MID-05	ATCAGACACG
MID-06	ATATCGCGAG
MID-07	CGTGTCTCTA
MID-08	CTCGCGTGTC
MID-11	TGATACGTCT
MID-13	CATAGTAGTG
MID-14	CGAGAGATAC
MID-15	ATACGACGTA
MID-16	TCACGTACTA
MID-17	CGTCTAGTAC
MID-18	TCTACGTAGC
MID-20	ACGACTACAG

Table B-7: Percentage proportion of phospholipid fatty acids (PLFAs) in different depths of the submarine permafrost core BK2.

	depth [m bsf]					
PLFAs [%]	**8.10**	**12.85**	**24.03**	**24.30**	**24.60**	**24.70**
12:0	1.29	1.36	2.71	1.93	1.49	1.07
***iso*14:0**	1.20	0	0	0	0	0
14:0	4.20	3.06	4.61	2.94	4.19	1.86
***iso*15:0**	4.83	1.75	0.89	0.55	1.45	1.86
***ai*15:0**	7.27	1.92	1.31	0.95	1.32	1.15
15:0	1.90	1.87	2.12	1.26	1.92	1.12
***iso*16:0**	1.15	0.77	0	0	0	0
16:1ω7c	7.94	1.73	3.53	3.15	2.64	4.13
16:1ω5	1.73	0	0	0	0	0
16:0	26.30	27.86	32.26	31.21	32.00	30.72
10Me-16:0	1.08	0.00	0.00	0	0	0
***iso*17:0**	0.63	0	0	0	0	0
***ai*17:0**	0.99	1.52	3.67	0	0	1.35
***cy*17:0ω7,8**	1.73	0.00	0	0	0	0
17:0	1.78	2.85	2.02	2.03	2.04	1.32
18:2ω9,12	2.02	2.54	0	0	0	0
18:1ω9	4.77	6.39	10.73	8.62	9.44	3.23
18:1ω7c	10.54	3.25	5.38	8.62	4.94	4.54
18:0	18.66	43.13	30.78	38.73	38.58	47.63

Blue shaded area represents SMTZ sediment layers.

C. Appendix Manuscript III

Supporting Information manuscript III

Figures

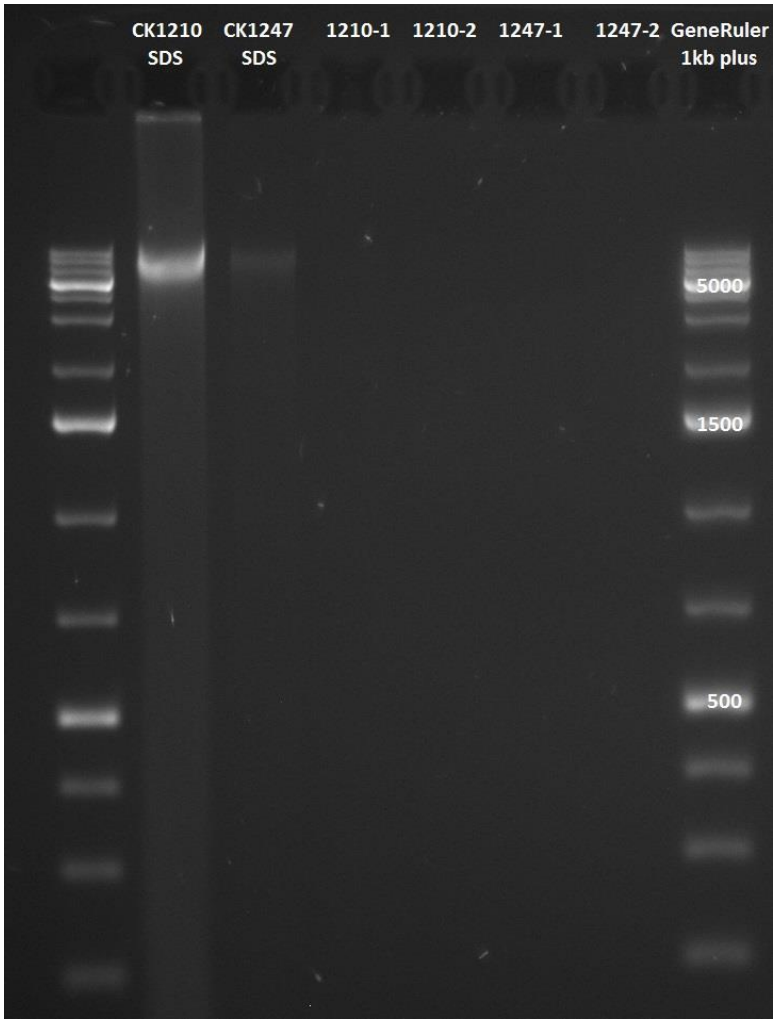

Figure C-1: Quality control of the extracted genomic DNA, exemplarily shown for two samples from core C2 (CK1210 SDS: 0.05 m bsf, 265 ng/g and CK1247 SDS: 52.7 m bsf, 33.4 ng/g). The examples show that there is not much fragmentation likely due to constantly freeze-locked conditions. Hence, we used the DNA extracts without gel purification for downstream analyses.

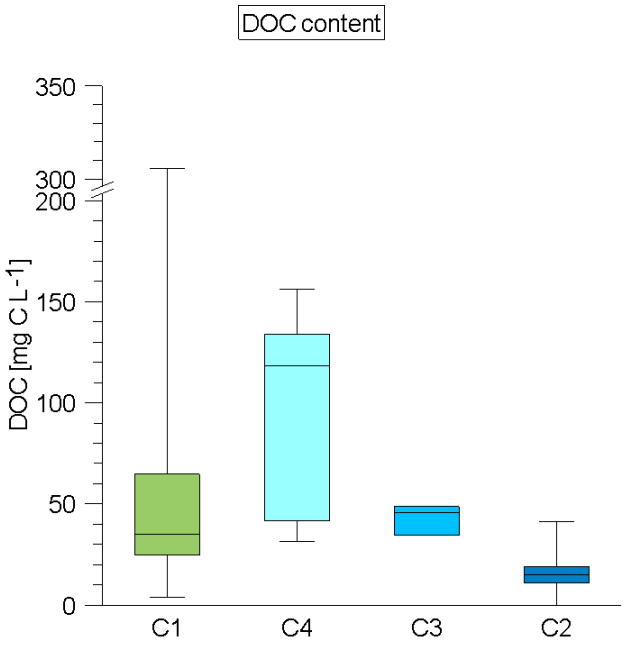

Figure C-2: Boxplot of DOC concentrations of Unit II in mg C L^{-1}. Median lines are indicated within the boxes of which the size corresponds to±25% of the data, whereas the whiskers show the minimum and maximum of all data. C1: n=74, C4: n=5, C3: n=3, C2: n =12.

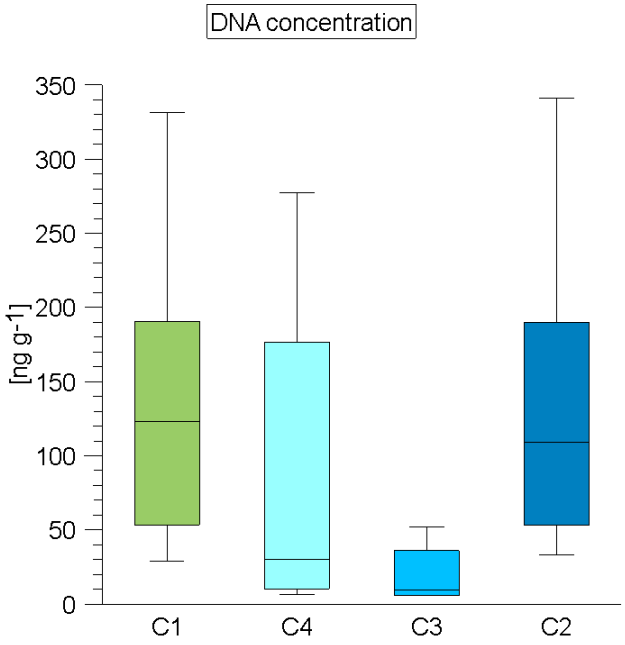

Figure C-3: DNA concentrations in ng g^{-1} sediment wet weight of the cores C1, C4, C3 and C2. Box plots contain the mean values of all samples, obtained from two technical replicates each. Median lines are indicated within the boxes of which the size corresponds to ± 25% of the data, whereas the whiskers show the minimum and maximum of all data. C1, C4 and C3: n=6, C2: n=17.

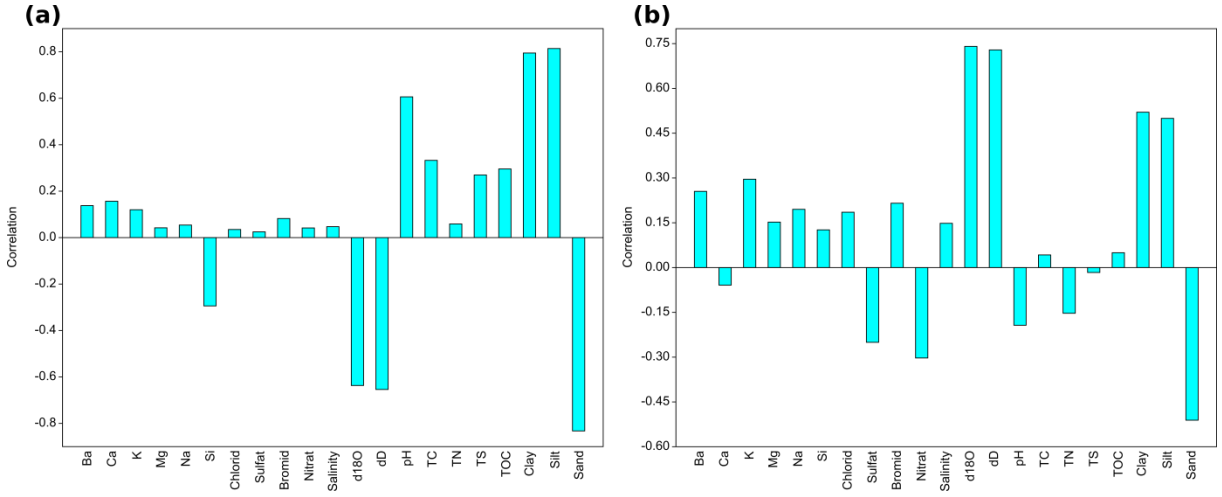

Figure C-4: Loadings plots belonging to Figure 6-1: PCA of environmental, sedimentological and pore water data from Unit II. Shown are the correlations to a) PC1 and b) PC2 which were used to choose the physicochemical factors that are mainly responsible for the variance between samples in the PCA.

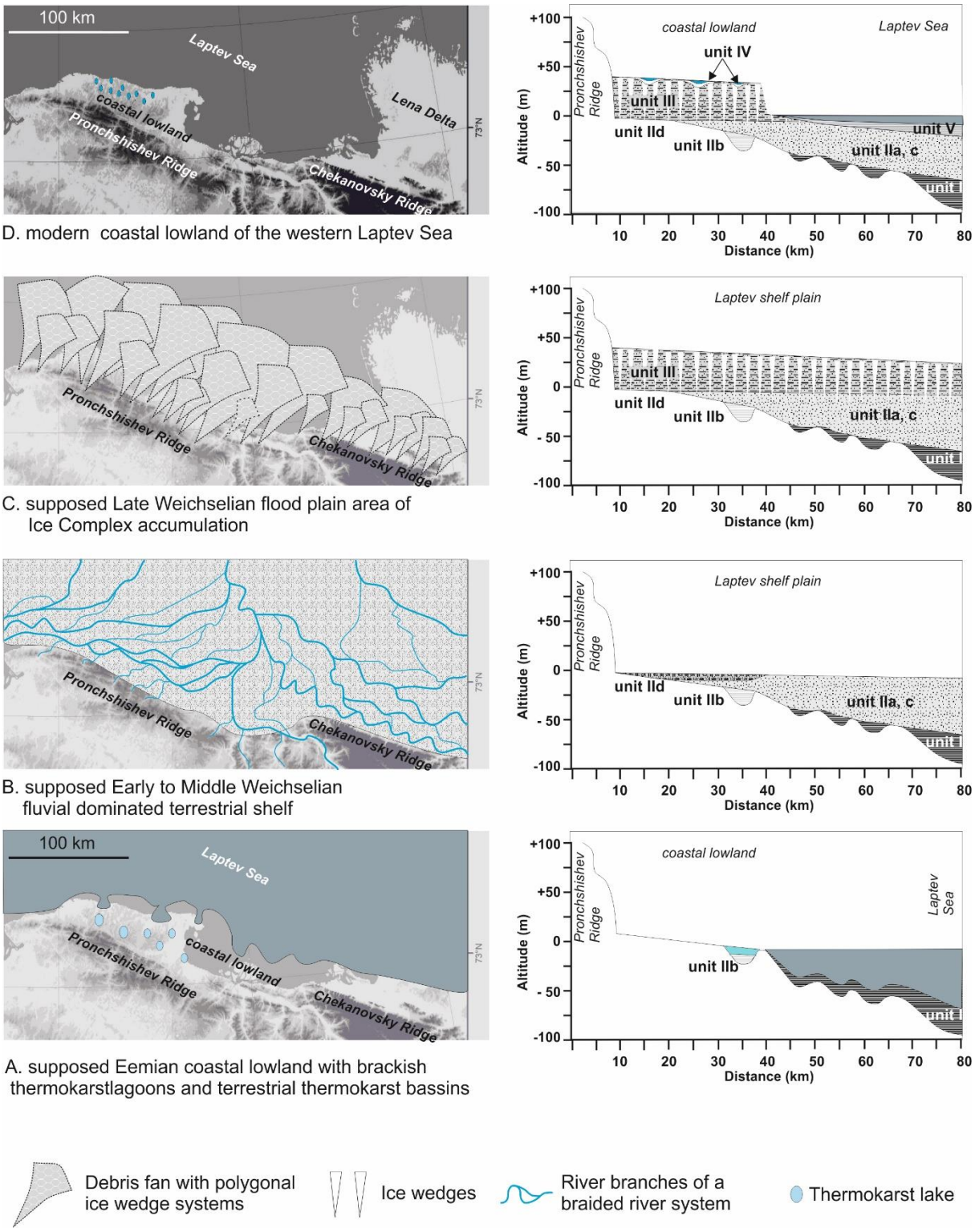

Figure C-5: Schematic representation of the late Quaternary landscape dynamics in the western Laptev Sea coastal region and formation of the sediments units (modified after *Winterfeld et al.* [2011]).

Tables

Table C-1: Site description of each borehole location. Mbsf stands for meters below seafloor and dedicates the depth in the submarine cores (C4, C3, C2), while mbs stands for meters below surface and is used for depth indication in the terrestrial core C1.

	C1	C4	C3	C2
Distance to coast [km]	0.1	1.0	3.0	11.5
Water depth [m]	-	2.2	4.4	6.0
Frost table depth [mbsf]	0.0	1.7	7.6	29.0
Upper boundary of Unit II [mbs/mbsf]	22.0	13.3	8.6	35.0
Lower boundary of Unit II	61.0	29.8	27.1	58.5
Uppermost sample depth [mbs/mbsf]	27.3	13.3	8.6	38.5
Lowermost sample depth	44.3	29.8	24.9	58.4

Table C-2: Minimum, maximum and mean values of environmental factors in Unit II significantly contributing to the bacterial community composition and microbial abundance.

	Core	Minimum	Maximum	Mean	n
Temperature [°C]	C1	-12.5	-12.4	-12.4	8
	C4	-7.1	-5.8	-6.4	4
	C3	-1.8	-1.2	-1.4	4
	C2	-1.6	-1.5	-1.5	4
Salinity [PSU]	C1	0.0	1.6	0.5	184
	C4	0.9	17.6	5.6	10
	C3	0.5	3.7	1.0	38
	C2	0.0	12.5	0.8	67
$\delta^{18}O$ [(‰) vs. SMOW]	C1	-30.8	-14.9	-22.3	184
	C4	-27.7	-18.8	-22.8	10
	C3	-20.6	-19.1	-20.1	38
	C2	-30.0	20.2	-27.6	67
δD [(‰) vs. SMOW]	C1	-241.8	-115.7	-177.2	184
	C4	-219.1	-144.0	-178.8	10
	C3	-162.9	-149.4	-158.4	38
	C2	-232.7	-156.8	-213.3	67

Table C-3: Geochemical, pore water and environmental data of all samples at each drill site.

This table was provided as separate .pdf file.

Table C-4: Sample names of the molecular samples, their depth relative to sea level (meters below sea level, m bsl), relative to surface (meters below surface (m bs) in the terrestrial core and meters below seafloor (m bsf) in the submarine cores), and their corresponding lithology.

Sample Name	Depth [m bsl]	Depth [m bs/ m bsf]	Lithology
C1-1	1.3	27.3	sandy
C1-2	9.9	35.9	sandy
C1-3	12.1	38.1	sandy
C1-4	17.2	43.2	plant/wood detritus
C1-5	17.4	43.4	plant/wood detritus
C1-6	18.4	44.4	plant/wood detritus
C4-1	15.5	13.3	plant/wood detritus
C4-2	22.0	19.8	small peat inclusions
C4-3	25.0	22.8	small peat inclusions
C4-4	28.5	26.3	sandy with quartz gravel
C4-5	30.0	27.8	sandy with quartz gravel
C4-6	32.0	29.8	sandy with quartz gravel
C3-1	13.0	8.6	small peat inclusions
C3-2	16.0	11.6	small peat inclusions
C3-3	19.0	14.6	small peat inclusions
C3-4	21.5	17.1	sandy
C3-5	24.6	20.2	sandy
C3-6	29.2	24.8	sandy
CK1232	44.5	38.5	
C2-1	46.0	40.0	sandy
C2-2	48.1	42.1	sandy
CK1235	49.3	43.3	
CK1236	50.7	44.7	
CK1237	51.8	45.8	
C2-4	52.2	46.2	sandy
C2-5	54.6	48.6	plant/wood detritus
CK 1241	54.7	48.7	
C2-7	55.0	49.0	plant/wood detritus
C2-8/1244	56.1	50.1	plant/wood detritus
CK1245	57.8	51.8	
CK1246	58.2	52.2	
CK1247	58.7	52.7	
CK1248	61.6	55.6	
C2-9	62.9	56.9	plant/wood detritus
C2-10	64.4	58.4	sandy silt

Table C-5: Oligonucleotide primers for Illumina MiSeq sequencing and quantitative PCR.

Target	Primer Sets	Primer Sequence 5'-3'	Size bp	T (°C)	No. of PCR Cycles	References
		Illumina MiSeq sequencing				
Bacterial 16S rRNA	S-D-Bact-0341-b-S-17	CCT ACG GGA GGC AGC AG	464	55	35	(Muyzer et al., 1993)
	S-D-Bact-0785-a-A-21	GAC TAC HVG GGT ATC TAA TCC				(Herlemann et al., 2011)
		Quantitative PCR				
Bacterial 16S rRNA	S-D-Bact-0341-b-S-17	CCT ACG GGA GGC AGC AG	193	55.7	40	(Muyzer et al., 1993)
	S-D-Bact-0517-a-A-18	ATT ACC GCG GCT GCT GG				(Muyzer et al., 1993)

Table C-6: Barcode sequences for Illumina MiSeq sequencing.

Barcode ID Forward Primer	Barcode Sequence	Barcode ID Reverse Primer	Barcode Sequence
Bac-01-For	ACGAGTGCGT	Bac-01-Rev	ACGAGTGCGT
Bac-02-For	ACGCTCGACA	Bac-02-Rev	ACGCTCGACA
Bac-03-For	AGACGCACT	Bac-04-Rev	AGCACTGTAG
Bac-06-For	ATATCGCGAG	Bac-05-Rev	ATCAGACACG
Bac-07-For	CGTGTCTCTA	Bac-06-Rev	ATATCGCGAG
Bac-08-For	CTCGCGTGT	Bac-07-Rev	CGTGTCTCTA
Bac-11-For	TGATACGTCT	Bac-08-Rev	CTCGCGTGTC
Bac-13-For	CATAGTAGTG	Bac-11-Rev	TGATACGTCT
Bac-15-For	ATACGACGTA	Bac-13-Rev	CATAGTAGTG
Bac-16-For	TCACGTACTA	Bac-14-Rev	CGAGAGATAC
Bac-17-For	CGTCTAGTA	Bac-17-Rev	CGTCTAGTAC
Bac-19-For	TGTACTACT	Bac-18-Rev	TCTACGTAGC
Bac-23-For	TACTCTCGTG	Bac-19-Rev	TGTACTACTC
Bac-24-For	TAGAGACGAG	Bac-22-Rev	TACGAGTATG
Bac-25-For	TCGTCGCTCG	Bac-23-Rev	TACTCTCGTG
Bac-26-For	ACATACGCGT	Bac-24-Rev	TAGAGACGAG
Bac-27-For	ACGCGAGTAT	Bac-25-Rev	TCGTCGCTCG
Bac-28-For	ACTACTATGT	Bac-26-Rev	ACATACGCGT
Bac-31-For	AGCGTCGTCT	Bac-28-Rev	ACTACTATGT
Bac-33-For	ATAGAGTACT	Bac-30-Rev	AGACTATACT
Bac-34-For	CACGCTACGT	Bac-31-Rev	AGCGTCGTCT
Bac-35-For	CAGTAGACGT	Bac-33-Rev	ATAGAGTACT
Bac-36-For	CGACGTGACT	Bac-34-Rev	CACGCTACGT
Bac-38-For	TACACGTGAT	Bac-35-Rev	CAGTAGACGT
Bac-39-For	TACAGATCGT	Bac-36-Rev	CGACGTGACT
Bac-40-For	TACGCTGTCT	Bac-37-Rev	TACACACACT
Bac-41-For	TAGTGTAGAT	Bac-38-Rev	TACACGTGAT
Bac-42-For	TCGATCACGT	Bac-39-Rev	TACAGATCGT
Bac-44-For	TCTAGCGACT	Bac-40-Rev	TACGCTGTCT

Bac-45-For	TCTATACTAT	Bac-41-Rev	TAGTGTAGAT
Bac-49-For	ACGCGATCGA	Bac-44-Rev	TCTAGCGACT
Bac-50-For	ACTAGCAGTA	Bac-45-Rev	TCTATACTAT
		Bac-46-Rev	TGACGTATGT
		Bac-49-Rev	ACGCGATCGA
SfiA-MW00	ACACGT	SfiB-MW10	CAGTCA
SfiA-MW01	ACGTAC	SfiB-MW11	CATGAC
SfiA-MW02	ACTGCA	SfiB-MW12	GACTAG
SfiA-MW02	ACTGCA	SfiB-MW13	GAGATC
SfiA-MW03	AGAGTC	SfiB-MW14	GATCGA
SfiA-MW04	AGCTGA	SfiB-MW14	GATCGA
SfiA-MW05	AGTCAG	SfiB-MW15	GTACAC
SfiA-MW06	ATATCG	SfiB-MW15	GTACAC
SfiA-MW07	ATCGAT	SfiB-MW16	GTCACA
		SfiB-MW17	GTGTGT
		SfiB-MW18	TCAGAG
		SfiB-MW19	TCGAGA

Table C-7: Overview of sequencing reads: number of reads after the removal of singletons, number of reads that were removed when the background filter of 0.5% was applied, number of reads representing chloroplast, mitochondrial and archaeal taxa and finally the number of quality reads after the application of all filters. Critical samples with less than 15.000 raw reads are shaded red. Critical samples where the relative abundances within duplicates are comparable are colored light red. The dark red colored sample was not used for the calculation of the mean relative abundance as the relative abundances within duplicates differed.

	Raw reads	Background Reads (0.5%)	Chloro-plast	Mitochondrial Taxa	Archaeal taxa	Quality reads
C1-1a	74760	20214	0	0	0	54546
C1-1b	89992	22879	0	0	0	67113
C1-2a	23789	15150	0	0	0	8639
C1-2b	25100	16330	0	0	0	8770
C1-3a	41727	24707	0	0	0	17020
C1-3b	8666	5185	0	0	0	3481
C1-4a	31071	22620	0	0	0	8451
C1-4b	5142	3761	0	0	0	1381
C1-5a	208578	100128	0	0	0	108450
C1-5b	147753	69180	0	0	0	78573
C1-6a	244866	100302	0	0	1790	142774
C1-6b	255535	113256	0	0	6331	135948
C4-1a	231425	70205	0	0	0	161220
C4-1b	103692	30996	0	0	0	72696
C4-2a	312930	64767	0	0	0	248163
C4-2b	18603	2840	0	0	0	15763

C4-3a	269853	99103	1765	0	0	168985
C4-3b	94463	33930	0	0	0	60533
C4-4a	170018	49851	0	0	1050	119117
C4-4b	180556	52147	0	0	0	128409
C4-5a	9823	4402	0	0	0	5421
C4-5b	17374	7566	0	0	0	9808
C4-6a	56201	23871	0	0	0	32330
C4-6b	20949	8951	0	0	0	11998
C3-1a	52885	27176	0	0	588	25121
C3-1b	180772	94154	1165	0	2402	83051
C3-2a	35528	13955	0	0	1511	20062
C3-2b	102122	39090	652	0	4780	57600
C3-3a	73935	22562	0	0	0	51373
C3-3b	25589	7940	0	0	0	17649
C3-4a	53553	16543	0	0	1899	35111
C3-4b	22552	6552	0	0	398	15602
C3-5a	128366	34045	1091	0	0	93230
C3-5b	16643	4179	152	0	0	12312
C3-6a	80004	20997	0	0	1349	57658
C3-6b	89902	21079	867	0	0	67956
CK1232-1	127284	59052	0	0	0	68232
CK1232-2	161752	70043	0	0	0	91709
C2-1a	53571	16678	0	0	0	36893
C2-1b	25615	7060	0	0	0	18555
C2-2a	55698	20602	0	0	0	35096
C2-2b	84301	25809	0	0	0	58492
CK1235-1	206215	122462	11152	0	0	72601
CK1235-2	74429	43777	4130	0	0	26522
CK1236-1	20564	11265	0	0	0	9299
CK1236-2	55725	30832	0	0	0	24893
CK1237-1	102376	62617	0	0	0	39759
CK1237-2	139700	86444	0	0	0	53256
C2-4a	136761	74460	0	0	0	62301
C2-4b	216318	118201	0	0	0	98117
C2-5a	48354	27604	0	0	0	20750
C2-5b	92506	55950	0	0	0	36556
CK1241-1	177526	115666	0	0	0	61860
CK1241-2	142667	88091	0	0	0	54576
C2-7a	63745	36419	0	0	0	27326
C2-7b	159960	88818	0	0	0	71142
C2-8a	22420	14376	0	0	0	8044
C2-8b	130842	85938	0	0	0	44904
CK1244-1	99934	54354	0	0	0	45580
CK1244-2	15808	9077	0	0	0	6731
CK1245-1	81822	42330	0	0	0	39492
CK1245-2	49130	24254	0	0	0	24876
CK1246-1	52169	30142	0	0	0	22027

CK1246-2	70027	43178	0	0	0	26849
CK1247-1	32592	14991	0	0	0	17601
CK1247-2	21821	9398	0	0	0	12423
CK1248-1	25455	16365	0	0	0	9090
CK1248-2	48980	32070	0	0	0	16910
C2-9a	37303	24313	0	0	0	12990
C2-9b	43272	26410	0	0	0	16862
C2-10a	1889	1288	0	0	0	601
C2-10b	213822	155149	1128	0	0	57545

Table C-8: Spearman correlation of DNA concentration, bacterial 16S rRNA gene abundance and total cell counts. P-values are shown above the diagonal and the correlation coefficient r_s below.

	DNA	16S rRNA gene copies	TCC
DNA		**>0.0001**	**>0.0001**
16S rRNA gene copies	0.87		**0.0001**
TCC	0.68	0.61	

Table C-9: Minimum. maximum. mean values and standard deviation of microbial and bacterial abundance. n indicates the number of samples.

	Core	**Min**	**Max**	**Mean**	**Std. dev.**	**n**
DNA concentration	C1	28.6	331.3	141.6	105.6	6
[ng g^{-1}]	C4	6.2	277.5	88.5	102.6	6
	C3	5.6	51.9	19.8	17.8	6
	C2	8.7	341.5	106.9	94.0	17
16S rRNA gene copies	C1	2.4E+07	4.3E+08	1.6E+08	1.4E+08	6
[g^{-1} sediment]	C4	1.7E+06	1.6E+08	3.6E+07	5.8E+07	6
	C3	4.1E+06	6.2E+07	1.7E+07	2.1E+07	6
	C2	5.4E+06	1.5E+09	2.9E+08	4.0E+08	17
16S rRNA gene copies	C1	7.6E+05	1.4E+06	1.0E+06	2.6E+05	6
[ng^{-1} DNA]	C4	5.8E+04	5.8E+05	2.7E+05	1.6E+05	6
	C3	4.9E+05	1.2E+06	7.6E+05	2.2E+05	6
	C2	2.6E+05	1.7E+07	2.7E+06	4.2E+06	17
TCC	C1	6.8E+06	8.2E+07	5.0E+07	2.8E+07	6
[g^{-1} sediment]	C4	1.6E+06	4.4E+07	1.3E+07	1.5E+07	6
	C3	3.4E+05	3.4E+06	1.5E+06	1.0E+06	6
	C2	1.4E+06	4.9E+07	1.5E+07	1.3E+07	17

Table C-10: Rank-based Spearman correlation of DNA concentration, bacterial 16S rRNA gene abundance and total cell counts with environmental factors and pore water data. Values in bold are significant (< 0.05) when omitting a p-value correction. Rs- values highlighted red show a negative correlation, whereas rs-values highlighted green show a positive correlation.

	16S Bacteria	16S/DNA	TCC	Temp	Salinity	Depth [mbsl]	Depth [mbs/ mbsf]	Ba^{2+}	Ca^{2+}	K^{+}	Mg^{2+}	Na^{+}	Si_{aq}	Cl^{-}	SO_4^{2-}	Br^{-}	NO_3^{-}	δ18O	δD	pH	TC	TN	TS	TOC	Clay	Silt	Sand	Grav. Water Content
p-value																												
DNA	**>0.001**	**>0.001**	**>0.001**	**0.030**	**0.039**	0.813	0.076	0.658	0.604	**0.020**	0.061	**0.021**	0.872	**0.011**	0.410	**0.015**	0.593	**0.027**	0.055	**0.008**	**0.017**	0.329	0.175	**0.045**	0.307	0.111	0.130	**0.006**
16S Bact.		**>0.001**	**>0.001**	0.173	**0.003**	0.164	**0.002**	0.860	0.248	**0.003**	**0.005**	**>0.001**	0.475	**>0.001**	0.128	**0.001**	0.587	**0.023**	0.054	**0.002**	**0.009**	0.175	0.056	**0.021**	0.821	0.886	0.926	**0.007**
16S / DNA			**0.03**	0.503	**>0.001**	0.216	**0.004**	0.799	**0.005**	**0.001**	**>0.001**	**>0.001**	0.268	**>0.001**	**0.016**	**>0.001**	0.425	0.369	0.528	**0.001**	0.218	0.171	0.135	0.284	0.055	0.102	0.084	0.153
TCC				**>0.001**	**0.008**	0.465	0.138	**0.024**	0.193	**0.012**	**0.029**	**0.002**	0.262	**0.001**	0.593	**0.002**	0.890	**0.028**	**0.027**	0.097	0.749	0.759	0.233	0.429	0.184	0.572	0.524	0.369
correlation coefficient r_s																												
DNA	0.87	0.47	0.68	-0.37	-0.35	0.04	0.30	-0.08	-0.09	-0.39	-0.32	-0.39	-0.03	-0.43	-0.14	-0.41	0.09	-0.37	-0.33	-0.44	0.40	0.17	-0.23	0.34	0.18	0.27	-0.26	0.47
16S Bact.		0.79	0.61	-0.24	-0.48	0.24	0.51	0.03	-0.20	-0.49	-0.46	-0.57	-0.12	-0.56	-0.26	-0.54	0.09	-0.38	-0.33	-0.52	0.44	0.23	-0.33	0.39	-0.04	0.03	-0.02	0.47
16S / DNA			0.36	-0.12	-0.63	0.21	0.47	0.04	-0.47	-0.55	-0.60	-0.71	-0.19	-0.67	-0.40	-0.66	-0.14	-0.16	-0.11	-0.54	0.21	0.24	-0.26	0.19	-0.33	-0.28	0.30	0.26
TCC				-0.64	-0.44	-0.13	0.26	-0.38	-0.23	-0.42	-0.37	-0.50	-0.19	-0.52	-0.09	-0.50	0.02	-0.37	-0.37	-0.28	0.06	0.05	-0.21	0.14	-0.23	-0.10	0.11	0.16

Table C-11: Significance of the variance introduced by environmental factors into the microbial community tested by Permutational MANOVA (PerMANOVA).

	Dim1	Dim2	r^2	p-value
Depth [mbs/msbf]	**-0.53174**	**-0.84691**	**0.3322**	**0.006**
Temperature	**0.13632**	**0.99067**	**0.2487**	**0.015**
Ba	**0.94807**	**0.31805**	**0.1859**	**0.031**
Si	0.90304	-0.42956	0.1541	0.056
Ca	0.50032	0.86584	0.0100	0.835
K	0.81761	0.57578	0.0612	0.341
Mg	0.80879	0.58809	0.0684	0.297
Na	0.99177	0.12804	0.0813	0.241
Nitrate	-0.81210	0.58351	0.0280	0.637
Chloride	0.98966	0.14344	0.0527	0.391
Sulfate	-0.28689	0.95796	0.1014	0.161
Bromide	0.92727	0.37439	0.0629	0.326
Salinity	0.99532	0.09660	0.0459	0.443
δ18O	**0.99329**	**-0.11569**	**0.3753**	**0.001**
δD	**0.98430**	**-0.17648**	**0.3914**	**0.001**
pH	**-0.42785**	**0.90385**	**0.6412**	**0.001**
TC	0.41379	-0.91037	0.1053	0.149
TN	-0.38942	-0.92106	0.0268	0.640
TS	**0.03653**	**0.99933**	**0.2694**	**0.004**
TOC	0.40692	-0.91346	0.0974	0.170
Clay	0.47503	0.87997	0.1123	0.132
Silt	0.76336	0.64597	0.0532	0.405
Sand	-0.70792	-0.70629	0.0630	0.330
Conductivity	0.98987	0.14199	0.0419	0.478

Table C-12: One-way PerMANOVA of OTU data from each drill site. Summary presents the overall test statistics. Pairwise analysis shows Bonferroni corrected p-values above the diagonal and F-values below.

Summary		**Pairwise**				
Permutation N:	9999		**C1**	**C4**	**C3**	**C2**
Total sum of squares:	26.49	**C1**		**0.0012**	**0.0006**	**0.0006**
Within-group sum of squares:	19.41	**C4**	4.014		**0.0006**	**0.0006**
F:	8.276	**C3**	12.400	7.368		**0.0006**
p (same):	0.0001	**C2**	5.833	5.156	16.350	

Table C-13: Analysis of variance (ANOVA) of DOC concentrations between all four cores and Tukey's pairwise post-hoc test with p-values adjusted according to Copenhaver-Holland above and the Tukey's Q below the diagonal.

	Sum of squares	df	Mean square	F	p (same)
Between groups:	24714.2	3	8238.06	4.814	0.003712
Within groups:	155731	91	1711.34		**Permutation p (n=99999)**
Total:	180446	94			0.02357

	C1	C4	C3	C2
C1		0.066	0.996	0.052
C4	3,540		0.299	**0.002**
C3	0.310	2.490		0.739
C2	3.676	5.209	1.441	

Table C-14: Fossil bioindicators according to *Schirrmeister et al.* [2008)] *Winterfeld et al.* [2011]; *Müller et al.* [2009)]and their stratigraphical and paleoenvironmental interpretation.

Units	Bioindicator	Stratigraphy	Landscape, facies	Vegetation	Climate
IId	• Pollen*:* Cyperaceae, Poaceae*, Artemisia, Salix* • Spores: *Encalypta, Glomus* • Green algae: *Botryococcus, Pediastrum* • Ostracodes • Plant macro remains: Carex, *Salix* sp., *Saxifraga hirculus*, *Dryas Kobresia myosuroides, Thlaspitea rotundifolii* • Testacea: hygrophillic (Difflugia), sphagnobiotic (*Heleopera, Nebela, Argynnia* sp.) • Mammals: *Equus caballus, Mammuthus primigenius*	Middle Weichselian Interstadial	Floodplain, alluvial, boggy, periodically flooded	Grass-sedge tundra	Moderate, humid
IIc	No determinable fossil records found	Early Weichselian Stadial	fluvial		
IIb	Pollen: *Larix, Alnus fruticosa*, *Betula nana*, Ericales	Eemian Interglacial	Thermokarst lake	Shrub tundra	Temperate

IIa	No determinable fossil records found	Early Weichselian Stadial	fluvial	
I	• Marine diatoms: *Hyalodiscus* sp., *Paralia sulcata, Porosira glacialis, Thalassiosira* sp., *Thalassiothrix longissima, Centralea* ind. • Fresh water diatoms: *Naicula radiosa, Eunotia praerupta, Pinnularia gibba, tetracyclus lacustris* • Sponge spicula • Pollen: *Larix, Alnus fruticosa*, *Betula nana*, Ericales • Spores: *Sphagnum*	Eemian Interglacial	Thermokarst lagoon	Shrub tundra temperate